https://doi.org/10.61092/iaea.zr3b-121v

INDC(NDS)-0791
Distr. Web

IAEA
International Atomic Energy Agency

INDC International Nuclear Data Committee

A GLOBAL FITTING METHOD WITH THE R-MATRIX CODE RAC

Zhenpeng Chen
Tsinghua University, Beijing, China

Yeying Sun
Tsinghua University, Beijing, China

December 2019

IAEA Nuclear Data Section
Vienna International Centre, P.O. Box 100, 1400 Vienna, Austria

Selected INDC documents may be downloaded in electronic form from
http://nds.iaea.org/publications
or sent as an e-mail attachment.
Requests for hardcopy or e-mail transmittal should be directed to
NDS.Contact-Point@iaea.org
or to:
Nuclear Data Section
International Atomic Energy Agency
Vienna International Centre
PO Box 100
1400 Vienna
Austria

Printed by the IAEA in Austria

December 2019

INDC(NDS)-0791
Distr. Web

A GLOBAL FITTING METHOD WITH THE R-MATRIX CODE RAC

Zhenpeng Chen*
Tsinghua University, Beijing, China

Yeying Sun
Tsinghua University, Beijing, China

ABSTRACT

This report introduces the evaluation method RAC-CERNGEPLIS and the results obtained for the project "R-matrix Codes for Charged-particle Induced Reactions in the Resolved Resonance Region" that is coordinated by the Nuclear Data Section. In fact, this method has been used before in the evaluation of the compound systems $n+^{6}Li$ and $n+^{10}B$, for the IAEA Neutron Standards (2006 and 2017 release). The main characteristics of the RAC code are that i) the eliminated channel width is included in the R-matrix algorithm and ii) the Generalized-Least Square method is used in the fitting procedure. In this report we discuss different approaches to R-Matrix fitting that are used in nuclear data evaluation. Practice shows that the RAC-CERNGEPLIS method is a reasonable, useful and powerful tool for evaluation of nuclear data.

* E-mail：zhpchen@mail.tsinghua.edu.cn

Report on the work performed under a Special Service Agreement

December 2019

Contents

1. INTRODUCTION

Charged-particle induced reactions at low energy are important for Ion Beam Analysis (IBA) applications in materials analysis, cultural heritage and preservation, environment and climate control, and forensics, to mention but a few examples. The Nuclear Data Section (NDS) of IAEA is the international center collecting and disseminating nuclear data for IBA. For this purpose it maintains the Ion Beam Analysis Data Library (IBANDL) that contains over 6000 datasets of experimental differential and total cross section for charged-particle induced reactions in the low-energy region below several MeV.

Other applications where charged-particle reactions in the resolved-resonance-region are relevant include management of reactor fuel in nuclear reactors. For the most widely used fuel material UO2, UF6, PuF4, and PuO2, the dominant neutron producing reactions are (α,xn) reactions on isotopes of O and F occurring in the resolved resonance region. A survey of evaluated library reveals lack of reliable (α,xn) data on these isotopes in the low-energy resolved resonance region.

In nuclear astrophysics, stellar synthesis models are based on thermonuclear reactions at temperatures of tens of millions of degree Kelvin to produce both the energy of the stars and the light and medium elements up to iron. In the earth laboratory these conditions correspond to charged-particle induced reactions on light and medium mass nuclei at energy of few tens of KeV. Efforts have been made over past decades to measure these cross sections and provide theoretical description, R-Matrix fits and/or evaluation of the data that would allow extrapolating to the lower energies needed for the stellar models.

To address the above-mentioned data needs the IAEA-NDS is coordinating an international effort to (1) perform an inter-comparison of all available R-matrix Code, (2) evaluate cross sections of charged-particle induced reaction in the resolved resonance region (RRR), (3) produce evaluated nuclear data files for further processing and finally (4) disseminate these data through the general purpose evaluated nuclear data libraries, and therefore make them available to the broader user community.

This report mainly introduces the results obtained within the project “R-matrix Codes for Charged-particle Induced Reactions in the Resolved Resonance Region” [1] using the evaluation method RAC-CERNGEPLIS. This method has already been used in the evaluation of n+^{6}Li and n+^{10}B for the IAEA Neutron Standard (2006 [2] and 2017 [3] (way be released later). The main characteristics of the RAC code are that (i) the eliminated channel width is included in the R-matrix algorithm and (ii) the Generalized-Least Square method is used in the fitting procedure. Different approaches to R-Matrix fitting adopted in nuclear data evaluation are also discussed. Our practice demonstrates that the RAC-CERNGEPLIS method is a reasonable, useful and powerful tool for evaluation of nuclear data.

The structure of the report is as follows: in Section 2 we introduce the formulas used in RAC, including the new calculation method; in Section 3 we discuss the computational accuracy of RAC and present the results in comparison with other R-matrix codes; in Section 4 we present the different evaluation methods based on Approximate Least Squares (ALS), Conventional Least Squares (CLS) and Generalized Least Squares (GLS) in detail, and in particular we

discuss the differences between the RAC code and EDA R-matrix code (Los Alamos R-matrix code); the importance of selecting a suitable level scheme for the evaluation is presented in Section 5; in Section 6 we demonstrate the different schemes used for the ALS, CLS and GLS and show that the differences in the end are observed in the chi2 the covariance matrix of evaluated values; in Section 7 we discuss some important issues related to the evaluation process; the final complete evaluation of ^{7}Be is presented in Section 8; our conclusions are given in Section 9 while the 6 files produced by this evaluations are appended in the Appendix.

2. BASIC FORMULAS OF THE R-MATRIX CODE RAC

In this section we introduce the R-matrix expressions and approximations implemented in the R-matrix code RAC. In Section 2.1 we present the improved formalism implemented in RAC which leads to small differences when compared with the results obtained by the other standard R-matrix codes for the same input parameters. Then in Section 2.2 we introduce the statistical theory of covariances and the method used to build a covariance matrix based on experimental data. Finally, in Section 2.3 we introduce the classical Reduced R-matrix formalism of Lane and Thomas [4].

2.1. Improved level width and energy shift

The level width and energy shift formulas given below are an extreme approximation that is valid for one single level

$$\Gamma_{\lambda c} = 2P_c\gamma_{\lambda c}^2$$

$$\Delta_{\lambda c} = -S_c\gamma_{\lambda c}^2 \qquad (2.1)$$

In Ref. 4 (see page 273, Eqs. 1.17, 1.18, 1.19), the correct general formulas for the 'level width' and 'level shift' are given as follows:

$$\Gamma_{\lambda c} = 2P_c\gamma_{\lambda c}^2/d_c \qquad (2.2)$$

$$\Delta_{\lambda c} = \frac{P_c(R_{cc}^0P_c)-S_c^0(1-R_{cc}^0S_c^0)}{d_c}\gamma_{\lambda c}^2 \qquad (2.3)$$

$$d_c = (1-R_{cc}^0S_c^0)^2 + (R_{cc}^0P_c)^2 \qquad (2.4)$$

where R_{cc}^0 is the constant background. In RAC we have implemented the Multi-channel and Multi-level R-Matrix formula without constant background. Instead, in the calculation of an energy level's width and shift, the contribution of the remaining levels are taken as a constant background, which is an accurate equivalent of using R_{cc}^0. Due to the complexity of the algorithm described in Eqs. (2.2-2.4), the calculation time required for adjusting the parameters in the fitting process increases by a factor of 5.

In this work we have used all the information on the experimental level widths and branching ratios available in the literature, which is absolutely essential to accurately calculate the width and shift in some cases. For example, we use

$$\Gamma_{\lambda\gamma}^{obs} = 2P_c\,\gamma_{\lambda c}^2/(1+\sum k\;\gamma_{\lambda k}^2\;(\frac{dS_k}{dE})_{E_\lambda}) \qquad (2.5)$$

where $\Gamma_{\lambda\gamma}^{obs}$ represents the observed width, P_c is the penetrability, $\gamma_{\lambda c}^2$ the reduced width amplitudes in the calculation.

Note that the improved level width and energy shift formulas are absolutely necessary when very narrow levels are considered. For example, in the evaluation for $^{12}C(\alpha,\gamma)^{16}O$, γ transitions play the most important role, but since all the information used is level width or level half-life for the bound levels, the improved formulas have to be used to get accurate results.

We obtain accurate wave functions of positive energy by using the continued fractions method in the (α,α) and γ–particle channels. This ensures that the wave functions calculated by RAC agree with the results of Barnett [5] by more than fourteen significant figures.

2.2. Covariances, generalized least squares and error propagation law

The book of D. Smith [6] presents the most advanced theory for evaluation of nuclear data and is a guide to developing computer programs. The IAEA Neutron Standards reports [2,3] are the best examples of applications of the theory of nuclear data evaluation and can be considered as 'best practice'. Key components of nuclear data evaluation and of self-contained methods are (i) the theory of error distribution and error propagation, (ii) the formulae for covariance fitting, (iii) the theory of generalized least squares, (iv) the experimental method for modification of Pearl's Pertinent Puzzle (PPP), (v) Lett's criteria for minimizing the effect from occasional 'outliers', and (vi) the test for the definiteness of the covariance matrix. These components cannot be ignored if one wants to obtain an accurate evaluated value and describe the experimental nuclear data objectively and with high precision. The basic reason for this is that nuclear measurements involve long-range, middle-range and short-range errors of the observables objectively, and this can never be avoided completely. The long-range and middle-range errors are connected via correlations.

The code RAC13 makes use of a suitable reaction model, employs the most advanced evaluation methods, and uses the most complete global experimental database, to obtain evaluated values close to the expectation values combined with the most reasonable error information. In previous efforts, we used the 'Conventional Least Squares fitting' fitting procedure - but neglecting the problem of PPP - which in theory cannot give an unbiased estimation for complex samples.

In this work, we use the 'covariance fitting' approach, because, in theory, the systematic error always exists no matter how exact the evaluation of the experimental data (ED) is. As long as the systematic error exists, the correlation between the experimental data (ED) and the off-diagonal elements of the covariance matrix can never be removed. The 'Conventional Least Squares fitting' fitting only considers the diagonal elements of the covariance matrix, while it ignores the off-diagonal elements and that part of the correlations of experimental data (ED). Therefore, the optimal calculation is only a rough approximation of the expected value according to the 'maximum likelihood principle'. Fitting the data using covariances is an accurate method. When the inverse of the covariance matrix is used in the optimization procedure, the values of χ^2_{Mean} are accurately estimated. Table 6.1 shows the significant

difference in the χ^2_{Mean} obtained with the 'Conventional Least Squares fitting' and the 'Covariance Fitting'.

In the following, we describe how to construct the covariance matrix with error information taken from the experimental data:

Suppose $U_i^2, S_i^2, L_i^2, M_i^2$ and Y_i^2 are total variance, statistical variance, long-range component (LERC) of systematic variance, medium-range component (MERC) of systematic variance and total systematic variance of the ith ED point respectively, and let $U_i^2 = S_i^2 + L_i^2 + M_i^2$, $Y_i^2 = L_i^2 + M_i^2$. The diagonal elements C_{jj} of correlation coefficient matrix C are 1 for all. The non-diagonal elements for integral cross sections are

$$C_{ij} = C_{ij}^L + C_{ij}^M \tag{2.6}$$

Here C_{ij}^L refers to the LERC of systematic errors, C_{ij}^M to the MERC of systematic errors, and

$$C_{ij}^L = L_i\, L_j/(U_i U_j) \tag{2.7}$$

$$C_{ij}^M = M_i\, M_j/(U_i U_j) \cdot f_{ij} \tag{2.8}$$

$$f_{ij} = \text{Exp}\ \{-[(E_i - E_j)/\text{W}]^2/2\} \tag{2.9}$$

where W is a distribution width parameter, and E_i and E_j stand for energy points of the data. The non-diagonal elements of C for AD are

$$C_{ij} = \left(C_{ij}^L + C_{ij}^M\right) \cdot G_{ij} \tag{2.10}$$

$$G_{ij} = \text{Exp}\ \{-[(\theta_i - \theta_j)/160]^2/2\} \tag{2.11}$$

Here 160 is a distribution parameter related to angle, θ_i and θ_j are angle values.

It can be seen from the formulas given above that the correlation coefficient is determined by the total error and systematic error, and a larger systematic error leads to a larger correlation coefficient. The absolute covariance matrix elements of the simulated data can be calculated from the corresponding correlation coefficients as follows:

$$V_{ij} = C_{ij} \cdot U_i \cdot U_j \tag{2.12}$$

The theoretical formula for error propagation within the R-matrix model fitting is as follows:

$$\text{y} - y_0 = D(P - P_0) \tag{2.13}$$

$$D_{ki} = (\partial y_k/\partial P_i)_0 \tag{2.14}$$

Here y refers to the vector of calculated values, D to the sensitivity matrix, P to the vector of R-matrix parameters. Subscript 0 means optimized original value, k and i are for fitted data and R-matrix parameter subscript respectively. The covariance matrix of parameter P is

$$V_P = (D^+ V^{-1} D)^{-1} \tag{2.15}$$

Here V refers to the covariance matrix of the data to be fitted, and its inversion matrix can be expressed as follows:

$$V^{-1} = \begin{pmatrix} V_1^{-1} & & 0 \\ & V_2^{-1} & \\ 0 & & \ddots \\ & & & V_k^{-1} \end{pmatrix} \tag{2.16}$$

Here $V_1, V_2 \cdots V_k$ refer to the covariance matrixes of the sub-set data, which are independent of each other. The covariance matrix of calculated values is

$$V_y = DV_P D^+ \tag{2.17}$$

The formula adopted for optimizing the R-matrix fitting is

$$\boldsymbol{\chi^2 = (\eta - y)^+ V^{-1}(\eta - y) \Rightarrow minimum} \tag{2.18}$$

Here η refers to the vector of ED, y refers to the vector of calculated values.

2.3. Basic formulas used in RAC2015

The practical formulas implemented in RAC are taken from the literature [4,6,7,8]. Regarding the R-matrix and reaction cross section calculations, the algorithms were implemented in strict accordance with the formulas in Ref. [4] without introducing any approximation. Here we present that part of the algorithm that was further developed.

For the positive energy channel, the incoming (I) and outgoing wave (O) function is defined as follows

$$I_c^+ = (G_c - iF_c)\exp(i\omega_c);\ O_c^+ = (G_c + iF_c)\exp(-i\omega_c) \tag{2.19}$$

For the negative energy channel, only the outgoing wave (O) function is defined as

$$O_c^- = W\left(-\eta_\alpha, l + \frac{1}{2}; 2\rho_\alpha\right), \tag{2.20}$$

$$\omega_c \equiv \omega_{\alpha l} = \sigma_{\alpha l} - \sigma_{\alpha 0} = \sum_{n=1}^{l} tan^{-1}(\eta_\alpha / n) \tag{2.21}$$

The logarithmic derivative of O-type wave function is designated as

$$L_c \equiv \left(\frac{\rho_c O_c'}{O_c}\right)_{r_c = a_c} = S_c + iP_c \tag{2.22}$$

The real and imaginary parts of which are given by, according to Eqs. (4.4a), (4.4b) in Ref. [4], respectively,

$$S_c^+ = \left[\frac{\rho_c(F_c F_c' - G_c G_c')}{F_c^2 + G_c^2}\right]_{r_c = a_c} \tag{2.23}$$

$$S_c^- = \left(\frac{\rho_c W_c'}{W_c}\right)_{r_c = a_c} \tag{2.24}$$

$$P_c^+ = \left[\frac{\rho_c}{F_\ell^2 + G_\ell^2}\right]_{r_c = a_c} \tag{2.25}$$

$$P_c^- = zer. \tag{2.26}$$

In the case of the positive energy channels, the ratio is defined as

$$\Omega_c^+ = (I_c/O_c)_{r_c=a_c}^{1/2} \tag{2.27}$$

It is a unit-modulus complex number which is expressible as

$$\Omega_c^+ \equiv \Omega_{\alpha l}^+ = exp\ \ i(\omega_c - \phi_c^+)$$

$$\phi_c^+ \equiv \phi_{\alpha l}^+ = tan^{-1}(F_c/G_c) \tag{2.28}$$

We also introduce

$$\mathfrak{L}_c = (\rho_c I_c'/I_c)_{r_c=a_c};\ \mathfrak{B}_c = (\rho_c/I_c O_c)_{r_c=a_c} \tag{2.29}$$

The Wronskian is

$$\omega = (O_c' I_c - I_c' O_c)_{r_c=a_c}. \tag{2.30}$$

The relation between the R-matrix and the collision matrix U is

$$\mathrm{U^J} = \ \Omega \mathrm{W}^J \Omega \tag{2.31}$$

$$\mathrm{W}^J = 1 + \mathfrak{B}^{\frac{1}{2}}(1 - \mathrm{R^J L^0})^{-1} \mathrm{R^J} L \mathfrak{B}^{\frac{1}{2}} w \tag{2.32}$$

where,

$$\mathrm{L^0} = \mathrm{L} - \mathrm{B} \tag{2.33}$$

$$B_c \equiv \frac{\delta_{\lambda c}}{\gamma_{\lambda c}} = \frac{D_{\lambda c}}{V_{\lambda c}}. \tag{2.34}$$

The formulas for the R-matrix, level matrix and energy shift are

$$(\mathrm{R}_{(E)}^J)_{\alpha' s' l', \alpha s l} = \sum_{\lambda\mu}^N \gamma_{\alpha' s' l'}^J \gamma_{\alpha s l}^J A_{\lambda\mu} \delta_{J J_0} \tag{2.35}$$

$$[A^{-1}]_{\lambda\mu} = \left[E_\lambda^r - E - \Delta_{\lambda\mu}^r(E_\lambda^r)\right]\delta_{\lambda\mu} + \Delta_{\lambda\mu}^e(E_\lambda^r) - \frac{i}{2}\Gamma_{\lambda\mu}^e \delta_{\lambda\mu} \tag{2.36}$$

$$\Delta_{\lambda\mu}^r = -\sum_{\alpha s l}^N (\mathrm{S}_{\lambda\mu} - \mathrm{B}_\alpha)\gamma_{\alpha' s' l'}\gamma_{\alpha s l} \tag{2.37}$$

Let $\Delta_{\lambda\mu}^e(E_\lambda^r) \equiv 0.0$ or take it as an adjustable parameter.

With the relation between T-matrix and U-matrix the cross-section formulas are:

$$T^{J}_{\alpha' s' l',asl} = e^{2i\,\omega_{\alpha l}}\delta_{\alpha' s' l',\alpha sl} - U^{J}_{\alpha' s' l',\alpha sl} \tag{2.38}$$

$$\sigma_{\alpha',a} == \frac{\pi}{k^2_{\alpha}} \sum_{sl's'lJ}\, g_J \left|T^{J}_{\alpha' s' l',asl}\right|^2 \tag{2.39}$$

$$\sigma_{tot} = \frac{\pi}{k^2_{\alpha}} \sum_{slJ}\, 2g_J\,(1 - \mathrm{Re}U^{J}_{asl,asl}) \tag{2.40}$$

$$g_J = \frac{(2J+1)}{(2I_1+1)(2I_2+1)} \tag{2.41}$$

$$\frac{d\sigma_{\alpha\alpha'}}{d\Omega_{\alpha'}} = \frac{1}{(2I_1+1)(2I_2+1)} \sum_{ss'\nu\nu'} \left|A_{\alpha' s'\nu',as\nu}\,(\Omega_{\alpha'})\right|^2 \tag{2.42}$$

$$A_{\alpha' s'\nu',\alpha s\nu} = \frac{\sqrt{\pi}}{k_{\alpha}}(-C_{\alpha'}(\theta_{\alpha'})\delta_{\alpha' s'\nu',\alpha s\nu} +$$

$$i\sum_{JMl'm'} \sqrt{2l+1}(sl\nu 0|JM)(s'l'\nu' m'|JM) T^{J}_{\alpha' s' l',\alpha sl}\, Y^{(l')}_{m'}(\Omega_{\alpha'})) \tag{2.43}$$

RAC also includes Eqs. (2.2 - 2.12) from page 292 of Ref. [4], as well as some formulas from Ref. [29] as follow:

$$d\sigma_{\alpha\to\lambda_f}/d\Omega = 1/((2I_{\alpha 1}+1)(2I\alpha_2+1))\,\frac{1}{k^2_{\alpha}} \sum_k B_k P_k\,(\theta) \tag{2.44}$$

with the following definitions:

$$B_k = \sum_{s,L,L',\iota,\iota' J,J',\epsilon,\epsilon'} [\,]\,(-1)^{1+s-J_f}\,/4Z_1(\iota,J,\iota' J';sk) \times Z_2\left(L\,J\,L'\,J'\,;\,J_f k\right)$$
$$T^{*J'}_{\alpha s\iota',\epsilon' L'\lambda_f}\;\; T^{J}_{\alpha s\iota,\epsilon L\lambda_f} \tag{2.45}$$

$$Z_1(\iota J\,\iota' J';sk) = \hat{\iota}\,\hat{J}'\,\hat{\jmath}\,\hat{\jmath}'\,(\hat{\iota}\,0\,\hat{\iota}\,'0\,|\,k0)\mathrm{W}(\iota J\iota' J';sk) \tag{2.46}$$

$$Z_2\left(LJL'J';J_f k\right) = \hat{L}\,\hat{L}'\,\hat{f}\,\hat{f}'\,(L1L'-1|\mathrm{k}0)W\left(LJL'J';J_f\,k\right) \tag{2.47}$$

$$\hat{\iota} = (2\iota+1)^{1/2}\,, \hat{J} = (2J+1)^{1/2} \tag{2.48}$$

$$[\,] = \frac{1}{2}\,[1 + (-1)^{L'+L+k+\epsilon+\epsilon'}] \tag{2.49}$$

Eqs. (2.45 -2.49) are suitable when γ is assumed to be a transverse wave with intrinsic spin 1.

3. COMPUTATIONAL ACCURACY OF THE CODES

This section presents the computational accuracy achieved by the RAC code and how this compares with other R-matrix codes. The accurate wave functions of positive energy are obtained by the continued fractions method. This ensures that the wave functions calculated by RAC are in conformance with the results of Ref. [5].

All the results demonstrate that the computational accuracy of RAC is reliable and satisfactory for the needs of evaluating nuclear data.

3.1. The comparison of RAC13 with EDA, SAMMY and NJOY

EDA [9] is an R-matrix code for light nucleus systems and has been developed for data evaluation at Los Alamos National Laboratory. A systematic comparison between EDA and RAC was completed within the international cooperation project on Neutron Cross Section Standards coordinated by the International Atomic Energy Agency [2]. The calculation of the ^{6}Li(t,α)^{4}He neutron standard cross section by both codes is consistent within 5 or 6 digits. In Fig. 3.1 (a), the black curve corresponds to the calculated values of EDA, while the red curve represents the calculation by RAC: the two curves are in agreement with each other without any significant difference.

SAMMY [10] is the R-Matrix code developed at Oak Ridge National Laboratory to evaluate mainly neutron-induced reactions of heavier systems. NJOY [11] is a nuclear data processing code which is used to reconstruct resonance cross sections from resonance parameters provided in the ENDF-6 format. Using the same R-Matrix parameters produced by SAMMY, the reconstructed cross sections from RAC and NJOY are identical to 4 to 6 digits. In Fig. 3.1 (right), the black line indicates the calculated values of NJOY, while the red line represents the calculation by RAC, and these two lines are in agreement with each other without any significant difference.

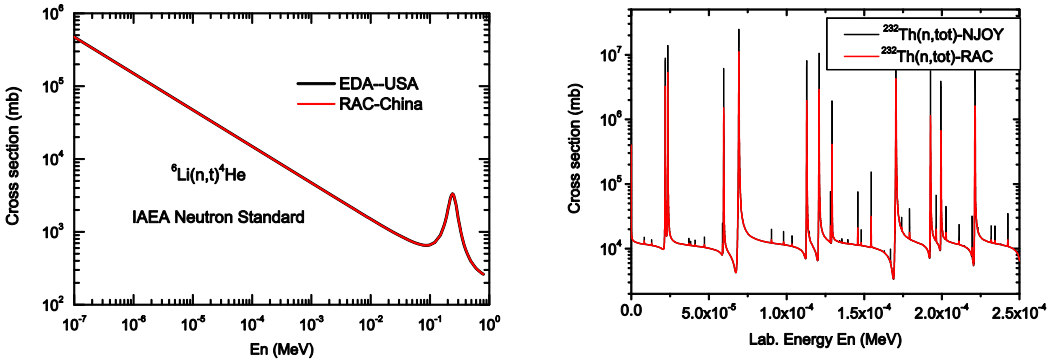

FIG 3.1. (Left) The calculated cross sections from RAC and EDA obtained with the same parameters. (Right) The reconstructed resonance cross sections of RAC and NJOY obtained with the same parameters of SAMMY.

Figure 3.2 shows the comparison of calculated results from RAC and EDA obtained with the same parameter set of EDA for ^{7}Be system evaluation. The parameter set was taken from the evaluation file of ^{7}Be system produced by the LANL group [46]. The agreement looks good.

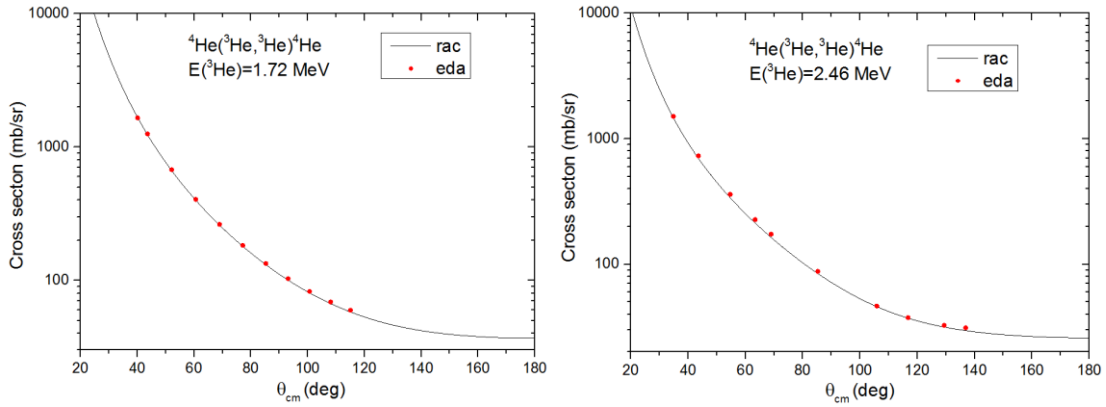

FIG 3.2. (Left) The calculated DA of ^{4}He(^{3}He,^{3}He)^{4}He from RAC and EDA at 1.72 MeV. (Right) The calculated DA of ^{4}He(^{3}He,^{3}He)^{4}He from RAC and EDA at 2.46 MeV.

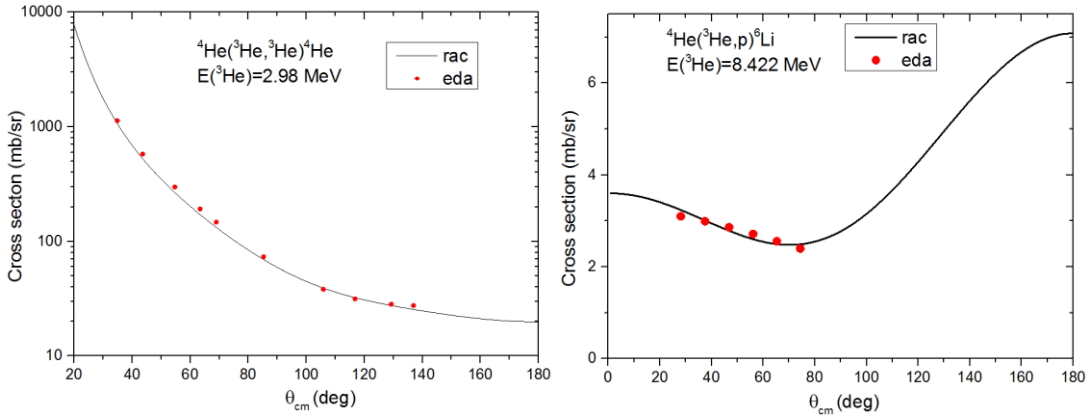

FIG 3.3. (Left) The calculated DA of ^{4}He(^{3}He,^{3}He)^{4}He from RAC and EDA at 2.98 MeV. (Right) The calculated DA of ^{4}He(^{3}He,^{3}He)^{4}He from RAC and EDA at 8.422 MeV.

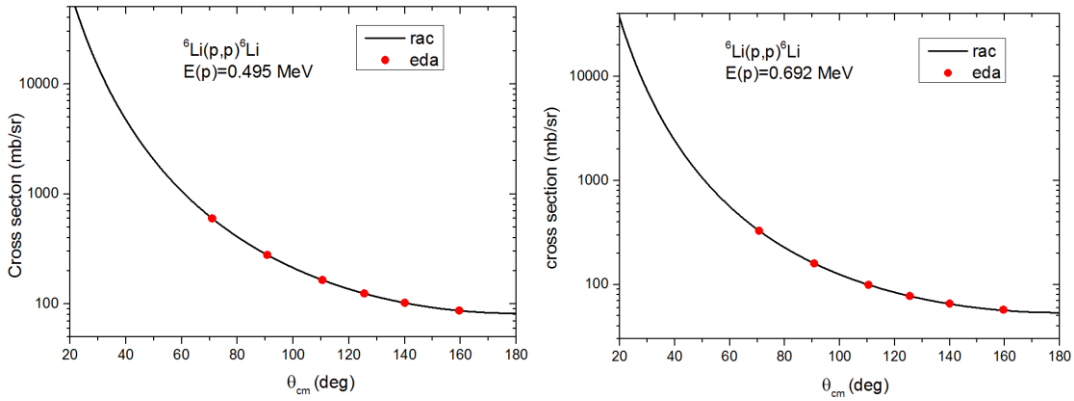

FIG 3.4. (Left) The calculated DA of ^{6}Li(p, p)^{6}Li from RAC and EDA at 0.495 MeV. (Right) The calculated DA of ^{6}Li(p, p)^{6}Li from RAC and EDA at 0.692 MeV.

3.2. Alpha spectrum results

The delayed alpha spectrum following β decay in ^{16}N (alpha spectrum) is calculated by RAC using the original parameters given in Ref. [12]. Figure 3.5 shows that the curve of the alpha spectrum of RAC is in agreement with the curve of Ref. [12] and is also very similar to the normalized alpha spectra of Ref. [13]. The calculated wave contribution of RAC is very similar

to that of Ref. [14]. The conclusion is that the calculation of the alpha spectrum using RAC is correct.

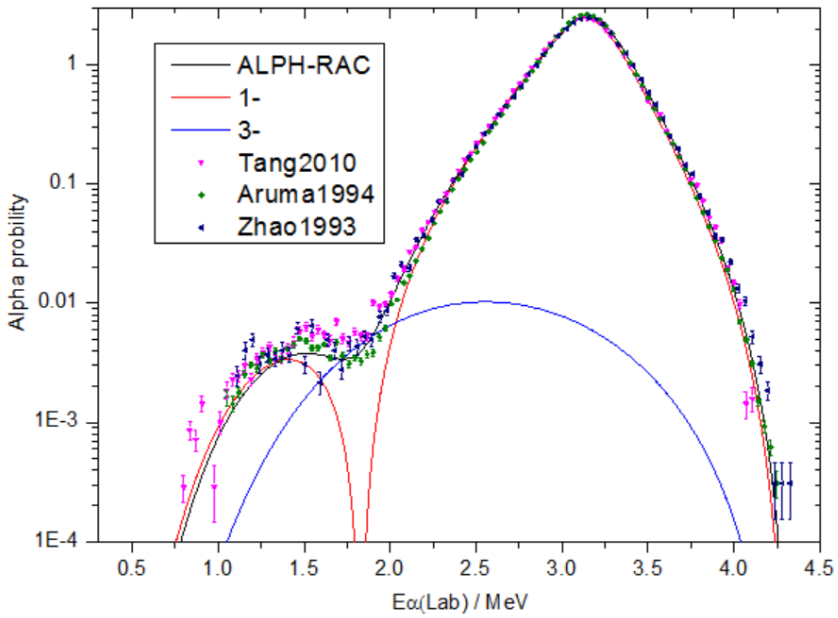

FIG 3.5. The data and calculated normalized alpha spectrum.

3.3. The Test1a results

Test1a was an exercise carried out within the IAEA project on R-matrix Codes for Charged-particle Reactions in the Resolved Resonance Region [1] with the aim of systematically comparing the various R-matrix codes used in nuclear data evaluation. The exercise required the calculation of cross sections using the same R-matrix parameter-set provided by the AMUR code (R-Matrix code developed at JAEA) and the same energy points for the following reactions: ^{6}Li(p,p)^{6}Li, ^{6}Li(p,^{4}He)^{3}He,^{3}He(^{4}He,^{4}He)^{3}He and ^{3}He(^{4}He,p)^{6}Li. The results of the inter-comparison (also published in [15]) show that SAMMY (ORNL), AZURE2 (Univ. Notre-Dame) and FRESCOX (Lawrence Livermore National Laboratory) agree very well, while EDA (LANL) and AMUR (JAEA) are close but with some differences. The results of RAC (Tsinghua Univ.) agree well with these of other codes for the (p,p) channels where these channels are open, but have obvious differences in the case of (p,p) channels where these channels are closed.

From the point of view of computational physics and overall experience, different nuclear codes based on many different approximations will unavoidably give different calculated cross sections. Differences of 2% are acceptable in the smooth energy region, while in the near threshold energy region differences of 5% are reasonable, and near the narrow pole energy region or very low energy region differences of 10% are expected. Based on this, the accuracy of the calculations obtained with all the participating codes (RAC, SAMMY, AZURE2 , FRESCOX, EDA, AMUR and CONRAD) is acceptable, however the reasons for the larger differences still need to be investigated.

The first possible reason for the differences between RAC and the other codes may be that RAC uses the corrected formulas for 'Width of level' and 'Energy shift' when multi-level calculations are performed, while the other codes use the 'extreme one-level approximation' formulas shown

instead (see Section 2.1). The corrected formulas are explained clearly in the classical reference of Lane and Thomas [4] on pp. 273 (an excerpt from the original publication is in following on the left side):

The extreme one-level approximation of (1.16) can be relaxed to some extent without much complication by retaining the contribution to R_l from all the other levels as a contribution R_l^0:

$$R_l = R_l^0 + \gamma_{\lambda l}^2/(E_{\lambda l} - E). \qquad (1.18)$$

The phase shift may then be expressed as

$$\delta_l = \tan^{-1}\left(\frac{\frac{1}{2}\Gamma_{\lambda l}'}{E_{\lambda l} + \Delta_{\lambda l}' - E}\right) - \phi_l', \qquad (1.19)$$

where

$$\tfrac{1}{2}\Gamma_{\lambda l}' = \gamma_{\lambda l}^2 P_l', \quad \Delta_{\lambda l}' = -\gamma_{\lambda l}^2 S_l',$$
$$\phi_l' = \phi_l - \tan^{-1}[R_l^0 P_l/(1 - R_l^0 S_l)],$$
$$S_l' = [S_l(1 - R_l^0 S_l) - R_l^0 P_l^2]/d_l, \quad P_l' = P_l/d_l,$$
$$d_l = (1 - R_l^0 S_l)^2 + (R_l^0 P_l)^2.$$

If R_l^0 is chosen to make (1.18) exact, then (1.19) is also exact like (1.15a). Although (1.19) has the same form as (1.17a), the level width, $\Gamma_{\lambda l}'$, the level shift $\Delta_{\lambda l}'$, and the potential scattering phase ϕ_l' are now modified by the contribution from the other levels. It is shown later (Sec. XI, 4) that the contribution to ϕ_l' from the other levels is of the same order of magnitude as the hard sphere contribution ϕ_l. Therefore, there is little justification to the interpretation of the observed potential scattering as that caused by a hard sphere.

(*ii*) *Negative energies.*—The only physically significant solution is the exponentially decaying one,

$$u_l = W(-\eta, l+\tfrac{1}{2}, 2\rho)$$

with the asymptotic form

$$W \sim \exp(-\rho - \eta \log 2\rho). \qquad (A.4)$$

This W function is the "Whittaker function" which has the integral representation

$$W(-\eta, l+\tfrac{1}{2}, 2\rho)$$
$$= \frac{\exp(-\rho - \eta \log 2\rho)}{\Gamma(1+l+\eta)} \int_0^\infty t^{l+\eta} e^{-t} \left(1 + \frac{t}{2\rho}\right)^{l-\eta} dt. \qquad (A.5)$$

For the case $\eta = 0$ (neutron channels), W becomes simply related to a modified Bessel function of the second kind:

$$W(0, l+\tfrac{1}{2}, 2\rho) = \left(\frac{2\rho}{\pi}\right)^{\frac{1}{2}} K_{l+\frac{1}{2}}(\rho). \qquad (A.6)$$

It is hard to give a precise estimate of the differences produced by these different formulas, but, in Ref. [4] it is mentioned that 'the contribution to ϕ_l' from the other levels is of the same order of magnitude as the hard sphere contribution ϕ_l, therefore more importance is attached to this potential source of differences than any other. In theory, a multi-level R-matrix code using the correct formulas for 'level width' and 'energy shift' should produce more reasonable results, but at the cost of using much longer CPU time.

The second possible reason is that RAC uses the integrated method to calculate the 'Whittaker Function' for 'negative energies' (refer to the right side in above text from Ref. [4], pp. 349). Other codes use different methods to calculate the wave function for 'negative energies'. In physics, in principle, using the integrated method to calculate the 'Whittaker Function' should be more reliable but again at the cost of using much longer CPU time.

In the following figures we present the results obtained using 4 different approaches to calculating the wave function for 'negative energies':

a. AMUR: the results obtained with the code AMUR which uses the 'continued fraction method' to calculate the wave function for 'negative energies'.

b. Int-Whittaker: the results from RAC obtained with the accurate integrated formulas for the Whittaker function (see Ref. [4], pp. 349, A.5). This is an exact calculation, therefore its precision must be better than that of other approximate methods, such as for example, the 'continued fraction method'. The drawback is that it costs much longer CPU, about 10 times as much as the 'continued fraction method'.

c. Asymp-Thompson: the results from RAC using the subroutine developed by I. Thompson. The asymptotic formulas (see Ref. [4], pp. 349, A.4) are used to calculate

the Whittaker function. In this case one obtains a relative value for the wave function while the scaling factor is 1.60. This is not an exact calculation.

d. MM-Bessel: the results from RAC using the approximate formulas for the Whittaker function (see Ref. [4], pp. 349, A.6). A modification factor 1.18 is used. This is not an exact calculation.

At E_α = 9.27 MeV the ^{3}He (α,p) ^{3}He channel is open. So in the 4 approaches mentioned above, a common requirement is that at E_α = 9.20 MeV they produce the same cross sections for ^{3}He(α, α)^{3}He, in order to get smooth and continuous cross sections for ^{3}He(α,α)^{3}He.

In the following figures one can see that all the results agree very well for the (p,p) channel in the open energy region; as for the ^{3}He(^{4}He,^{4}He)^{3}He channel, the 4 approaches agree in the energy region E_α > 9.27 MeV, but there exist obvious differences in the region of E_α < 8.5 MeV. It is clear that the different methods for calculating the wave function at 'negative energies' produce different results.

The third source of differences could be the intrinsic precision of a computer which includes the error from word length truncation among others. In computer calculations, the procedure (a+b) c may be different to ac+bc, in other words the different calculation order used in the different codes may give rise to different results. These errors cannot be avoided and may impact the very complex calculations performed in R-matrix analysis.

There may be other reasons for the R-matrix codes giving different results given the same input but as they are of minor importance we do not list them here.

As a general comment， the comparison performed in exercise Test1a can indicate if there is something wrong with the codes, for example if a specific code shows very large differences compared to the others. But it is not really possible to conclude which code is the most accurate one, or which code can be taken as a reference. The fact that more than one code give a certain value does not necessarily mean that the value is the best one. It may be that the codes use the same approximation or that they contain the same subroutines from another code or share subroutines. Therefore, it does not make much sense to set '0.1% to 0.3%' as the standard differences expected in R-matrix calculations using different codes.

Furthermore, the Test1a exercise is based on a very simple case that does not allow all the aspects of R-matrix analysis to be revealed and compared. For example, in the final evaluation exercise, new reaction channels (p,p_1), (p,p_2), (p,γ_0), (p, γ_1), (^{3}He,p_1), (^{3}He,p_2), (^{3}He, γ_0) and (^{3}He, γ_1) are involved, and additionally the polarization or analyzing data have to be included, so all the participating codes will have to prove that they can produce these types of observables as well.

To conclude, in order to be able to draw a reliable conclusion on the various R-matrix codes, more studies on more complex cases need to be performed.

In the following we present the figures comparing the results of Test1a obtained with RAC and AMUR codes.

3.3.1. ^{6}Li(p,p)^{6}Li reaction

The cross sections obtained for ^{6}Li(p,p)^{6}Li using the 4 approaches to calculating the Whittaker functions are completely identical.

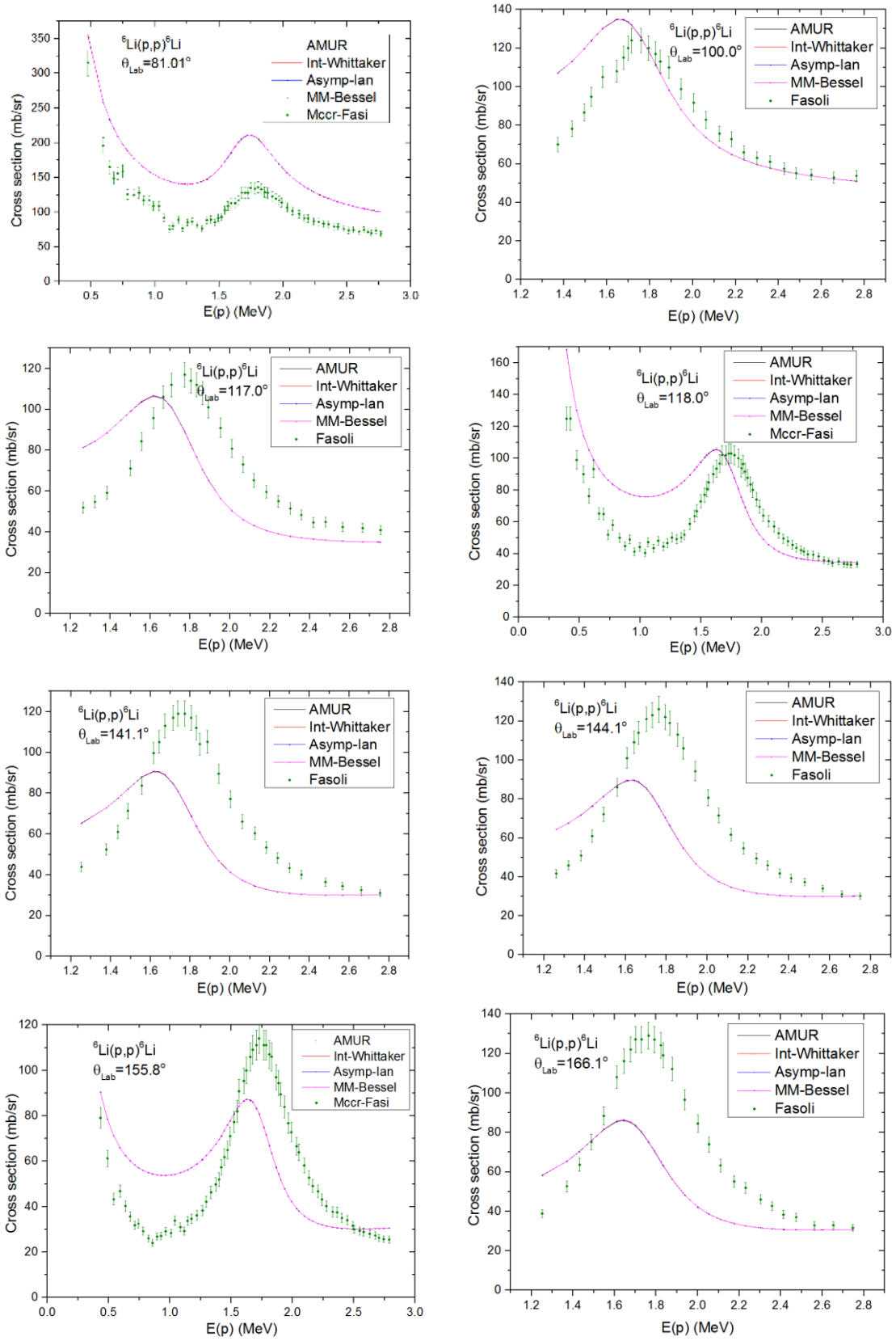

FIG 3.6. DA calculated using different Whittaker functions in RAC compared with AMUR results for ^{6}Li(p,p)^{6}Li.

3.3.2. $^{6}Li(p,^{4}He)^{3}He$

The calculations for the $^{6}Li(p,^{4}He)^{3}He$ reaction using the 3 approaches implemented in RAC are identical. The RAC and AMUR results however have very small differences for some energies.

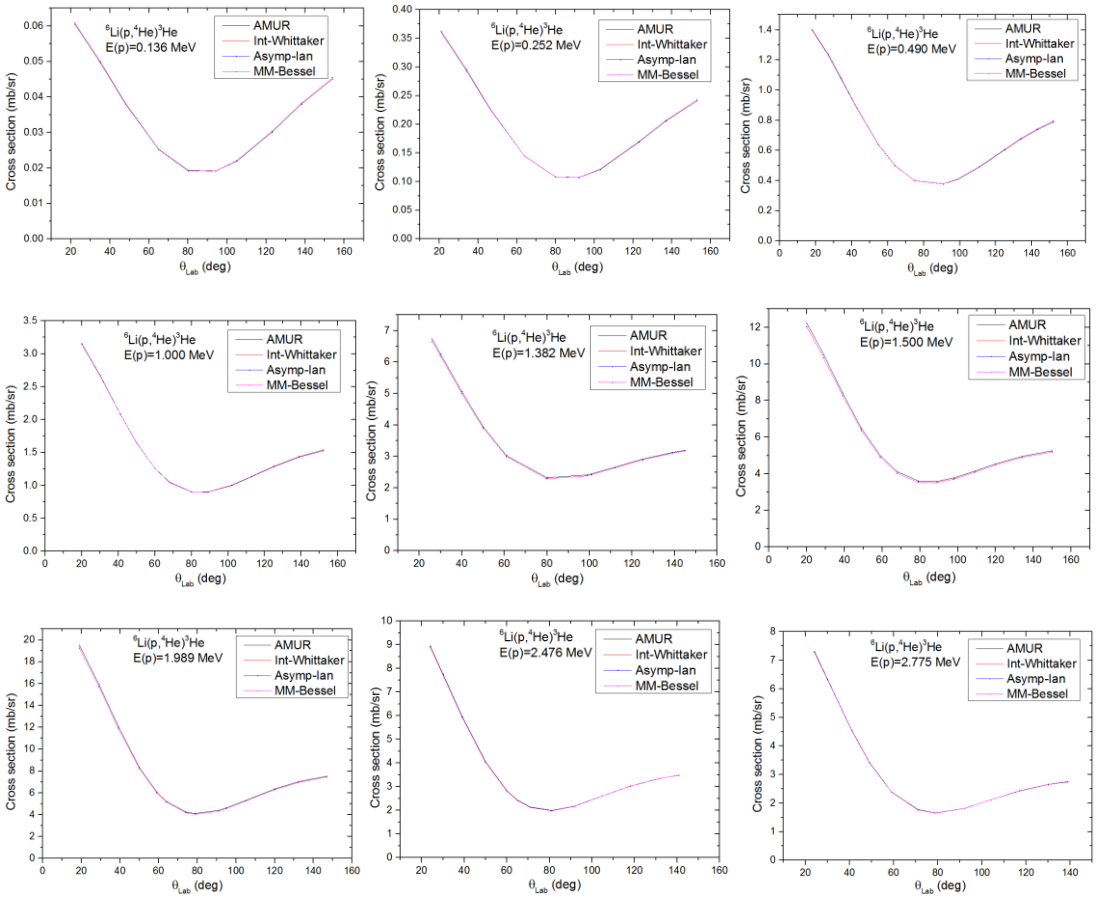

FIG 3.7. Same as in FIG 3.6 but for $^{6}Li(p,^{4}He)^{3}He$.

3.3.3. $^{3}He(^{4}He,^{4}He)^{3}He$

There are obviously differences for the $^{3}He(^{4}He,^{4}He)^{3}He$ reaction in the energy range from 1.5 MeV to 6.5 MeV. Some reasons for these differences have been given in the previous section.

At E_{α} = 9.27 MeV the $^{3}He(\alpha,p)^{3}He$ channel opens. So in the 4 approaches used in the calculations, a common requirement is that at E_{α} = 9.20 MeV they give the same cross sections for $^{3}He(\alpha,\alpha)^{3}He$, in order to get smooth and continuous cross sections for $^{3}He(\alpha,\alpha)^{3}He$ reaction.

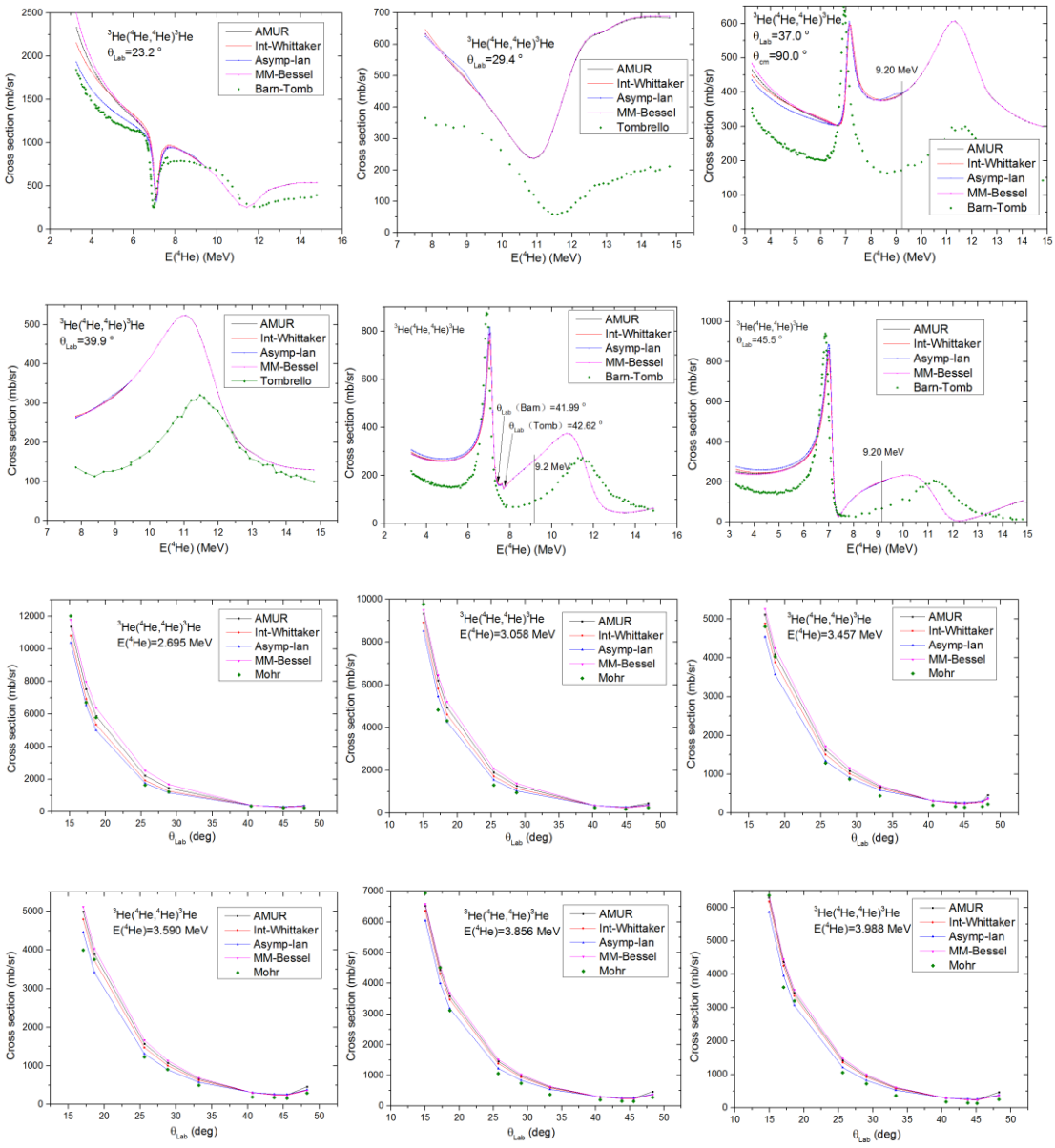

FIG 3.8. Same as in FIG 3.6 but for $^{3}He(^{4}He,^{4}He)^{3}He$.

3.3.4. $^{3}He(^{4}He,p_0)^{6}Li$

The calculated cross sections for the $^{3}He(^{4}He,p_0)^{6}Li$ reaction are identical using the 3 approaches implemented in RAC. AMUR gives small differences at the energies near the threshold.

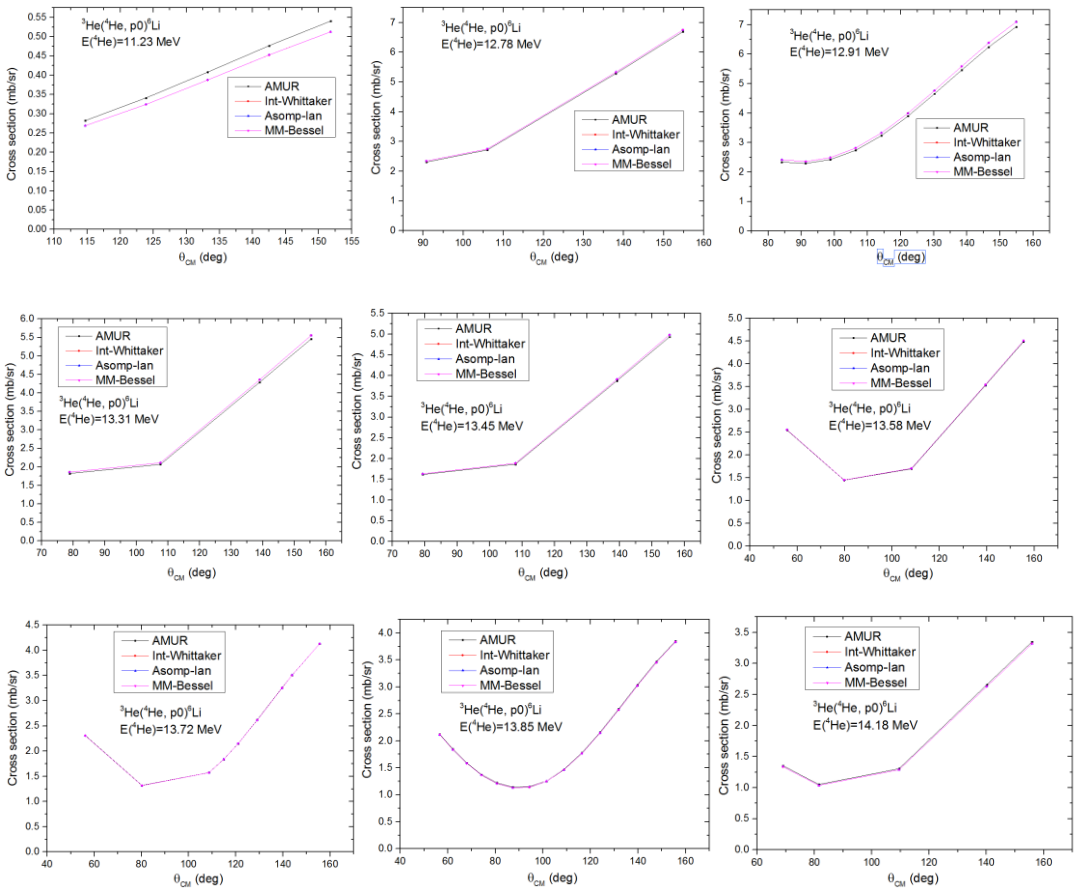

FIG 3.9. Same as in FIG 3.6 but for $^{3}He\ (^{4}He,p_0)^{6}Li$.

4. EVALUATION METHODS

In this section we discuss the evaluation methods based on Conventional Least Squares and Generalized Least Squares in detail. In particular, we describe the differences between the codes RAC and EDA. The opinions expressed herein are open to debate as undoubtedly further discussions on the issues will benefit future evaluation work.

4.1. Introduction to evaluation theory and terminology

At present, the 'Conventional Least Squares method' (CLS), as defined in p. 188 of Ref. [6], is commonly accepted and used worldwide to evaluate nuclear data. The objective of the operations performed under CLS is:

$$\chi^2 = (\vec{\eta} - \vec{y})^+ V^{-1} (\vec{\eta} - \vec{y}) \Rightarrow \text{minimum} \qquad (4.1)$$

The actual nuclear measurement samples must have statistical error s_i and system error y_i, and the covariance matrix of experimental data is composed of statistical error and system error. Many different expressions are used to calculate χ^2. In order to identify the differences between the various expressions of χ^2, the definitions and formulas of the covariance matrix, and error propagation theorem are introduced following the prescriptions in [6] (see p. 118 of this reference).

Error propagation theorem

If the vector Y is a linear function of vector x, that is $y = \sum_{i=1,n} t_i x_i$, $\delta Y = T^+ \delta x$, where T is a $n \times m$ matrix, then the following relations exist between the covariance matrix V_x of x and Y covariance matrix V_y,

$$V_y = T^+ V_x T \tag{4.2}$$

Formula of covariance matrix

The realization of Least Squares fitting must meet the requirements of linear regression, that is, the calculated value must be a linear function of the fitting model parameters. So if an initial parameter vector $\vec{P_0}$ was selected for parameter vector $\vec{P}$, the approximate linear function can be obtained by using the bench expansion:

$$\vec{Y} - \vec{Y_0} = D(\vec{P} - \vec{P_0}) \tag{4.3}$$

$$D_{kl} = (\partial y_k / \partial P_l)_0 \tag{4.4}$$

Here, Y is the said calculated value vector, D represents the 'Sensitivity Matrix', k is the subscript of calculated value vector, l is the subscript of parameter vector. The formula for calculation of covariance of parameter vector $\vec{P}$ is as follows:

$$V_P = (D^+ V^{-1} D)^{-1} \tag{4.5}$$

Here V represents the covariance matrix of all experimental data sets, V^{-1} represents the inverse matrix of V,

$$V^{-1} = \begin{pmatrix} V_1^{-1} & & 0 \\ & V_2^{-1} & \\ 0 & & V_k^{-1} \end{pmatrix} \tag{4.6}$$

Here, V_1, $V_2 \ldots V_k$ represent independent subsets.

According to the theory of Error Propagation (Eq. (4.2)), the covariance matrix of the final calculated value (also known as the evaluation value) is as follow:

$$V_y = D V_P D^+ \tag{4.7}$$

Here, V_P is the covariance matrix of the optimal parameter set, D is the sensitivity matrix of the final experimental data set with respect to the optimal parameter set. Formulas (4.5, 4.7) clearly show according to Ref. [6]:

1. If the non-diagonal element of V is ignored, that is the correlation between the systematic error of the experimental data is ignored, it is impossible to get the correct covariance matrix of the optimal parameter set V_P, and then it is impossible to get the correct covariance matrix value of evaluation value V_y. However, this is a common practice in the field of nuclear data evaluation.
2. V_y is the covariance matrix of evaluation values. The covariance information obtained from the 'non model' evaluation of experimental data can be used as initial data for 'Global evaluation', but, absolutely cannot be regarded as the covariance matrix of evaluation value V_y, while the V_y also includes the influence of the model parameters, which through the sensitivity matrix D play a major role.
3. When we consider all the matrix elements of V, it is possible to get the correct value of the covariance matrix, however this can only be achieved by using the 'Generalized Least Squares method' (GLS) (see pp. 188 of Ref. [6]). However, it is necessary to have accurate systematic errors to use the GLS. This is precisely the goal of our current efforts.

4.2. Systematic uncertainties

In the experimental data files accumulated over the past decades in the international experimental cross-section databases [16], the vast majority of experimental data have clearly assigned statistical errors， but the same does not hold for systematic errors. A large part of the available experimental data consists of only relative measurements without any systematic errors. On the other hand, of those experimental data files containing absolute measurements, the majority do not have information on systematic errors or in the best case provide rough estimates. Only a small fraction of the newly measured experimental data sets contains complete information on the system errors, however, if in these cases the systematic error is much larger than the statistical error, this is extremely unfavorable for nuclear data evaluation. There are many sources of systematic errors such as (i) systematic deficiencies of the experimental devices (accelerator, detector, electronics, data acquisition, etc.), (ii) systematic deviations in data processing, (iii) systematic bias of the treated model, and many others. There is no exact information about these factors in most of the relevant literature. Therefore, in the process of data evaluation, in order to get the systematic error, evaluators have to use skills similar to those used by archaeologists to 'dig out' information buried in publications or reports or hidden in the data themselves. These 'archaeological skills', as was mentioned in Ref. [6], are very often combined with unreliable operations such as 'hypothesis', 'guess', 'analog' and 'estimate' and so on. If the 'archaeological approach' reveals lack of adequate original records, then the systematic errors have to be assumed arbitrarily. In other words, the accurate determination of the systematic errors of a single experimental data set is the core issue of nuclear data evaluation. It is also the most vexing problem and a major obstacle which the nuclear data reviewers have been struggling to overcome for decades.

Past experience in nuclear data evaluation shows that the problem of poor knowledge of systematic errors cannot be overcome by treating different nuclear data as isolated cases and evaluating them using local approaches. It has been demonstrated that only by applying the theory of unitarily in the physical models, and through the systematic and comprehensive evaluation of all available nuclear data for a given nuclear system（global as opposed to local

fitting), is there a chance to solve the problem. This is because it is possible to obtain accurate and self-consistent fitting values for all types of data that can be considered to be very close to their 'expectation' values. Once the 'expectation values' are obtained, the systematic error of each experimental data set can be determined.

For example, let's assume an experimental data set Y_i, and by adjusting the normalization coefficient n_i we convert it to $n_i Y_i \Rightarrow X_i(P) \approx E$, where $n_i Y_i$ is the final practical experimental data, $X_i(P)$ is the final fitting value, and E is the expected value of such data. If we use σ_i as the standard error of $X_i(P)$, it is possible to have the following relations

$$n_i Y_i - k\sigma_i \le E \le n_i Y_i + k\sigma_i, (k=1 \text{ to } 2) \tag{4.8}$$

The $k\sigma_i$ can be considered as a systematic error of $n_i Y_{i,}$, which corresponds roughly to a 70% to 95% confidence interval. The value of k is based on the principle that PPP does not occur.

It should be emphasized that only when there exist good enough evidence to support that the final evaluated value is very close to the expectation value, can the kσ be taken as the systematic error of the normalized experimental data that was obtained finally. Otherwise it's better to use the original systematic error.

Two main criticisms have been expressed of formula (4.8): (a) in the evaluation of nuclear data one cannot change the original experimental information, and (b) the error of the evaluation value one obtains is too small. In the following we will focus on these two key arguments.

4.3. Improved least-squares method (ILS)

In the Least Square method, often the statistical error and systematic error of the experimental data are considered simultaneously ($V_i^2 = S_i^2 + Y_i^2$), however, the non-diagonal elements of the covariance matrix of experimental data are not considered. This in theory means that, the 'unbiased estimate' of the sample is not guaranteed. However, the systematic error is taken into account, and is also conveniently calculated, so this approach is widely used in the field of nuclear data evaluation. In this paper, we call this approach as 'Improved Least Square method' (ILS). Since this method ignores the non-diagonal elements of the covariance matrix V of the experimental data, it cannot give the correct value of the covariance matrix. In the ILS one can have different expressions for χ^2, and two practical examples are given below.

4.3.1. EDA-Improved least-squares method

EDA [9] is a well-known R-matrix analysis program that has been extensively used for the evaluation of light systems, in particular for the evaluated nuclear data files in ENDF/B7 and ENDF/B8. The optimization expression for χ^2 used in EDA (Ref. [2], p. 3235) is

$$\chi^2_{\mathrm{EDA}} = \sum_i \left[\frac{nX_i(\mathbf{p}) - R_i}{\Delta R_i}\right]^2 + \left[\frac{nS-1}{\Delta S/S}\right]^2, \tag{4.9}$$

where n is the normalization coefficient, $X_i(\mathrm{P})$ indicates the fitting value, R_i is the value of the experimental data, ΔR_i is the data error, S is the shape factor of the experimental data, $\Delta S/S$ is the relative systematic error. Obviously, the first item in (4.9) refers to the contribution from the

statistical error， while the second term is the contribution form the systematic error.

There is a particularly important issue that needs to be discussed related to Eq. (4.9) and that is **how to normalize the experimental data.**

One approach is to treat the normalization as 'a subset of the experimental data', by taking its initial value R_i as the standard, then changing the fitted values $X_i(P)$ by adjusting the normalization coefficient n, and finally letting $nX_i(P) \rightarrow R_i$. This is the method adopted in EDA as shown above.

It is obvious from Eq. (4.9) that the principle behind this kind of 'normalization' is that '**one cannot change the original experimental information**'. Is this a reasonable approach?

In theory， in the classical Least Squares method, one uses $[X_i(P)\text{-}R_i]^2/(\Delta R_i)^2$ to calculate χ^2, where $X_i(P)$ is the calculation value; in EDA they use $[nX_i(P)\text{-}R_i]^2/(\Delta R_i)^2$ to calculate χ^2, where the $nX_i(P)$ is a modification of the calculation value. This has the following consequences:

1. The χ^2 expression of EDA is inconsistent with the original definition of classical Least Squares method,
2. It does not meet the established requirements for "maximum likelihood principle",
3. It is not obvious that the $X_i(P)$ will have maximum probability,
4. It is not obvious that it can lead to "unbiased estimates",
5. The obtained minimum χ^2 of EDA has no real physical meaning,
6. In the end, the evaluated data have to take the original values, so there is a big possibility that the difference between experimental data and the evaluated data will be much larger (refer to Appendix 1).

Most likely it just an empirical expression without a rigorous statistical theoretical basis.

In the data fitting procedure, the fitting values of EDA depend entirely on the original experimental data, even if the original data values have serious defects. For example, in the case of experimental data sets with very large systematic errors, the latter essentially reflect the experimenter's lack of confidence in the experimental data. But in the EDA approach, this kind of data with serious defects always contribute to the fitting value.

Another consequence of Eq. (4.9) is that it is impossible to use the 'Generalized Least Squares method'.

Also, because the calculated value must be lower than the experimental data systematically, this leads to the occurrence of PPP. Of course, the 'Smith-NOppp-method' can be used to overcome PPP, but the essence of the 'Smith-NOppp-method' is to overcome PPP by modifying the original systematic error, which is in conflict with the principle of not changing the original experimental information (refer to Section 5 for more details).

In fact, the premise of doing this kind of normalization is to change the original experimental data, i.e. is to 'pre-evaluate' the experimental data which includes the following steps in the RAC CLS procedure before performing a GLS fitting:

i. Determine the shape factor S for all relative data, make it close to 1, and change the original relative value to the absolute value;

ii. Determine their 'systematic error' $\Delta S/S$ for all relative data;

iii. For absolute data without systematic errors, give the 'systematic errors'.

iv. For absolute data with very large systematic errors, make pre-evaluation.

EDA ignores the correlation between errors of the experimental data， On the whole, it is impossible to get an accurate fitting value and the corresponding covariance matrix directly. See Appendix 1 for details.

4.3.2. RAC-Improved least-squares method

At the beginning of the analysis work, RAC used the 'RAC-Improved least-squares method' to fit experimental data. The optimization expression used by RAC was (taking an independent data subset as an example):

$$\chi^2=\sum_{i=1}^{i=n}[X_i(\mathrm{P})-\mathrm{n}R_i/((\varepsilon_s+\varepsilon_t)\mathrm{n}R_i)]2 \Rightarrow \text{minimum} \quad (4.10)$$

where n_i is the normalization coefficient， $X_i(\mathrm{P})$ indicates the fitting value, R_i is the value of the experimental data, ε_s is the relative statistical error, ε_t is the relative systematic error. As can be seen from this formula, 'RAC-normalization' means taking the fitting value $X_i(\mathrm{P})$ as standard (because the final $X_i(\mathrm{P})$ is close to the expected value), and then adjusting the normalized coefficient n_i to let $n_iR_i \rightarrow X_i(\mathrm{P})$, or adjusting the shape factor S_i to let $S_iR_i \rightarrow X_i(\mathrm{P})$.

It is obvious from Eq. (4.10) that the principle of this normalization is the following: the original experimental information is adjusted in a 'global fitting' procedure, taking the fitting values $X_i(\mathrm{P})$ as standard, and under the constraints of 'unitarily', 'self-consistency' and 'identity' which include the following:

1. The total neutron cross section equals the sum of the cross sections of all reaction channels;
2. The integrated value of the differential cross section is equal to the reaction cross section;
3. The experimental data of the same reaction cross section should be equal, and so on;
4. The experimental data of the positive reaction cross section and the cross-section data of the inverse cross section should match;
5. Different types of experimental data (cross section, polarization, width, etc.) should match.

The χ^2 expression of RAC in Eq. (4.10) is fully consistent with the classical 'Least Squares method' that uses $[X_i(P)\text{-}R_i]^2/(\Delta R_i)^2$ to calculate χ^2， where $X_i(P)$ is the fitting value. In other words, RAC strictly implements the statistical theory thus satisfying the 'maximum likelihood principle', leading to 'unbiased estimates'， and producing a χ^2 that has real physical meaning.

In the data fitting procedure, the fitting value obtained from the expression is related to the original experimental data. However, it is not entirely dependent on the original experimental

data, since in the iterative fitting procedure the defects of the original experimental data are corrected. As a result, the defects no longer have a negative impact on the evaluated values. On the other hand, the systematic errors change with changing normalization coefficient, and finally become 1 to 2 times the value of the standard error of the calculated value, which is usually significantly less than the statistical error. Using this kind of 'normalization' formula and the modified systematic error, the non-diagonal elements of the covariance matrix of experimental data can be introduced directly, that is one can use the 'Generalized Least Squares method' directly. This will significantly improve the fitting value and give a more accurate covariance matrix at the same time, as will be discussed in more detail in the following section.

4.4. Generalized Least Squares method (GLS)

In the Least Squares method, if the full covariance matrix of the experimental data is considered, then we have what is called the 'Generalized Least Squares (GLS) method' (see pp. 188 of Ref. [6]).

In GLS， both the statistical error and systematic errors are considered simultaneously, which means that the sample no longer satisfies a strictly normal distribution, which is in fact the actual state of our experimental data set. To date, there is no rigorous statistical theory that can prove that the least squares method described above can lead to the generation of an 'unbiased estimate'. But according to a famous classical statistical theorem, the 'Gauss-Markev' theorem, under certain conditions GLS can lead to the minimum variance estimation, which is exactly what we need.

'Gauss-Markev' theorem

Let's assume that $\overrightarrow{\theta_0}$ is a set of parameters， it has an a priori value $\overrightarrow{\theta_a}$ and a corresponding covariance matrix $\overrightarrow{V_a}$. In addition, let's assume the existence of a linear relationship between observable $\vec{y}$ and $\vec{\theta}$. Finally, let's assume that $\vec{\eta}$ is a group of measured data, and the corresponding covariance matrix is V. Then the least squares formula in Eq. (4.11) will produce an estimate of $\vec{\theta}$ for $\overrightarrow{\theta_0}$ that is of minimum variance

$$\chi^2 = (\vec{\theta} - \overrightarrow{\theta_a})^+ V_a^{-1} (\vec{\theta} - \overrightarrow{\theta_a}) + (\vec{\eta} - \vec{y})^+ V^{-1} (\vec{\eta} - \vec{y}) \Rightarrow \text{minimum} \qquad (4.11)$$

The applicability of this theory depends only on the initial parameters and the observed data having an average value and the corresponding covariance, not on the normalcy of the probability distributions. Of course, there must be a linear relationship between the parameters and the observed data. Here are a few specific issues.

1. Assume the functional relationship between $\vec{y}$ and $\vec{\theta}$ to be $\overrightarrow{y} = \vec{\theta}$. This is an absolutely accurate linear relationship where the parameter is the observable itself, and formula (4.11) can be used to estimate the observable with the minimum variance. The fitting Code GMA of IAEA used for the evaluation of the neutron standard cross sections is working with the assumption $\overrightarrow{y} = \vec{\theta}$.
2. Assume the functional relationship between $\vec{y}$ and $\vec{\theta}$ to be $\vec{y} = f(\vec{\theta})$,where $\vec{\theta}$ is the fitting model parameters. Using the initial condition $\overrightarrow{y_a} = f(\theta_a)$ and the Taylor expansion, an approximate linear relationship can be obtained as $\vec{Y} - \overrightarrow{Y_a} = D\,(\vec{\theta} - \overrightarrow{\theta_a})$. By using

formula (4.11), an estimation with least variance can be given to $\vec{\theta}$ and the covariance matrix V_θ of $\vec{\theta}$. According to the formula $V_y = DV_\theta D^+$, the covariance estimates of $\vec{y}$ observables can be given. But having obtained a $\vec{\theta}$ of minimum variance does not mean that we have the minimum variance of the Y observables, nor that the value of the estimated y is very close to the expectation value. Analytical experience shows that if the systematic error is too large, that is, if the distribution of the sample deviates from the normal distribution significantly, the estimated value of Y will deviate from the expected value significantly. At which point, the fitting value is probably systematically lower than the average value of the experimental data, which is the so-called PPP phenomenon. Based on experience from using the GLS, if the systematic error of the analysis sample is greater than 30% of the statistical error, a mild PPP phenomenon is observed, while if it is more than 50% then a pronounced PPP phenomenon is observed. In the following section we discuss the PPP phenomenon in more detail.

3. At the beginning of the analysis work, RAC uses the 'RAC-Improved least-squares method' to fit experimental data. After obtaining a good parameter set $\vec{\theta}$ and its covariance matrix V_θ, then we use the optimization formula of 'Generalized Least–squares Method' (Eq. (4.11)). That is, this group of $\vec{\theta}$ and V_θ is used as the initial value $\overrightarrow{\theta_a}$ and V_a. RAC then uses an iterative process to continuously improve the estimated value of $\vec{\theta}$, and decrease the χ^2 with respect to $\vec{\theta}$ and with respect to $\vec{\eta}$ at the same time. The evaluated values of the experimental data sets are continuously improved. This of course comes at the cost of using 100 times more CPU time than what is required when using CLS or ILS. Of course, the most obvious advantage of GLS is able to use the error propagation theorem to produce an accurate covariance matrix for the evaluation value at the same time. Something that is impossible to do by using the 'Conventional Least Squares method' or the 'Improved Least Square method'.

4.5. Solution to PPP

Pearl's Pertinent Puzzle (PPP) refers to the phenomenon where the sample fitting value is systematically lower than the sample mean value. From the statistical point of view, the occurrence of 'PPP' is due to the fact that the sample deviates from the normal distribution too much. From the numerical calculation we to make an intuitive explanation.

In the 'Improved Least Squares method' (see Sect. 4.1.3.2), $\chi^2 = (\vec{\eta} - \vec{y})^+ V_{dia}^{-1} (\vec{\eta} - \vec{y})$,

where V_{dia} are the diagonal elements of the covariance matrix of experimental data, and each element is the sum of the statistical and systematic variances of the experimental data. V_{dia}^{-1} is the inverse matrix of V_{dia}. From a statistical point of view, this approach amounts to treating the systematic variance as statistical variance, the used experimental data sample is a purely statistical sample in fact too, only the statistical error is increased, therefore the fitting value may reach the average value and PPP does not occur.

In the GLS, where $\vec{\theta} = \overrightarrow{\theta_a}$, the final χ^2 is $\chi^2 = (\vec{\eta} - \vec{y})^+ V^{-1} (\vec{\eta} - \vec{y})$, V is the covariance matrix of the experimental data, and V^{-1} is the inverse matrix of V. The diagonal

element (number n) of V is the sum of the statistical variance and the systematic variance, and the non-diagonal element (number n^2-n) is the product of systematic errors of different data points. The number of non-diagonal elements is much larger than the number of diagonal elements. Because of the huge number of summations in the non-diagonal elements of χ^2, the χ^2 in the GLS is quite sensitive to the systematic error.

As is well known, the smaller the error of the experimental data, the larger the weighting factor of this data in the determination of χ^2. The systematic errors of experimental data are usually expressed in percentages, leading to the small experimental values in the sample having relatively small error compared to the larger experimental values that have larger errors. This means that the smaller data points have relatively larger weighting factors. Although the differences of these weighting factors are very small, because of the large number of non-diagonal elements these small data points end up contributing significantly to the fitting. Consequently, the resulting fitting values are systematically lower than the mean value of the sample and the PPP phenomenon is observed. The greater the systematic error is, the worse the PPP.

The explanation given above may seem simplistic, but it can be verified by a series of practical examples. In the following we present a few examples where we use the same sample of experimental data for the ^{7}Li system but apply different data fitting methods, thus obtaining different fitting values. Figure 4.1 shows the ratios of the total cross sections relative to that obtained with purely statistical fitting (ii).

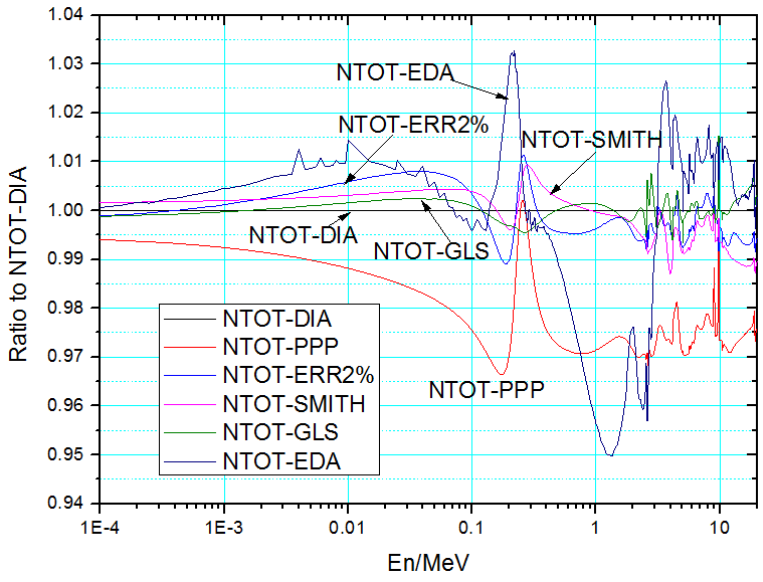

FIG 4.1. The ratios of cross sections obtained with 6 different fitting methods for ^{6}Li(n,tot).

In Fig. 4.2 we compare the different fitted total cross sections with experimental data， It can be seen that the curves corresponding to NTOT-GLS, NTOT-DIA, NTOT-Smith and NTOT-mod2% are within the errors of the experimental data, while the NTOT-PPP and NTOT-EDA curves lay roughly beyond the experimental data error line.

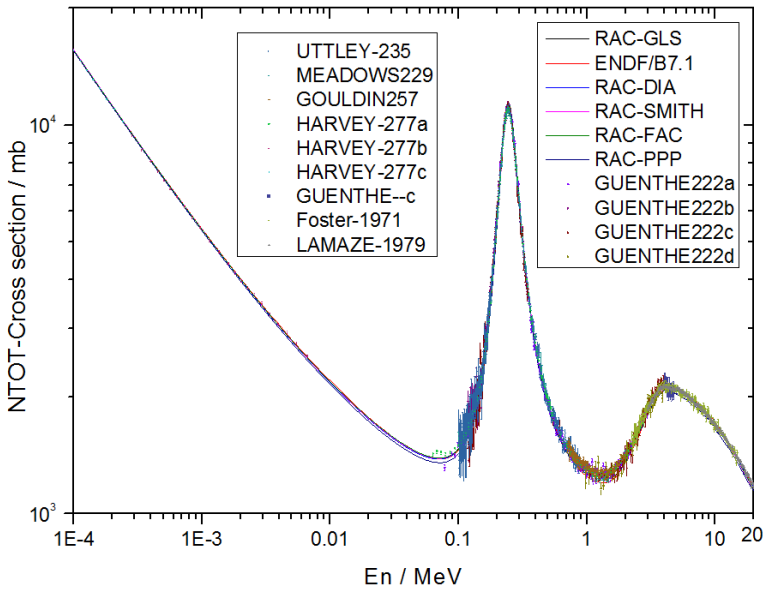

FIG 4.2. Comparison of fitting values and experimental data for ^{6}Li(n,tot).

The six different cases that are compared are described below:

I. Using 'Improved least squares method' (NTOT-DIA), the variance of the experimental data is the sum of the statistical variance and the variance of the systematic variance, without considering the correlations between systematic errors. The fitting values are quite close to the sample average values， and PPP does not occur. These fitted values were taken as the reference values for the comparison shown in Fig. 4.1 where we plot the ratios of the cross sections obtained with the other methods over the cross sections obtained with this method.

II. Using the 'Generalized least squares method' (NTOT-PPP) and the original covariance matrix of the experimental data, that is we consider the correlations between statistical error and systematic errors, we obtain fitting values that are systematically lower than the sample average values. This is obviously a case of PPP (red line in Fig. 4.1). The largest discrepancies are of the order of 3.5%.

III. Using the 'Generalized least squares method' (NTOT-mod2%), keeping the statistical error of experimental data unchanged, and adjusting the systematic error of the experimental data so that if it is less than the average value (NTOT-DIA) it is increased by 2% and the fitting weight is reduced, whereas where it is greater than the average value it is reduced by 2% and the fitting weight is increased. The covariance matrix is constructed by using the original statistical error and the modified systematic error. The resulting fitting value of the whole sample is close to the sample average (violet line in Fig. 4.1), while the maximum difference is about 1.2%. This example intuitively explains why PPP occurs and how it is possible to overcome it in a very simple way. In principle, experimental data deviate differently and regulating the corresponding weight factor by using a fixed correction coefficient is not the proper way of dealing with PPP. A different approach is discussed below.

IV. Using the 'Generalized least squares method' (NTOT-Smith), keeping the statistical error of the experimental data unchanged， and replacing the absolute error of the experimental data by the corresponding fitting value multiplied by the relative systematic error. Essentially what is done is that for the experimental data points whose values are less than the average, the absolute systematic error is increased a little, thus reducing the fitting weight; while for the experimental data points whose values are larger than the average, the absolute systematic error is decreased a little, thus increasing the fitting weight. Thus, it can be seen that the larger the deviation of experimental data points, the greater the degree of adjustment of the fitting weight. The resulting fitting value is close to the sample average. The largest difference observed (purple line in Fig. 4.1) is about 1.5%. This is called the 'Smith-NOppp' method in this paper.

V. Using the 'Generalized Least Squares method' (NTOT-GLS), keeping the statistical error of experimental data unchanged, however, adjusting the systematic error to be 1 to 2 times the error of the fitting value. The principle behind this approach is that the systematic error is significantly smaller than the corresponding statistical error. The covariance matrix is constructed by using the original statistical error and the improved systematic error. Because the systematic error is very small, it is not necessary to use the 'Smith-NOppp' method to avoid PPP, and the fitting values are very close to the mean values (experimental) of the samples. This method of overcoming PPP is a reasonable physical correction and can be applied to the global evaluation of a nuclear system. The largest differences obtained (green line in Fig. 4.1) are about 0.5%.

VI. The NTOT-EDA curve (dark blue in Fig. 4.1) shows that the evaluation value of the total cross section of ENDF/B7.1 deviates systematically from the mean value (experimental) in most part of the energy region. The discrepancies are as high as 3% and as low as 5% (see also Appendix 1).

The R- matrix analysis is a phenomenological fitting method. Appendix 1 shows that NTOT-EDA significantly and systematically deviates from the experimental data, while NTOT-GLS is in good agreement with the experimental data.

4.6. Error analysis

It has been said that the error of the evaluation value given by RAC is too small. Our opinion is that this should be discussed after the actual evaluation is finished. As long as the theory and method that is used are both correct, the experimental data set is correct, the fitting results are good, and error propagation theorem is used to calculate the errors, then the size of the error is what it is.

According to the error propagation theorem, the final average relative error value (FERR) depends on the following factors:

1. The greater the number of parameters (M), the greater the FERR; FERR is proportional to $\sqrt{M}$;

2. The larger number of points (N) of the experimental data set, the smaller the FERR; FERR is inversely proportional to N;
3. The smaller the average relative error (DER) of the experimental data sets is, the smaller the FERR; FERR is approximately proportional to DER;
4. The smaller the optimal objective function χ^2 is, the smaller the FERR; FERR is approximately proportional to the mean χ.

For the 'Global fitting' of the ^{7}Li compound system, the number of adjusted parameters is 365, the number of experimental data points is 14400, the average value of the initial error of the data is about 3%, the mean χ^2 is about 1.8, so,

$$\text{FERR} \approx \sqrt{360}/\sqrt{14400} \cdot 0.03 \cdot \sqrt{1.8} \approx 19/126 \cdot 0.03 \cdot 1.35 = 0.005 = 0.5\%.$$

The error is therefore reasonable.

5. NUCLEAR STRUCTURE

In R-matrix fitting, the selection of a suitable level scheme is key to solving the problem. A bad level scheme will definitely result in a bad fit. In principal, the R-Matrix theory is based on a complete collection of quantum states, so one needs to include a complete level scheme in the analysis.

In this section we explore the effect of using different nuclear structure input, such as level schemes, on the R-matrix analysis. Eight fitting schemes based on different level schemes have been employed to analyze the given database of Test1b [1]. This database was augmented by adding the data of McCray 1961 at 90 degree [20], because these are the most accurate experimental data available for the ^{7}Be system. The database includes experimental cross sections and angular distributions for ^{3}He(^{4}He,^{4}He)^{3}He, ^{6}Li(p, p)^{6}Li, ^{3}He(^{4}He, p)^{6}Li and ^{6}Li(p, ^{4}He)^{3}He reactions. In Table 5.1 we display the details of the eight fitting schemes.

TABLE 5.1. The eight fitting schemes, where columns 2-11 give the number of levels for each J^{π}, Γ^{e} refers to the width of eliminated channels, and χ^2/free is χ^2 over the number of degrees of freedom. Column 14 gives a comment on the quality of the fit.

Name	+0.5	-0.5	+1.5	-1.5	+2.5	-2.5	+3.5	-3.5	+4.5	-4.5	Γ^{e}	χ^2/free.	Comment
James--03JP-07L				2		3		2			No	26.20	Very bad
Satoshi-10JP-14L	1	1	1	2	1	3	1	2	1	1	No	16.20	Very Bad
Chen1-07JP-13L	1	1	1	3	1	3		3			No	2.001	Not good
Chen2-07JP-15L	3	1	1	3	1	3		3			Yes	1.722	Good
Chen3-10JP-19L	3	1	1	3	1	4	1	3	1	1	Yes	1.042	Very good
Chen4-10JP-23L	3	2	2	4	1	4	1	4	1	1	Yes	0.958	Very good
Chen5-10JP-28L	3	2	2	4	2	5	2	4	2	2	Yes	0.844	Very good
Chen6-10JP-28L	3	2	2	4	2	5	2	4	2	2	No	2.515	Bad

James--03JP-07L: the original level scheme given in **test1b** was used. The resulting χ^2/freedom is 26.2, and the fit is very poor, which confirms that the level scheme has to be improved.

Satoshi-10JP-14L: the improved level scheme obtained as a result of **Test1a** [1] was used, the resulting χ^2/freedom is 16.2, and the fit is poor too. The level structure has to be improved.

Chen1-07JP-13L: starting from the level scheme of **Satoshi-10JP-14L**, 1 level with Jπ = 1.5– and one level with Jπ = 7/2– were added, while the levels with Jπ = 4.5+ and Jπ = 4.5– were removed. The resulting χ^2/freedom is 2.001, but the fit does not look that good. The problem lies in the first peak observed in the ^{6}Li(p,p)^{6}Li reaction with Jπ = 5/2– near E_p= 1.75 MeV, where the calculations give a very strong peak or 2 peaks in some Excitation Function (EF) datasets.

Chen2-10JP-15L: starting from the level scheme of **Chen1-07JP-13L**, 2 levels of Jπ = 0.5+ were added, and some 'widths of eliminated channels' were added. The χ^2/freedom is 1.701, the serious problem with the overestimated peaks seen in **Chen1**-07JP-13L has been solved and the resulting fit looks good.

Chen3-10JP-19L: starting from **Chen2-10JP-15L**, one level was added for each Jπ = 2.5–, 3.5+, 4.5+ and 4.5– was added, and the χ^2/freedom decreases to 1.042. The fit looks very good.

Chen4-10JP-23L: starting from **Chen3-10JP-19L**, more levels were added, and the χ^2/freedom decreased to 0.958, while the fit looks very good.

Chen5-10JP-28L: starting from **Chen4-10JP-23L**, more levels were added, and the χ^2/freedom decreased to 0.844. The resulting fit looks very good.

Chen6-10JP-28L: starting from **Chen5-10JP-28L**, the existing 'widths of eliminated channels' were removed, so the χ^2/freedom increases to 2.515 and the fit looks bad.

In statistics, for a pure statistical sample the fit that gives χ^2/freedom ≈ 1.00 is the best fit, but for a non-pure statistical sample no conclusion can be drawn. The database selected for Test1b is a non-pure statistical sample, which requires a strong background, so maybe χ^2/freedom < 1.5 can be considered as very good.

How many levels should be used? It depends on the evaluator. At the same time one should study the visual comparisons with the experimental data in detail to see if the calculations are close to the experimental data or within the error bars for all the data. In this example, maybe Chen3-10JP-19L is already good enough, while Chen5-10JP-28L is significantly improved.

In the following figures, 'Ori' indicates the original experimental data, 'Nor' means normalized data, which are the data used in the fitting actually. N or S means normalization factor or shape factor.

5.1. Results of Test1b

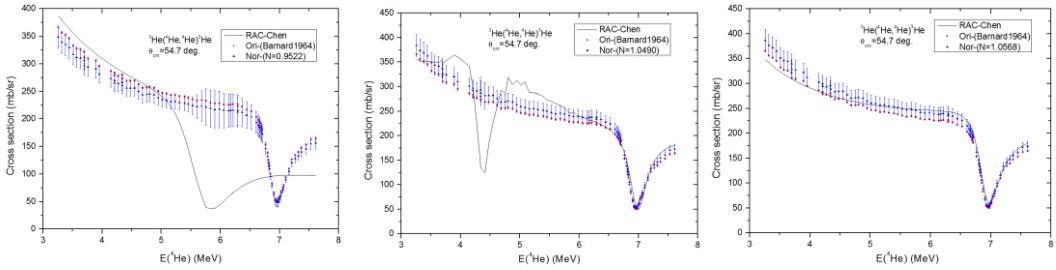

FIG 5.1. (Left) The $^3He(^4He,^4He)^3He$ cross sections at 54.7 degree for James-03JP-07L, (Middle) Satoshi-10JP-14L, and (Right) Chen1-07JP-13L. All the fits are poor.

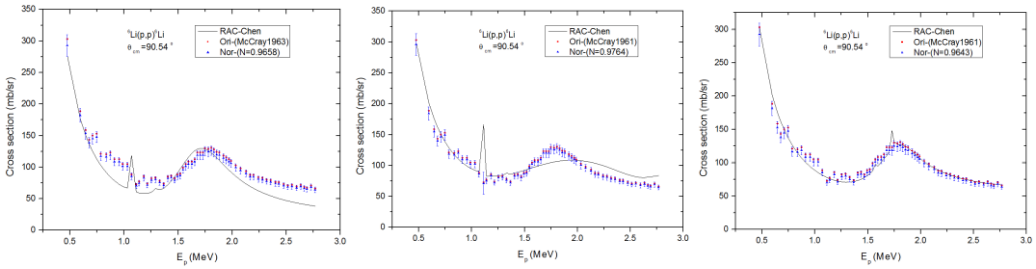

FIG 5.2. (Left) The $^3He(^4He,^4He)^3He$ at 90.54 degree for James-03JP-07L, (Middle) Satoshi-10JP-14L and (Right) Chen1-07JP-13L. All the fits are poor.

In the following figures we show the results for Chen5-10JP-28L. In this scheme, the systematic error given in the experimental papers is taken as a constraint for the normalization, i.e. the modification of the experimental data does not exceed the systematic error given by the authors in most of the cases. The whole fit is reasonable, the mean χ^2 is about 0.84, and for most of the data the calculated values are in good agreement with the experimental data. In this work, the parameter 'width of eliminated channels' represents the $^6Li(p,\gamma)^7Be$ channel and so on, so the strong interference have been removed.

In this fit, the $^3He(^4He,^4He)^3He$ and $^6Li(p, p)^6Li$ channels are the dominant channels, whereas the fitted values of $^3He(^4He, p)^6Li$ and $^6Li(p, ^4He)^3He$ depend on $^3He(^4He,^4He)^3He$ and $^6Li(p, p)^6Li$ to some extent.

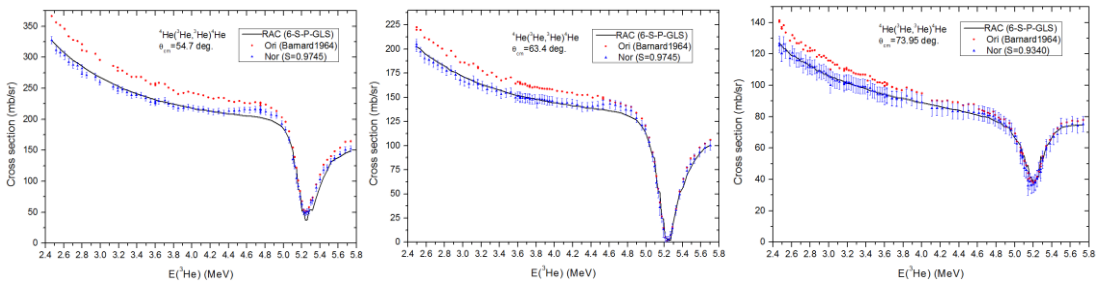

FIG 5.3. The $^3He(^4He,^4He)^3He$ cross sections of Barnard [21] at 54.7, 63.4 and 73.93 degrees.

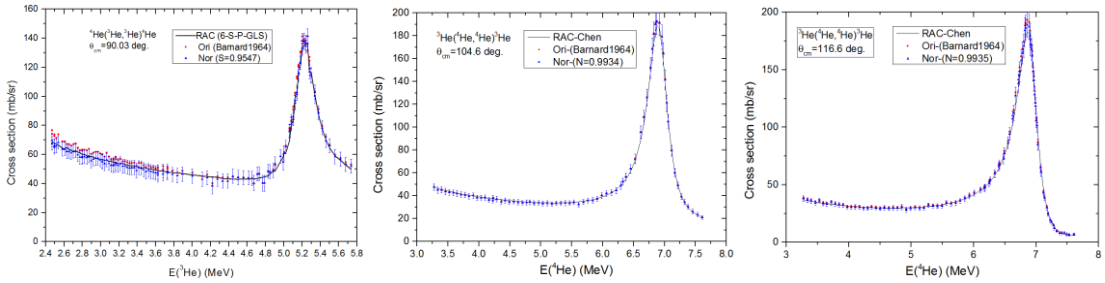

FIG 5.4. The $^{3}He(^{4}He,^{4}He)^{3}He$ cross sections of Barnard [21] at 90.03, 104.6 and 116.6 degrees.

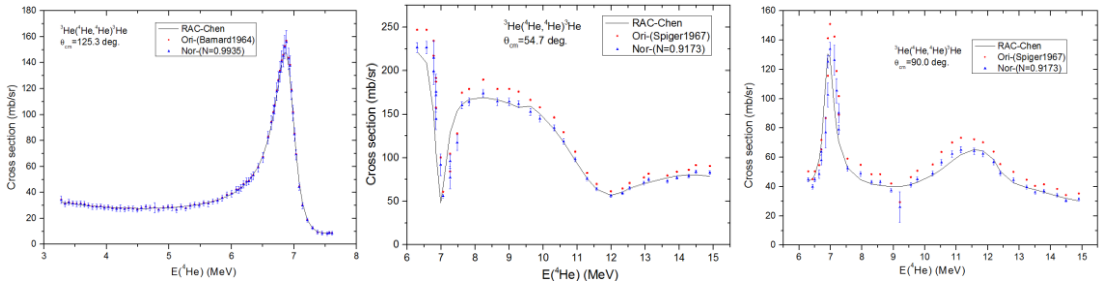

FIG 5.5. The $^{3}He(^{4}He,^{4}He)^{3}He$ cross sections of Barnard [21] at 125.3 degrees, and of Spiger at 54.7 and 90.0 degrees.

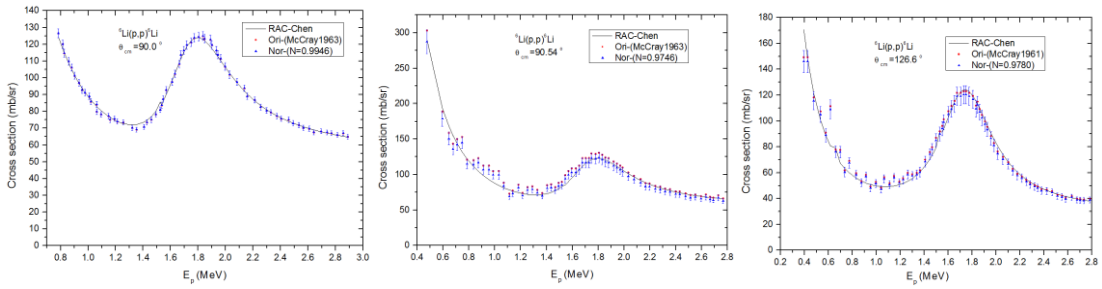

FIG 5.6. The ^{6}Li (p,p)^{6}Li cross sections of McCray at 90.0, 90.54 and 126.6 degrees [20]. The dataset at 90.0 degrees (left) was added to the Test1b database, because these data are the most accurate absolute experimental data with statistical error near 0.5% for the ^{7}Be system.

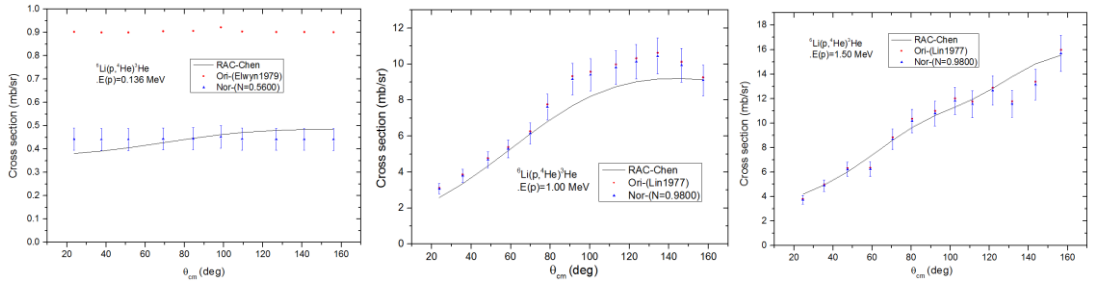

FIG 5.7. The ^{6}Li (p,$^{4}He)^{3}He$ cross sections of Elwyn et al [22] at 0.136 MeV (left): the shape indicates that there exists a 0.5^{+} level in the ^{7}Be system. The middle and right panels are for the data of Lin et al [23].

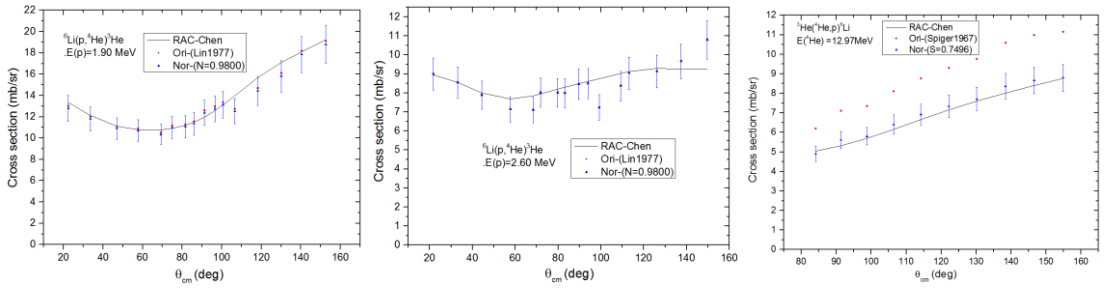

FIG 5.8. The ^{6}Li (p,^{4}He)^{3}He cross sections of Lin et al. [23] at 1.90 MeV(left) and 2.60 MeV (middle). The shape of these angular distributions indicates that these data are good. The right panel is for the ^{3}He(^{4}He,p)^{6}Li cross sections of Spiger et al. [24].

Remarks on Test1b exercise

1. The word 'global fitting' means that, with one set of R-matrix parameters one fits all kinds of available and useful experimental data for one nuclear system in a wide energy range (maybe from 1.0e-7 MeV to 20 MeV) simultaneously. The whole dataset may include normal reactions and inverse reactions. The most important advantages of 'global fitting' are that by comparing systematically the original data in the database, (i) existing errors can be found and removed; (ii) the discrepancies between different datasets can be found and minimized, and (iii) the systematic error of each dataset can be found and reduced. So finally the improved database will be much closer to the real and objective world, and the final unique evaluation result will be much closer to the real and objective world, that is the expectation value according to statistics.
2. In the complete 'database' used for a 'global fitting', there must exist a 'background'. This 'background' may come from:

   a. The contribution from levels in the higher energy region. This is a physical contribution;

   b. The contribution from non-compound nuclear reactions. These are physical contributions;

   c. The contribution from discrepancies between the many datasets; these are non-physical contributions;

   d. The contribution from experimental technology and data processing; these are non- physical contributions;

   e. Other sources.

   The shape of the 'background' is very complex and unknown. The following possibilities are valid:

   a. Smooth dependence on energy;

   b. Increasing with increasing energy;

   c. Decreasing with increasing energy;

   d. Fluctuating with energy;

   e. Other trends.

3. Due to the fact that the complete 'database' has a complex 'background', one should never expect to use only levels with obvious physical meaning or levels existing in the existing level scheme. It will be necessary to use additional levels to describe the complex 'background'. Only when the complex 'background' has been described correctly, can the physical contributions be described correctly.

4. Due to the fact that R-matrix fitting is a phenomenological fitting, there is no reason for the following:

   a. To limit the number of levels used; instead every level that is very sensitive to the total χ^2 must be used. In fact, the level set used finally should be **'not one more and not one less'**.

   b. To limit the number of the R-matrix parameters of the sub-channels used; instead all R-matrix parameters that are very sensitive to the mean χ^2/freedom should be used; the parameter set used finally should be '**not one more and not one less**'.

   c. To limit the energy position of any level or to fix the value of any R-matrix parameter. All R-Matrix parameter should be searched freely.

   In other words, every level and parameter used in the fit must be necessary to get the minimum χ^2. In the RAC fitting procedure, any non-necessary level and parameter is identified and flagged automatically, and is deleted in the iteration procedure.

5. The 'non-physical parameter' should not be considered as void of any meaning. In fact, it may mask the contribution from a non-physical part of the database, or it may represent the contribution of non-compound nuclei. It may even be a real level which has not been recognized in the past. If more than one code introduces the same identical new levels in order to get a good fit, then maybe the new levels can be recognized as real levels.

6. Evaluated libraries should in principle contain the complete and accurate Covariance matrix of the Evaluation value (CE) which includes both the contribution of data and model at the same time, and is associated with the Evaluation value in the corresponding ENDF file. A method which only evaluates data using mathematical approaches (Archaeology method), or only uses MC calculations, or misses the interference between statistical and systematic errors (CLS), will not be adequate.

7. The basic expression for the minimum of chi-squared should be $\chi^2 = (\text{Exp}\cdot N - \text{Cal})^2/\text{Err}^2$, in which the normalized target is the experimental value EXP (as in RAC). It should not be $\chi^2 = (\text{Exp} - \text{Cal}\cdot N)^2/\text{Err}^2$, in which the normalized target is the calculation value Cal (as in EDA). N is the normalization factor or shape factor, Err is the total error.

8. If some open channels have no data in the analyzed energy range, the Reduced R-matrix Theory should be used. If some open channels are ignored temporarily, then again the Reduced R-matrix theory should be used.

9. To obtain a good analysis of the resolved resonances, one has to consider also the non-resolved resonances simultaneously. There exist strong correlations between resolved and non-resolved resonances that can only be treated with the Reduced R-matrix theory.

10. Given that the complete experimental database includes strong contributions from non-

compound nuclei, and from levels at higher energies, distant levels have to be introduced in the R-matrix analysis.

11. If the complete database includes some very discrepant data which are 'outliers', then they have to be dealt with carefully. In some cases, one should use Lett's criteria' (χ^2/freedom > 9), or choose to increase the statistical error, or remove the data from the database.
12. The R-matrix fitting is a phenomenological fitting, so the best fit should correspond to the minimum χ^2, with the acceptable value being mean χ^2/freedom < 3.0
13. Different methods are used to deal with errors, so the best way to check whether a fit is good is to perform a visual comparison of data and fitted values.
14. The basic criteria for a good fit is that the calculated value is close to the data value, and that most of the calculated values for a given data-group are located within the error bar.
15. Using an 'iterative fitting process' has many advantages. The normalization factor changes little by little, the value of normalized data approaches the 'real value' little by little. At the same time, the relative statistical error is fixed always, but the relative systematic error of the data should be reduced little by little.
16. The modification of experimental data in the normalization procedure should be less than the systematic error given in the original paper.
17. In the normalization procedure, some data should not be changed, for example, the data which is considered to be the most accurate, and data which has no competition, i.e. they are the only existing data.

6. DIFFERENT EVALUATION SCHEMES

In this section we present the results of the evaluation of ^{7}Be system using ALS, CLS and GLS. The details of ALS, CLS and GLS, including all the formulas used to calculate χ^2 are provided in Section 4.

In the evaluation of the ^{7}Be system we used all the available experimental data from EXFOR. The evaluation of ^{7}Be consists of two separate evaluations: p+^{6}Li for lab projectile energies up to 20 MeV and ^{3}He+^{4}He for lab projectile energies up to 30 MeV.

We included data for the following reactions: ^{6}Li(p, p)^{6}Li, ^{6}Li(p, ^{3}He)^{4}He, the ^{6}Li(p,p$_1$)^{6}Li*, ^{6}Li(p,p$_2$)^{6}Li**, ^{6}Li(p,g$_0$)^{7}Li, and ^{6}Li(p,g$_1$)^{7}Li*, ^{4}He(^{3}He,^{3}He)^{4}He, ^{4}He(^{3}He,p)^{6}Li, ^{4}He(^{3}He,p$_1$)^{6}Li*, ^{4}He(^{3}He,g$_0$)^{7}Li, ^{4}He(^{3}He,g$_1$)^{7}Li*. Both cross sections and analyzing powers were fitted amounting to a total of 5032 data points. Seven different approaches to dealing with systematic errors and calculating the χ^2 were employed (see Table 6.1) while the level scheme of ^{7}Be remained the same. To our surprise, all the evaluated data are very close to the experimental values, the obvious differences existing in the resulting χ^2 and the covariance matrix of evaluated values.

Here we remind the reader of the most important formulas used in the seven approaches:

$$\chi^2 = (\vec{\eta} - \vec{y})^+ V_0^{-1} (\vec{\eta} - \vec{y}) + ((N-1)/S)^2 \Rightarrow \text{minimum} \qquad \text{(ALS) F1}$$

$$\chi^2 = (\vec{\eta} - \vec{y})^+ V_O^{-1} (\vec{\eta} - \vec{y}) \Rightarrow \text{minimum} \quad \text{(CLS) F2}$$

$$\chi^2 = (\vec{\theta} - \overrightarrow{\theta_a})^+ V_a^{-1} (\vec{\theta} - \overrightarrow{\theta_a}) + (\vec{\eta} - \vec{y})^+ V_M^{-1} (\vec{\eta} - \vec{y}) \Rightarrow \text{minimum} \quad \text{(GLS) F3}$$

In the above expressions of χ^2, the $\vec{\eta}$ are the normalized data (Modi) which are effectively used in the fitting. They are derived from the original experimental data (Origi) after multiplying by the normalization factor for absolute data, or multiplying by the shape factor for relative data; the $\vec{y}$ are the calculated values. This is the method that is always used in RAC for the normalization of experimental data.

6.1. Abbreviations

NAME OF SEVEN SCHEMES

For the second letter, 0 refer to 0.0, O refer to ORI, S refer to Standard error (STD);

For the third letter, N refer to No, P refer to Part, M refer to Modification, A refer to All.

ALS: Approximate Least Squares method;

CLS: Conventional Least Squares method;

GLS: General Least Squares method with 'Gauss-Markev' theorem;

DATA USED $\vec{\eta}$ IN FITTING

Origi: original experimental data;

Modi: normalized experimental data of part or full;

V OF $\vec{\eta}$

V: Covariance matrix of $\vec{\eta}$, which is produced with Statistic error and Systematic error;

V_0: all non-diagonal elements in V is 0.0;

V_O: For making V all original Systematic error is used;

V_M: For making V, the standard error of evaluation values is used as Systematic error;

STATISTICAL ERROR

ORI: use the original statistical error always;

SYSTEMATIC ERROR (%)

No (0.0 to 0.0): for building V, all systematic errors are 0.0;

ORI (1.5 to 10): for building V, all original systematic errors are used, the value ranging from 1.5% to 10%;

STD (0.2 to 2.5): for building V, the standard error of evaluated values is used, the value ranging from 0.2% to 2.5%;

$((N-1)/S)^2$

N: The real normalization factor obtained in fitting;

S: The normalization factor or shape factor of original data;

NOR-REL

Yes: The relative data are normalized always;

NOR-ABS

No: All absolute data are not normalized;

Part: Part of absolute data have been normalized;

All: All absolute data have been normalized;

EAE/EEE

EAE： the normalization is done for both 'Angle dependency' and 'Energy dependency'；

EEE： the normalization is done for 'Energy dependency' only；

FM OF χ^2: THE FORMULA OF χ^2

χ^2_{Mean}: the mean χ^2 for the whole database used.

6.2. Evaluation schemes

TABLE 6.1. Characteristics of the seven evaluation schemes

Scheme	Data	V ($\vec{\eta}$)	Stat. Error	Syst. Error (%)	$((N-1)/S)^2$	NOR-Rel.	NOR-Abs.	EAE/EEE	FM	χ^2_{Mean}	Comment
1-0-N-ALS	Origi	V_0	ORI	No (0.0 to 0.0)	Yes	Yes	No	EEE	F1	3.602	χ^2 too larger
2-0-P-ALS	Origi	V_0	ORI	No (0.0 to 0.0)	Yes	Yes	Part	EEE	F1	2.616	As a Reference
3-0-M-ALS	Origi	V_0	ORI	No (0.0 to 0.0)	Yes	Yes	Part	EEE	F1	2.116	Acceptable
4-O-P-CLS	Modi	V_O	ORI	ORI (1.5 to 10)	No	Yes	All	EEE	F2	0.961	As a Reference
5-S-M-CLS	Modi	V_M	ORI	STD (0.2 to 2.5)	No	Yes	Part	EAE	F2	1.462	Very good
6-S-M-GLS	Modi	V_M	ORI	STD (0.2 to 2.5)	No	Yes	Part	EAE	F3	1.542	The best one
7-S-A-GLS	Modi	V_M	ORI	STD (0.2 to 2.5)	No	Yes	All	EAE	F3	1.404	As a Reference

6.3. Results

All the results shown in the figures herein include:

a. The curves corresponding to the seven evaluation schemes.

b. The original experimental data points (Origi) and the normalized data points (Modi) which were used in the fitting. In practice, most of the Modi data points are located within the error bar of Origi, and for most of the datasets the changes are less than the original systematical error given in the original paper; which explains why the modification of the original dataset is reasonable.

   From the figures below it is clear that it is necessary to normalize some of the absolute experimental datasets, otherwise the χ^2 is not statistically acceptable as is that of scheme (1-0-P-ALS). It should be pointed out that decreasing χ^2 by the normalization n of the calculated values (which has been done in EDA) is absolutely wrong (refer to Nuclear Data Sheets 109 (2008) 2812–2816).

c. In the figures showing the elements of a row of the 3 dimensional Correlation factor(C) and Covariation matrix (COV), it is clear that the evaluated COV of General Least Squares (GLS) are larger than the evaluated COV of Conventional Least Squares (CLS); the evaluated COV of Conventional Least Squares are larger than the evaluated COV of Approximate Least Squares (ALS).

d. For those data which are not in direct competition with other data, we do not perform any normalization. Such data include, for example, integrated (p,p_1)and (p,p_2), the data on (p,p),(p,p1) and (p,p2) at 14 MeV; the data on γ capture and analyzing powers.

e. The results of the three evaluations (6-S-M-GLS), (5-S-M-CLS) and (3-0-P-ALS) can be taken as the final recommended evaluated results, where the (6-S-M-GLS) is better than (5-S-M-CLS), and (5-S-M-CLS) is better than (3-0-P-ALS).

6.3.1. $^{6}Li(p,p)^{6}Li$

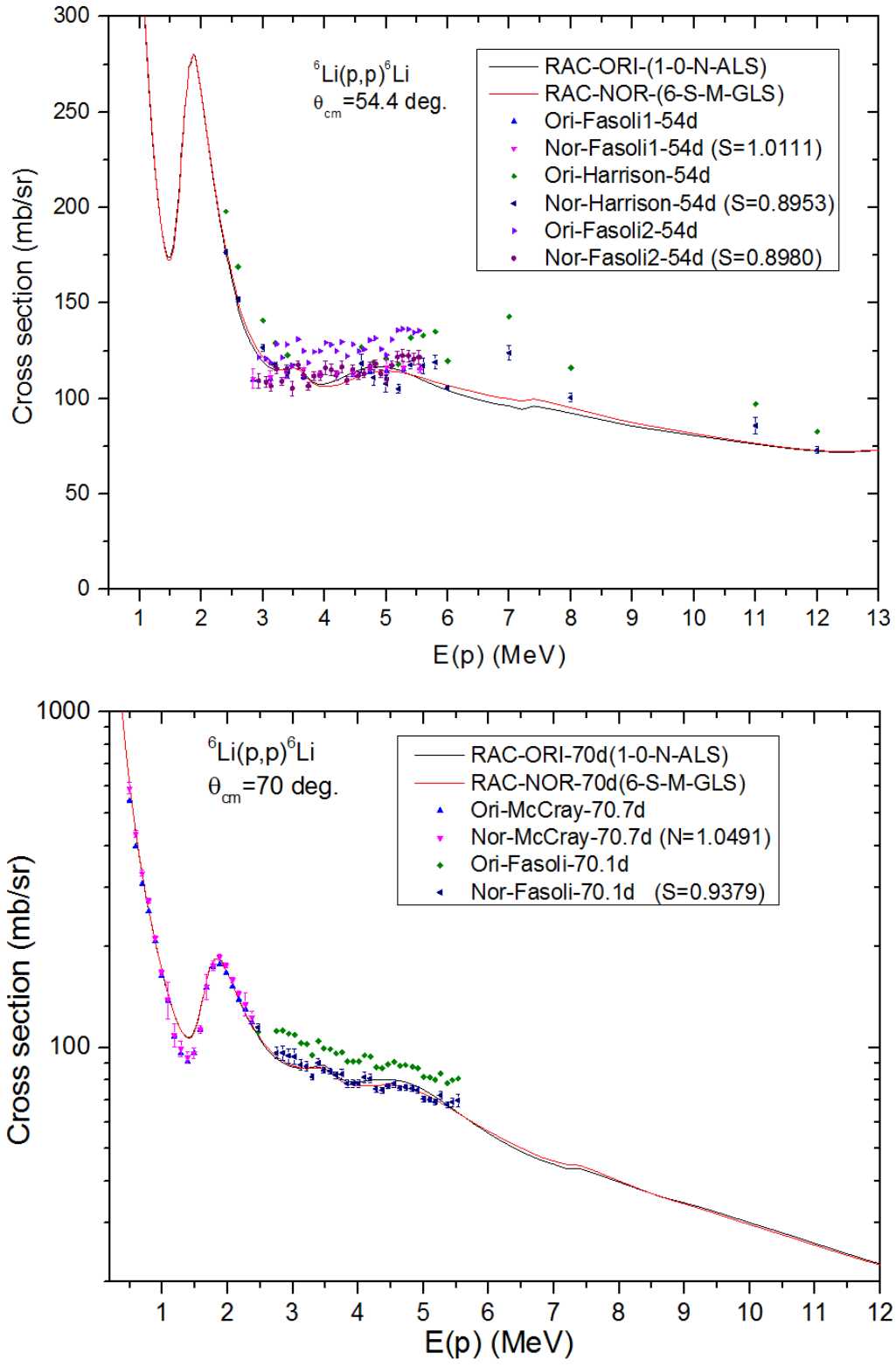

FIG 6.1. The ^{6}Li (p, p) ^{6}Li excitation function near 54 degrees and 70 degrees

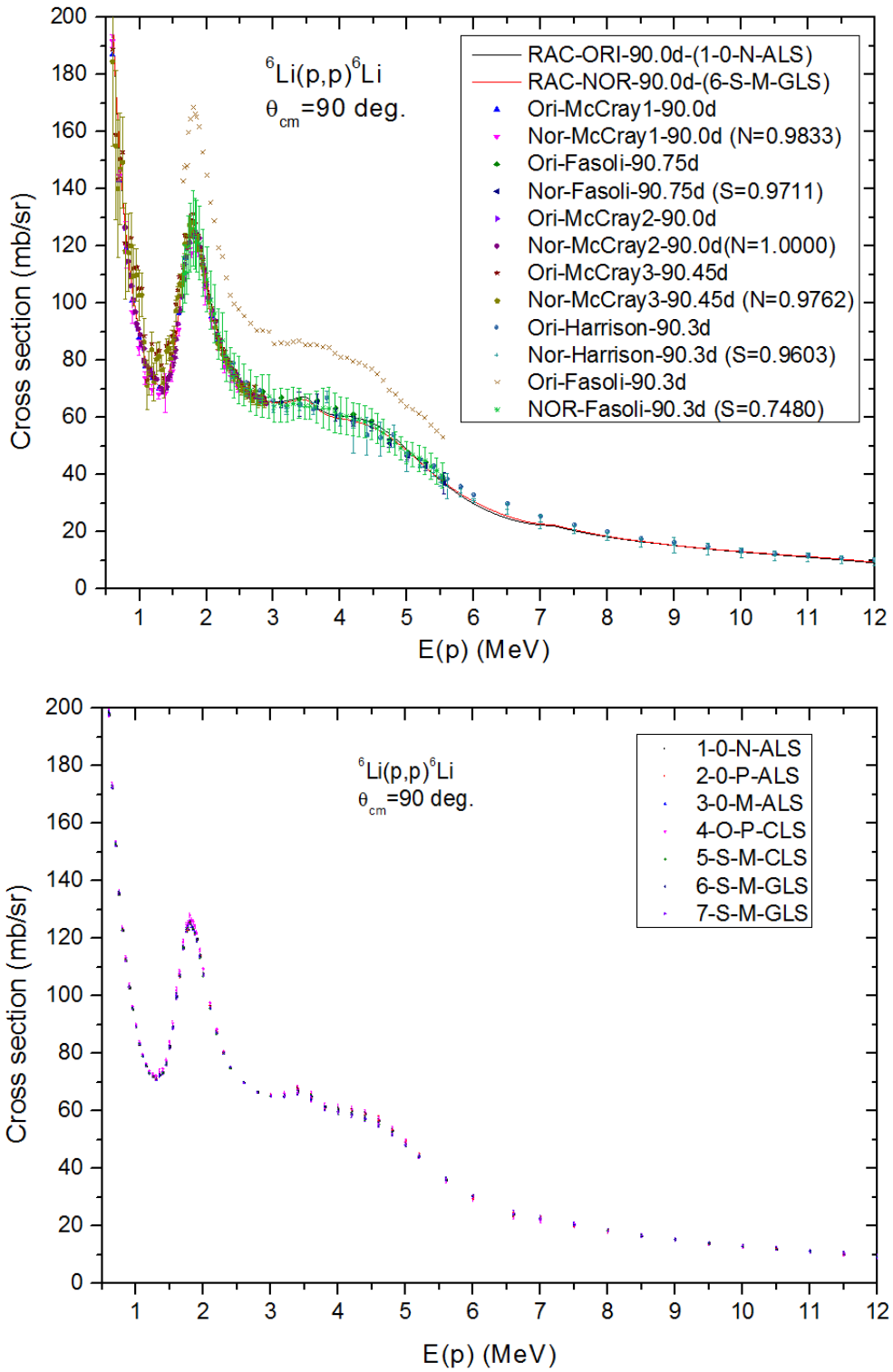

FIG 6.2. The ^{6}Li (p,p)^{6}Li excitation function at 90 degrees. The top panel shows that the fits are excellent. The shape and peak position of the relative data of Fasoli [28] is important information for fitting the data. The bottom panel shows the fits using the seven schemes: both the values and shapes are almost identical.

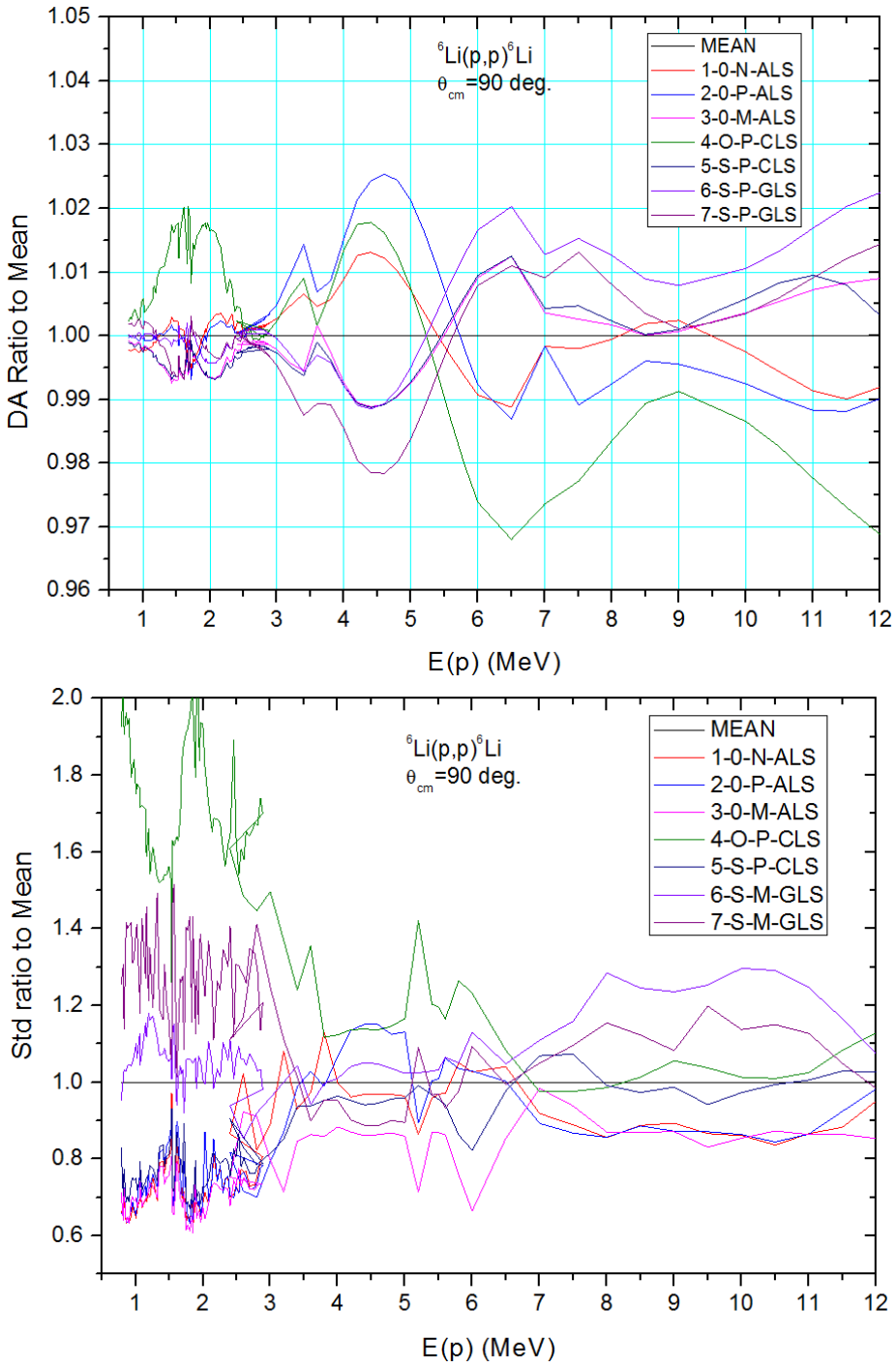

FIG 6.3. The top panel shows the ratios of the excitation functions calculated at 90 degrees using the seven schemes over their mean value for ^{6}Li (p,p) ^{6}Li. The maxima of the ratio range from 0.98 to 1.02 at $E_p < 4$ MeV, and from 0.97 to 1.03 for $E_p > 4$ MeV. The bottom panel shows the ratios of the STD for the seven schemes to their mean value. The figures shows rather large differences. The deviation of (4-O-P-CLS) is the largest one for $E_p < 7$ MeV because the original systematic errors were used in the diagonal elements of the experimental covariance matrix.

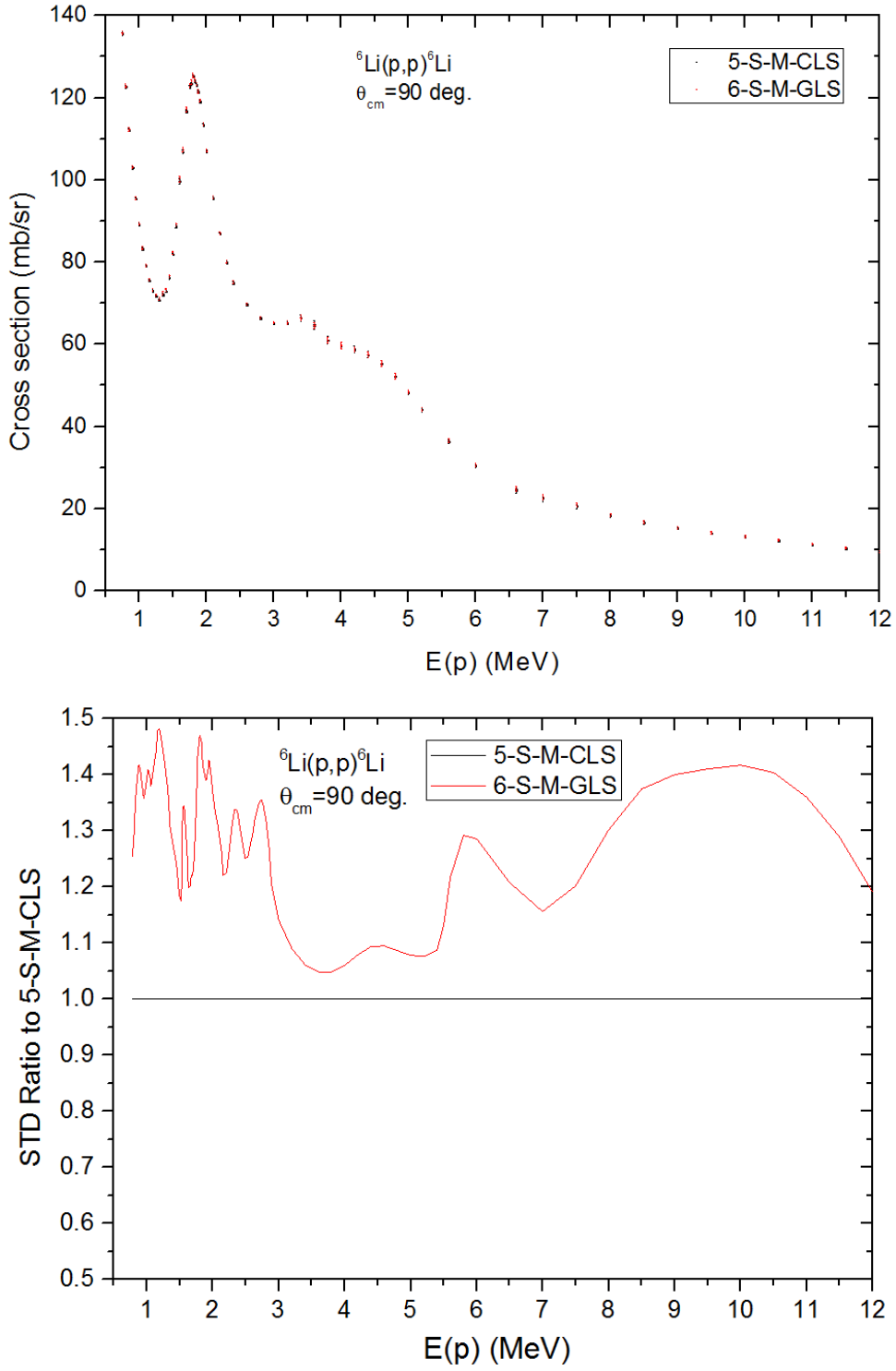

FIG 6.4. The top panel shows that among the seven schemes the 5-S-M-CLS is the best fit for CLS, 6-S-M-GLS is the best fit for GLS, while the maximum ratio of the corresponding evaluations range from 0.995 to 1.005. Thus, it is safe to say that both can be adopted as the final recommended values. The bottom panel shows the ratio of the STD of 6-S-M-GLS to that of 5-S-M-CLS, with the maximum ratio ranging from 1.2 to 1.4. This difference is due to the fact that data correlations are considered in the GLS fitting, but not in the CLS fitting. For the non-diagonal elements of the covariance matrix of the evaluation data, the differences are much larger by a factor of 3 (see Fig. 6.5).

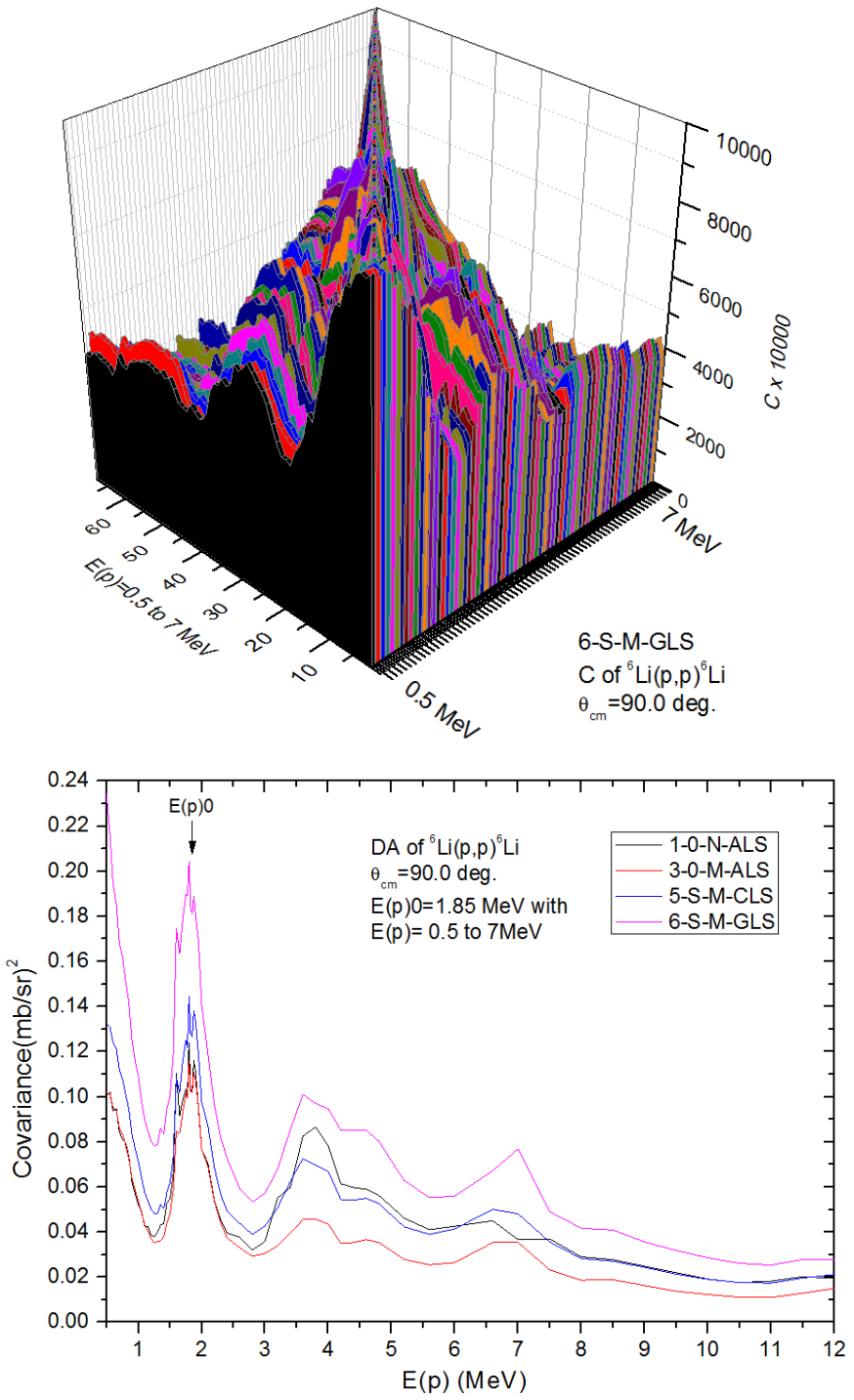

FIG 6.5. The top panel shows the correlation factor (C) for the excitation function of ^{6}Li(p,p)^{6}Li at 90 degrees, and E_p = 0.5 to 7 MeV. It is the result of the scheme (6-S-M-GLS). In the C matrix the diagonal elements $C_{ii} \equiv 1$. The bottom panel shows the covariance matrix elements for the excitation function of ^{6}Li(p,p)^{6}Li at 90 degree, and for the E_{p0} = 1.85 MeV with E_p = 0.5 to 7 MeV in the 4 scheme (1-0-N-ALS), (3-0-M-ALS), (5-S-M-CLS) and (6-S-M-GLS). It should be noted that the scheme (6-S-M-GLS) has the largest covariance matrix elements, because the correlations among the data are considered in GLS. On the other hand, the scheme (3-0-M-ALS) has the smallest covariance matrix elements, since the correlations of the data are not considered in ALS.

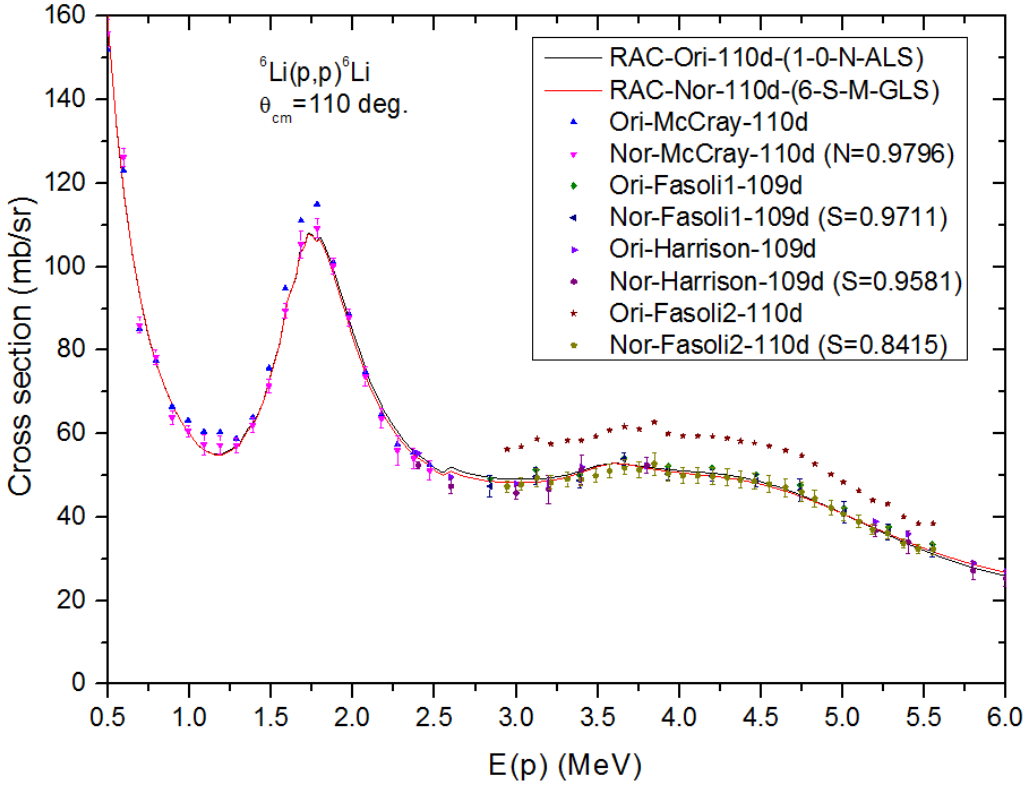

FIG 6.6. The ^{6}Li(p,p)^{6}Li excitation function near 110 degrees. The fit is excellent. The shape and peak position of the relative data of Fasoli [28] is important information for fitting the data.

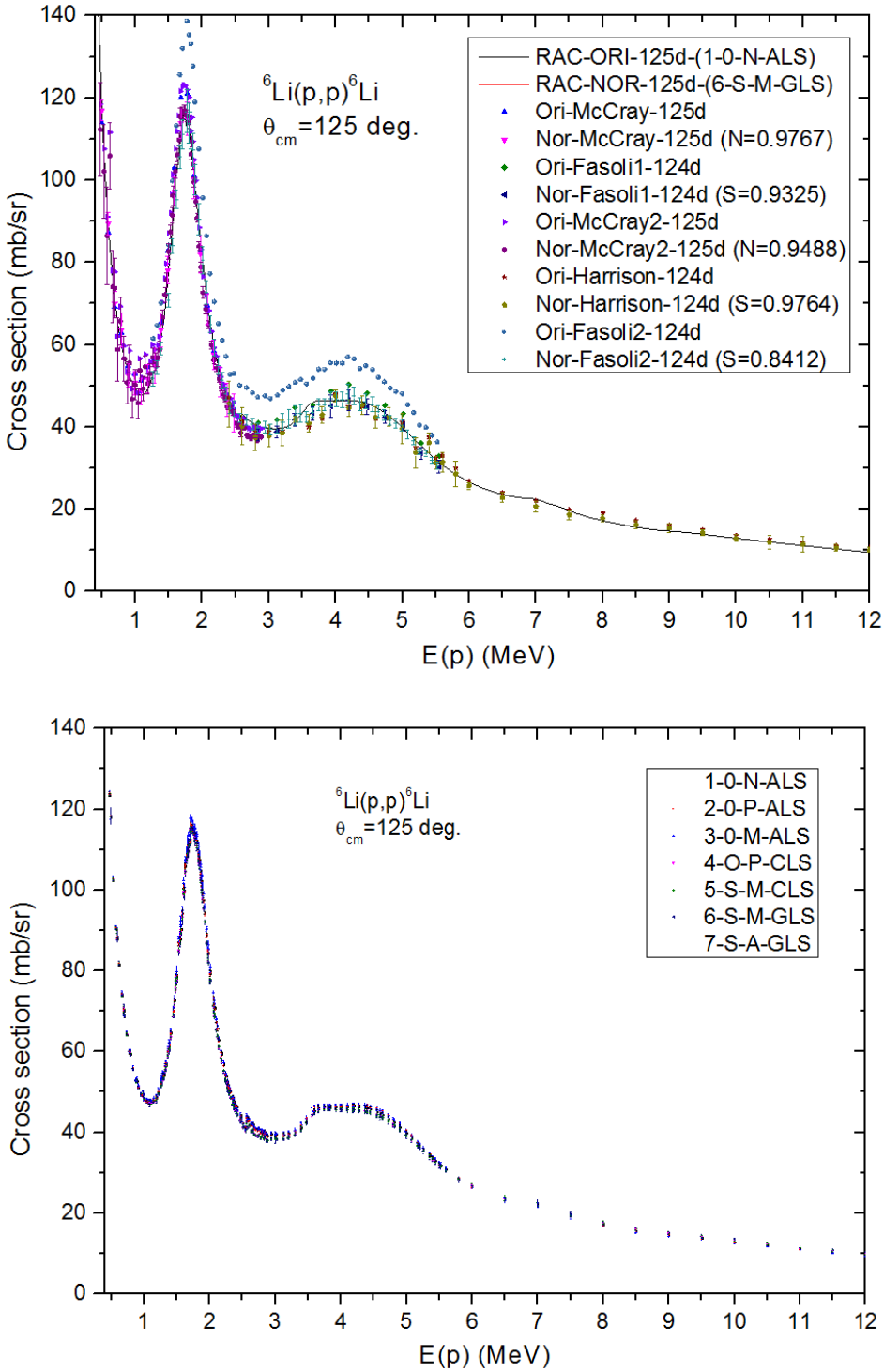

FIG 6.7. The top panel shows the ^{6}Li(p,p)^{6}Li excitation function of near 125 degree. The figure shows that the fit is excellent. The shape and peak position of the relative data of Fasoli [28] is important information for fitting. The bottom panel shows the ^{6}Li(p,p)^{6}Li excitation function near 125 degrees obtained with the seven schemes. The results agree very well both in magnitude and shape.

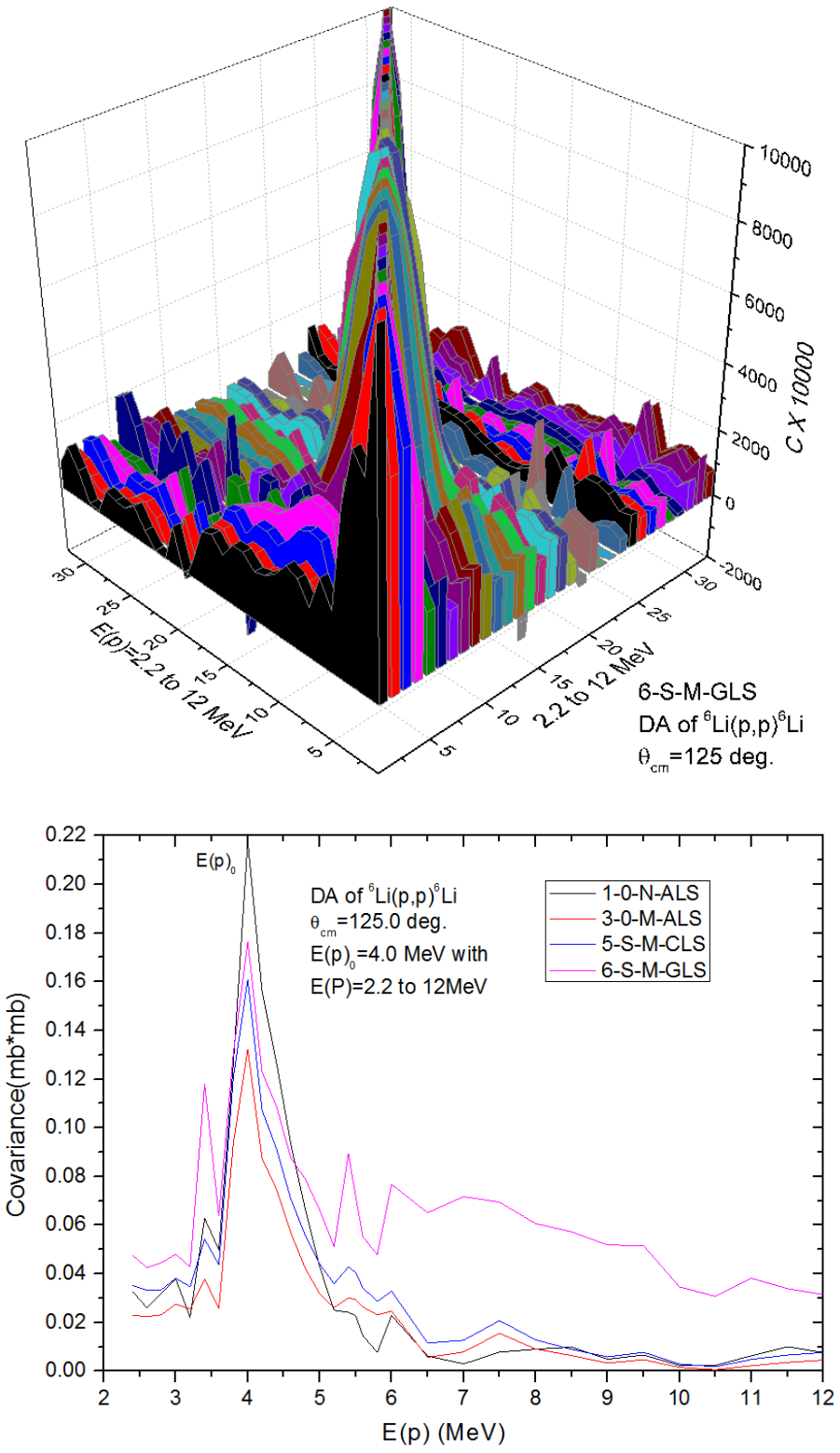

FIG 6.8. The top panel shows the correlation factor (C) for the excitation function of ^{6}Li(p,p)^{6}Li at 125 degrees, and E_p=2.2 MeV to 12 MeV obtained with the scheme (6-S-M-GLS). In the C matrix diagonal elements C_{ii}≡1. The bottom panel shows the covariance matrix elements for the same excitation function but for E_{p0}=1.85 MeV with E_p=2.2 to 12 MeV obtained with the 4 schemes (1-0-N-ALS), (3-0-M-ALS), (5-S-M-CLS) and (6-S-M-GLS). It should be noted that the scheme (6-S-M-GLS) has the largest covariance matrix elements in most of the energy region.

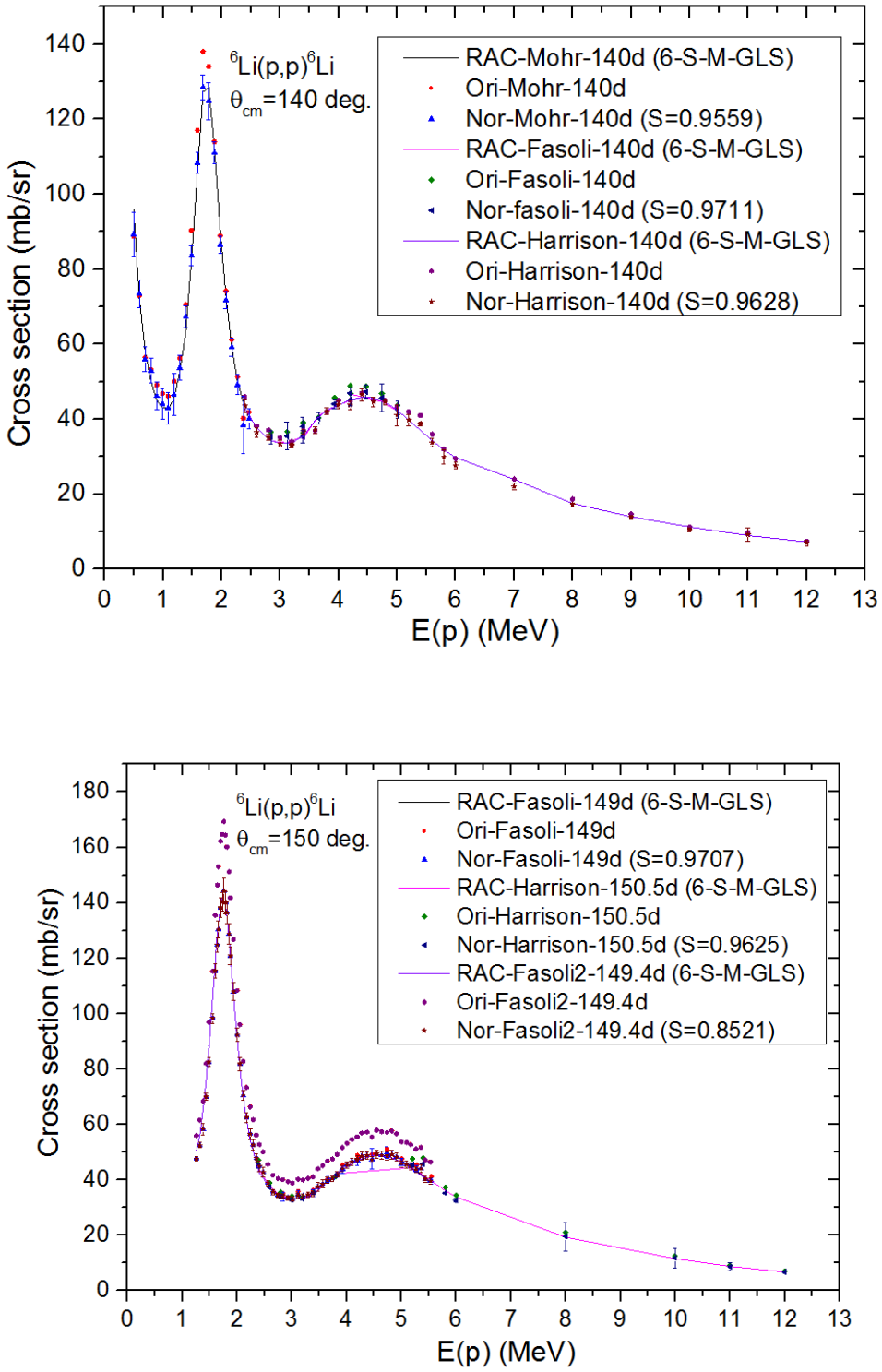

FIG 6.9. The top panel shows the ^{6}Li(p,p)^{6}Li excitation function near 140 degrees. The fit is good. The bottom panel shows the same but for 150 degrees. In the range 3.9-5.3 MeV there are no data points for Harrison [27] at 150.5 degrees, hence the straight line in calculated curve.

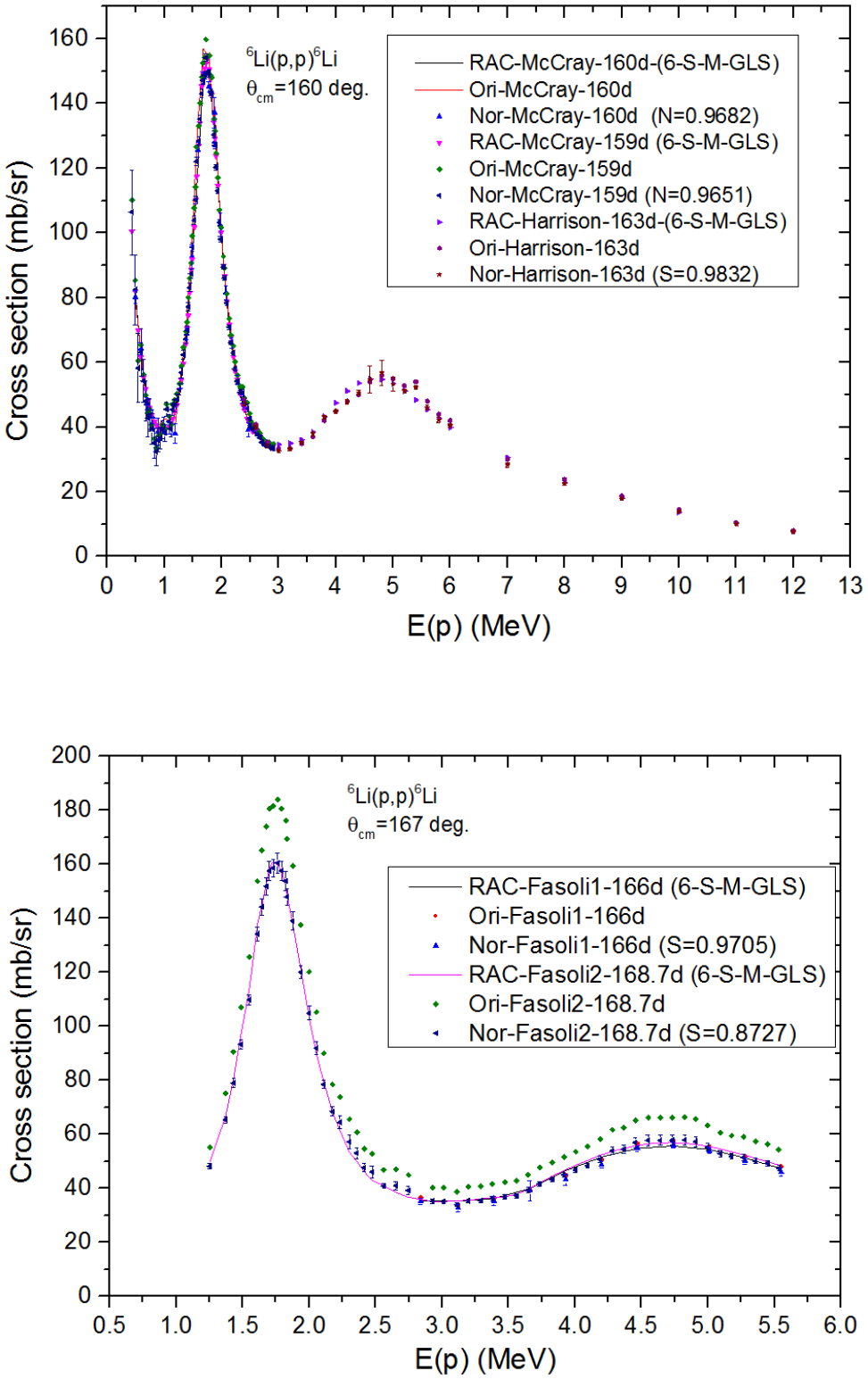

FIG 6.10. The top panel shows the ^{6}Li(p,p)^{6}Li EF near 160 degrees. The fit is very good. The shape and peak position of the relative data of Harrison [27] is important information for fitting the data. The bottom panel shows the same but at 167 degrees.

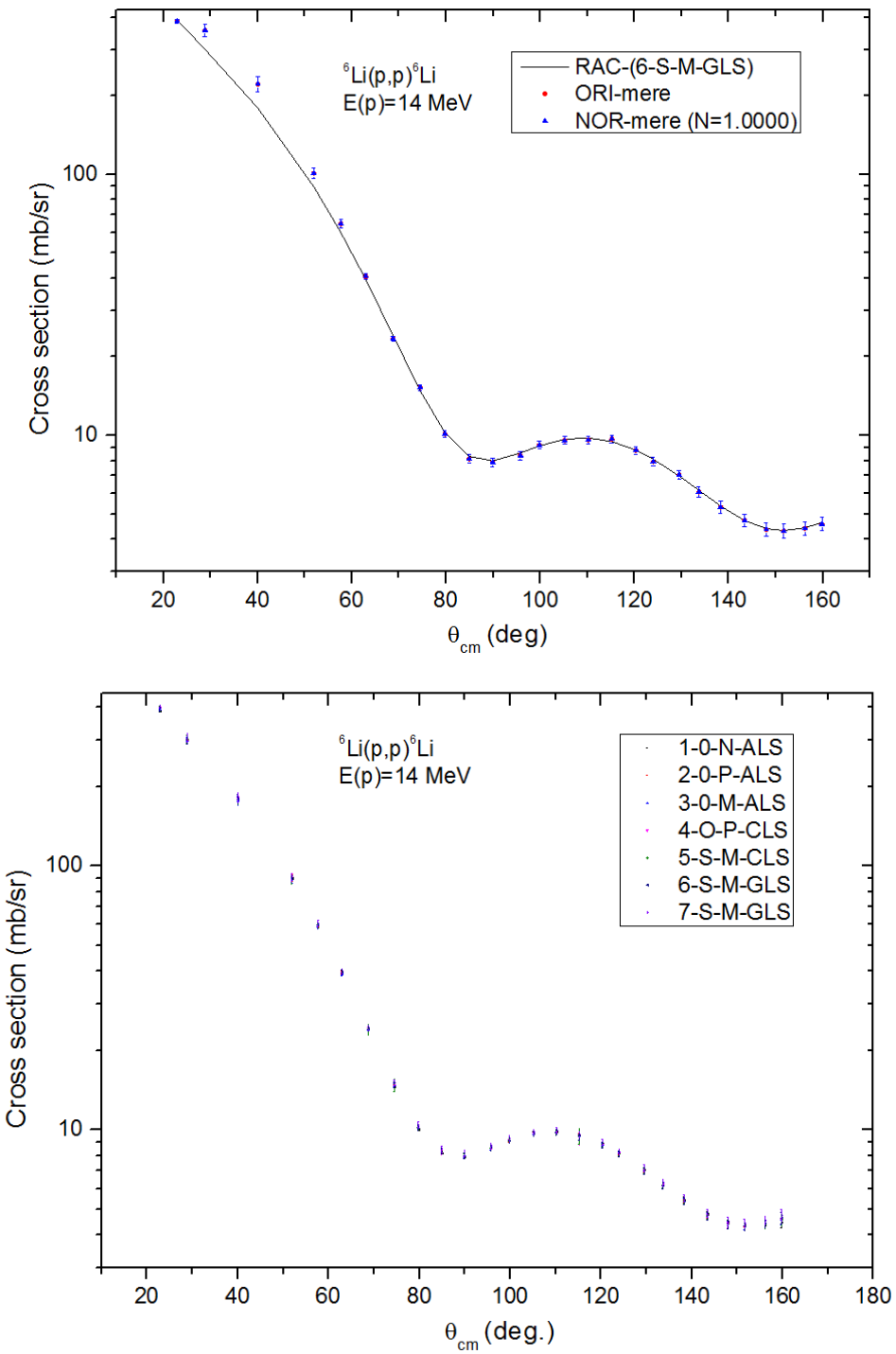

FIG 6.11. The top panel shows the fitted DA of ^{6}Li(p,p)^{6}Li at E_p=14 MeV, which is the largest energy used in the database. The fit is very good. This data are in the non-resolved resonance region, so the good fit shows that RAC has the ability to analyze the experimental data in the non-resolved resonance region as well. The bottom panel shows the corresponding calculated DA using the seven R-matrix schemes. The results agree very well both in magnitude and shape.

6.3.2. $^{6}Li(p,^{3}He)^{4}He$

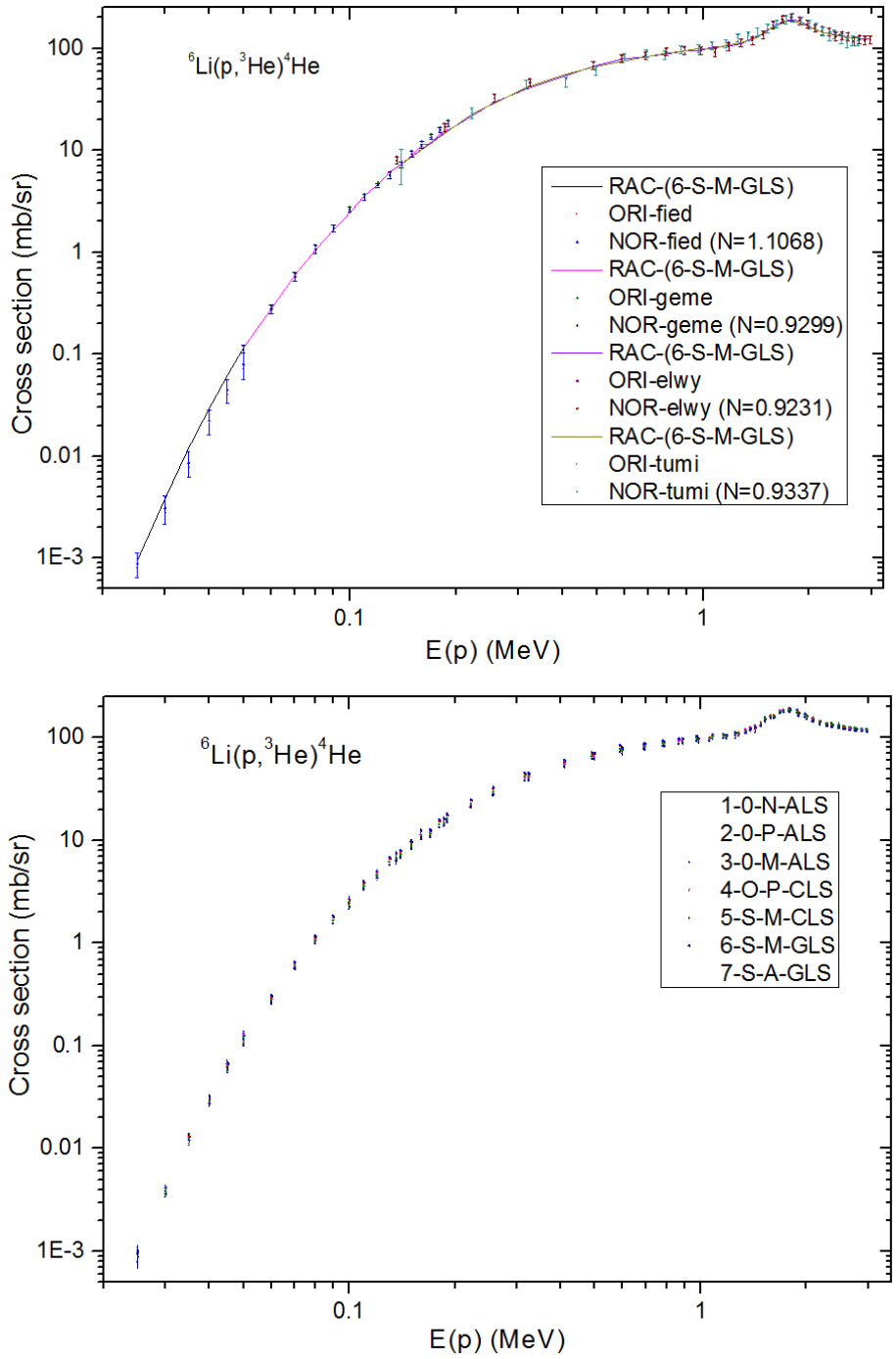

FIG 6.12. The top panel shows the fit of the integrated cross section of the $^{6}Li(p,^{3}He)^{4}He$ reaction.. The fit is very good. The bottom panel shows the corresponding calculated integrated cross sections obtained with the seven schemes. The results agree very well both in magnitude and shape.

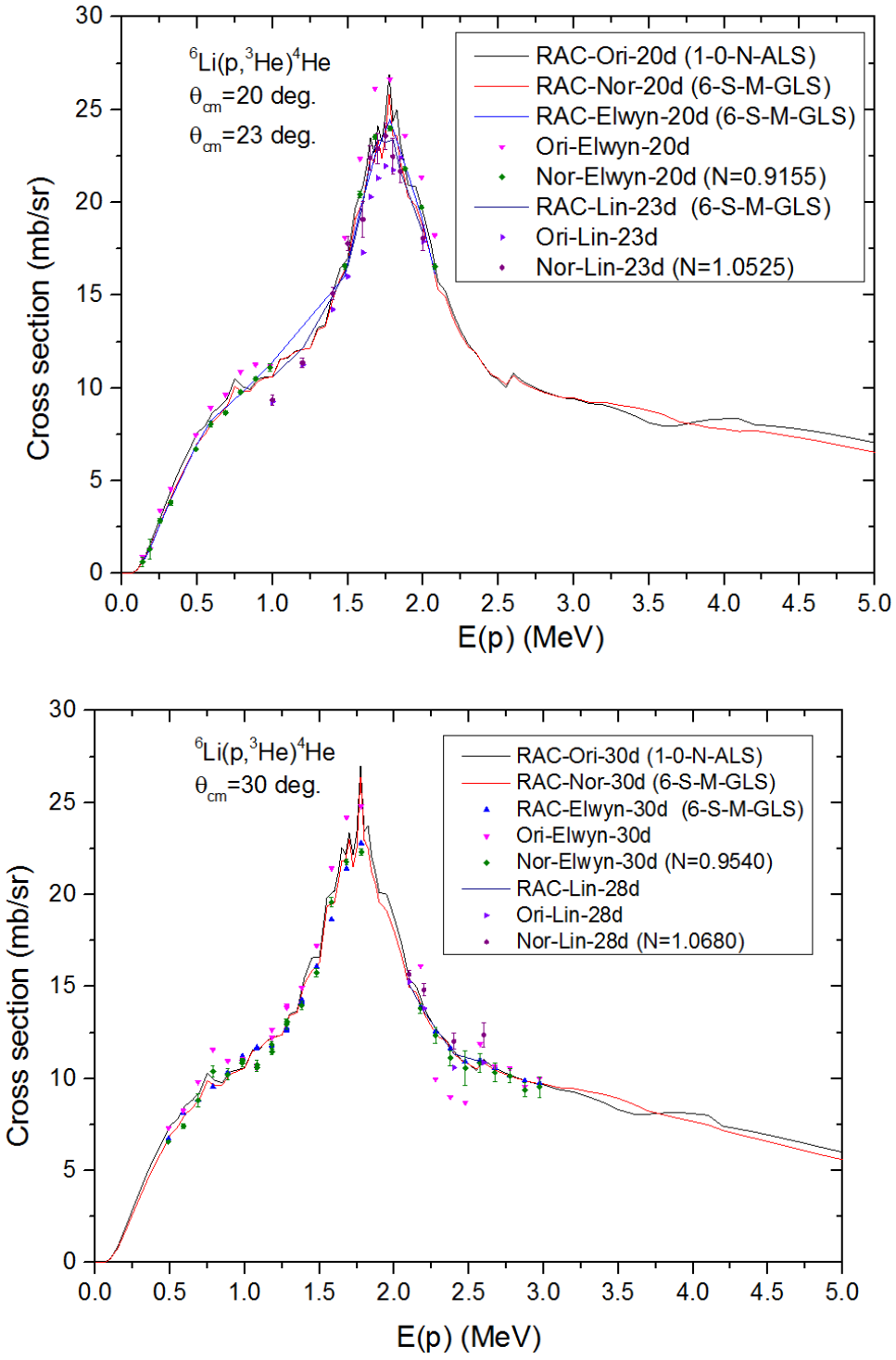

FIG 6.13. The top panel shows the ^{6}Li(p,^{3}He)^{4}He excitation function near 20 and 23 degrees. The bottom panel shows the same at 30 degrees. Both fits are very good.

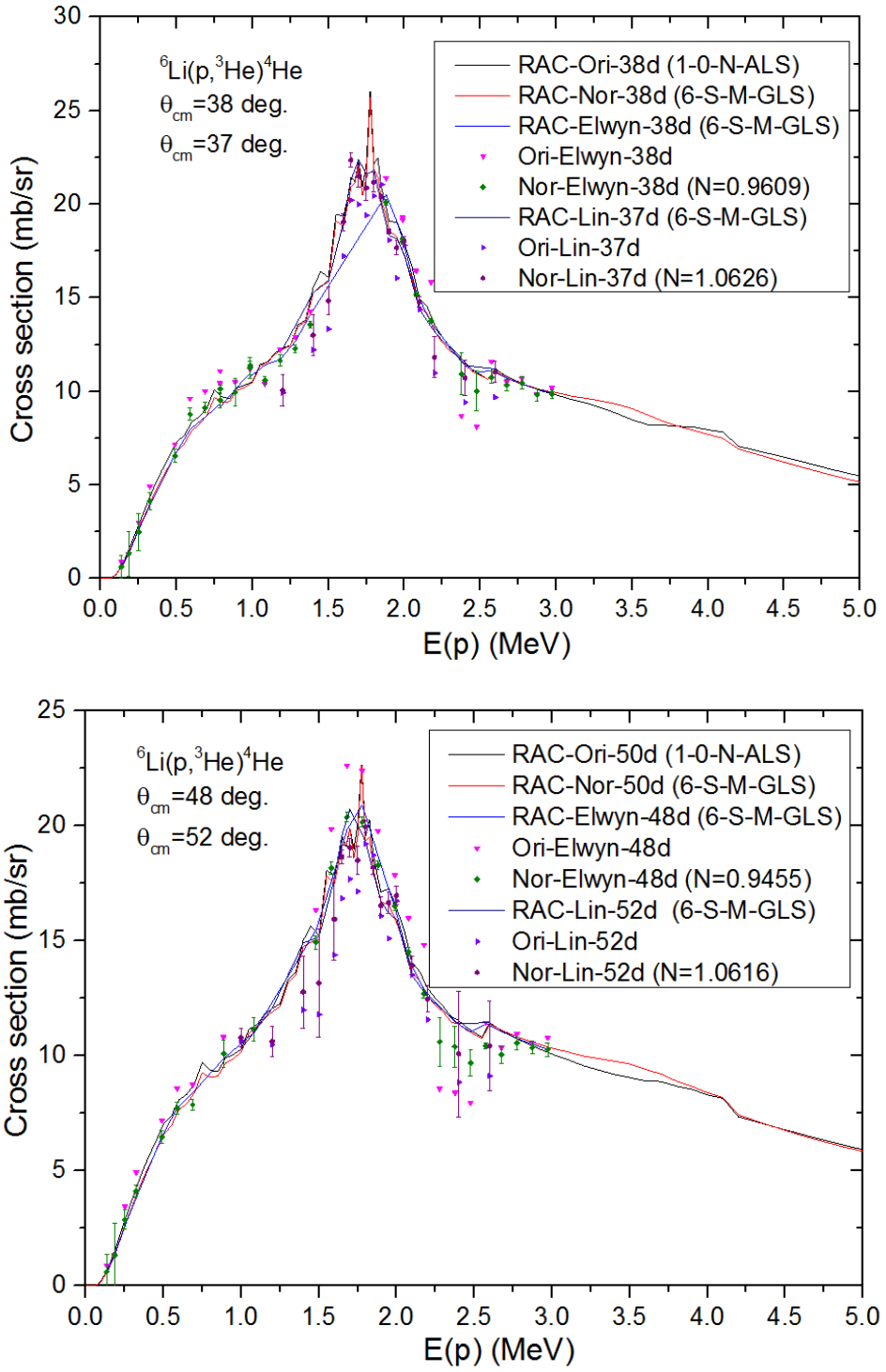

FIG 6.14. The top panel shows the ^{6}Li(p,^{3}He)^{4}He excitation function at 37 and 38 degrees, while the bottom panel shows the same at 48 and 52 degrees. Both fits are very good. It should be noted that near 2.5 MeV the experimental data of Elwyn [22] are systematically lower.

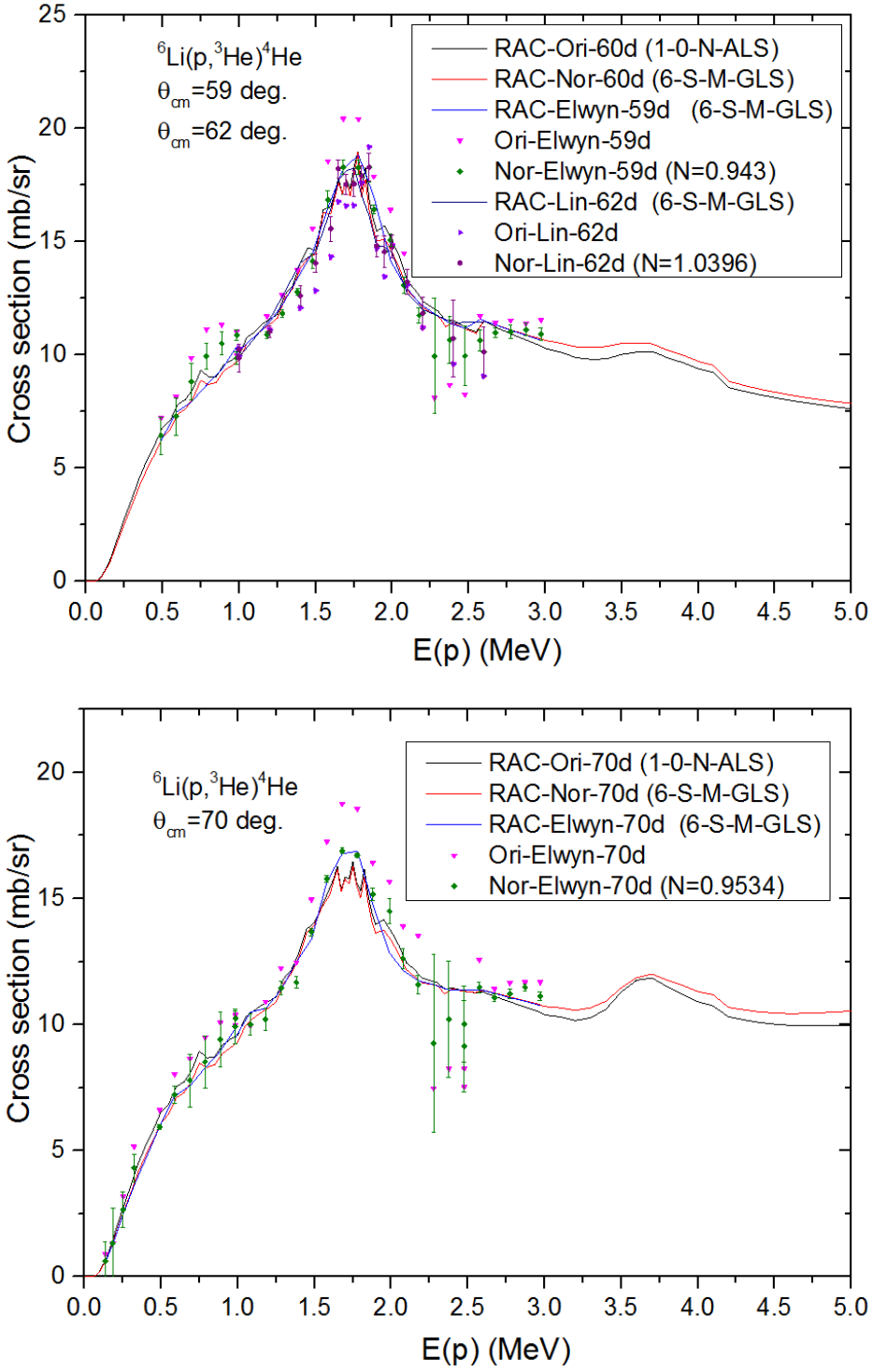

FIG 6.15. The top panel shows the ^{6}Li(p,^{3}He)^{4}He excitation function at 59 and 62 degrees, while the bottom panel shows the same at 70 degrees. Both fits are good. It should be noted that near 2.5 MeV the experimental data of Elwyn [22] are systematically lower.

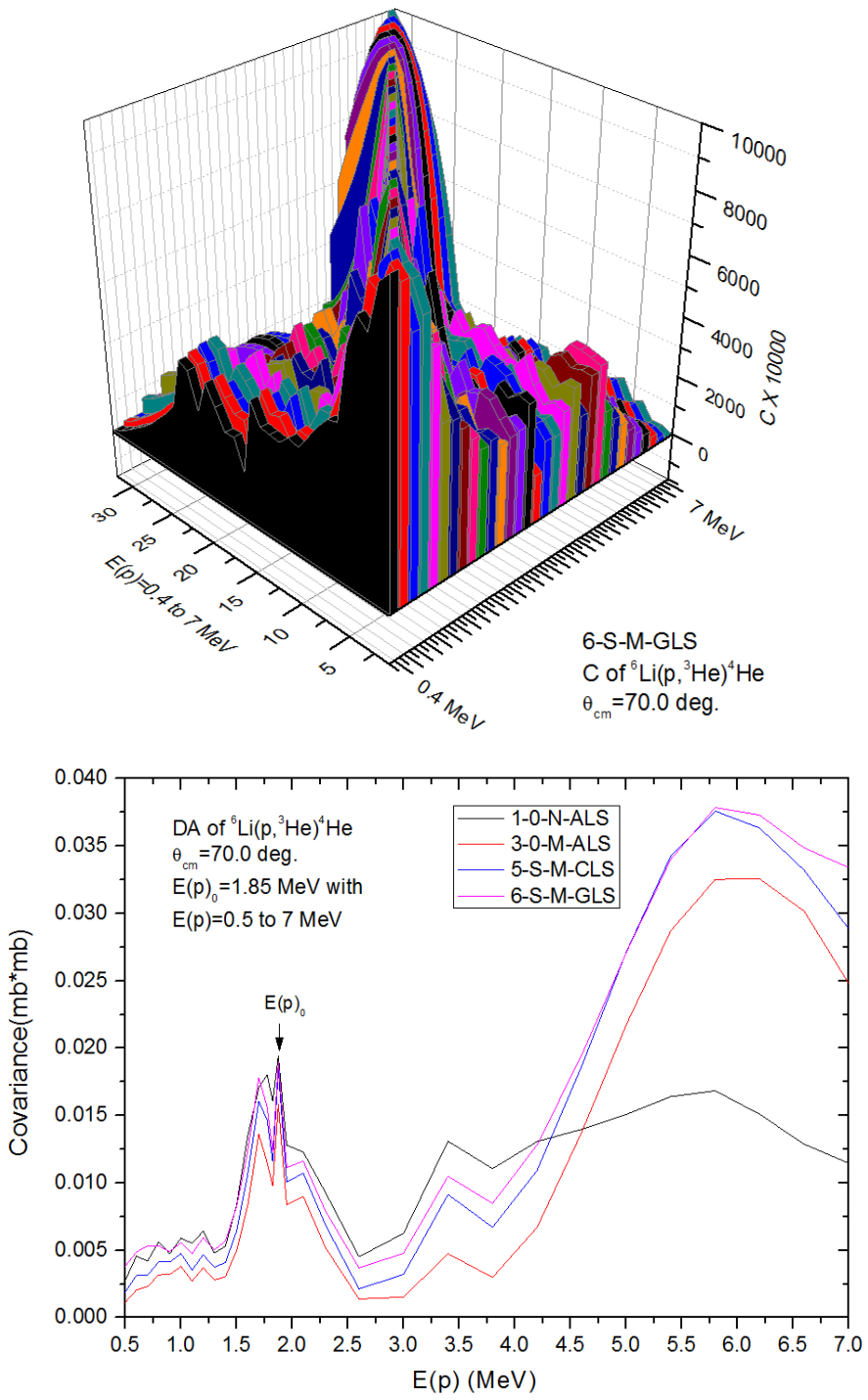

FIG 6.16. The top panel shows the correlation factor (C) for the excitation function of ^{6}Li(p, ^{3}He)^{4}He at 70 degrees, and E_p = 0.4 MeV to 7 MeV. It is the result of the scheme (6-S-M-GLS). The bottom panel shows the covariance matrix elements for the same excitation function, for E_{p0} = 1.85 MeV with E_p = 0.5 to 7 MeV obtained from the 4 schemes (1-0-N-ALS), (3-0-M-ALS), (5-S-M-CLS) and (6-S-M-GLS). It should be noted that the scheme (6-S-M-GLS) has the largest covariance matrix elements in most of the energy region.

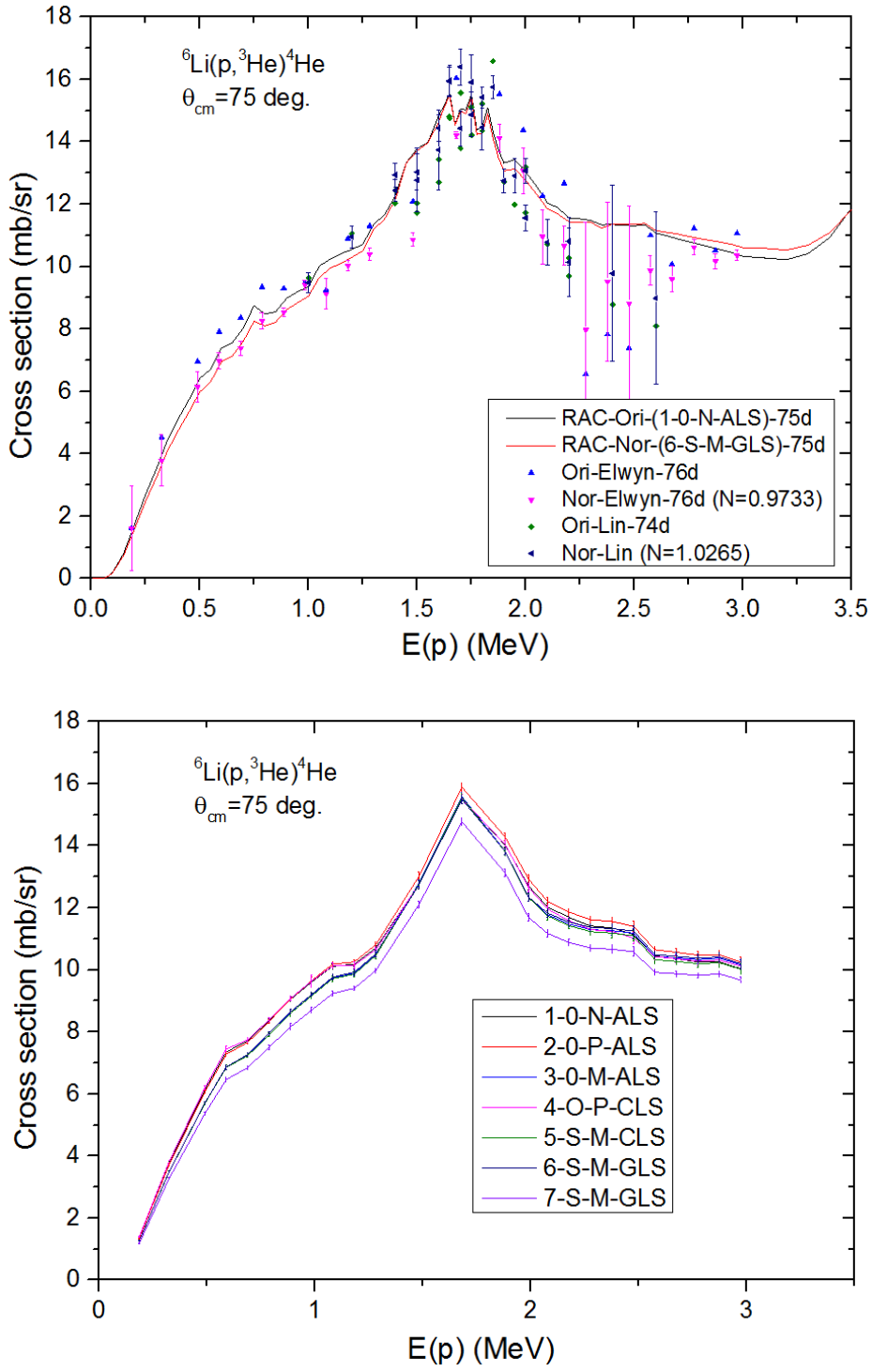

FIG 6.17. The top panel shows the excitation function of ^{6}Li(p,^{3}He)^{4}He at 75 degrees. The fit looks good. It should be noted that large differences are observed in the region E_p = 2.1 to 2.6 MeV, as in this energy range the experimental data have rather large systematic errors. The bottom panel shows the corresponding *calculated excitation function obtained with the seven schemes. The results agree both in magnitude and shape.*

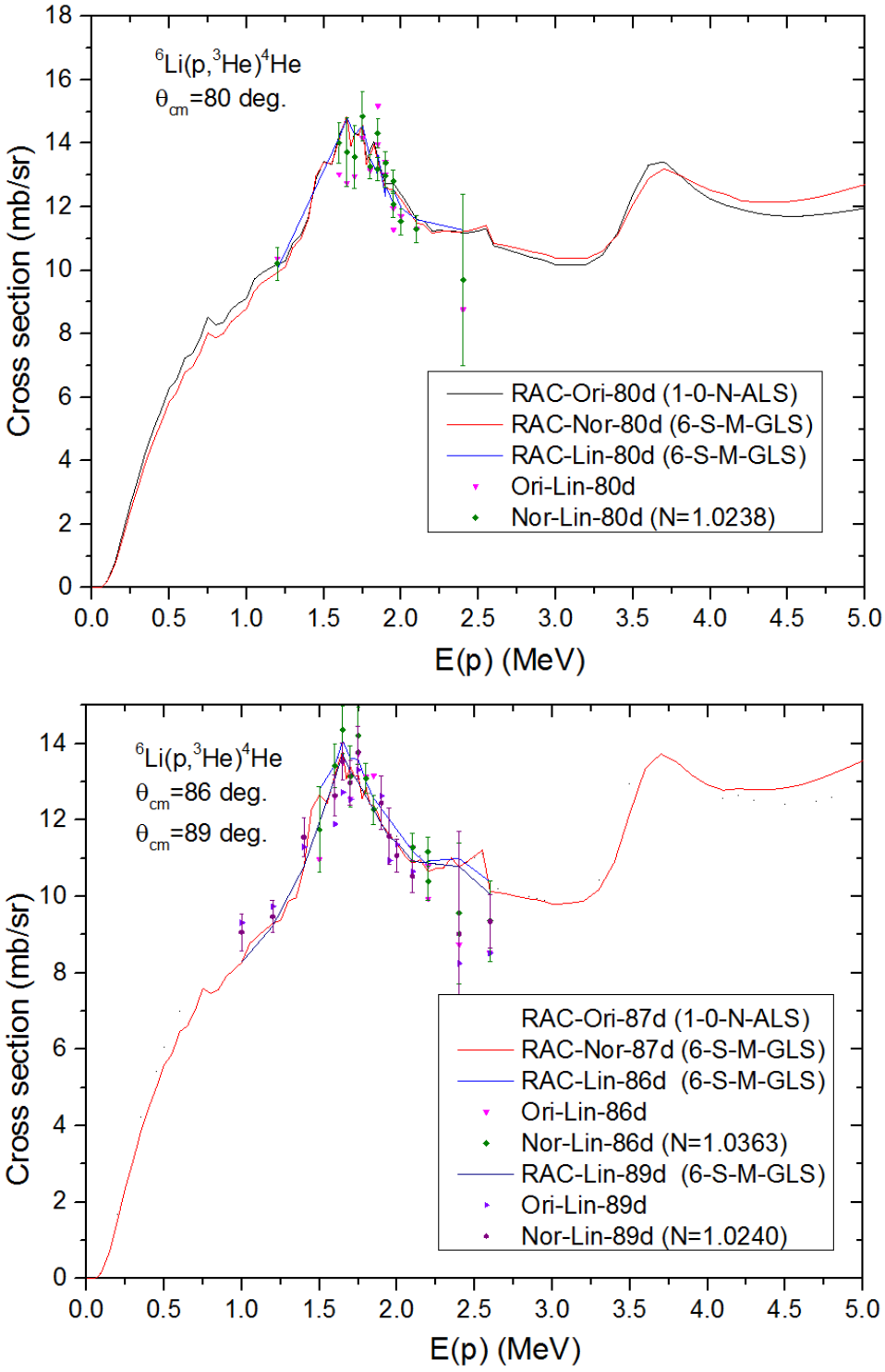

FIG 6.18. The top panel shows the excitation function of ^{6}Li(p,^{3}He)^{4}He at 80 degrees, while the bottom panel shows the same at 86 and 89 degrees. Both fits look good. It should be noted that near 2.5 MeV the experimental data are systematically lower.

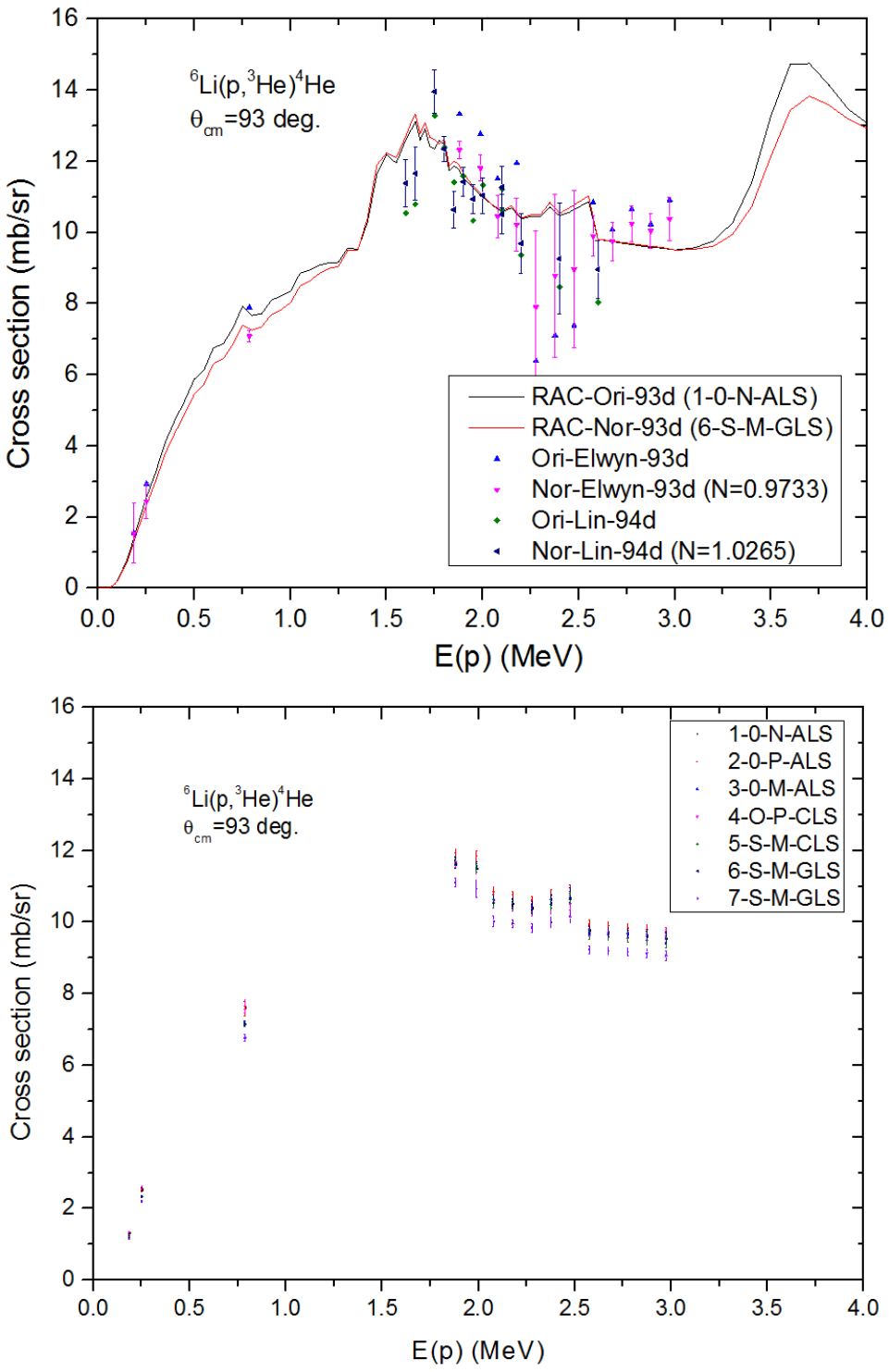

FIG 6.19. The top panel shows the excitation function of ^{6}Li (p, ^{3}He) ^{4}He at 93 degrees. The fit looks good however, it should be noted that near 2.5 MeV the experimental data are systematically lower. The bottom panel shows the corresponding calculated excitation functions obtained with the seven schemes. The absolute magnitudes are close and the shapes are similar.

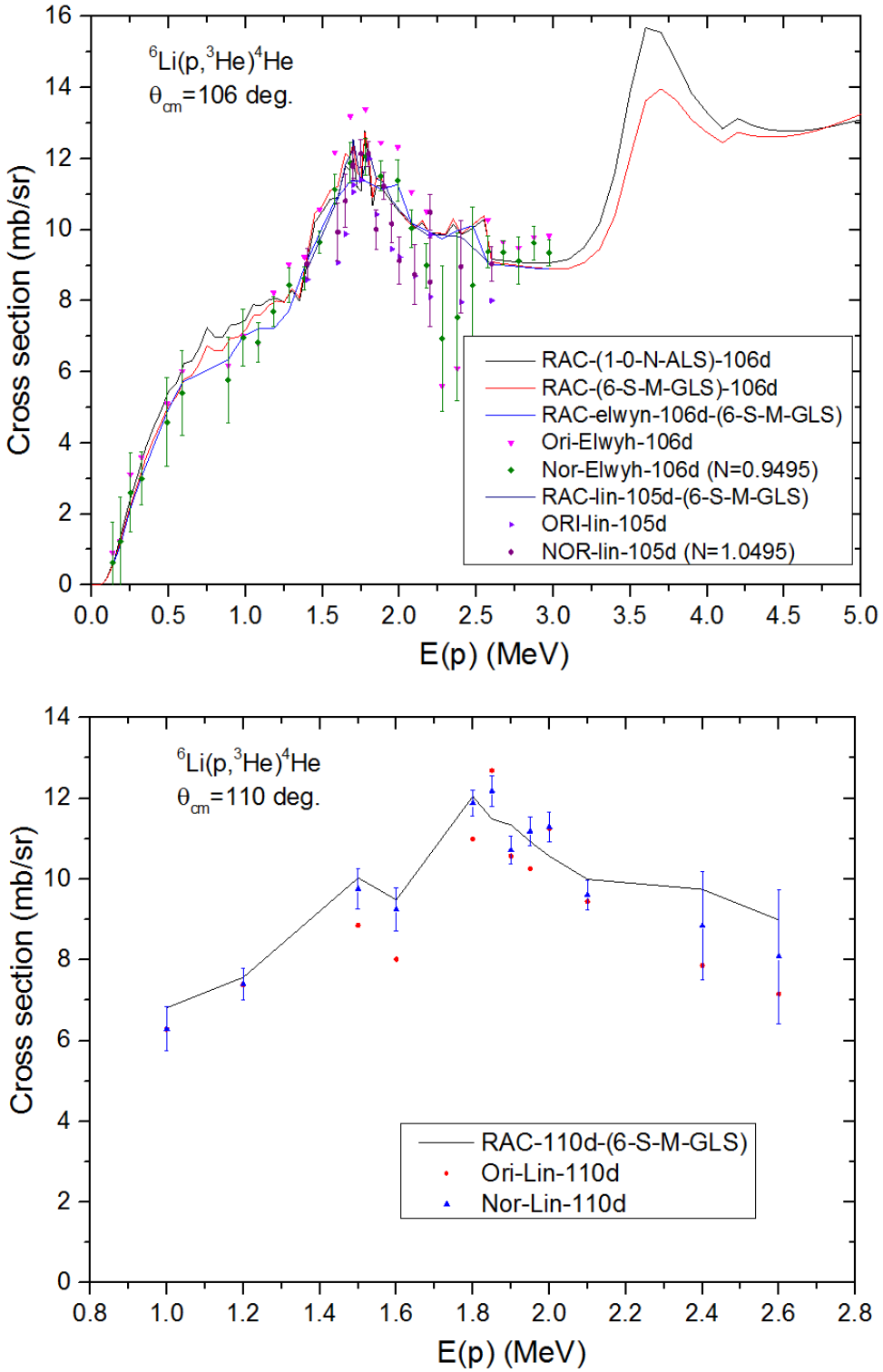

FIG 6.20. The top panel shows the excitation function of the ^{6}Li(p,^{3}He)^{4}He at 106 degrees, while the bottom panel shows the same at 110 degrees. The fits look good, however it should be noted that near 2.5 MeV the experimental data are systematically lower.

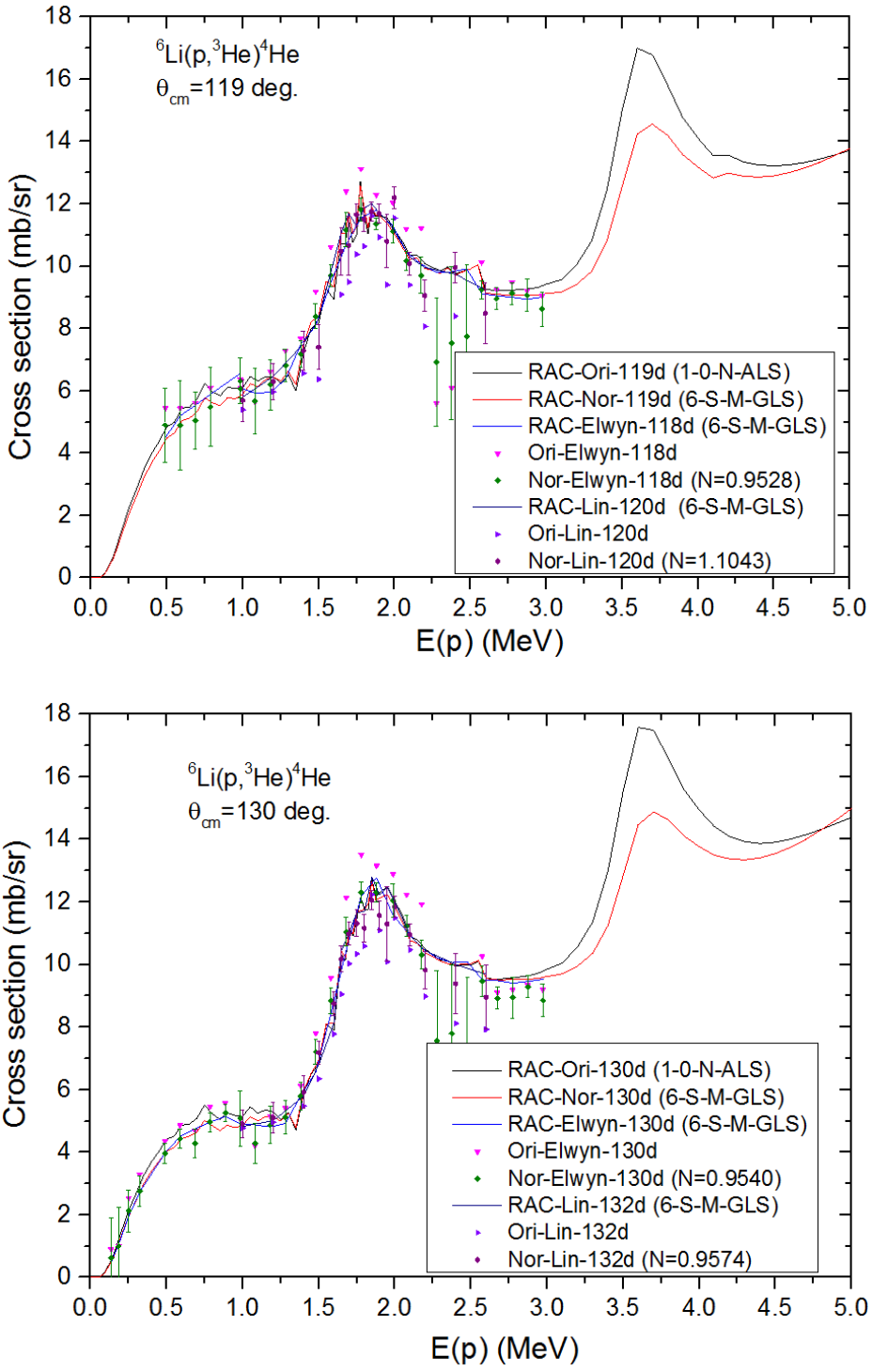

FIG 6.21. The top panel shows the ^{6}Li(p,^{3}He)^{4}He excitation function close to 119 degrees. The fit looks good. The bottom panel shows the same but close to 130 degrees. It should be noted that close to 2.5 MeV the experimental data are systematically lower.

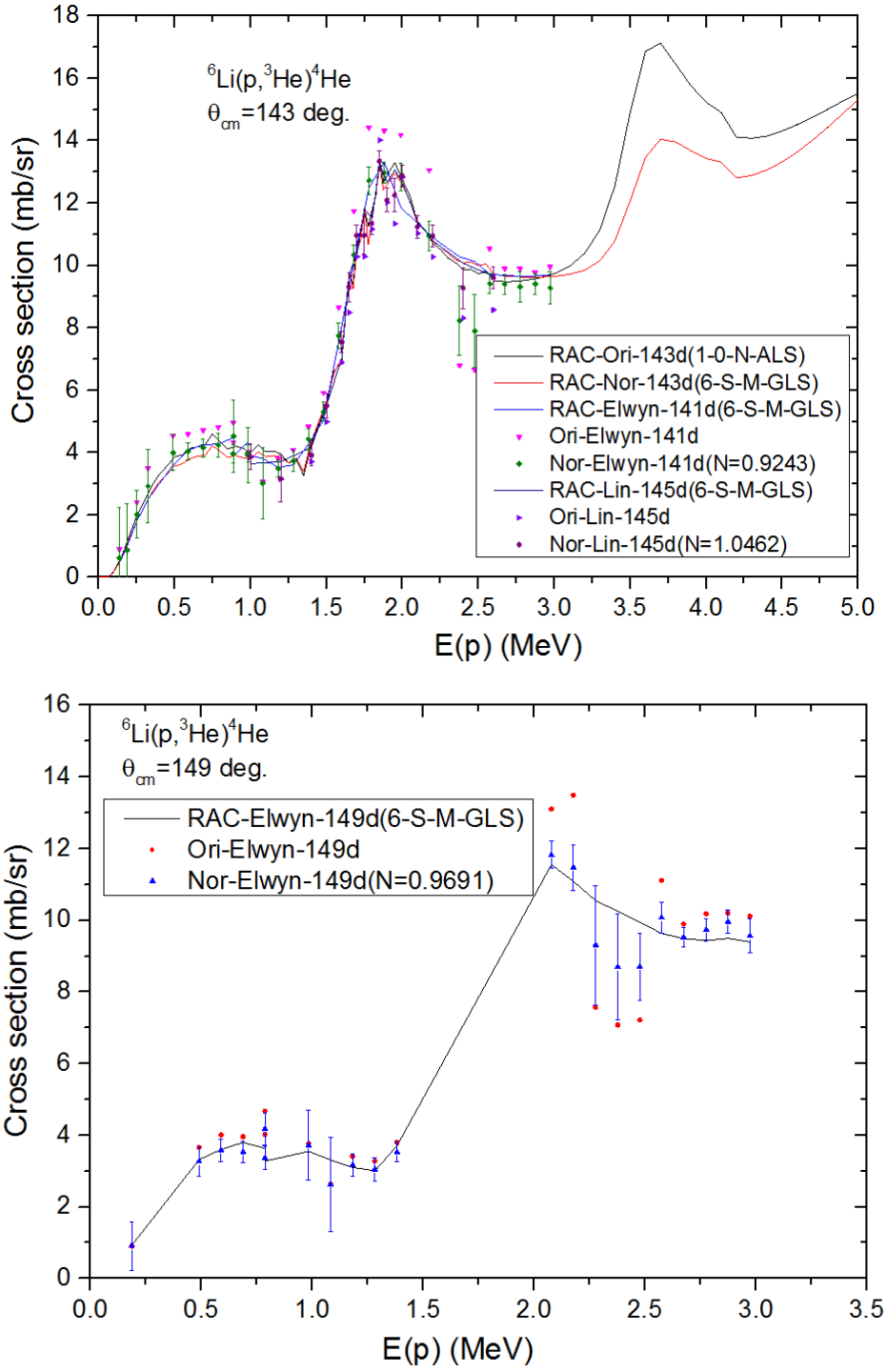

FIG 6.22. The top panel shows the ^{6}Li(p,^{3}He)^{4}He excitation function close to 143 degrees. The fit looks good. The bottom panel shows the same but for 149 degrees. It should be noted that near 2.5 MeV the experimental data are systematically lower.

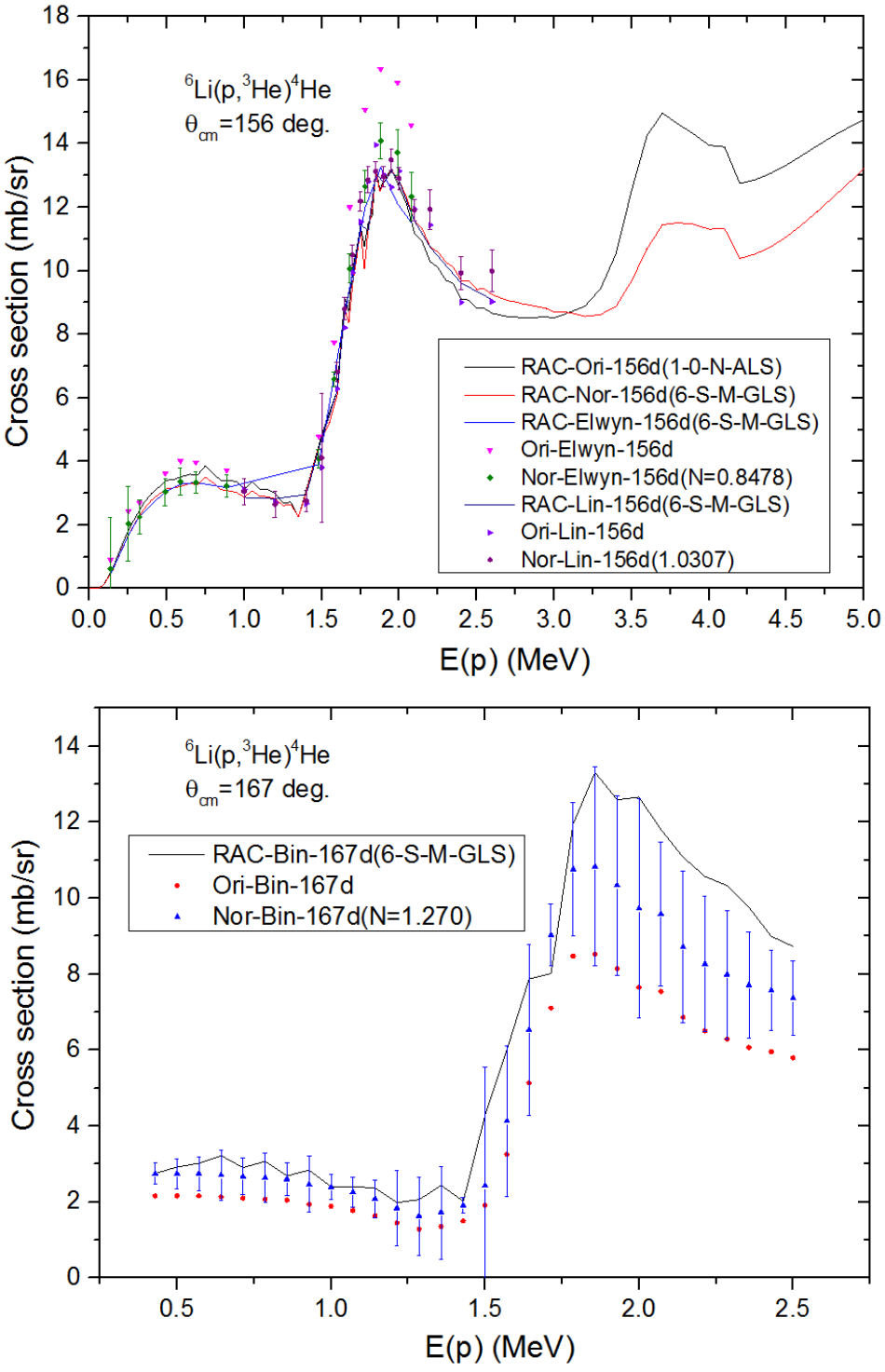

FIG 6.23. The top panel shows the ^{6}Li(p,^{3}He)^{4}He excitation function close to 156 degrees. The fit looks good. The bottom panel shows the same but for 167 degrees.

6.3.3. $^{6}Li(p,p_1)^{6}Li^{*}$

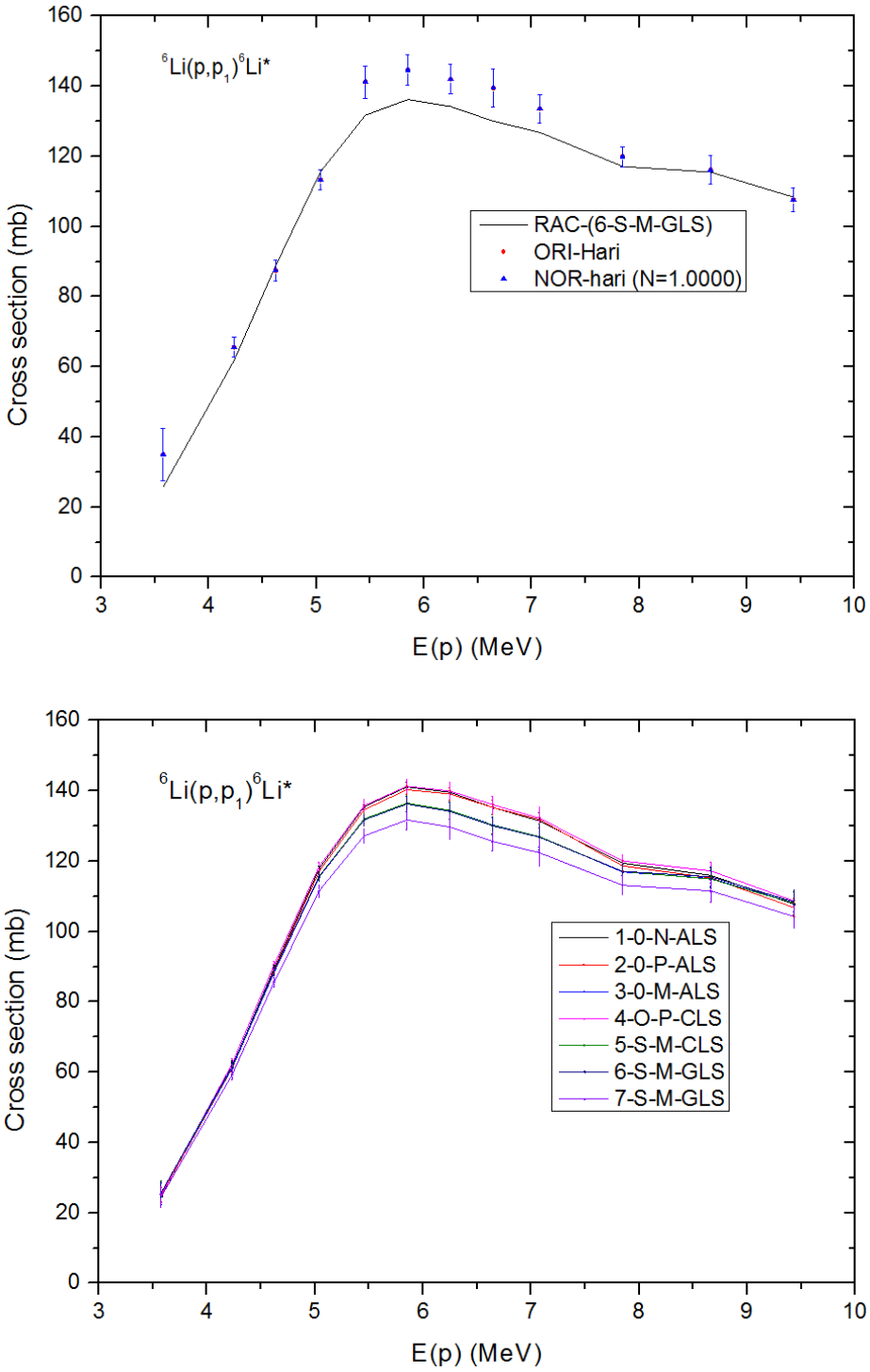

FIG 6.24. The top panel shows the fits for the integrated cross sections of $^{6}Li(p,p_1)^{6}Li^{*}$ using the scheme (6-S-M-GLS). The fit looks good. The bottom panel shows the calculated integrated cross sections for $^{6}Li(p,p_1)^{6}Li^{*}$ using all seven schemes. The results show that they agree reasonably.

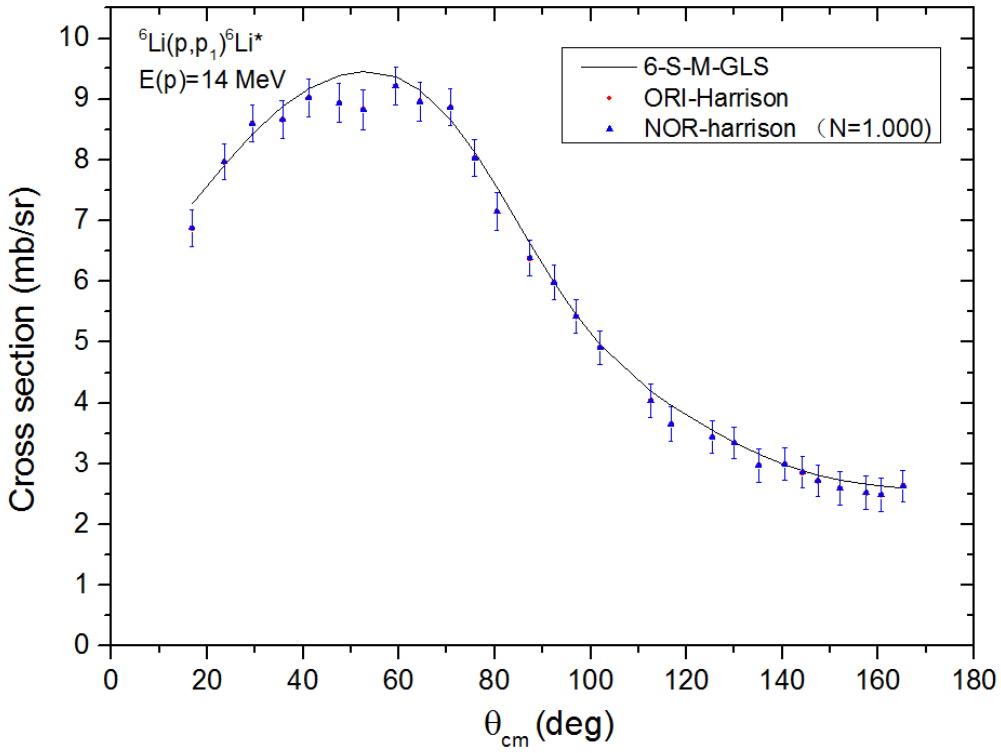

FIG 6.25. The fit of the DA of ^{6}Li (p,p$_1$) ^{6}Li* at E_p = 14 MeV, which is the largest energy used in database. The fit is very good. At this energy the reaction occurs in the non-resolved resonance region, therefore the results show that the code RAC is able to analyze the experimental data in the non-resolved resonance region as well.

6.3.4. $^{6}Li(p,p_2)^{6}Li^{**}$

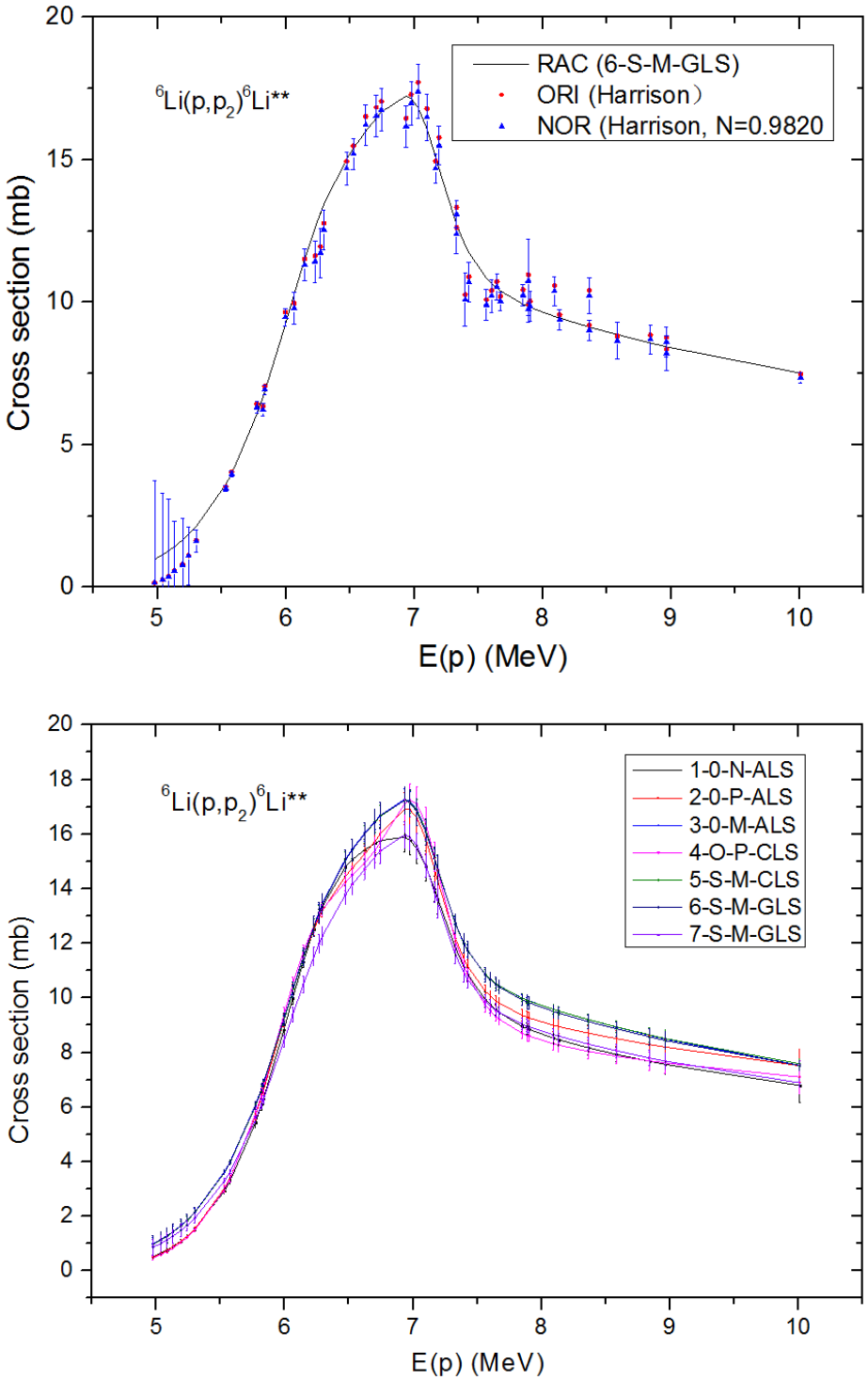

FIG 6.26. The top panel shows the fit of the integrated cross sections of $^{6}Li(p,p_2)^{6}Li^{**}$ using the scheme (6-S-M-GLS). N=1 means that the data are not normalized. The fit looks good. The bottom panel shows the calculated integrated cross sections of $^{6}Li(p,p_2)^{6}Li^{**}$ using all seven schemes. The results agree reasonably.

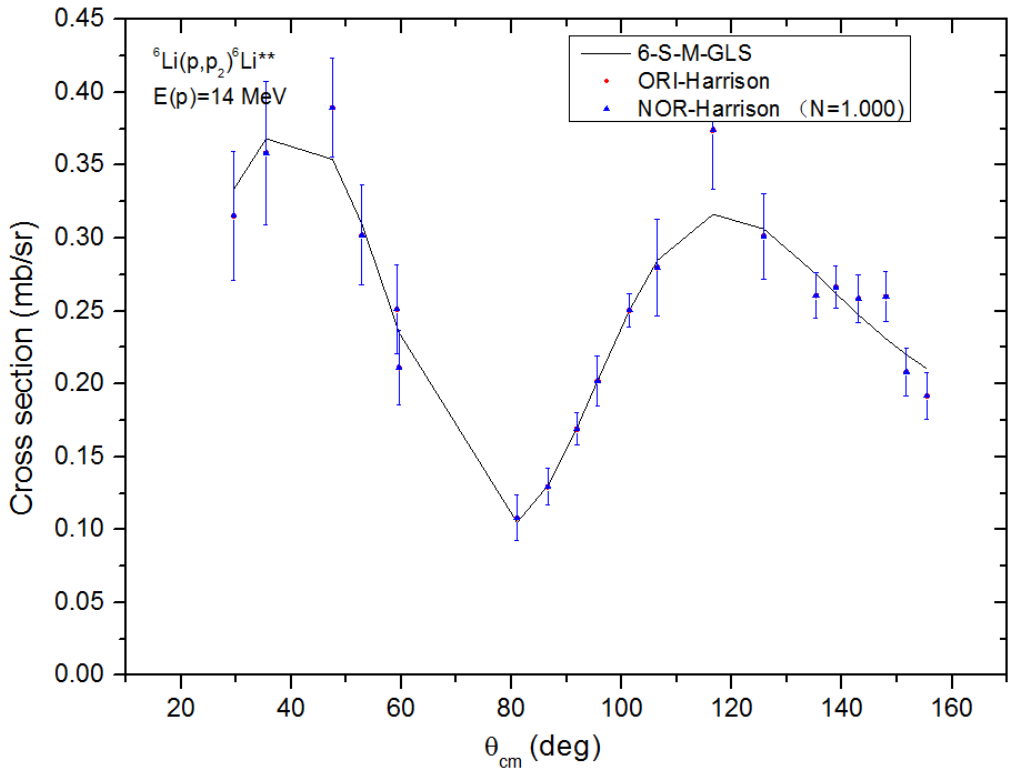

FIG 6.27. The fit for the DA of ^{6}Li(p,p$_2$)^{6}Li** at E_p = 14 MeV, which is the largest energy used in database. The fit looks good. The results show that the code RAC is able to analyze the non-resonance region as well.

6.3.5. $^{6}Li(p,\gamma_0)^{7}Be$

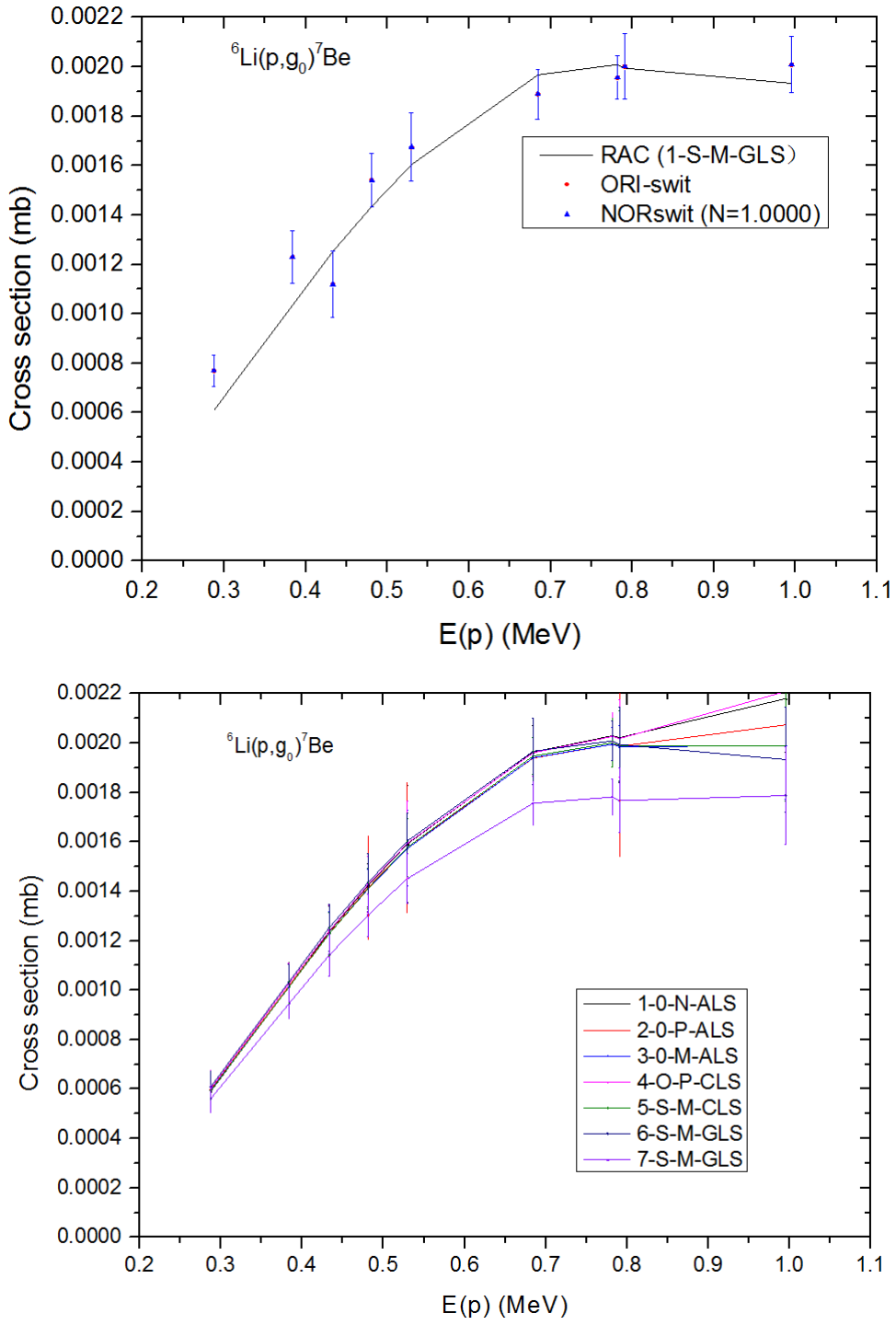

FIG 6.28. The left panel shows the fit for the integrated cross section of $^{6}Li(p,\gamma_0)^{7}Be$ using the scheme (1-S-M-GLS). N=1 means data are not normalized. The fit looks good. The bottom panel shows the calculated integrated cross sections obtained with the seven schemes. The results agree in magnitude and shape except for the scheme (6-S-M-GLS).

6.3.6. $^{6}Li(p,\gamma_1)^{7}Be^{*}$

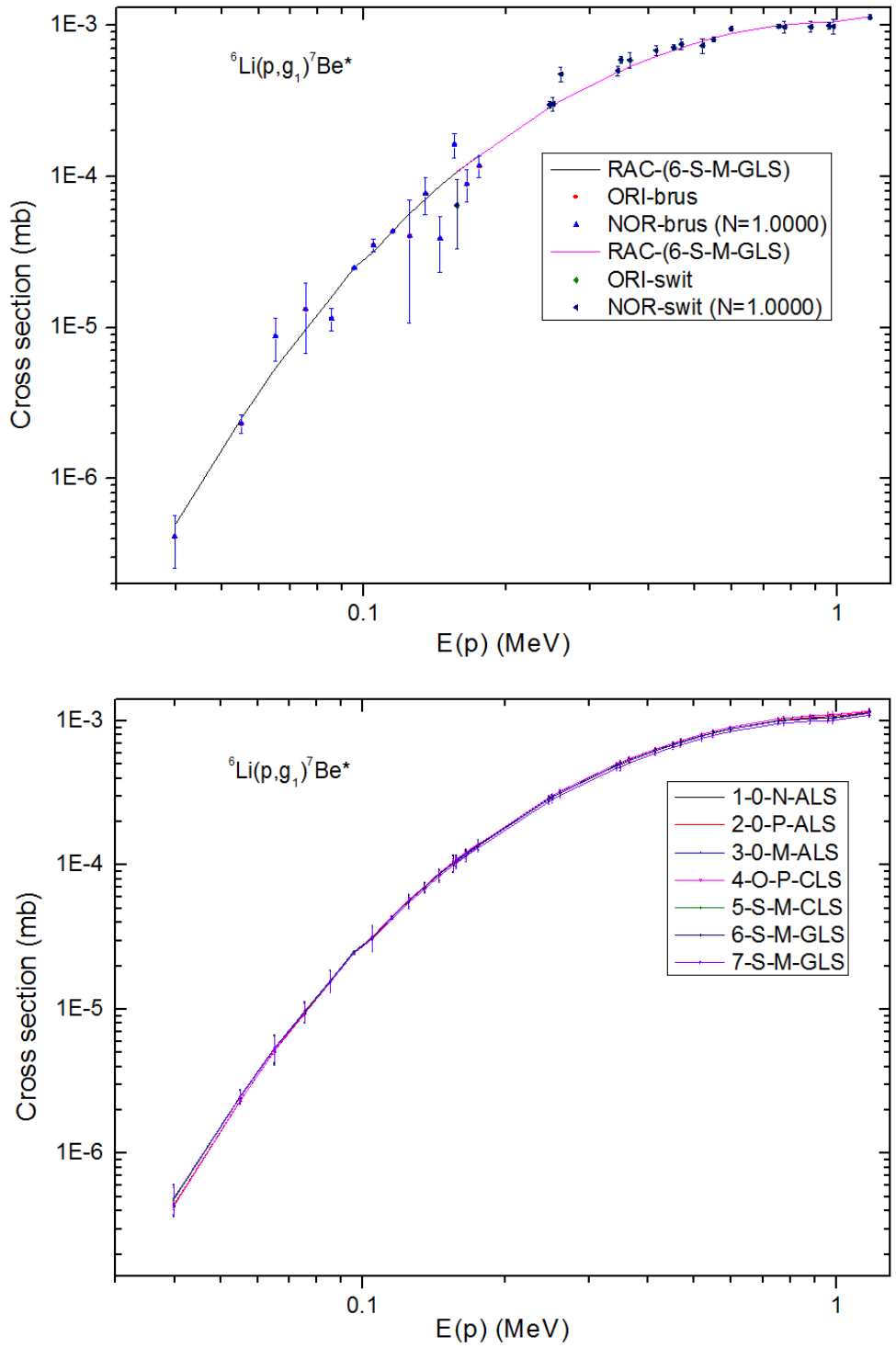

*FIG 6.29. The left panel shows the fit for the integrated $^{6}Li(p,\gamma_1)^{7}Be$ * using the scheme (6-S-M-GLS). N = 1 means that data are not normalized. The fit looks good. The bottom panel shows the calculated integrated cross sections obtained from the seven schemes. The results agree reasonably except for the scheme (6-S-M-GLS).*

6.3.7. $^4He(^3He,^3He)^4He$

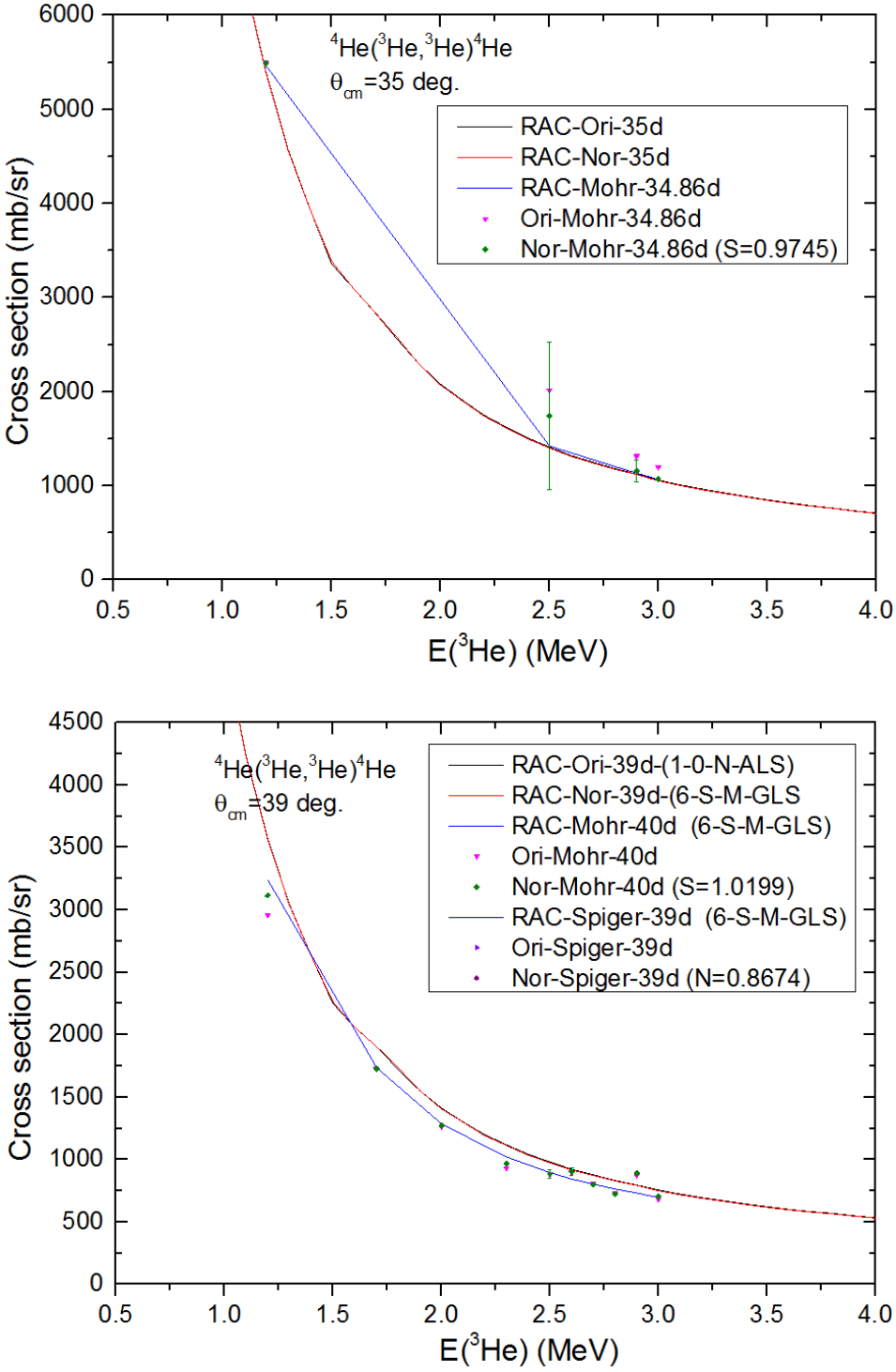

FIG 6.30. (Top) The fit for the excitation function of $^4He(^3He,^3He)^4He$ at about 35 degrees. The fit is very good. (Bottom) The same but at about 39 degrees. This fit also looks good.

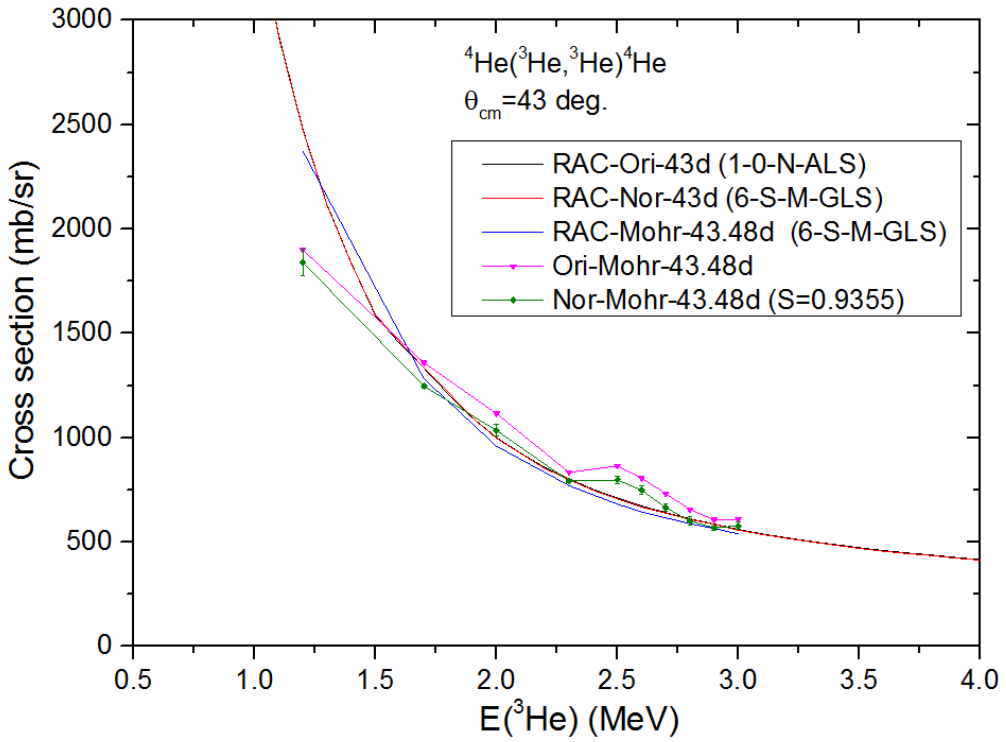

FIG 6.31. Fit for the excitation function of ^{4}He(^{3}He ^{3}He)^{4}He at about 43 degrees. The fit is good.

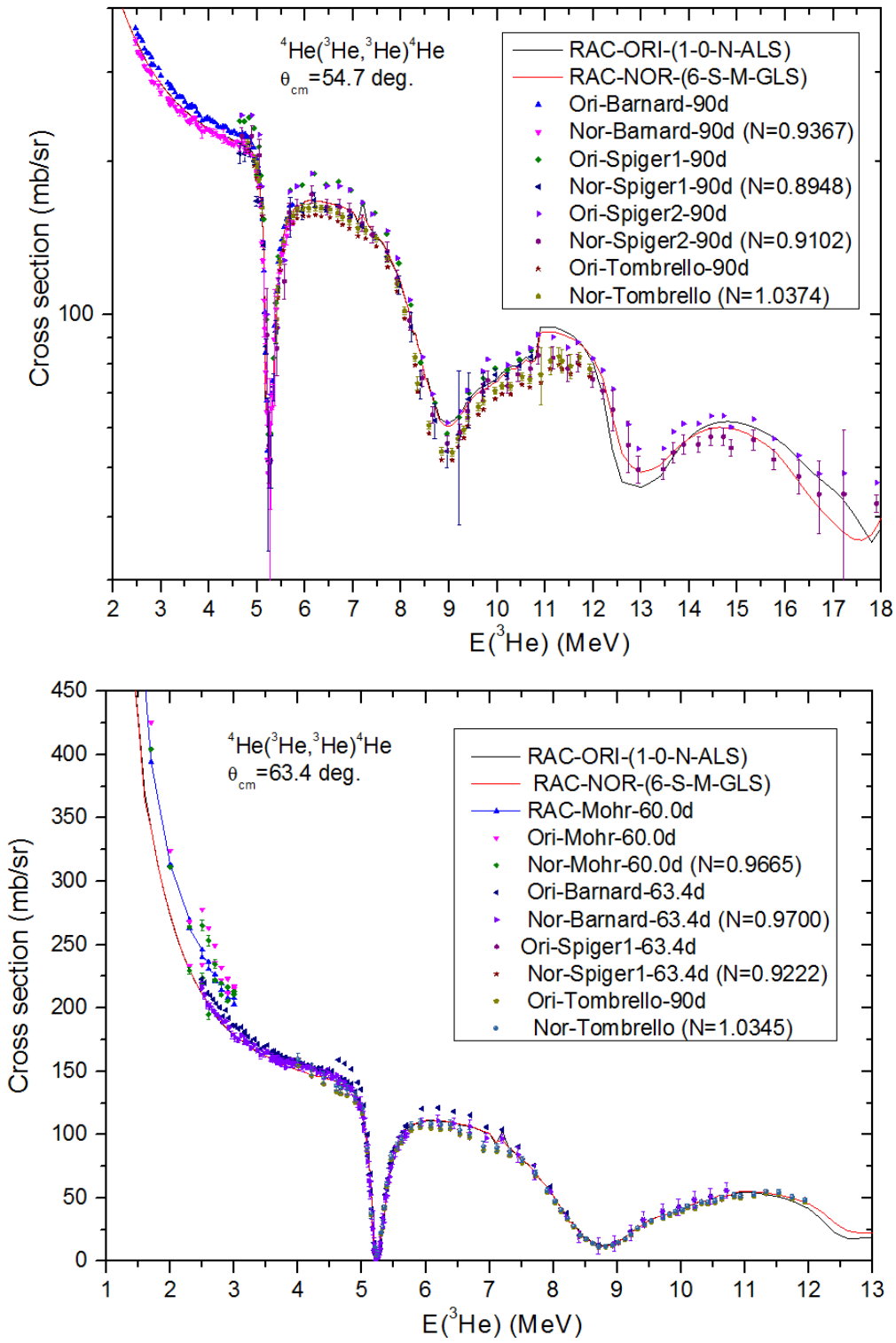

FIG 6.32. (Top) Fit of the excitation function of ^{4}He(^{3}He,^{3}He)^{4}He at about 54.7 degrees. The fit is very good. (Bottom) Then same but at about 63.4 degree. Again, the fit is very good.

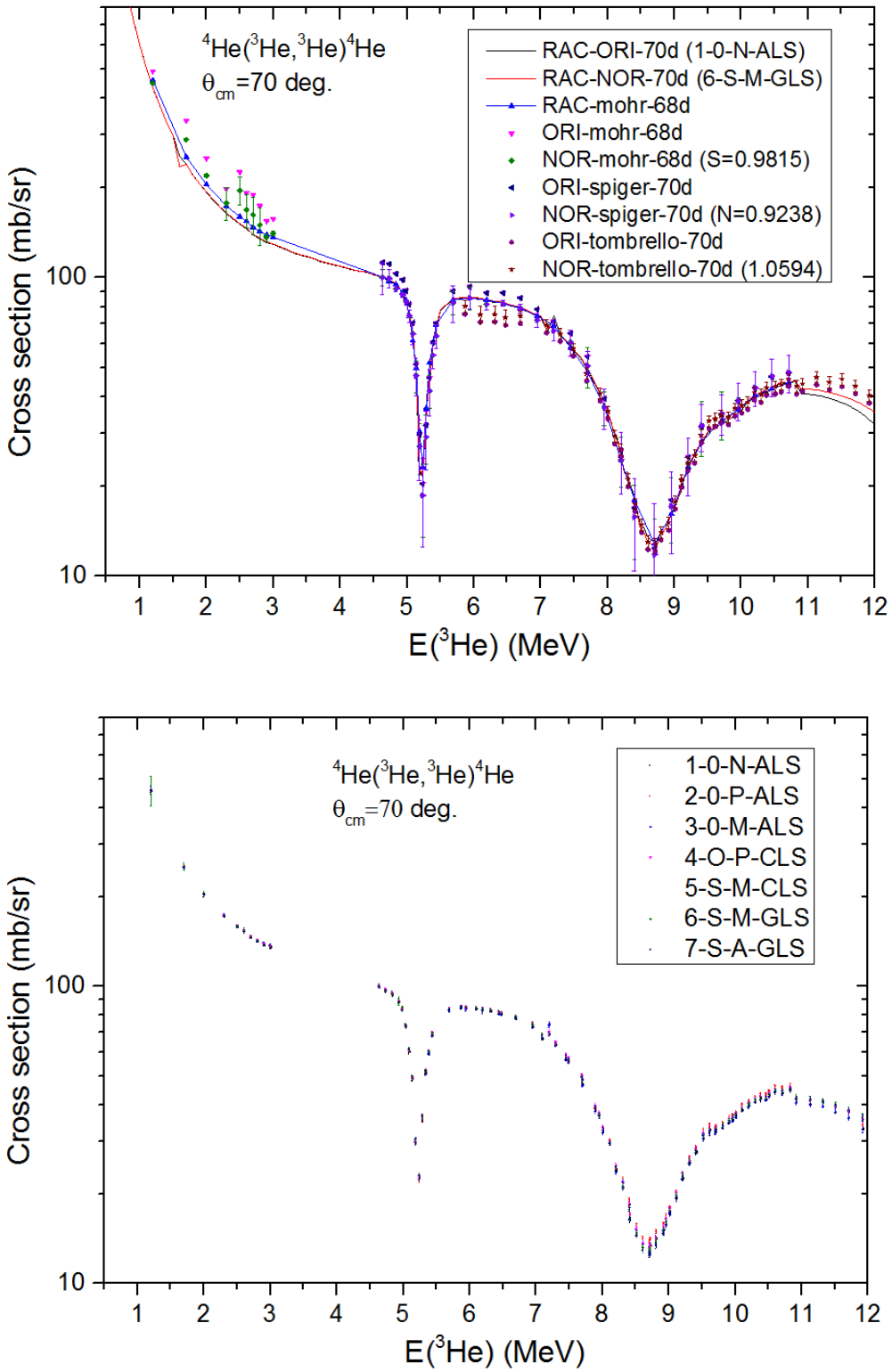

FIG 6.33. (Top) Fit for excitation function of ^{4}He(^{3}He,^{3}He)^{4}He at about 70 degrees. The fit is very good. (Bottom) The calculated excitation functions at about 70 degrees obtained with the seven schemes. The results agree both in magnitude and shape.

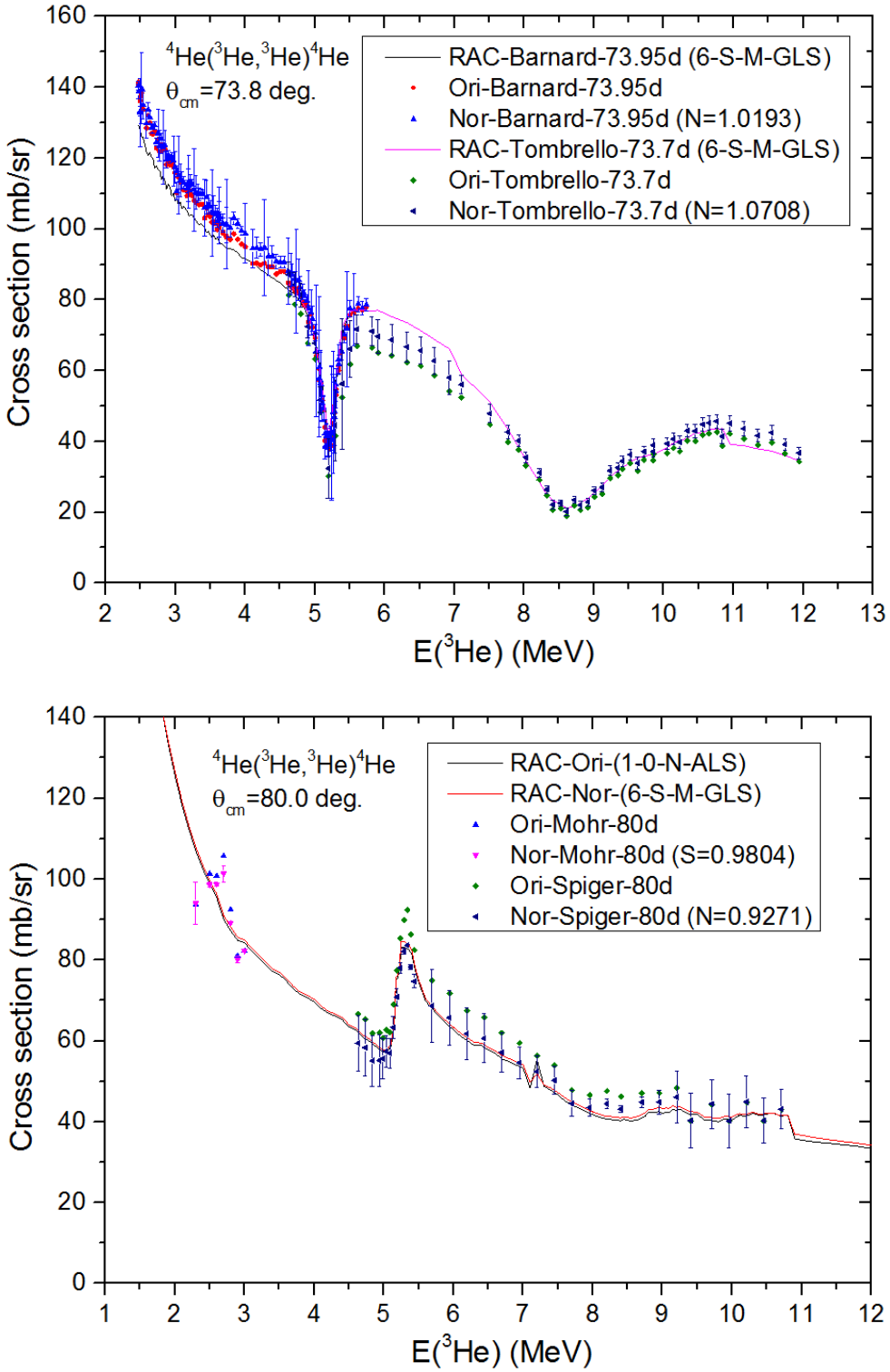

FIG 6.34. (Top) Fit for the excitation function of ^{4}He(^{3}He,^{3}He)^{4}He at about 73.8 degrees. The fit is very good. (Right) The same but for 80 degrees. Again, the fit is very good.

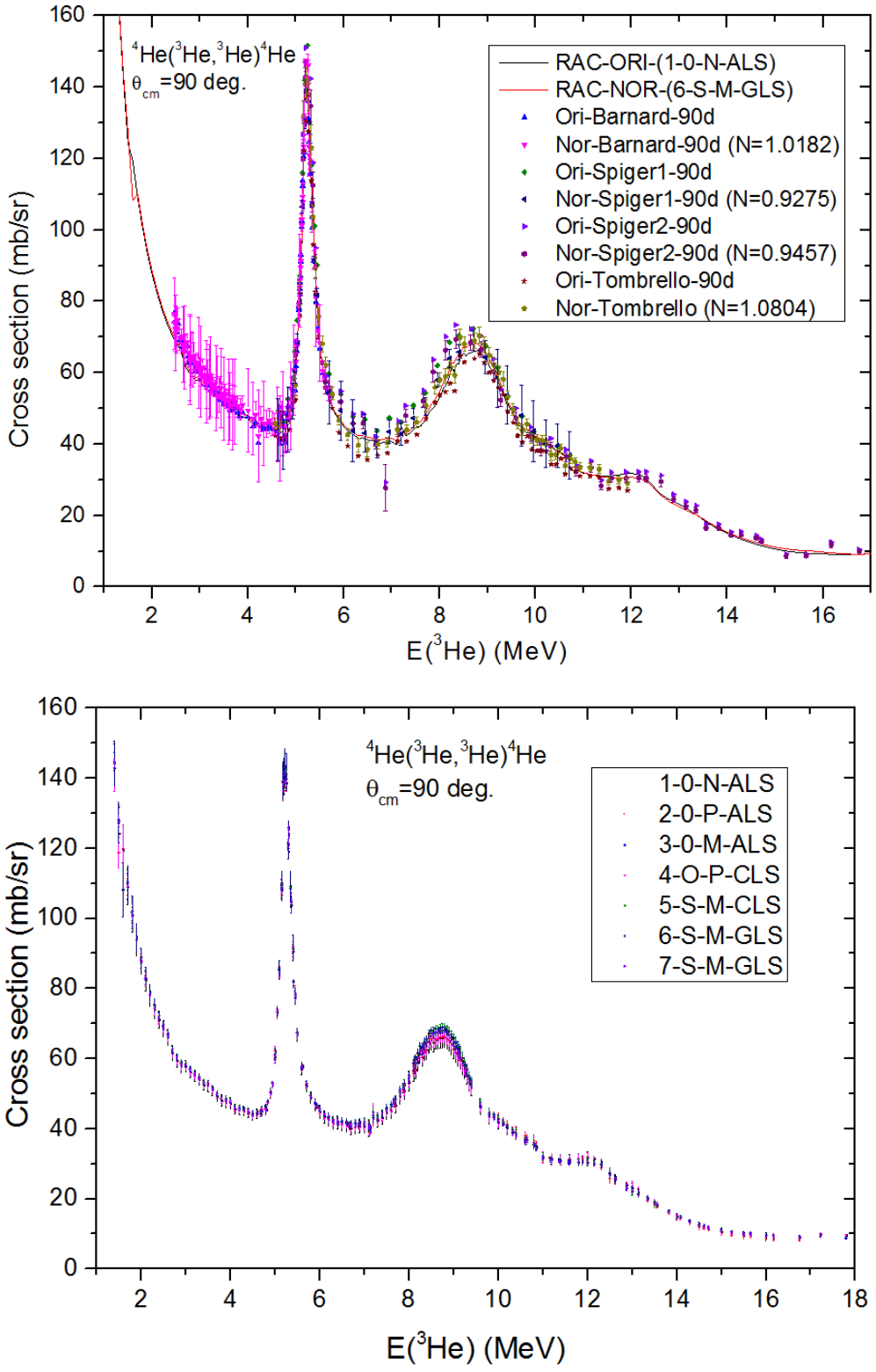

FIG 6.35. (Top) Fit for the excitation function of ^{4}He(^{3}He,^{3}He)^{4}He at 90 degrees. The fit is very good. The data from 14 to 18 MeV are in the non-resolved resonance region, so the good results show that RAC has the ability to analyze experimental data in the non-resolved resonance region. (Bottom) The calculated excitation functions of obtained with the seven schemes. The results agree both in magnitude and shape.

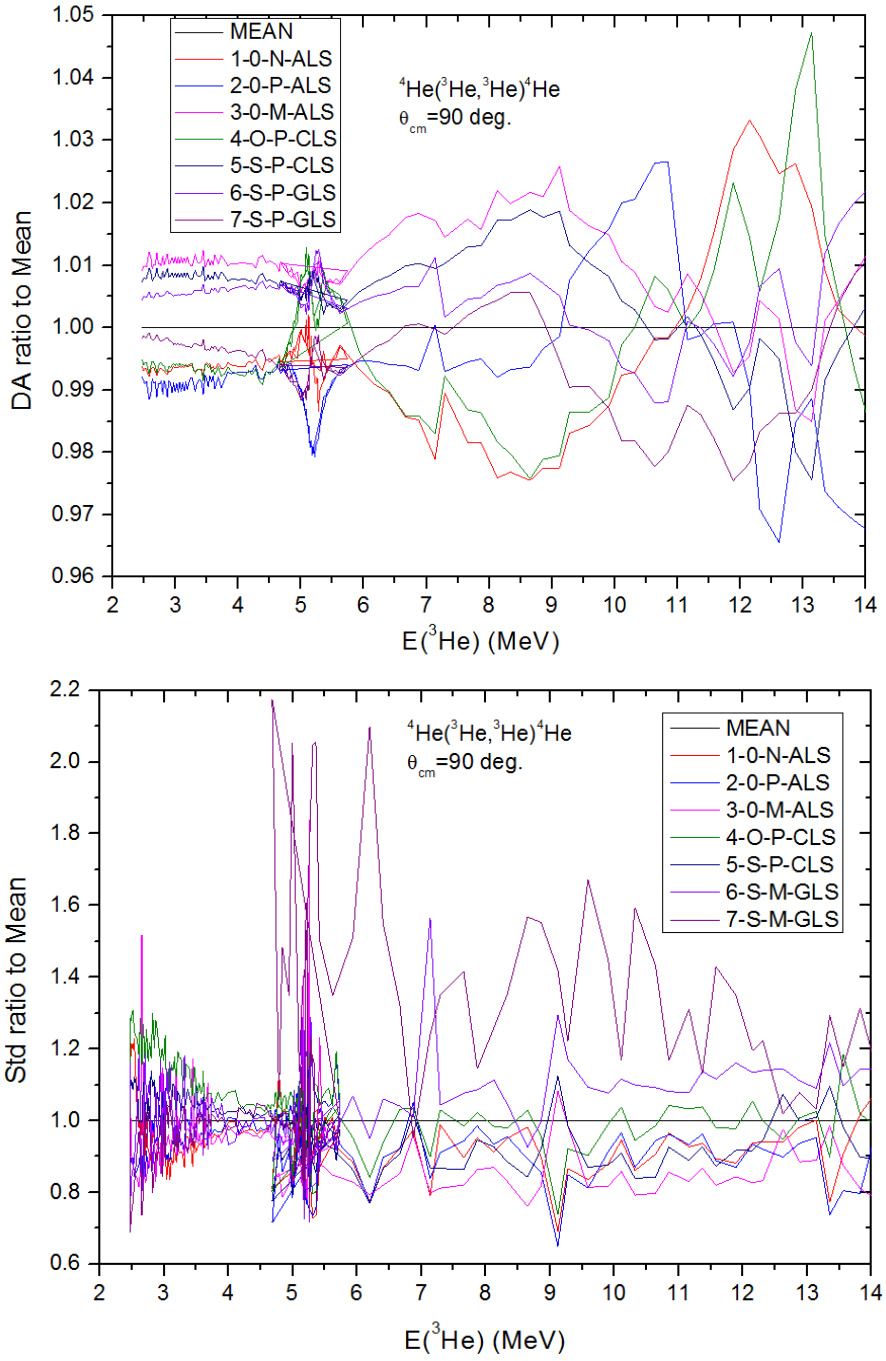

FIG 6.36. (Top) The ratio of calculated excitation functions of $^4He(^3He,^3He)^4He$ at 90 degrees for the seven schemes to their mean value. The maximum of the ratio ranges from 0.99 to 1.01, so it is fair to say that all seven schemes are acceptable. (Bottom) The ratio of the STD of the seven schemes to their mean value. The results show rather large differences. The STD obtained with (4-O-P-CLS) is the largest one for E_p below 4 MeV. This is because in this case the original systematic errors are considered in the diagonal elements of the experimental covariance matrix. The STDs of (6-S-M-GLS) and (6-S-M-GLS) are the largest ones for E_p greater than 4.5 MeV. The explanation is given in the text.

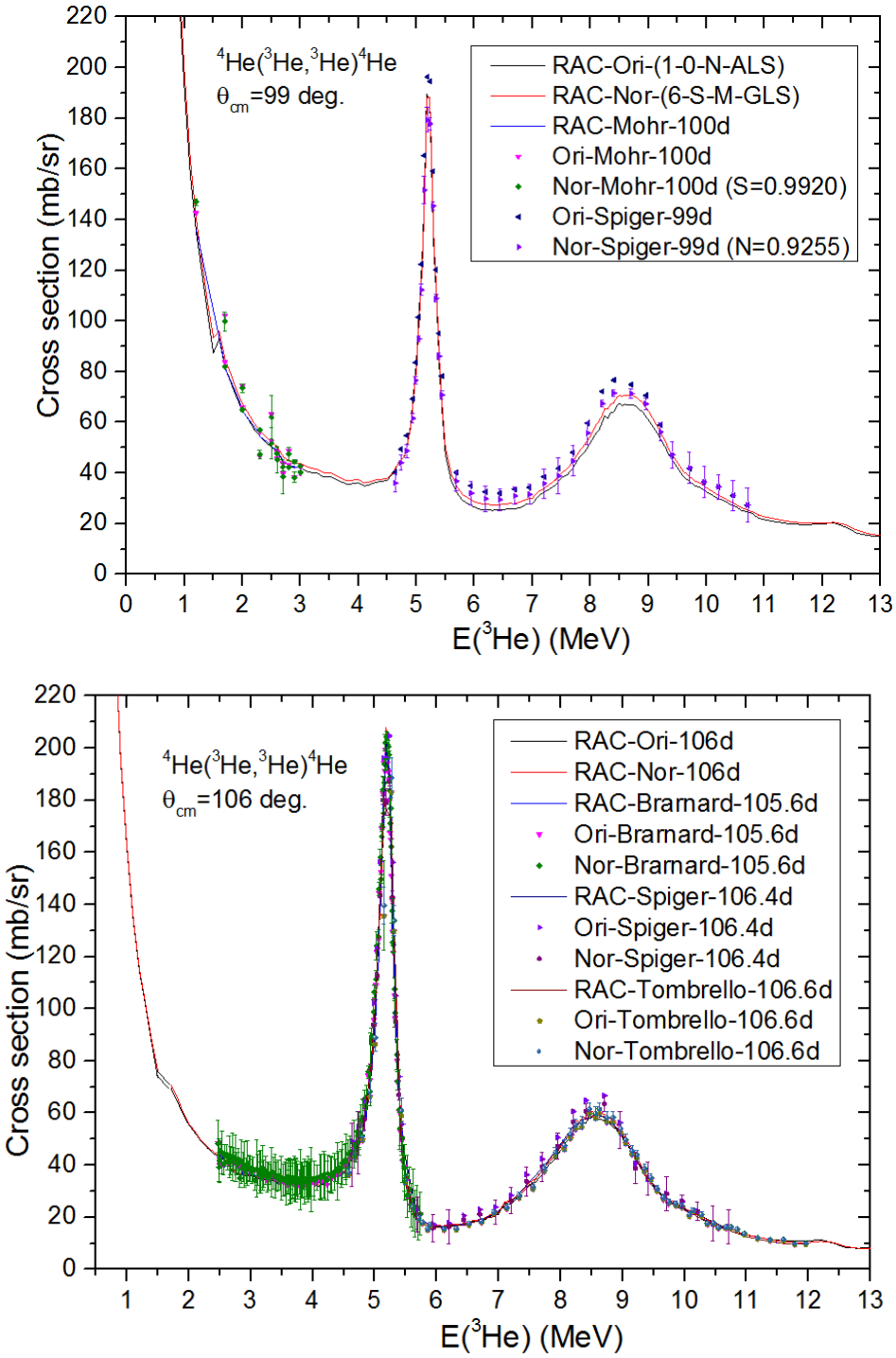

FIG 6.37. (Top) Fit for the excitation function of ^{4}He(^{3}He,^{3}He)^{4}He at about 99 degrees. The fit is very good. (Bottom) The same but at about 106 degrees. Again, the fit is very good.

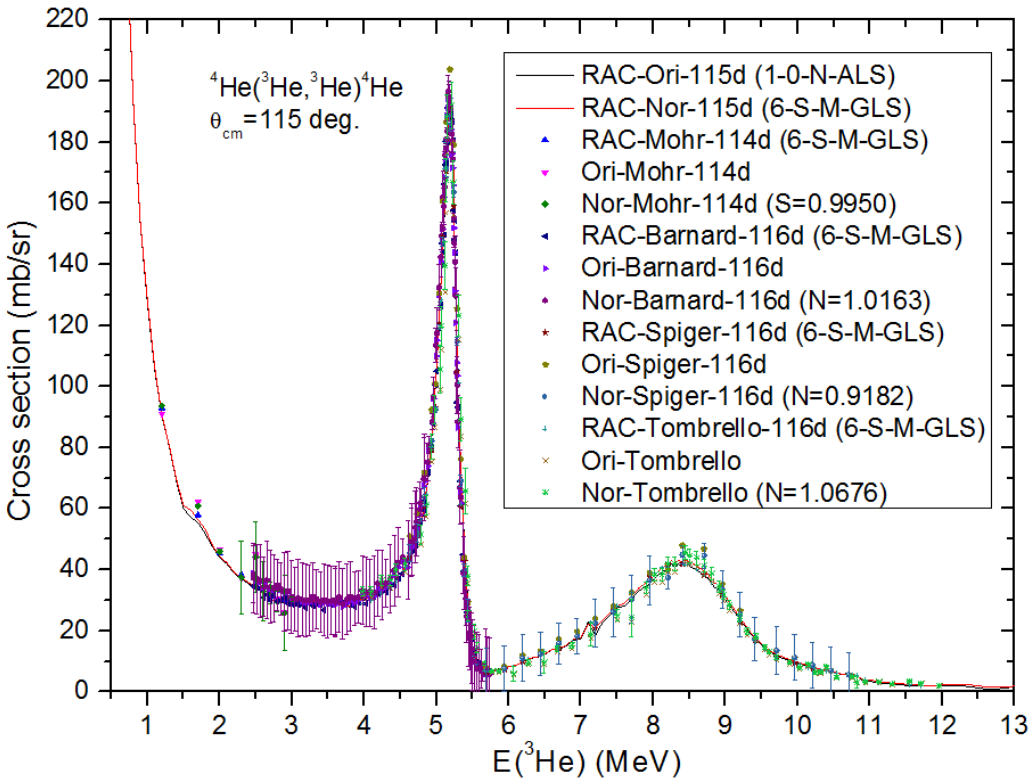

FIG 6.38. Fit for the excitation function of ^{4}He(^{3}He,^{3}He)^{4}He at about 115 degrees. The fit is very good.

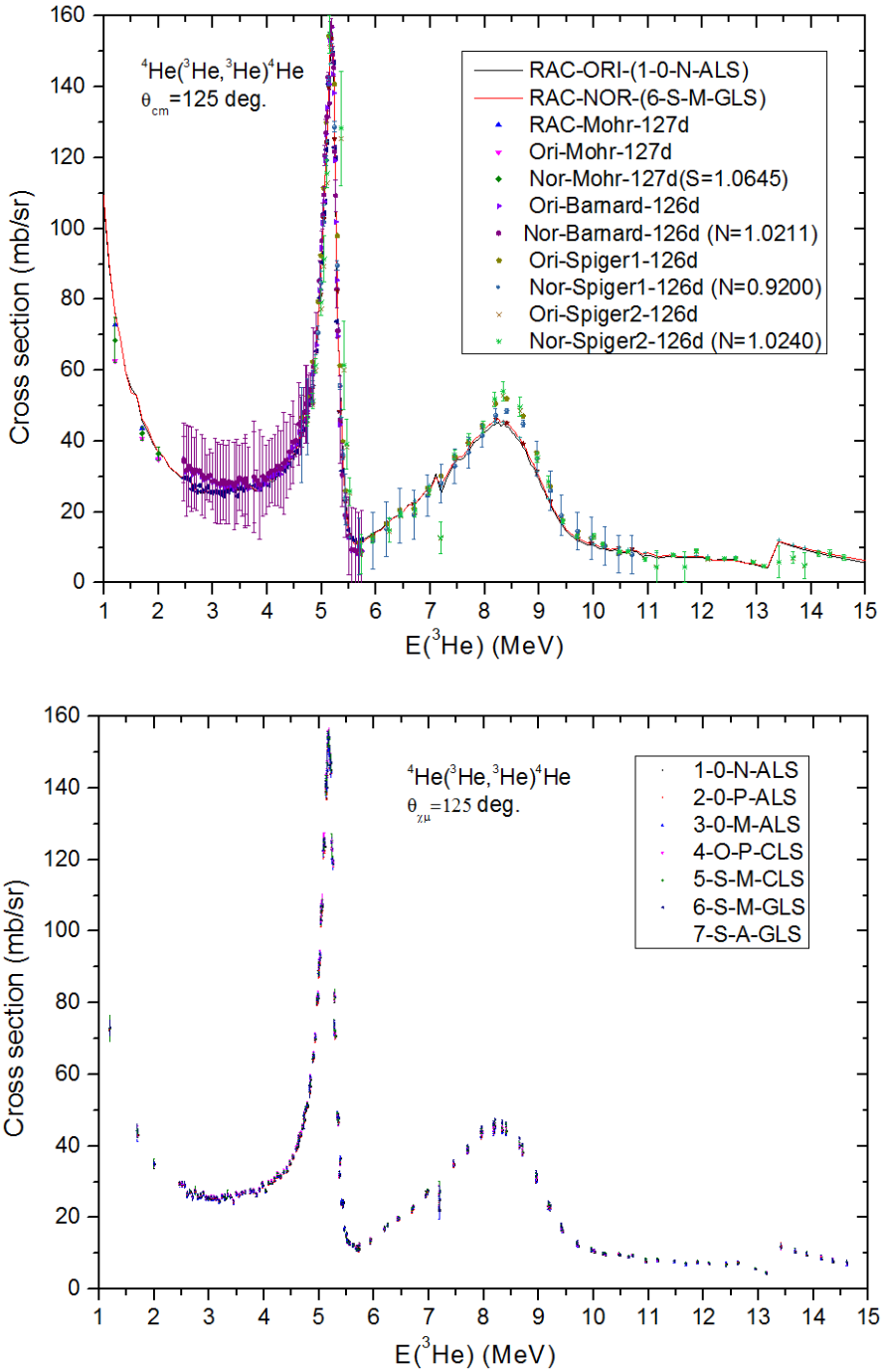

FIG 6.39. (Top) Fit for the excitation function of ^{4}He(^{3}He,^{3}He)^{4}He at 125 degrees. The fit is very good. (Bottom) The corresponding calculated excitation functions obtained with the seven schemes. The results agree both in magnitude and shape.

The figures show that the global fitting of the ^{7}Be system depends strongly on the reproduction of the four groups of experimental data on ^{4}He(^{3}He,^{3}He)^{4}He (Mohr [25], Barnard [21], Tombrello [26], Spiger [24]). These data have been measured at energies ranging from 1.0 to 18 MeV, so fitting them well requires an accurate R-matrix analysis of widely varying cross sections for all the open channels for which data exist. This in turn requires a suitable and reliable R-matrix code.

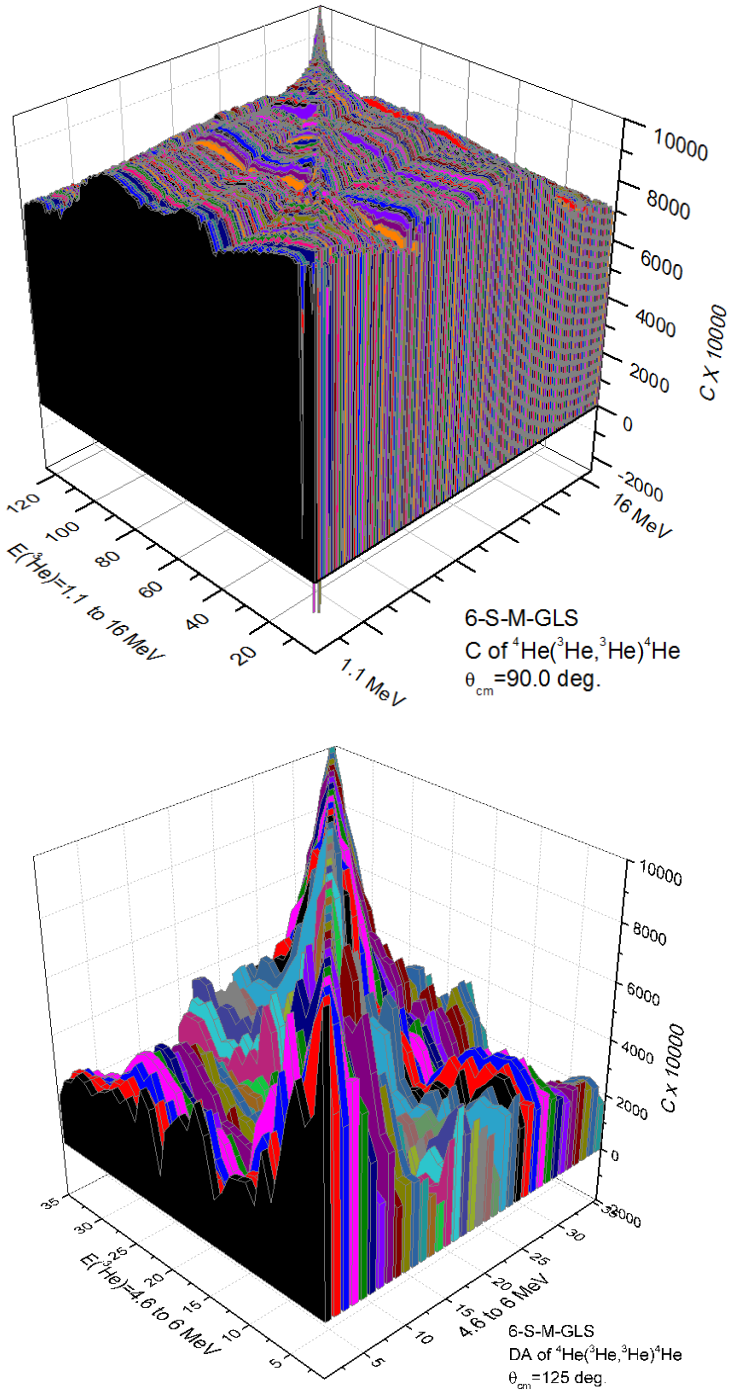

FIG 6.40. (Top) Correlation factor (C) for the excitation function of ^{4}He (^{3}He,^{3}He)^{4}He at 90 degrees for E_{3He} = 1.1 MeV to 16 MeV obtained with (6-S-M-GLS). The correlations are very strong. (Bottom) The same but at 125 degrees and for E_{3He} = 4.6 MeV to 6 MeV. In this case the correlations are not very strong.

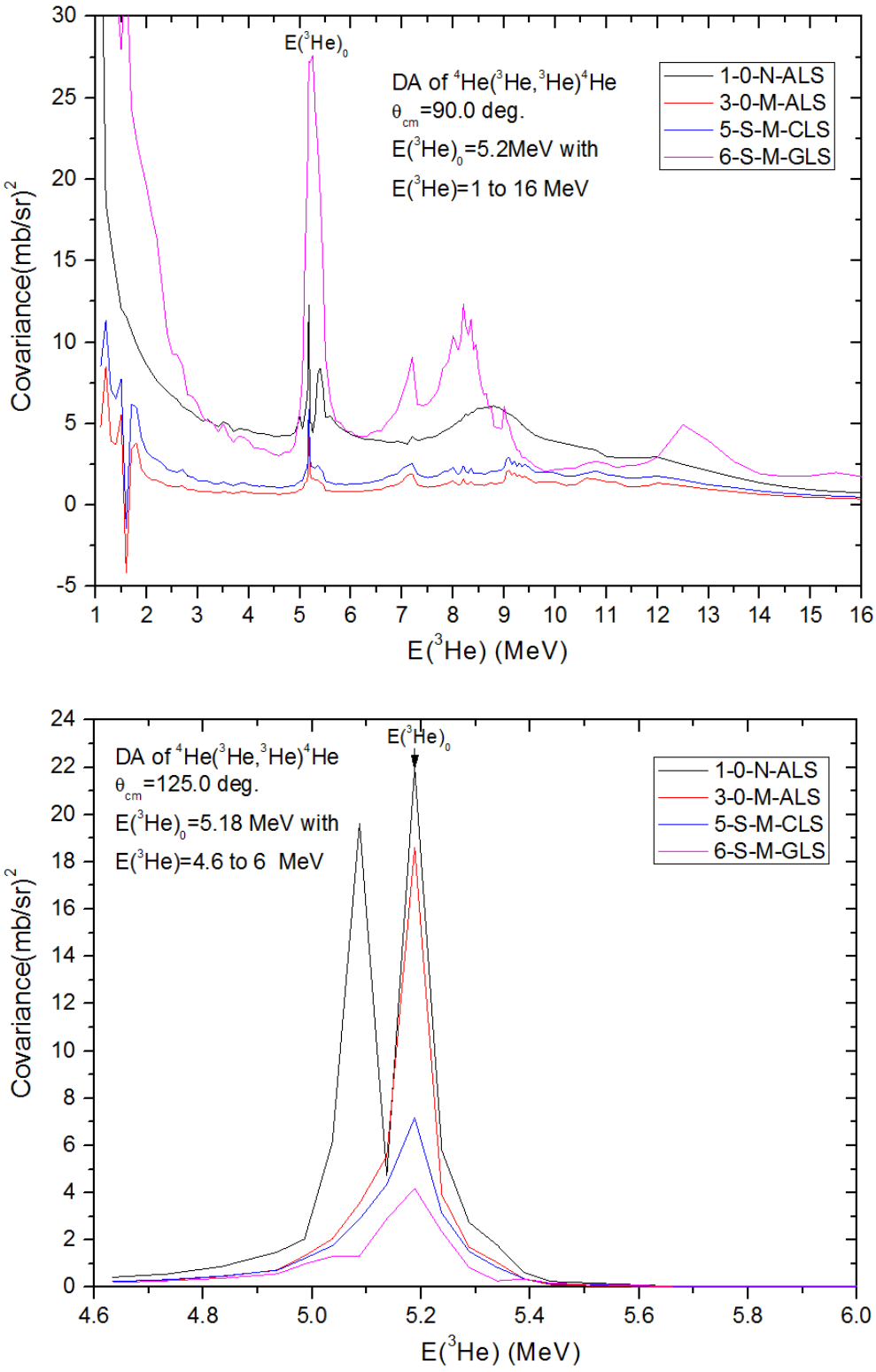

FIG 6.41. (Top) Covariance matrix elements for the excitation function of $^4He(^3He,^3He)^4He$ at 90 degrees and for E_{3He0} = 5.2 MeV with E_{3He}=1 to 16 MeV obtained with the 4 schemes (1-0-N-ALS), (3-0-M-ALS), (5-S-M-CLS) and (6-S-M-GLS). It should be noted that (6-S-M-GLS) has the largest covariance matrix elements. (Bottom) The same but at 125 degrees and for E_{3He0} = 5.18 MeV with E_{3He} = 4.6 to 6 MeV. Here the scheme (6-S-M-GLS) has the smallest covariance matrix elements.

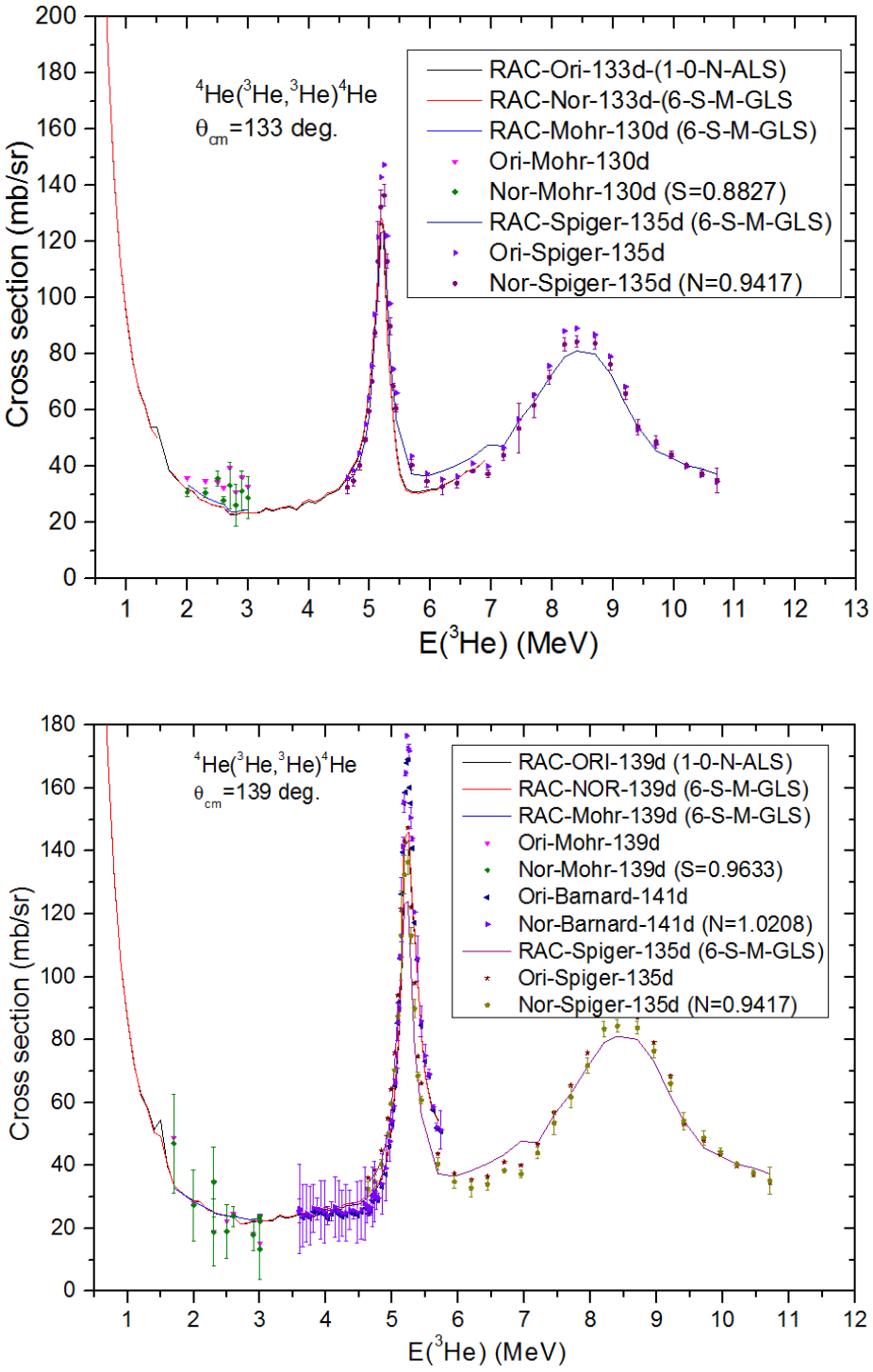

FIG 6.42. (Top) Fit for the excitation function of ^{4}He(^{3}He,^{3}He)^{4}He at 133 degrees. The fit is very good. (Bottom) The same but at 139 degrees. Again, the fit is very good.

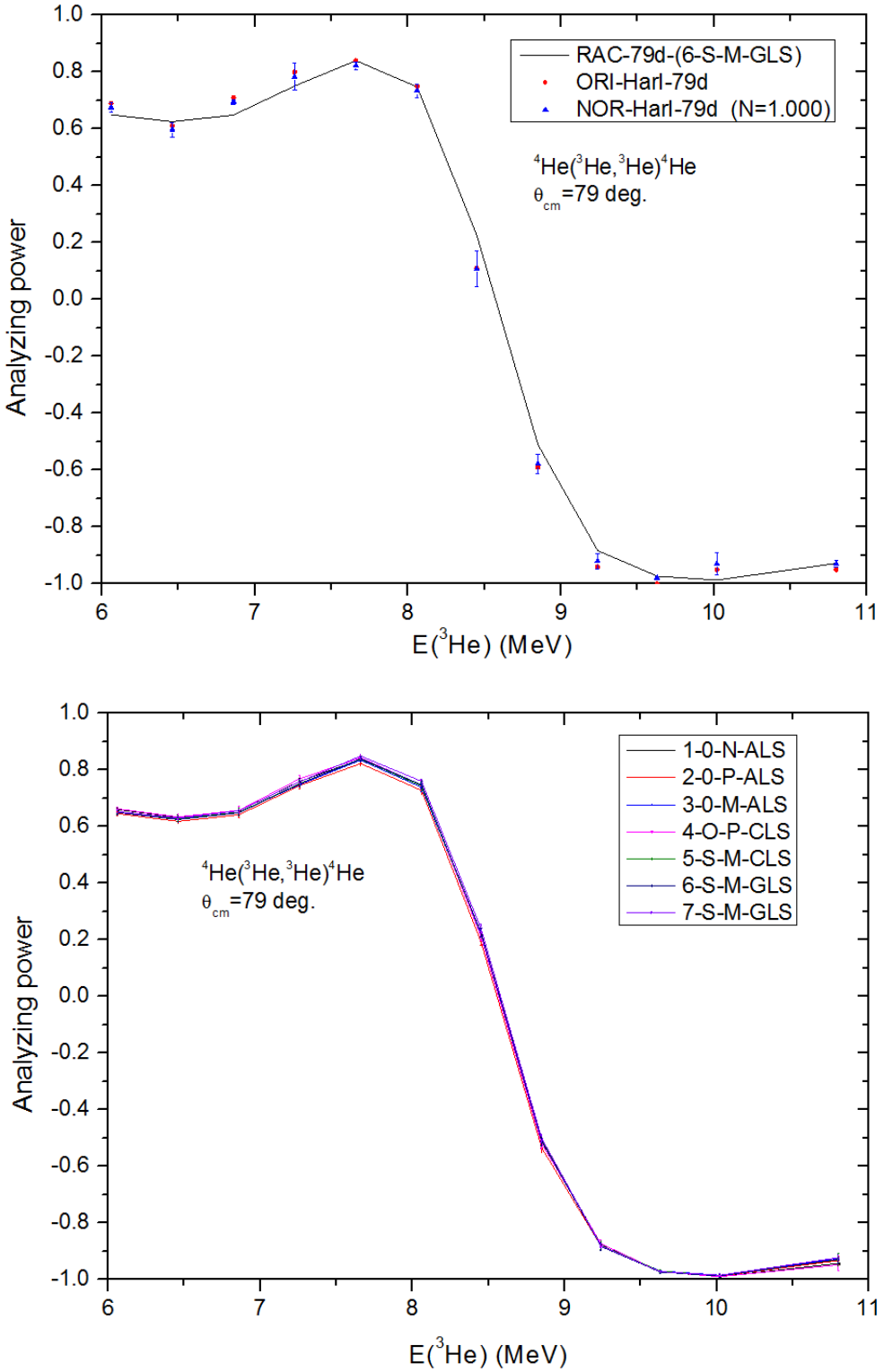

FIG 6.43. (Top)Fit for the analyzing power of ^{4}He(^{3}He,^{3}He)^{4}He at 79 degrees. N = 1.000 means that the data are not normalized. The fit is very good. (Bottom) Corresponding calculated analyzing powers obtained with the seven schemes. The results agree in magnitude and shape.

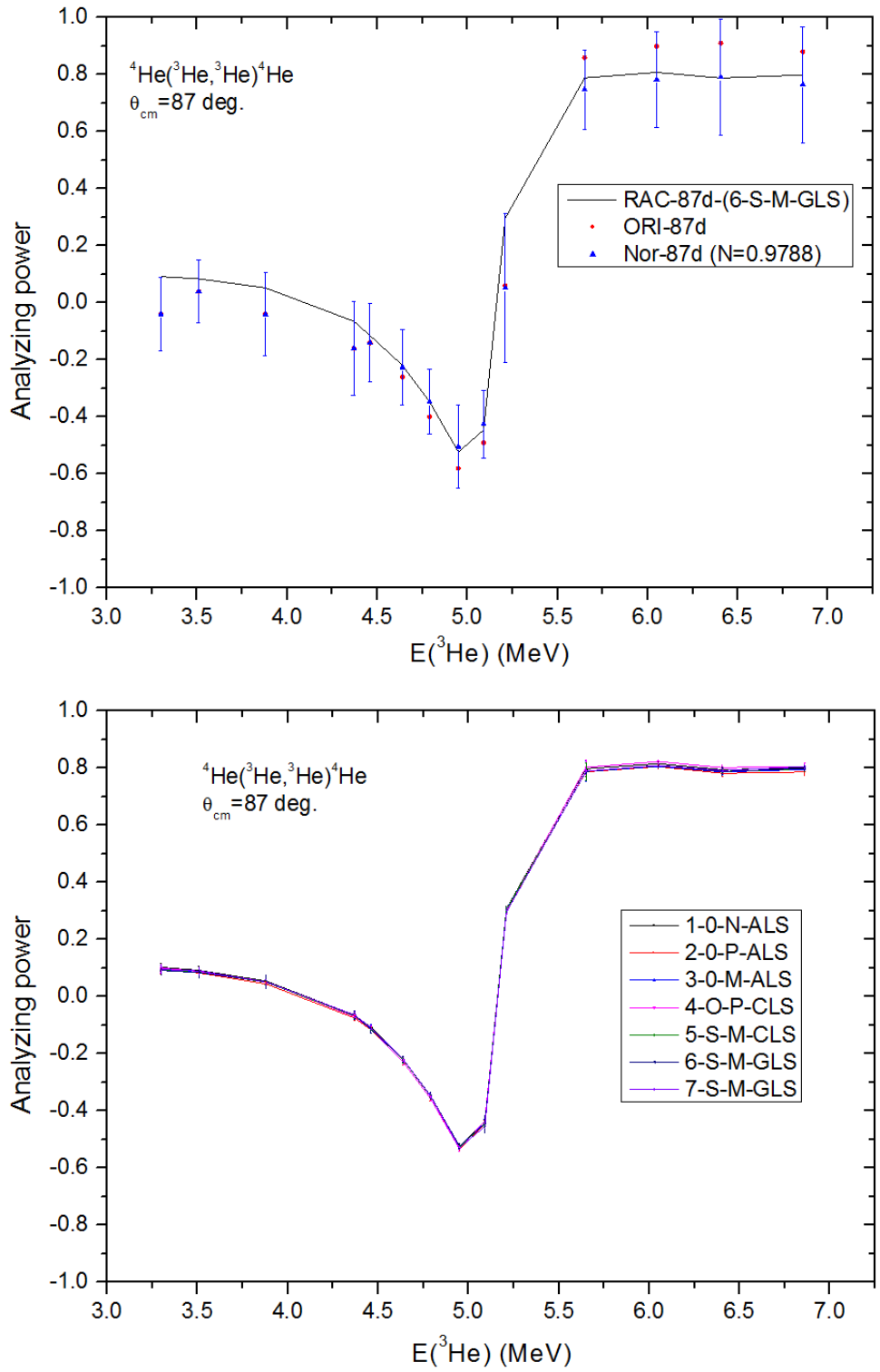

FIG 6.44. (Top) Fit for the analyzing power of ^{4}He(^{3}He,^{3}He)^{4}He at 87 degrees. N = 0.9788 is the normalization factor. The fit is very good. (Bottom) Corresponding calculated analyzing powers obtained with the seven schemes. The magnitudes agree and the shapes are identical.

6.3.8. $^{4}He(^{3}He,p)^{6}Li$

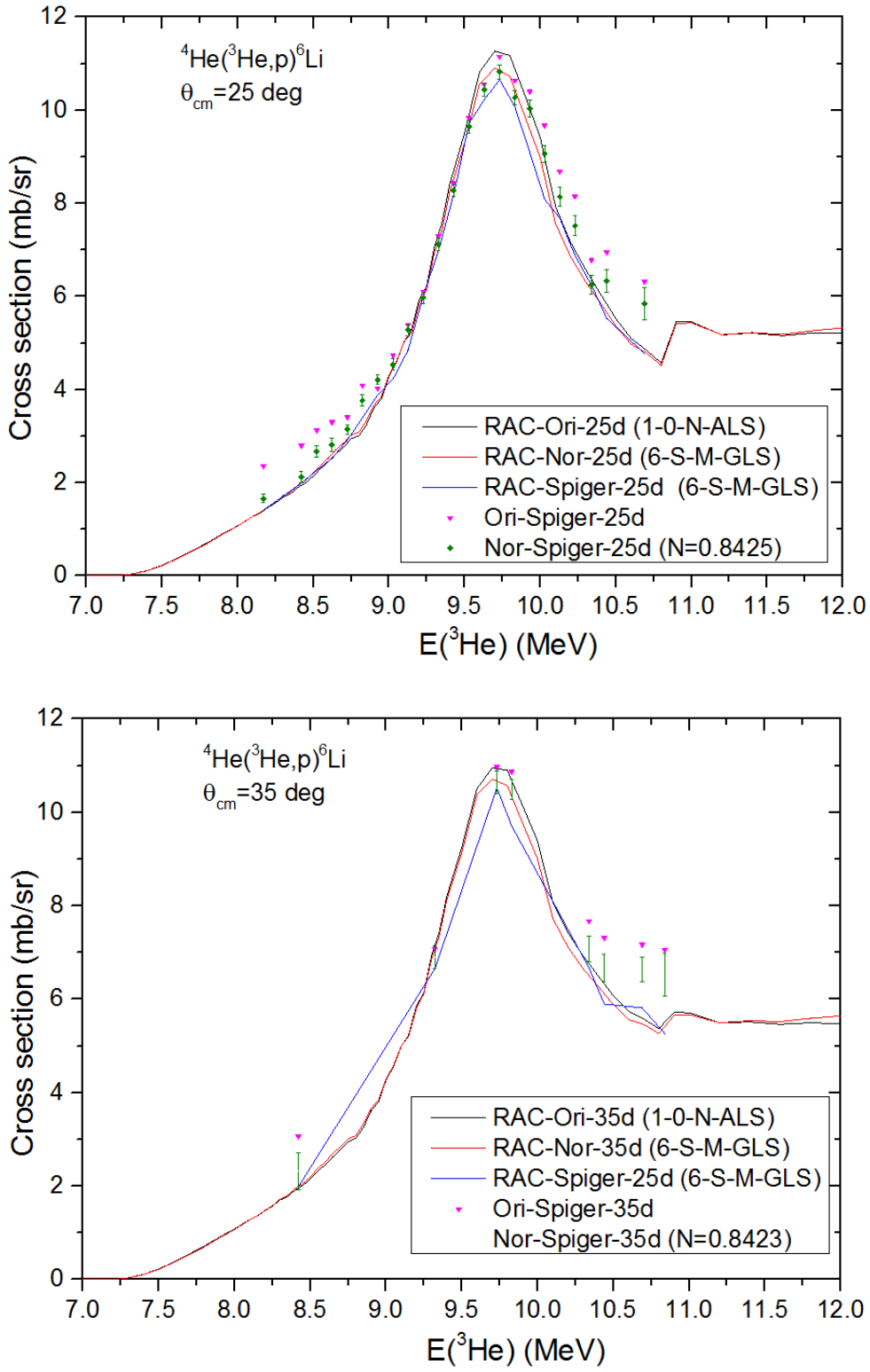

FIG 6.45. (Top) Fit for the excitation function $^{4}He(^{3}He,p)^{6}Li$ at about 25 degrees. N = 0.8425 is the normalization factor. The fit is good. (Bottom) The same but at 35 degrees.

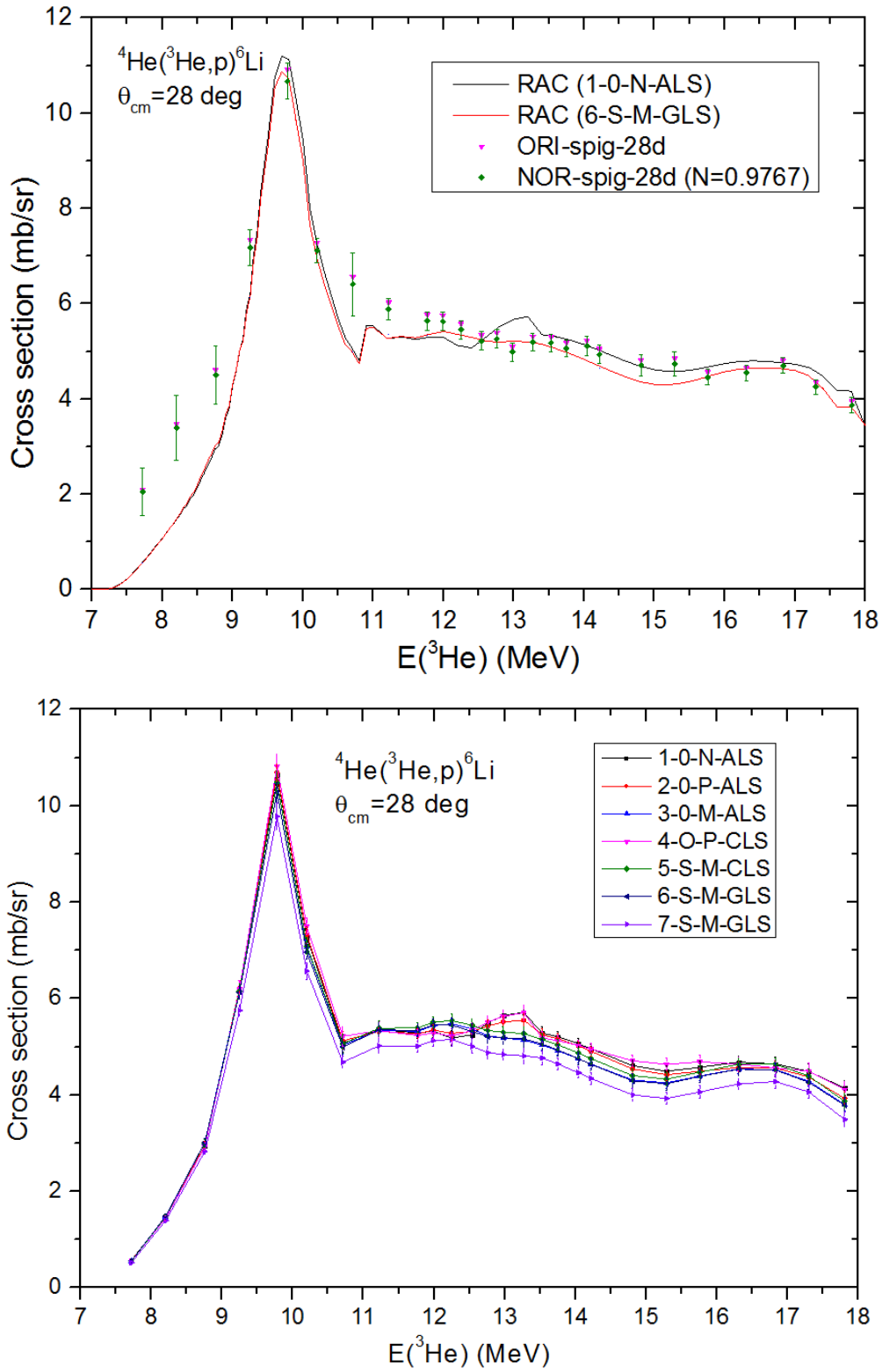

FIG 6.46. (Top) Fit for the excitation function of ^{4}He(^{3}He,p)^{6}Li near 28 degree. N = 0.9767 is the normalization factor. The fit looks good. The data from 14 to 18 MeV are in the non-resolved resonance region, which shows that RAC has the ability to analyze experimental data in the non-resolved resonance region as well. (Bottom) Corresponding calculated excitation functions obtained with the seven schemes. The results are in reasonable agreement both in magnitude and shape. The scheme (7-S-M-GLS) gives the smallest values.

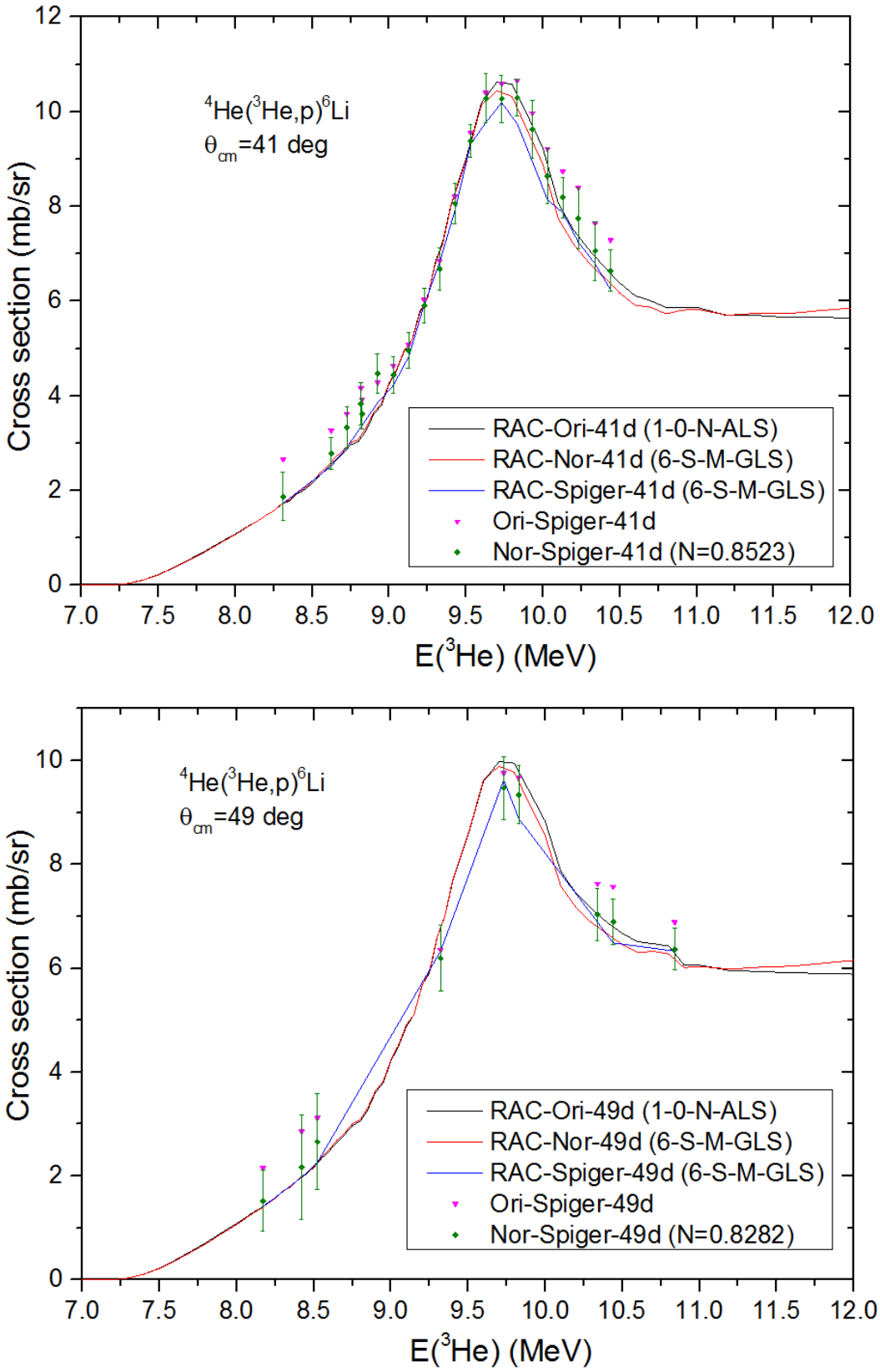

FIG 6.47. (Top) Fit for the excitation function ^{4}He(^{3}He,p)^{6}Li at 41 degrees. N = 0.8523 is the normalization factor. The fit looks good. (Bottom) The same but at 49 degrees.

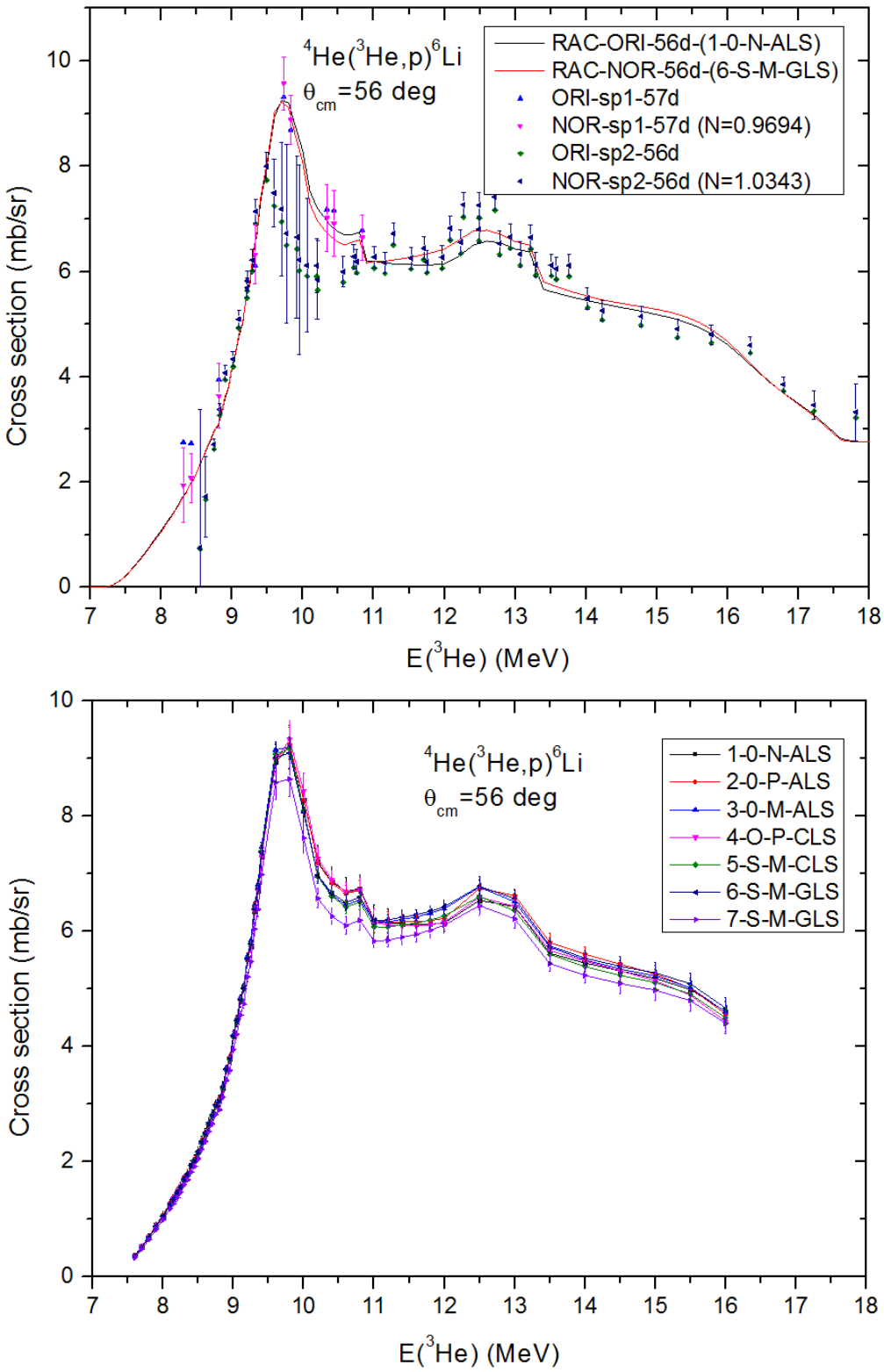

FIG 6.48. (Top) Fit for the excitation function of ^{4}He(^{3}He,p)^{6}Li at 56 degrees. N = 0.9694, 1.0343 are the normalization factors. The fit looks good. The data from 14 to 18 MeV are in the non-resolved resonance region, which proves that RAC is able to analyze the experimental data in the non-resolved resonance region. (Bottom) Corresponding calculated excitation functions using the seven schemes. The results agree well in magnitude and less in shape. The scheme (7-S-M-GLS) gives the smallest values.

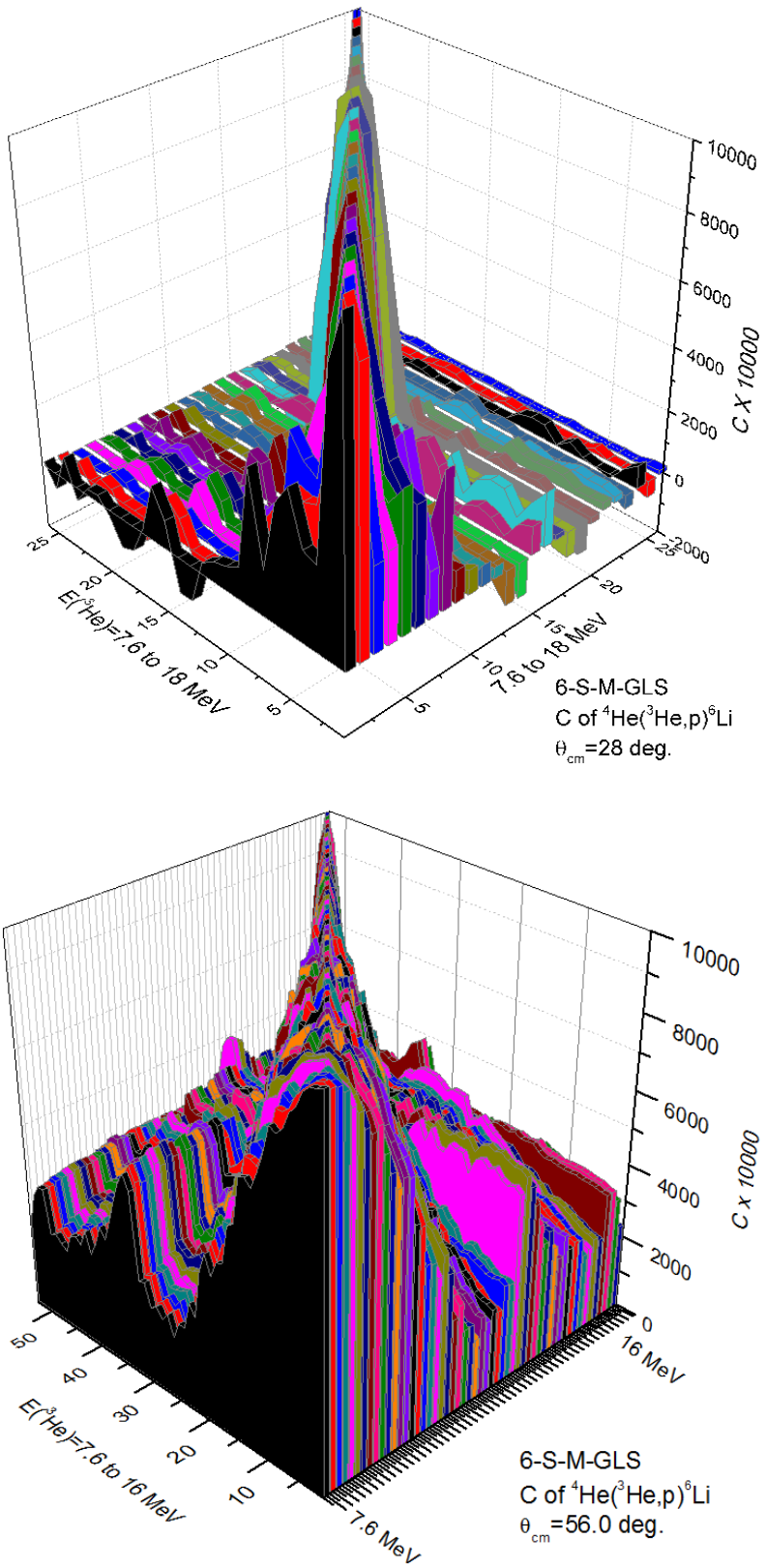

FIG 6.49. (Top) Correlation factor (C) for the excitation function of $^{3}He(^{4}He,p)^{6}Li$ at 28 degrees, E_{3He} = 7.6 MeV to 16 MeV, obtained with the scheme (6-S-M-GLS). (Bottom) The same but at 56 degrees and E_{3He} = 7.6 MeV to 16 MeV.

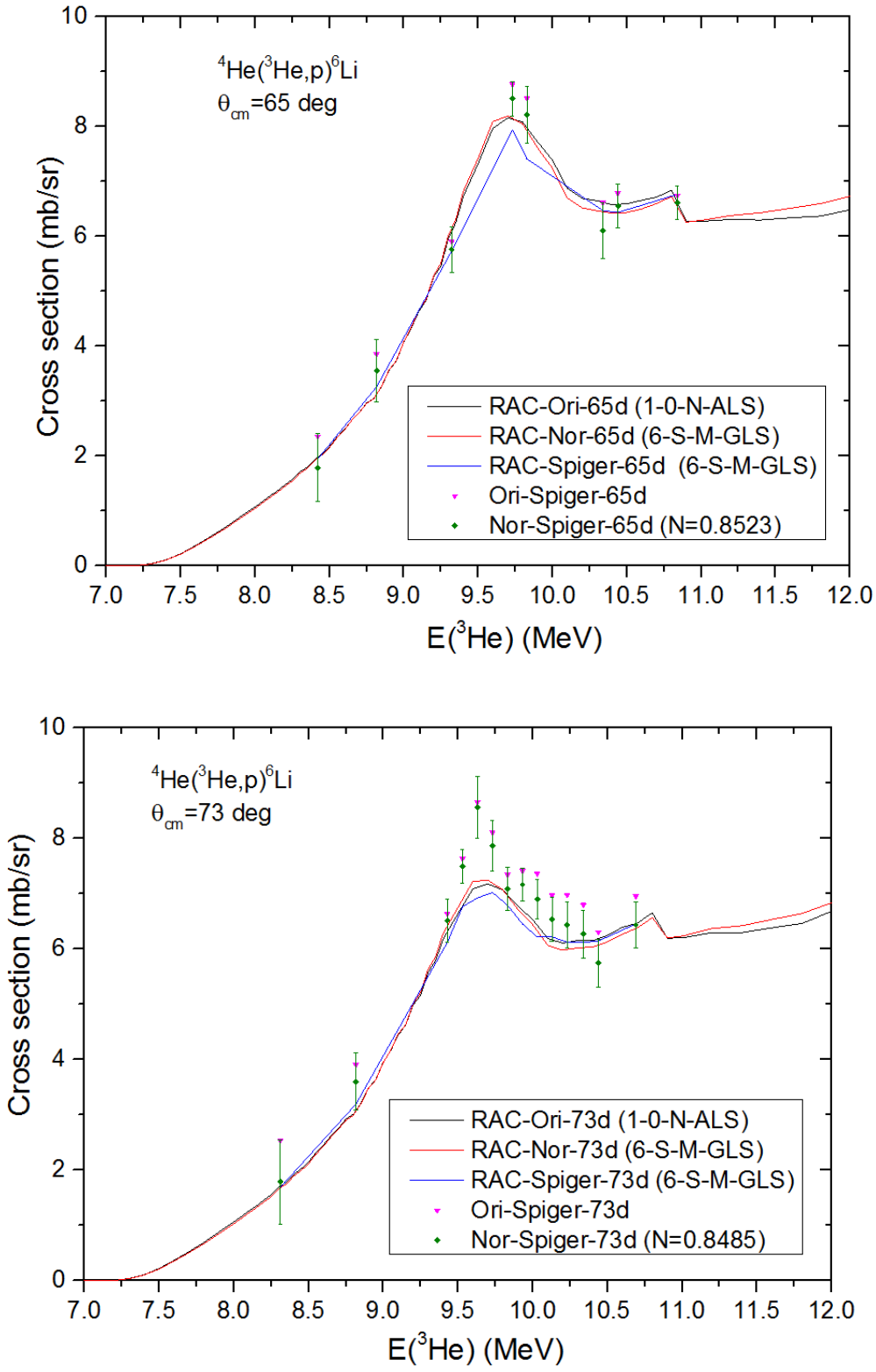

FIG 6.50. (Top) Fit for the excitation function of ^{4}He(^{3}He,p)^{6}Li at 65 degrees. The fit looks good. (Bottom) The same but at 73 degrees.

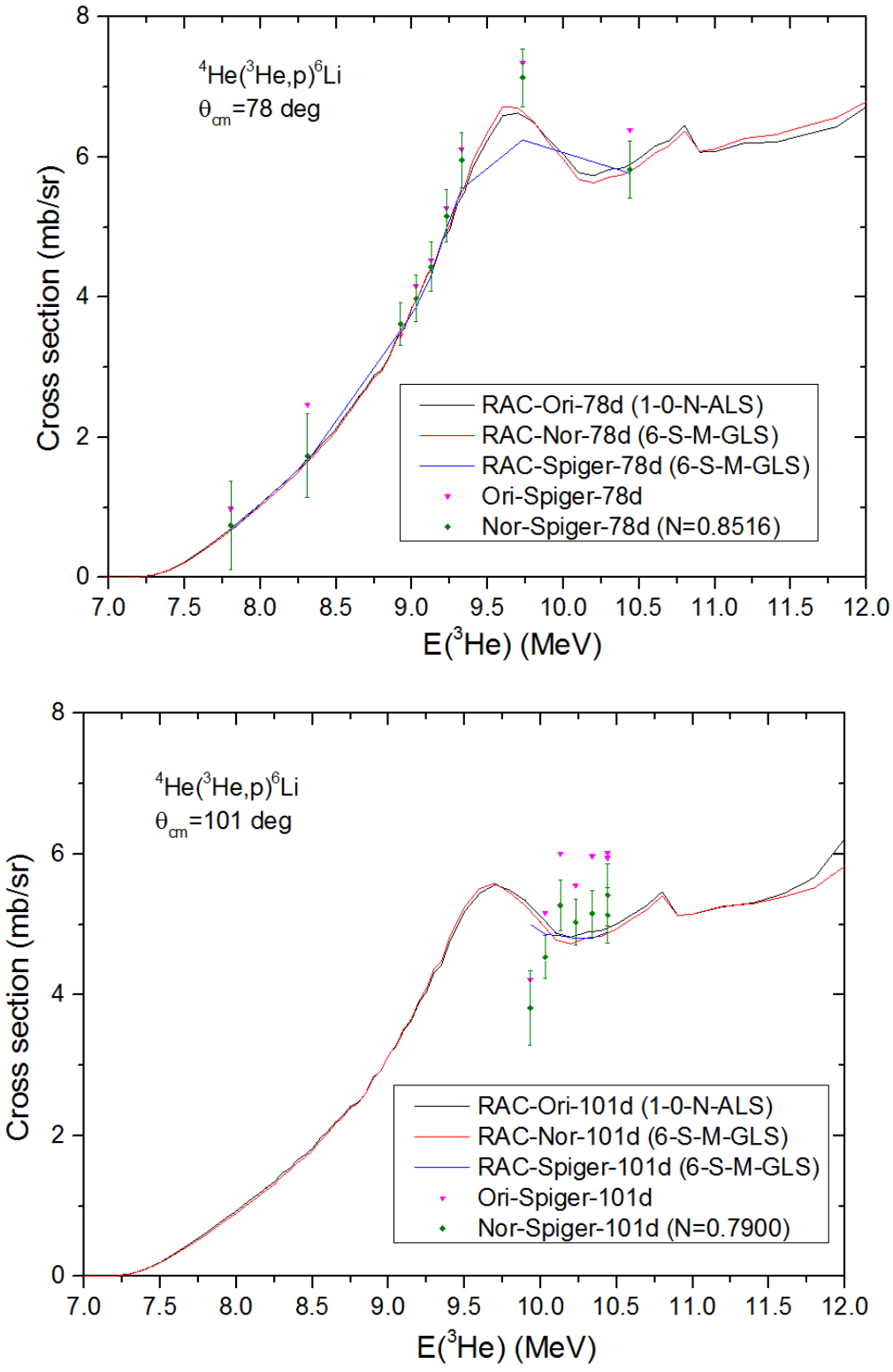

FIG 6.51. (Top) Fit for the excitation function of ^{4}He(^{3}He,p)^{6}Li at 78 degrees. The fit looks good. (Bottom) The same but at 101 degrees.

6.3.9. $^{4}He(^{3}He,p_1)^{6}Li^{*}$

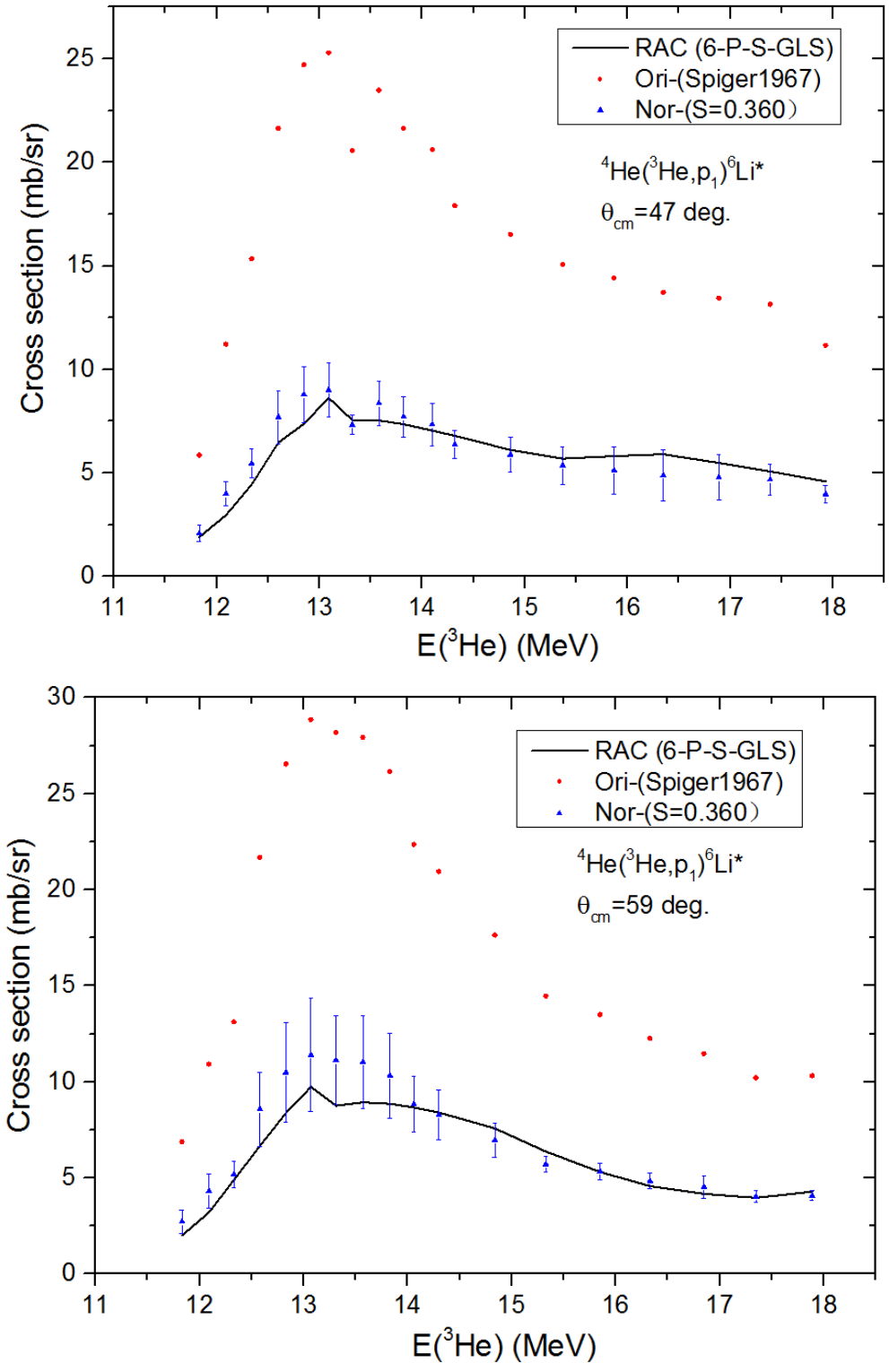

FIG 6.52. (Top) Fit for the excitation function of $^{4}He(^{3}He,p_1)^{6}Li^{*}$ at 47 degrees. The fit looks good, but these are shape data. (Bottom) The same but at 59 degrees. Again, the fit looks good, but these are shape data.

6.3.10. $^{4}He(^{3}He,\gamma_0)^{7}Be$

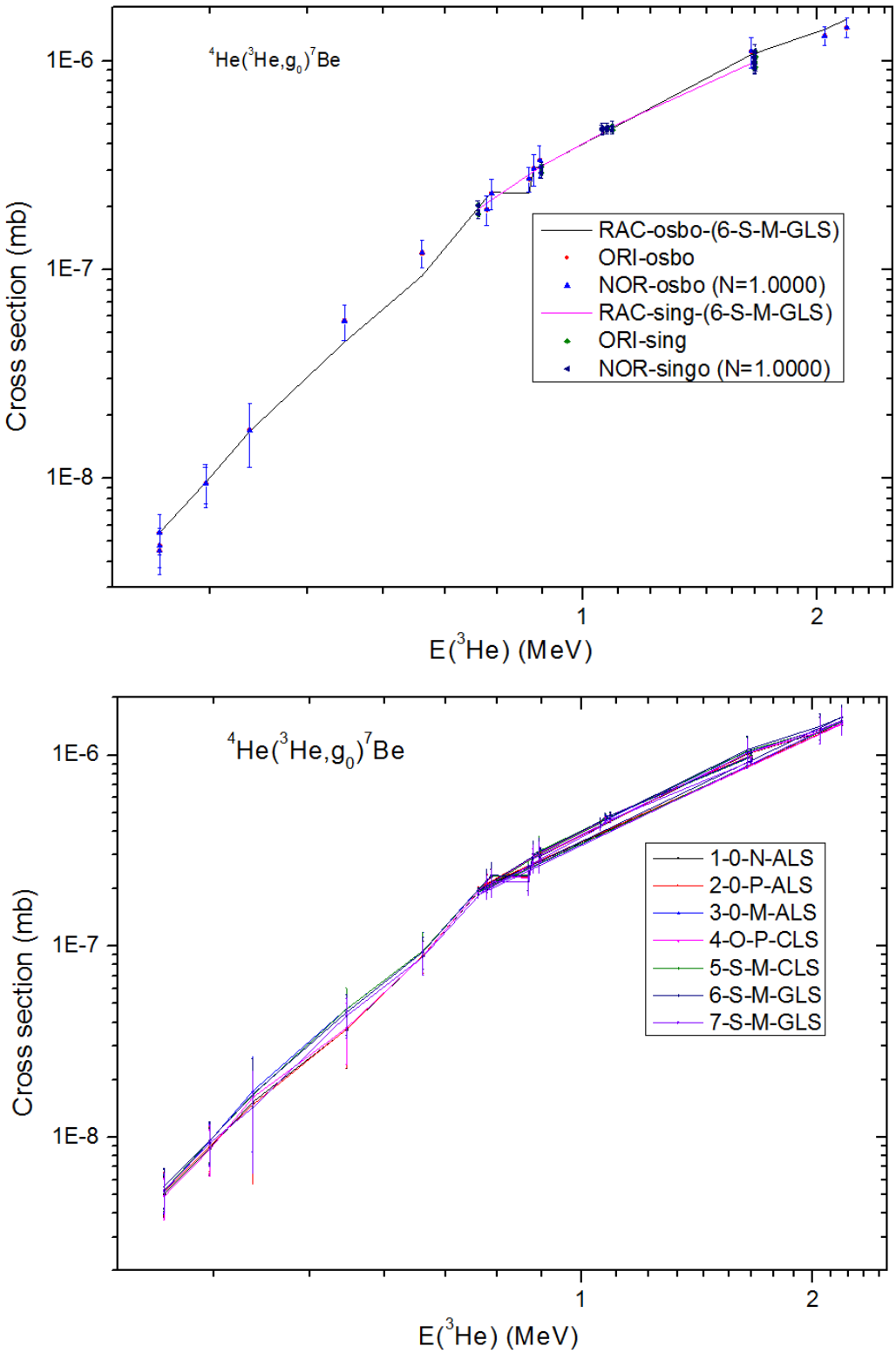

FIG 6.53. (Top) Fit for integrated cross sections of $^{4}He(^{3}He,\gamma_0)^{7}Be$. N = 1.000 means no normalization of data. The fit looks good. (Bottom) Calculated integrated cross sections using the seven schemes. The results agree reasonably in both magnitude and shape.

6.3.11. $^{4}He(^{3}He,\gamma_1)^{7}Be^{*}$

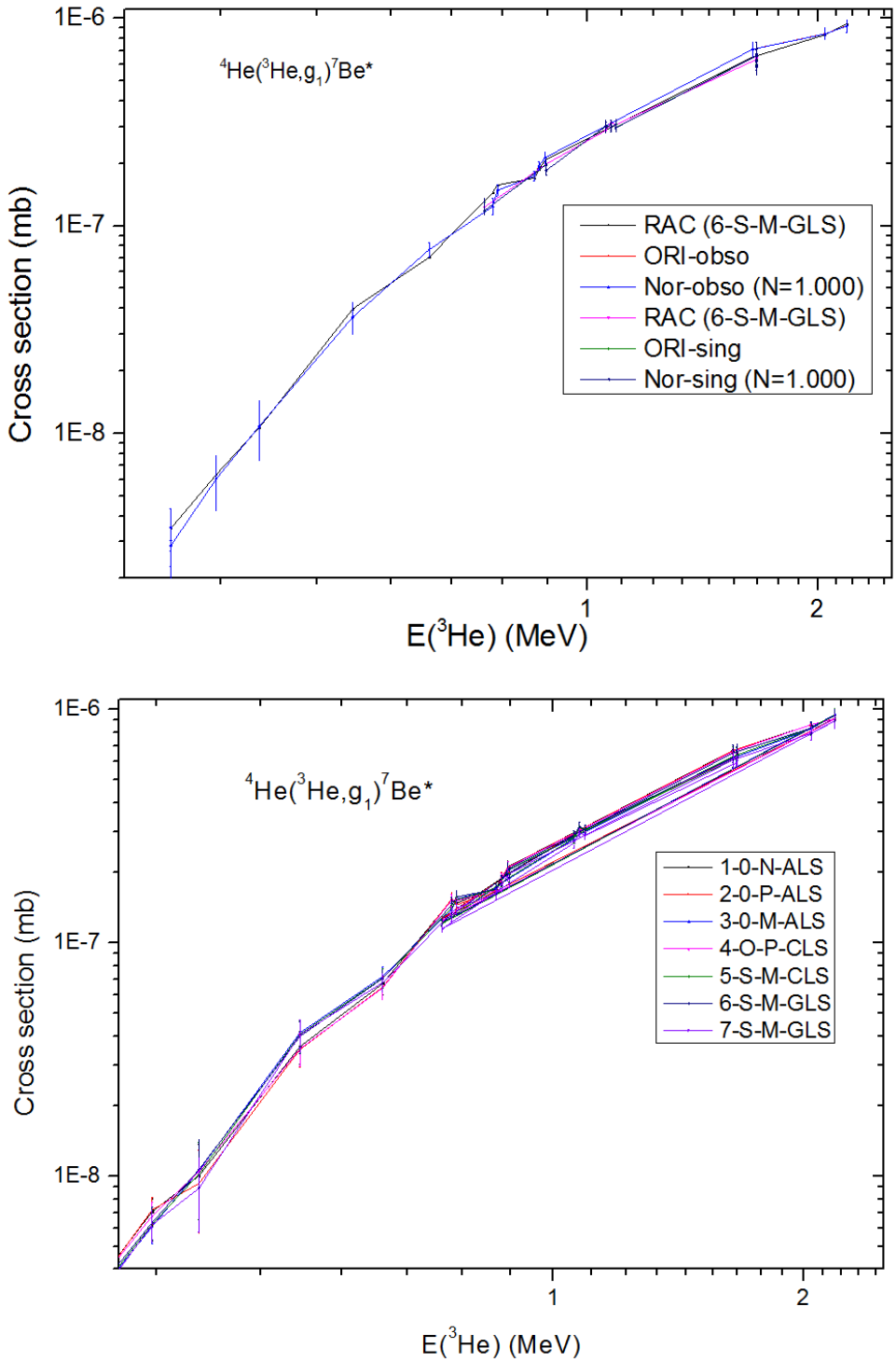

FIG 6.54. (Top) Fit for integrated cross sections of $^{4}He(^{3}He,\gamma_1)^{7}Be^{*}$. N = 1.000 means no normalization of experimental data. The fit looks good. (Bottom) Calculated integrated cross sections using the seven schemes. The results agree reasonably in magnitude and shape.

7. GLOBAL FITTING OF ^{7}Be SYSTEM (GLS)

In this section we present the final results for the evaluation of the ^{7}Be system, in which we have fitted all the available and useful experimental data in the energy region extending to 20 MeV. Each experimental data group is discussed separately in the following subsections in order to highlight the role of the data in the global fit, the status of the original data, the normalized values and the final fitted values.

We have performed a 'global fitting' which means that with we have used one R-Matrix parameter set to fit all the experimental data available simultaneously. The advantages of 'global fitting' have been detailed in the previous sections 4, 5 and 6. One other important advantage of a global fit is that the evaluation is done within the same approach/model and therefore is consistent for all the different experimental data. This ensures that unitarity is respected and there is no need to make any adjustments to meet it.

For the global fitting we have employed the Reduced R-Matrix theory (see Section 3) combined with the GLS statistical method in Section 4.

The selection of the level scheme (see Section 5) has been done as follows: for every J^{π} one background level with positive higher energy is introduced, and for some J^{π} one distant background level negative distant energy is assumed. The iterative fitting procedure will sort out if any one of the initial parameters is needed or not, and in case it is not needed, i.e. it does not contribute to the minimization of χ^2, then it will be removed from the next iteration. The goal is to get an improved fit to the entire database with every iteration.

The experimental data used in the global fit were taken from the EXFOR database. They include experimental data for the following reactions and energies:

^{6}Li(p,p)^{6}Li, ^{6}Li(p,^{3}He)^{4}He, ^{6}Li(p,p$_1$)^{6}Li*,

^{6}Li(p,p$_2$)^{6}Li**, ^{6}Li(p,γ_0)^{7}Li, ^{6}Li(p,γ_1)^{7}Li*,

for E_p = 0.4 to 22.5 MeV;

^{4}He(^{3}He,^{3}He)^{4}He, ^{4}He(^{3}He,p)^{6}Li, ^{4}He(^{3}He,p$_1$)^{6}Li*,

^{4}He(^{3}He,γ_0)^{7}Li, ^{4}He(^{3}He,γ_1)^{7}Li*,

for $E_{^3He}$ = 1.0 to 22.6 MeV.

The experimental database consists of both cross section and analyzing powers, about 6709 data points in total, which means nearly all the valuable and useful data have been used. Some details of the composition of the experimental database are given in Tables 7.1, 7.2.

TABLE 7.1. Reaction channels information in this work

Channel	A_C(fm)	If-search	Step-%	L_{max}	Threshold (MeV)
'P,^{6}Li'	0.39439688299650	y	0.2	4	0.000000
'^{3}He,^{4}He'	0.42415108711860	y	0.2	5	4.019800
'P1,^{6}Li*'	0.39439688299650	y	0.2	6	-2.186000
'P2,^{6}Li*'	0.39439688299650	y	0.2	7	-3.563000
'G0,^{7}Be'	0.39439688299650	y	0.2	2	5.610000
'G1,^{7}Be*'	0.39439688299650	y	0.2	2	5.180000
'RED-CH'	Used to represent 'P3,^{6}Li* ' and other channels				

TABLE 7.2. Reaction channels and data information

Reaction channel	Type of data	Energy range (MeV)	Data Groups	Data points	Final mean χ^2 /Comment
^{6}Li(p,p)^{6}Li	DA	0.3 to 14.1	8	2697	
^{6}Li(p,^{3}He)^{4}He	CS	0.1 to 3	4	92	
^{6}Li(p,^{3}He)^{4}He	DA	0.1 to 3	4	1134	
^{6}Li(p,^{3}He)^{4}He	AY	0.5 to 3	1	121	
^{6}Li(p,p1)^{6}Li*	CS	3 to 10.1	1	12	
^{6}Li(p,p1)^{6}Li*	DA	4 to 14.1	4	199	
^{6}Li(p,p2)^{6}Li**	CS	4 to 10.1	1	50	
^{6}Li(p,p2)^{6}Li**	DA	6 to 14.1	3	52	
^{6}Li(p,g0)^{7}Be	CS	0.3 to 1.1	1	9	
^{6}Li(p,g0)^{7}Be	DA	0.3 to 1.1	1	8	
^{6}Li(p,g1)^{7}Be*	CS	0.03 to 1.1	1	14	
^{6}Li(p,g1)^{7}Be*	CS	0.03 to 1.1	2	27	
^{4}He(^{3}He,^{3}He)^{4}He	DA	1.2 to 22.6	9	3611	
^{4}He(^{3}He,^{3}He)^{4}He	AY	3.3 to 11	1	65	
^{4}He(^{3}He,p)^{6}Li	DA	8 to 18	1	198	
^{4}He(^{3}He,p1)^{6}Li*	DA	11 to 18	1	36	
^{4}He(^{3}He,g0)^{7}Be	CS	0.28 to 1.7	2	40	
^{4}He(^{3}He,g1)^{7}Be*	CS	0.28 to 1.7	2	40	
Total or mean			49	6721	1.421

In this global experimental database, the most complete and accurate experimental data exist for the reactions ^{6}Li(p,p) ^{6}Li and ^{4}He(^{3}He,^{3}He)^{4}He, therefore they play a key role in the fitting; the fitting of the reactions ^{6}Li(p,^{3}He)^{4}He and ^{4}He(^{3}He,p)^{6}Li depends on the ^{6}Li(p, p)^{6}Li and ^{4}He(^{3}He, ^{3}He) ^{4}He fits, and of course ^{6}Li(p, ^{3}He) ^{4}He and ^{4}He(^{3}He,p) ^{6}Li are to some extent competing channels. For the channels ^{6}Li(p,p$_1$)^{6}Li*, ^{6}Li(p,p$_2$)^{6}Li**, ^{6}Li(p,γ)^{7}Li, ^{4}He(^{3}He p$_1$)^{6}Li, ^{4}He(^{3}He,γ)^{7}Li , we use a free parameter in the fitting, so most of the shape factors are keep equal to 1.00.

In the figures we display both the original experimental data points (Ori-(name of group) and the normalized data points (Nor-(S = K.xxx)) which were used practically in the fitting. It can be seen that most of the normalized data points lie within the error bars of the original data, and that for most of the data sets the changes are less than the original systematical error given in the original paper; this confirms that the modification of the original data sets are reasonable

We first show the evaluated cross sections that resulted from the global fitting.

7.1. Evaluation results

The evaluation has been performed for proton energies in the range E_p = 0.01 to 20 MeV and for ^{3}He energies in the range $E_{^{3}He}$ = 1 to 20 MeV. The angular distributions (DA) extend from 0.1 degree to 180 degree.

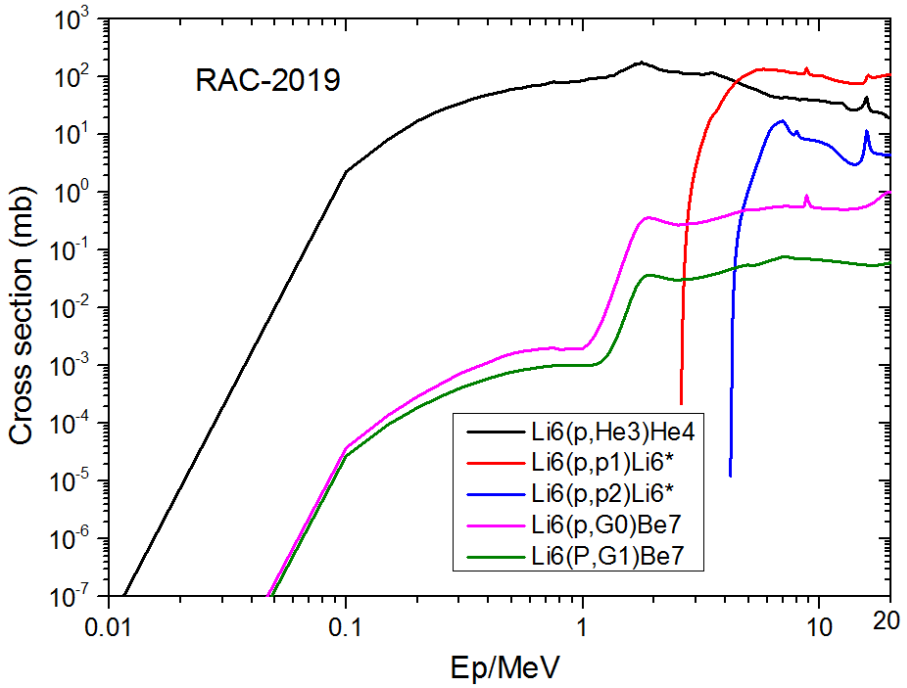

FIG 7.1. Integrated evaluated cross sections for p+^{6}Li.

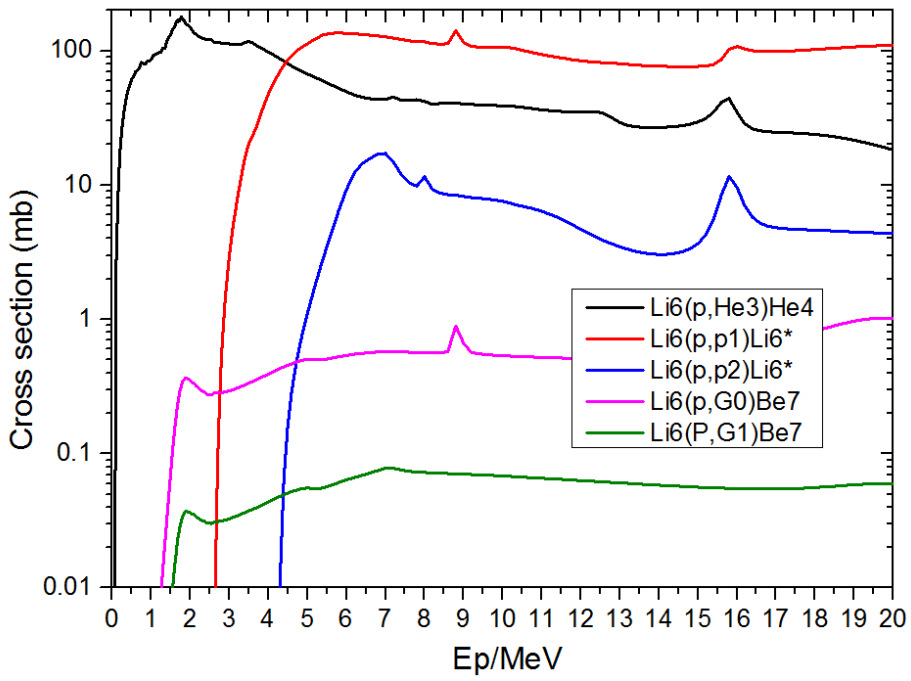

FIG 7.2. Evaluated integrated cross sections for p+^{6}Li.

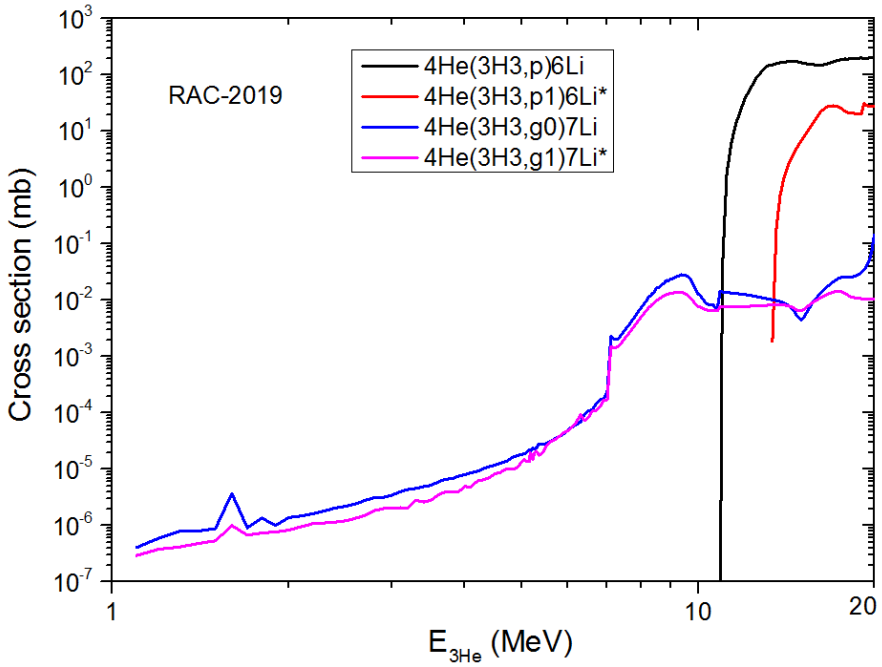

FIG 7.3. Evaluated integrated cross sections for ^{3}He+^{4}H.

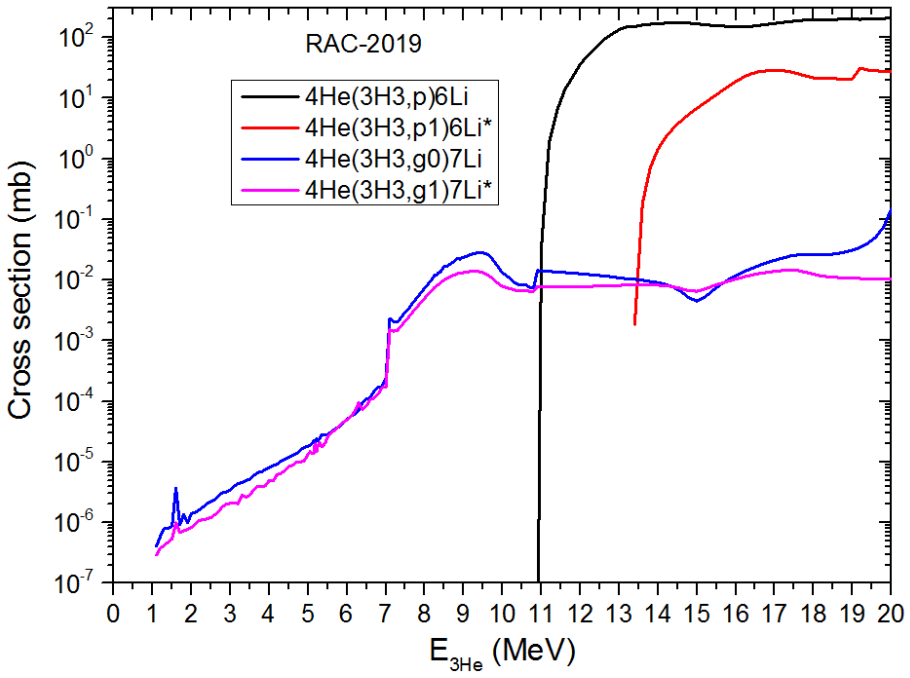

FIG 7.4. Evaluated integrated cross sections for $^{3}He+^{4}H$.

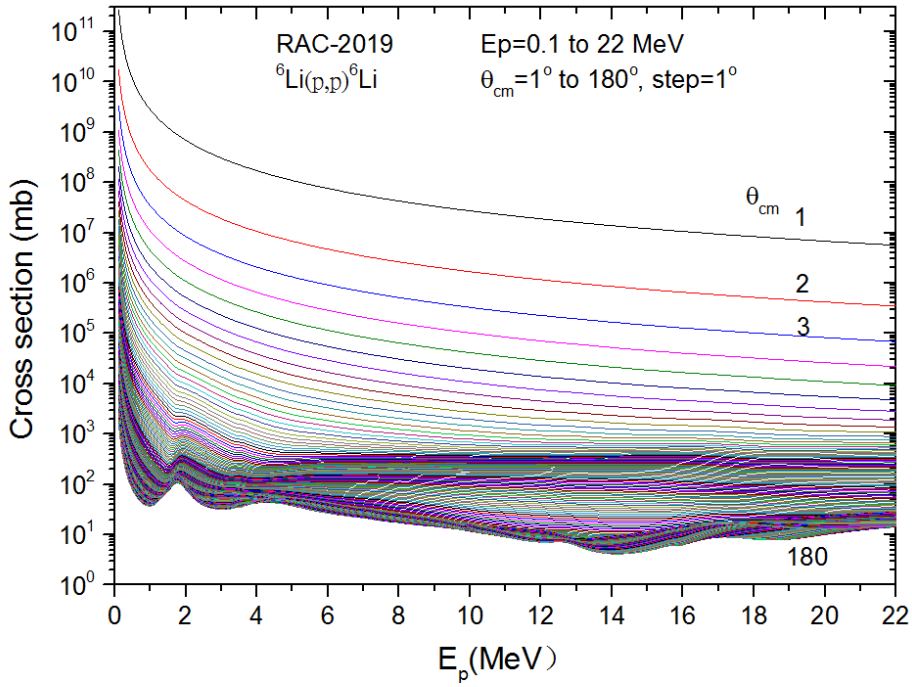

FIG 7.5. Evaluated DA for $p+^{6}Li$.

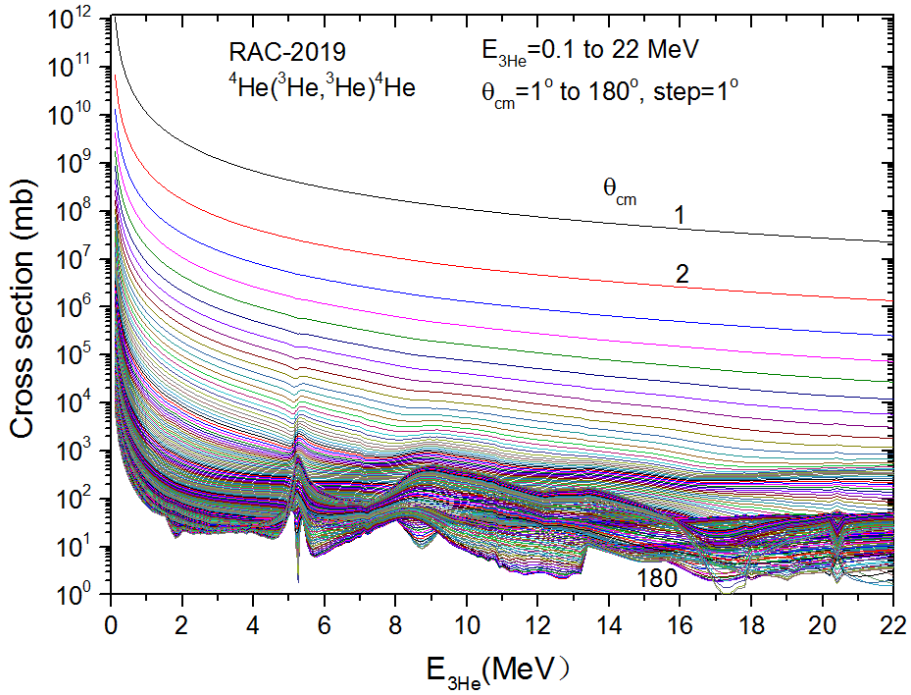

FIG 7.6. Evaluated DA for ^{3}He+^{4}He.

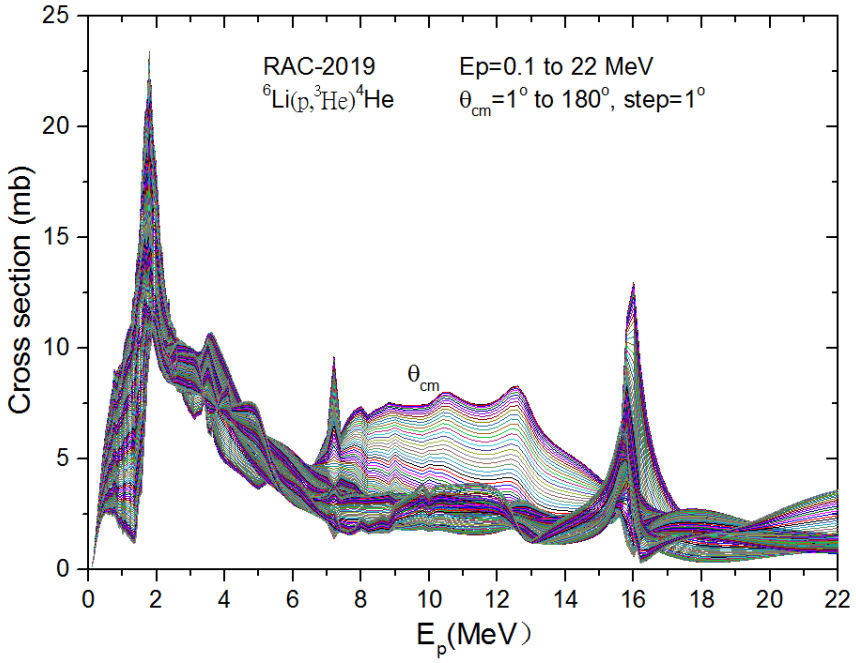

FIG 7.7. The Evaluated DA for ^{6}Li(p,^{3}He)^{4}He.

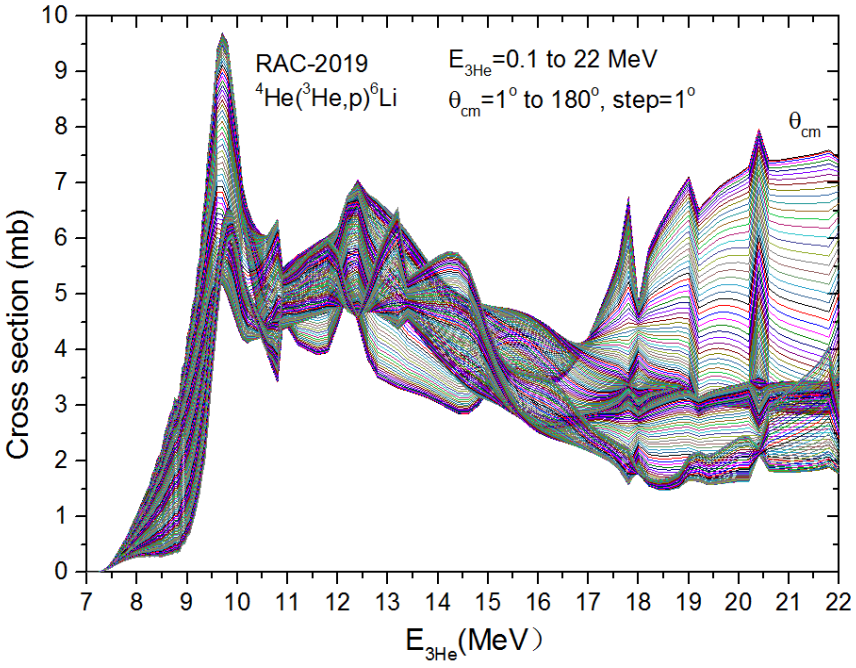

FIG 7.8. The Evaluated DA for ^{4}He(^{3}He,p)^{6}Li.

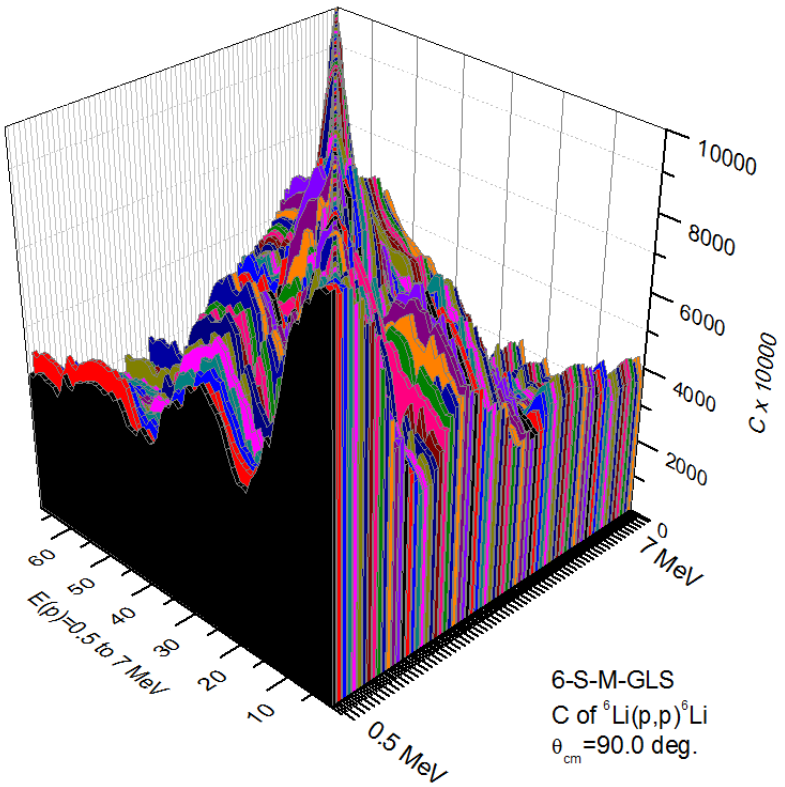

FIG 7.9. DA correlation factors at 90^0 for ^{6}Li(p,p)^{6}Li.

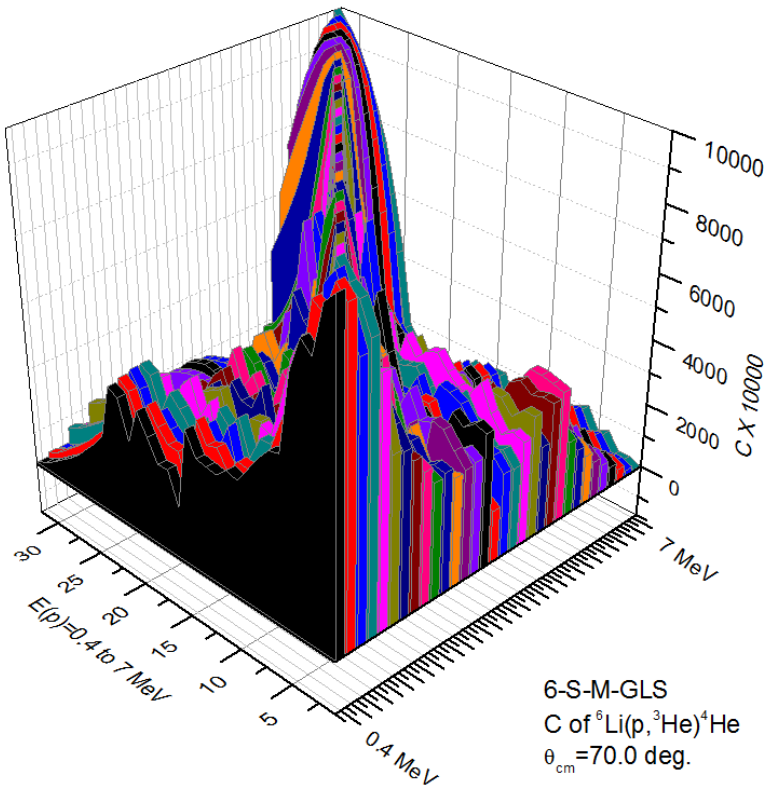

FIG 7.10. Cross section correlation factors for ^{6}Li(p,^{3}He)^{4}He.

7.2. Reaction channel ^{6}Li(p,p)^{6}Li

7.2.1. Data of McCray (1963) - group a

This data set of McCray [20] is the most accurate data set available for the ^{7}Be system. It is an absolute measurement with about 0.5% statistical error only at 90 degree. In the fitting procedure, its normalization factor is fixed at 1.00 initially, however in the final fitting procedure it is an adjustable parameter and the best fit value obtained is about 0.995.

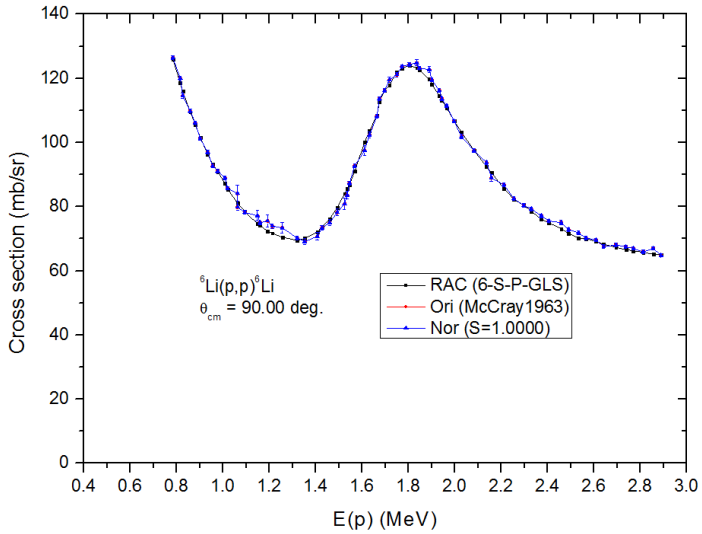

FIG 7.11. Evaluated DA for McCray data [20] at 90 deg.

7.2.2. Data of McCray (1963) - group b

This data set [20] is a rather accurate data set for the ^{7}Be system, as it is a relative measurement with respect to the Rutherford elastic scattering cross section at 3 angles. The statistical error is set to range from 3 to 5%.

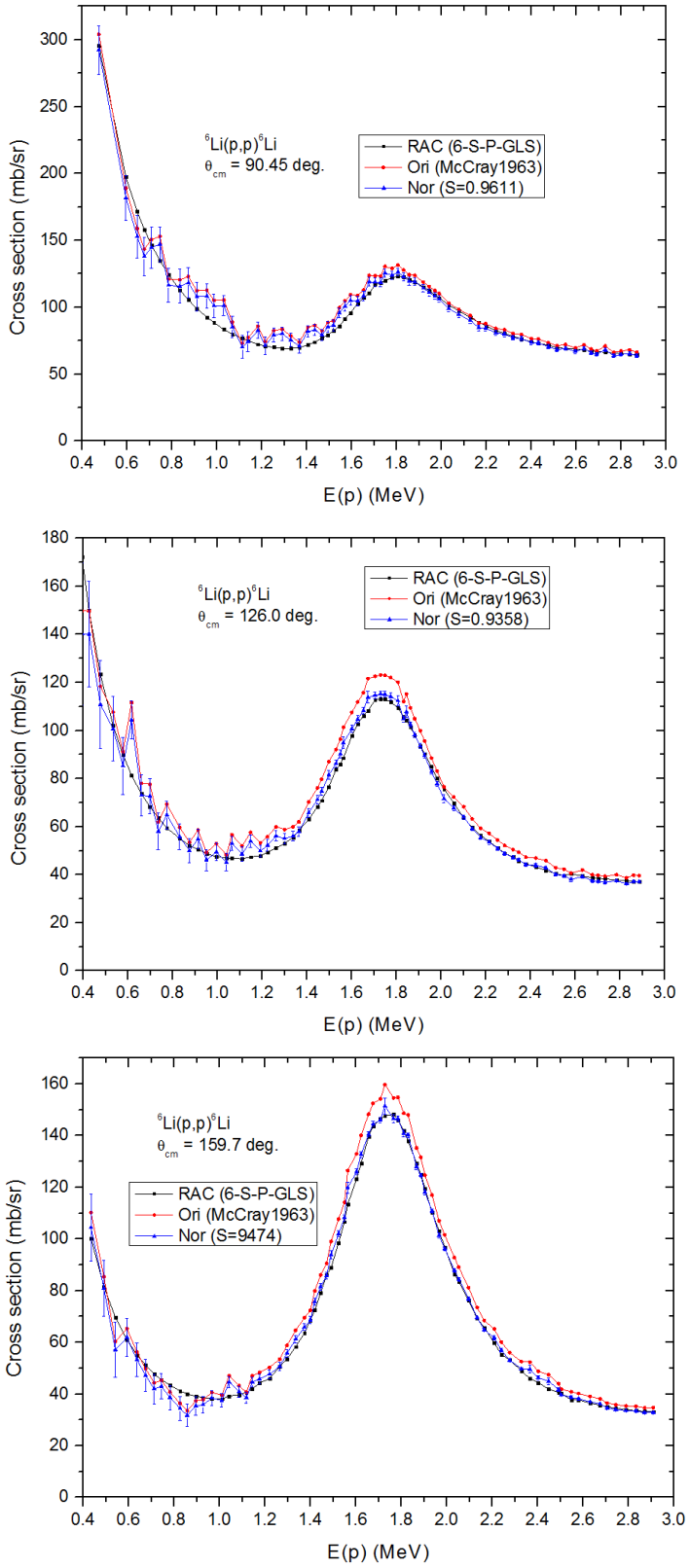

FIG 7.12. Evaluated DA for McCray data [20] at 90.45, 126, and 159.7 degrees.

7.2.3. Data of McCray (1963) - group c

This data set [20] is a rather accurate data set of the ^{7}Be system, as it is an absolute measurement at 5 angles. The statistical error is set to range from 3 to 5%. The data at 90.7 degree is in better agreement with group a (Sect. 7.2.1).

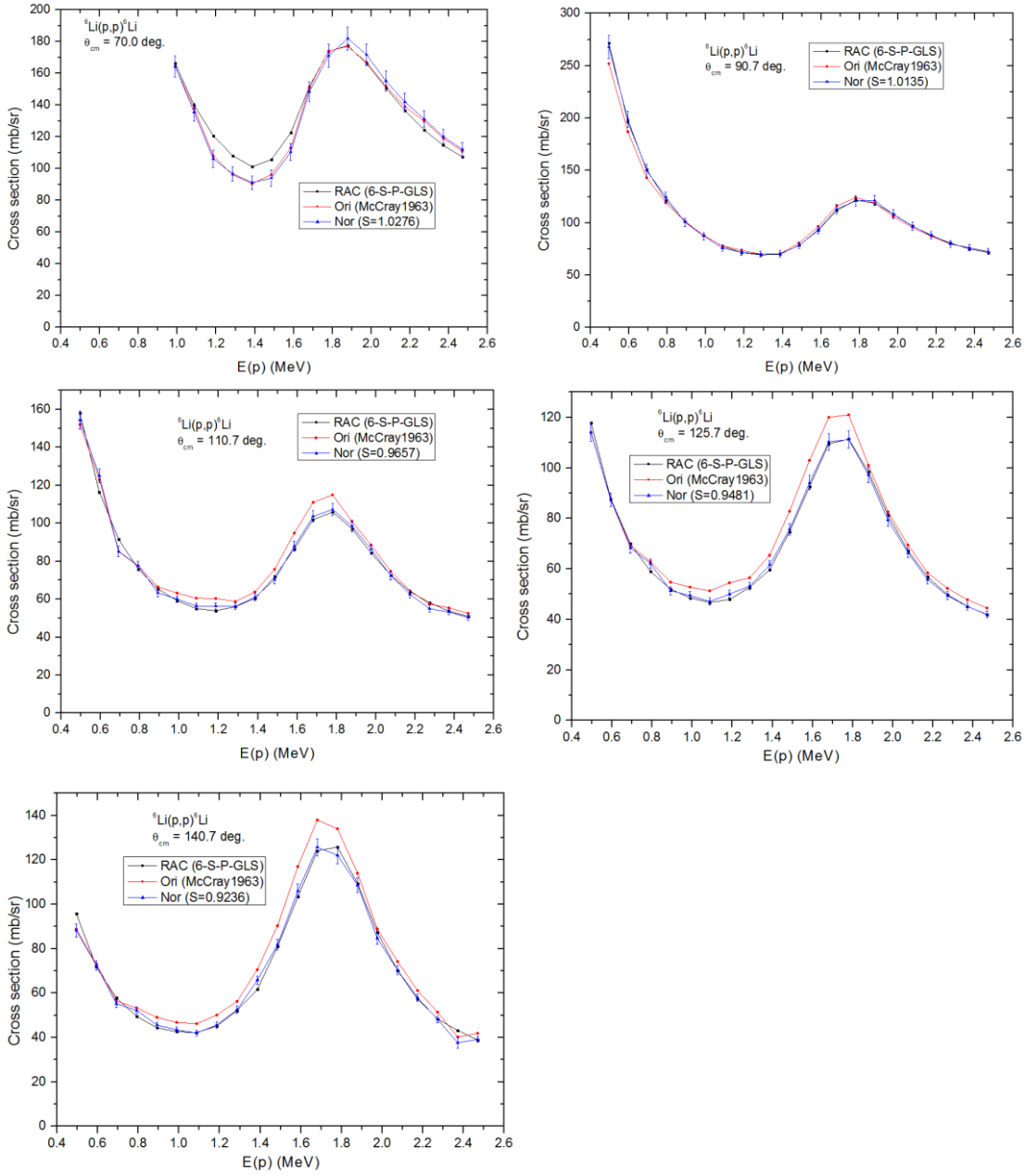

FIG 7.13. Evaluated DA for McCray data [20] at 70, 90.7, 110.7, 125.6, and 140.7 degrees.

7.2.4. DA of Merchez (1968)

This data set [30] is a rather accurate data set of the ^{7}Be system, as it is an absolute measurement at 14 MeV which is the highest energy for ^{6}Li(p,p) ^{6}L. The statistical error is set to range from 2 to 3%. It plays a key role in the fitting in the higher energy range and its normalization factor is fixed to 1.00.

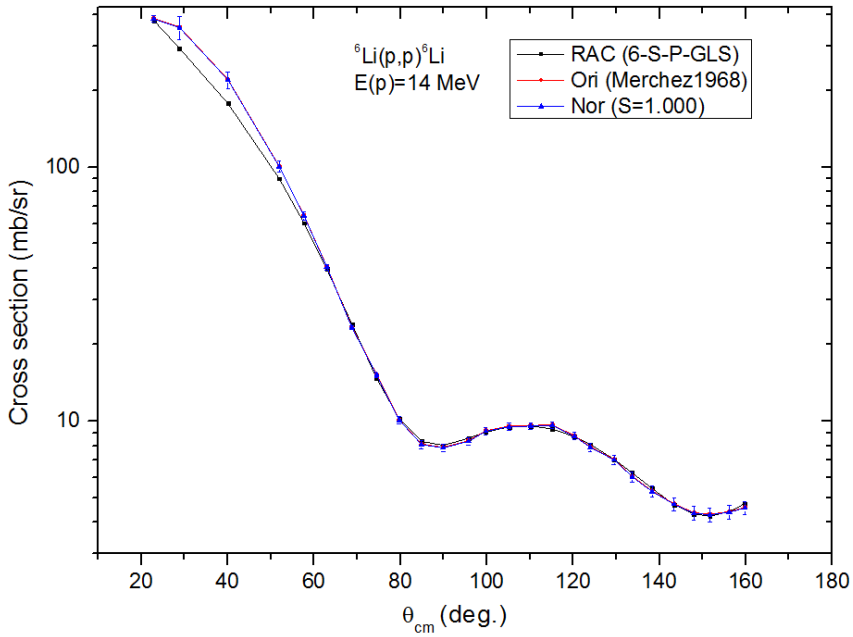

FIG 7.14. Evaluated DA for Merchez data [30] at 14 MeV incident energy.

7.2.5. Data of Fasoli (1974) - group a

This data set is from a relative measurement at 8 angles [28]. The statistical error is set to 5%. The mean value of the shape factor is about 0.95.

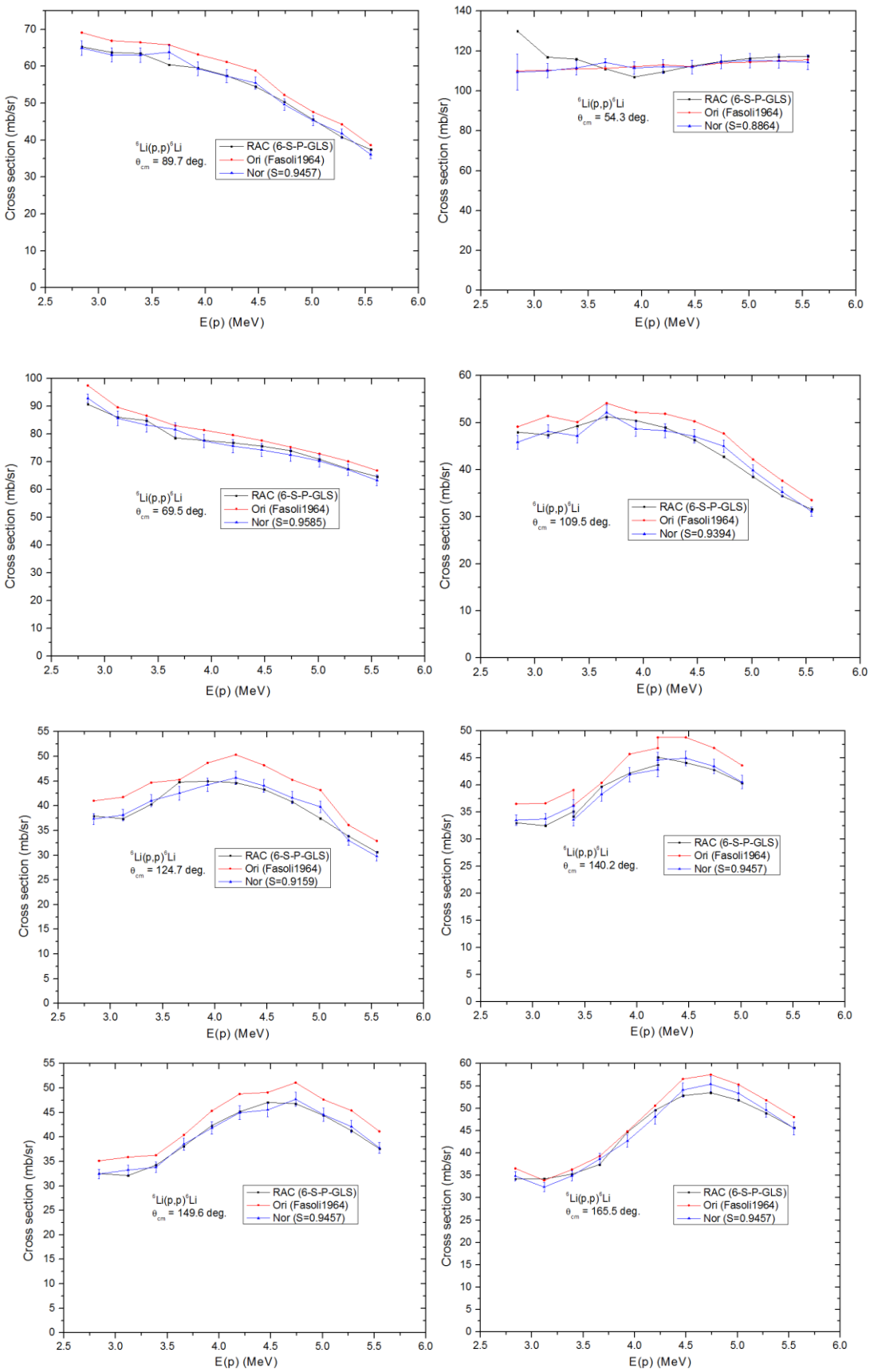

FIG 7.15. Evaluated DA for Fasoli data [28] – group a at 8 angles.

7.2.6. Data of Fasoli (1974) - group b

This data set is measured relative to group a (Sect. 7.2.5) at 8 angles for many more energies. The statistical error is set to 3%. The mean value of the shape factor is about 0.886. This data set shows that the shape of the data is important experimental information.

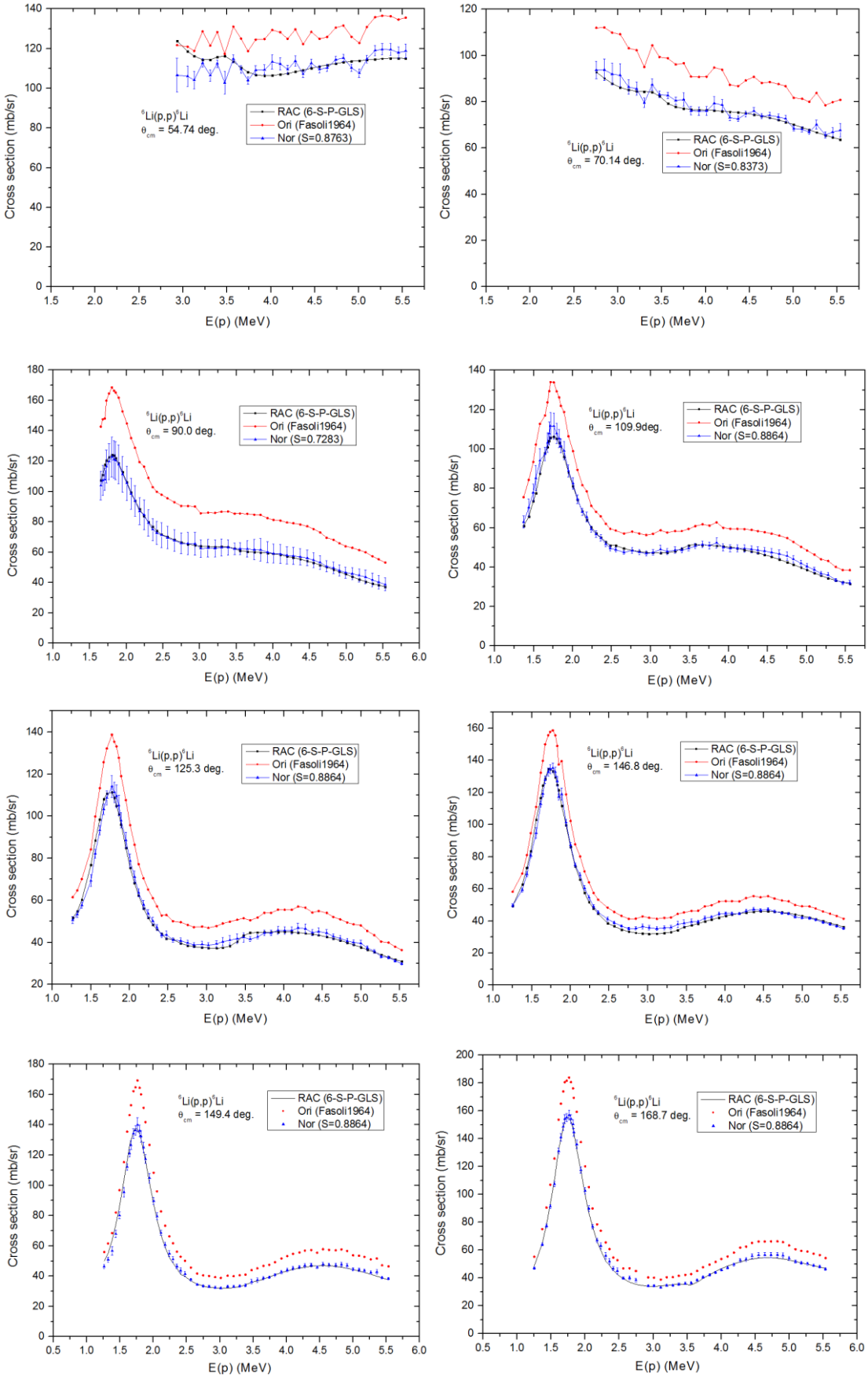

FIG 7.16. Evaluated DA for Fasoli data [28] – group b.

7.2.7. Data of Harrison (1963)

This data set [27] is from a relative measurement at 14 angles for a rather wide range of energies from 2 MeV up to 12 MeV. The statistical error is set to 3%. The mean value of the shape factor is about 0.95. This data set shows that the shape of the data is important experimental information. And plays a key role in the fitting of the data in the middle-to-high energy range.

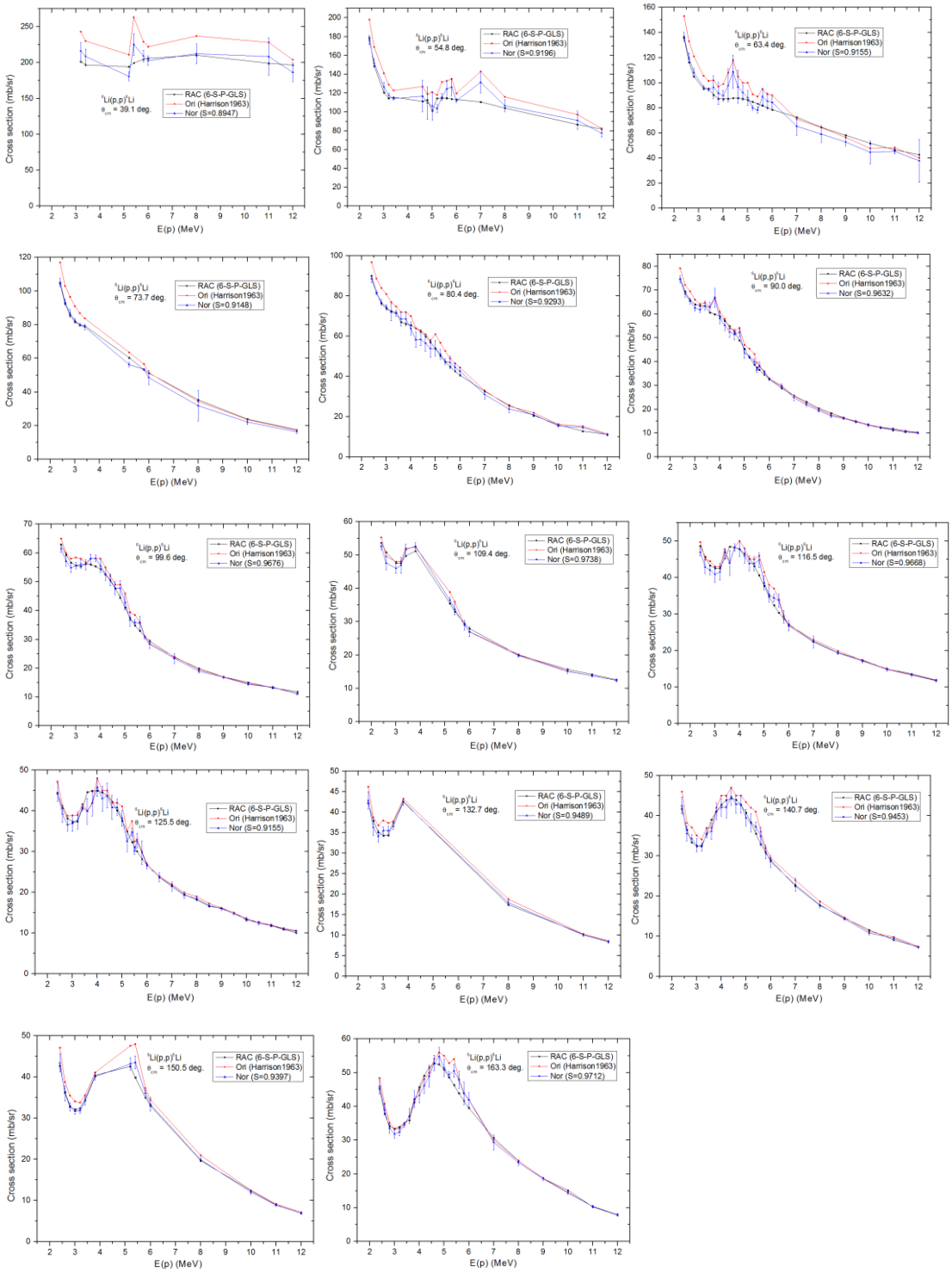

FIG 7.17. Evaluated DA for Harrison data [27].

7.2.8. Data of Haller (1989)

This data set [31] is from a relative measurement at 28 angles for a rather wide range of energies from 1.5 MeV up to 10 MeV. The statistical error is set to 3%. The mean value of the shape factor ranges from 0.95 to 0.98. The data at energies less than 2 MeV are not good, so they have been modified (energy shifted) and the errors have been increased. The main feature of these data is that they include many angles (total of 28).

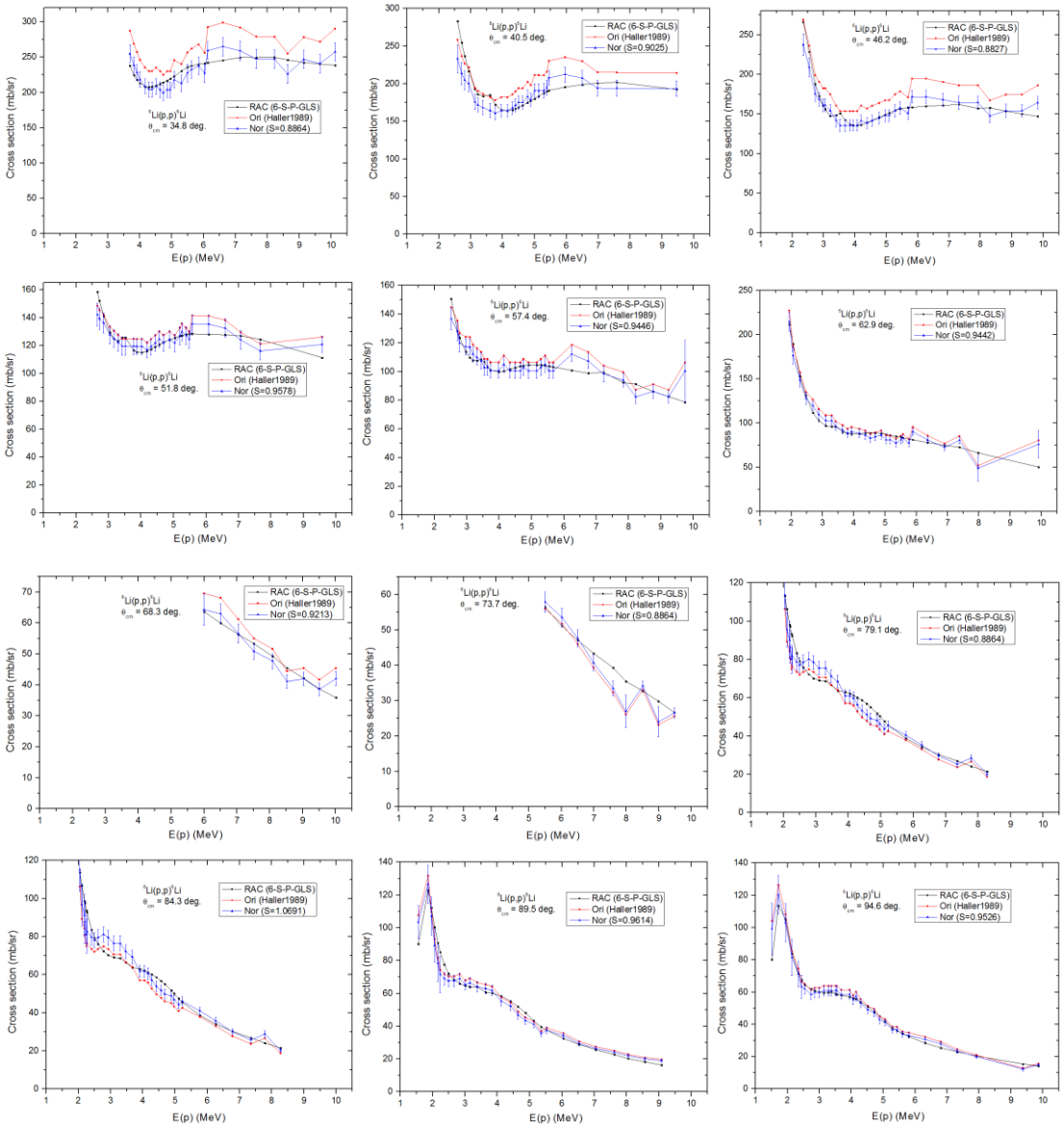

FIG 7.18(a). Evaluated DA for Haller data [31].

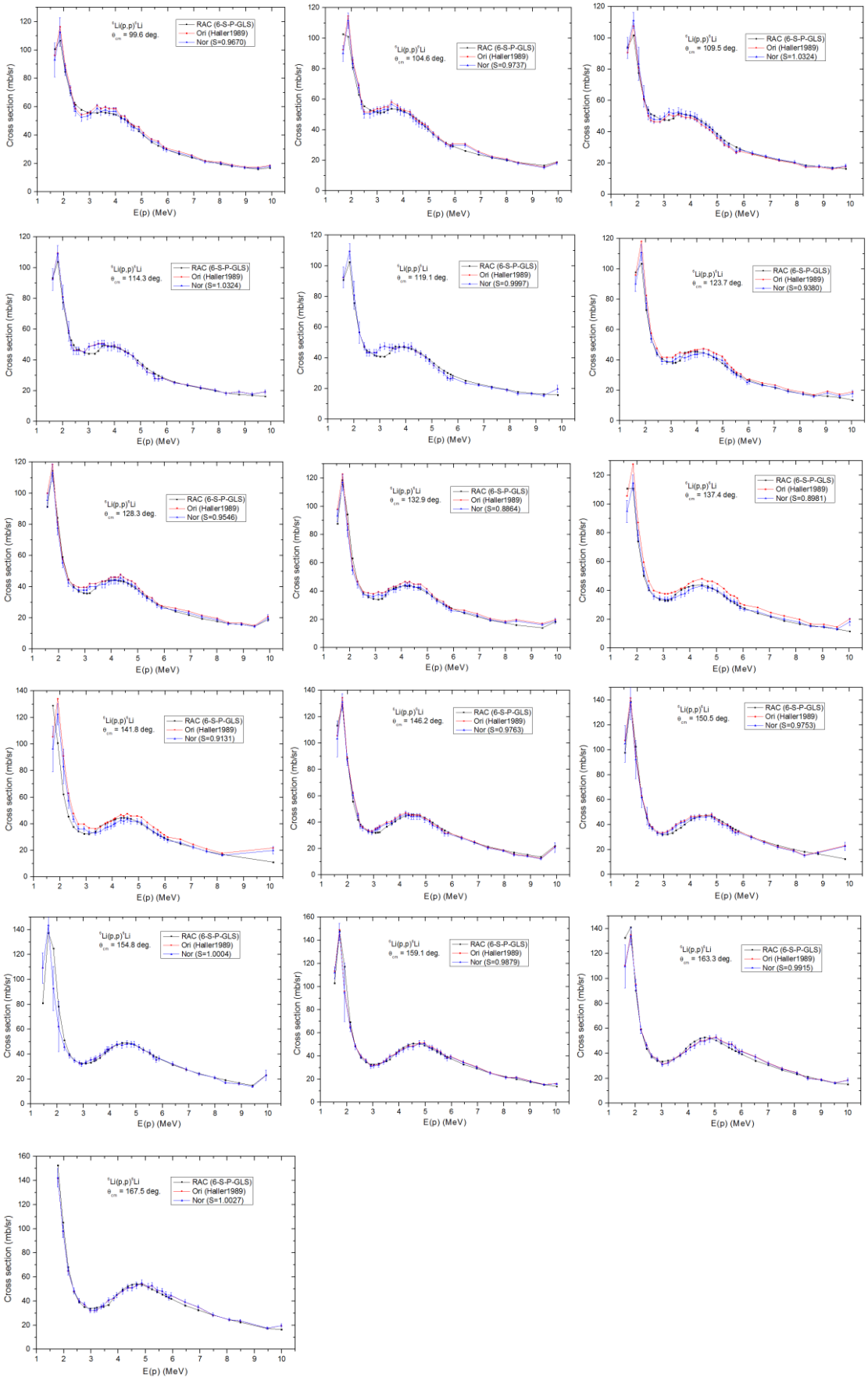

FIG 7.18(b). Evaluated DA for Haller data [31].

7.2.9. DA of Skill-1995

This data set is from a relative measurement at 10 angles and for 19 energies from 0.4 MeV to 2.2 MeV [32]. The statistical error is set to 7%. The mean value of the shape factor is about 1.2. The main feature is that it includes many energies at very small intervals.

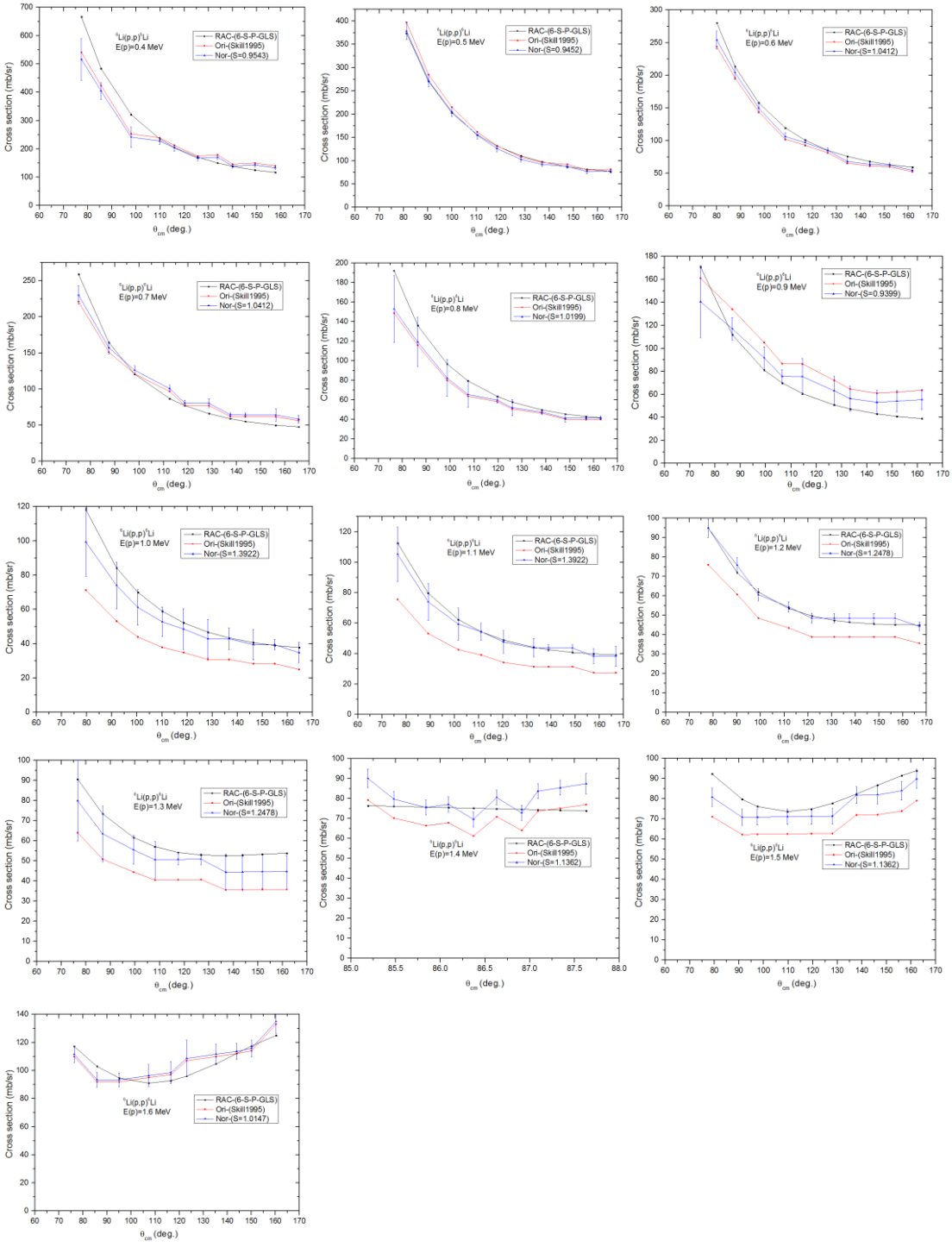

FIG 7.19(a). Evaluated DA for Skill data [32].

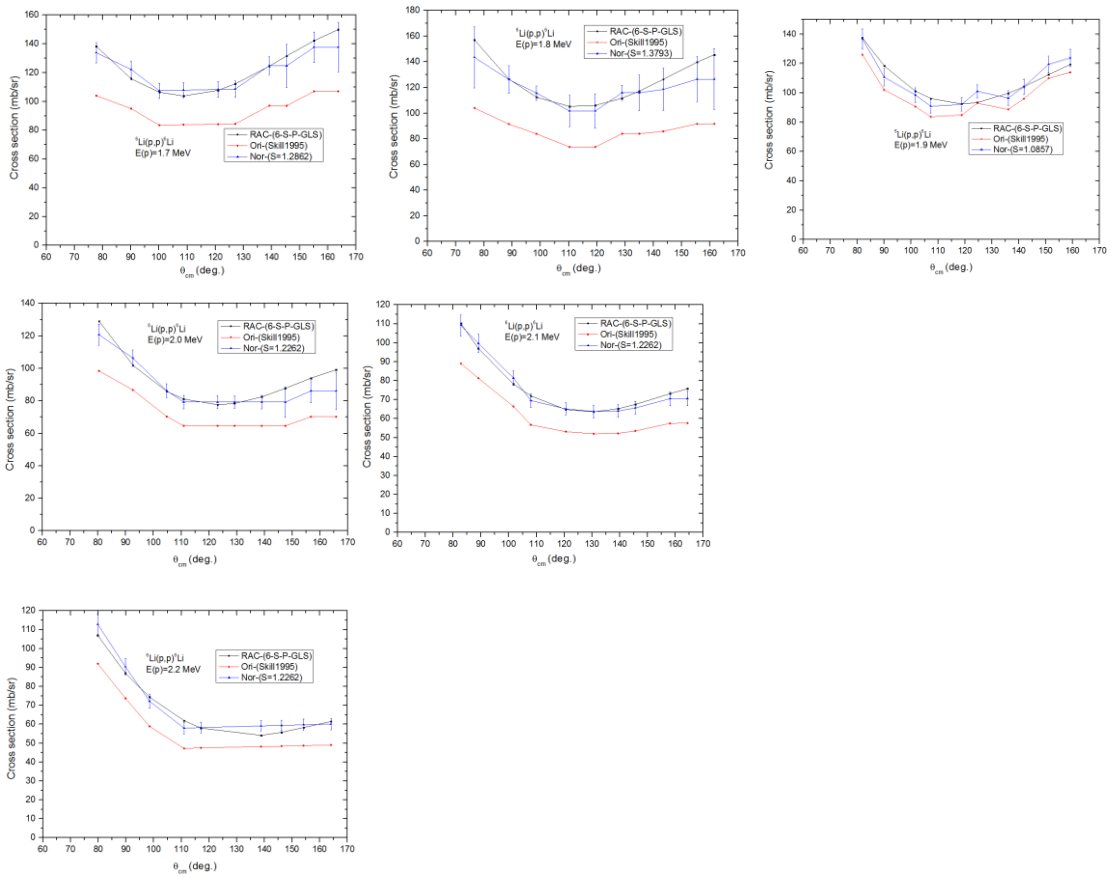

FIG 7.19(b). Evaluated DA for Skill data [32].

7.2.10. Comparison of 4 data sets

This figure compares the excitation function of 4 data sets at angles from 89.5 to 90.5 degrees. These data sets have a strong weighting factor in the fitting procedure.

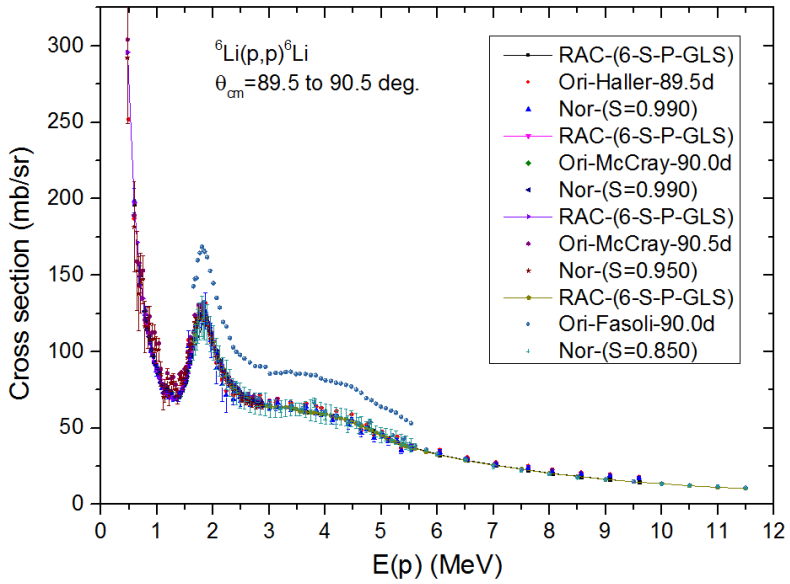

FIG 7.20. Evaluated DA for ^{6}Li(p,p)^{6}Li at angles 89.5 to 90.5 degrees.

7.3. Reaction channel $^{6}Li(p,^{3}He)^{4}He$

7.3.1. Integrated cross sections

These integrated cross-section data set are taken from the EDA evaluated file for the ^{7}Be system.

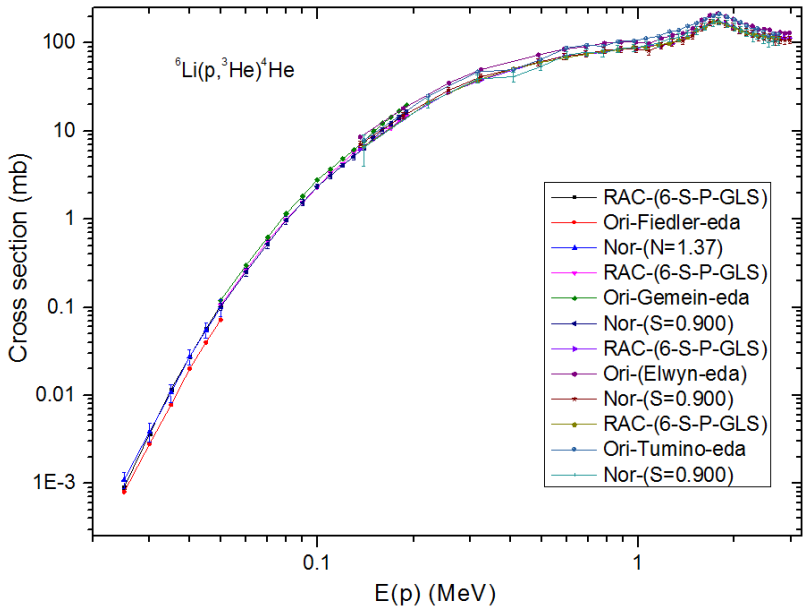

FIG 7.21. Evaluated intergated cross sections for $^{6}Li(p,^{3}He)^{4}He$.

7.3.2. Angular distributions at very low energies

This data set includes 3 groups of data (Kuan [33], Spinka [34] and Bouchez [35]) measured at very low energies from E_p = 0.15 to 0.33 MeV. They are relative values with similar smooth shapes, which is attributed to the 1S-wave being the dominant contribution. The statistical errors are rather large ranging from 10% to 20%. These data can only be reproduced if S-wave (0.5^+ or 1.5^+) levels are included in the level scheme used in the R-matrix analysis, even though levels with $J^{\pi} = 0.5^+$ or 1.5^+ do not exist in the current level scheme of ^{7}Be.

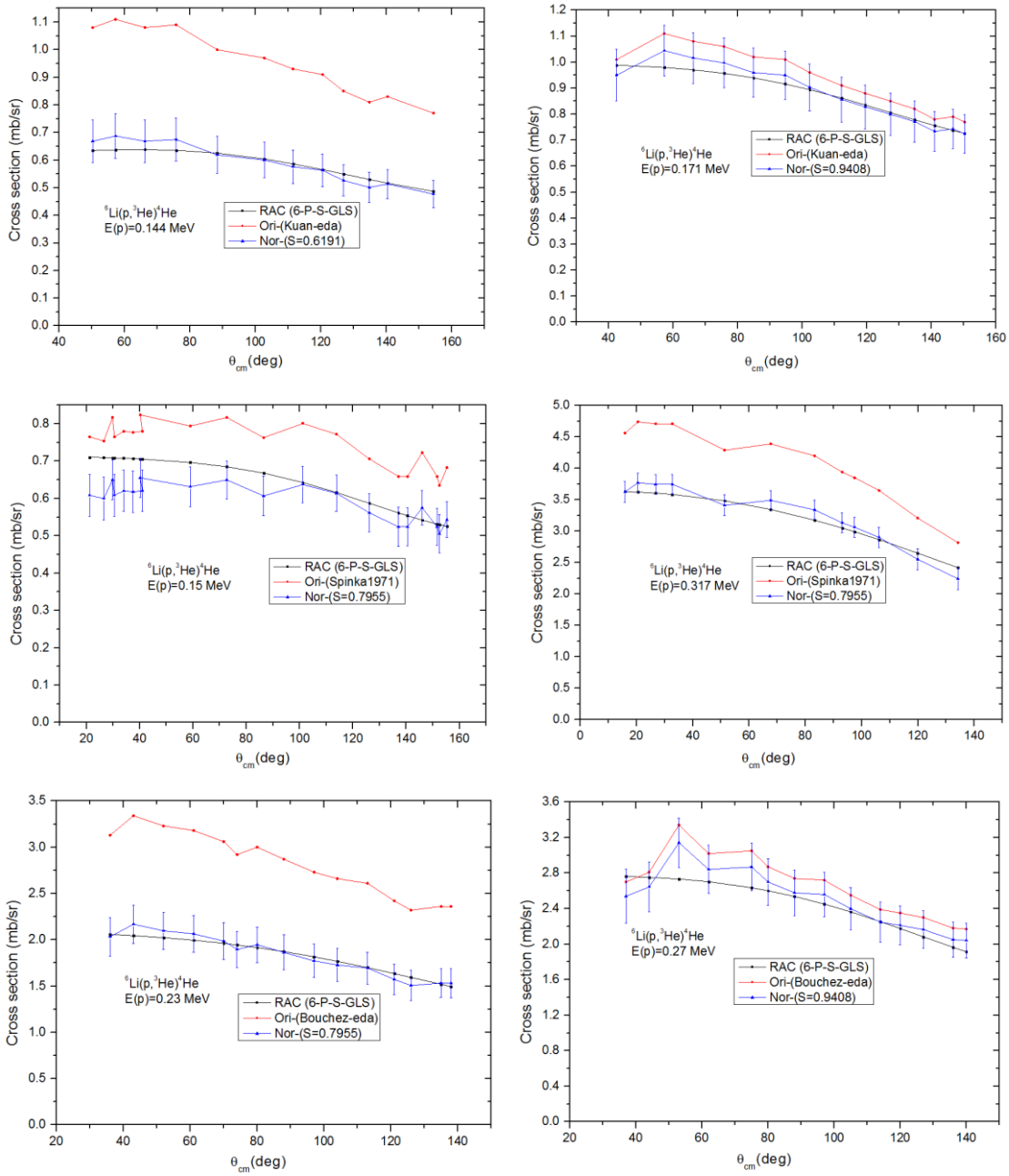

FIG 7.22. Evaluated DA of [33. 34,35] for $^{6}Li(p,^{3}He)^{4}He$ at very low energies.

7.3.3. Data of Elwyn (1979)

This data set of Elwyn includes 18 angles [22], with each angle covering an angle range in the CM system. Each angle range corresponds however to a detector located at a fixed angle in the LAB system. The figures clearly show that the data at 2.2, 2.4 and 2.56 MeV have a very larger negative systematic error, which cannot be attributed to a resonance because in this same energy range the ^{6}Li(p,p)^{6}Li and ^{4}He(^{3}He,^{3}He)^{4}He vary smoothly. In the same energy range the data set of Lin [23] also very smooth with energy.

For proton energies $E_p < 1$ MeV these data contribute strongly to the global fitting, while for $E_p > 1$ MeV, the data set of Lin (1977) dominates in the fitting.

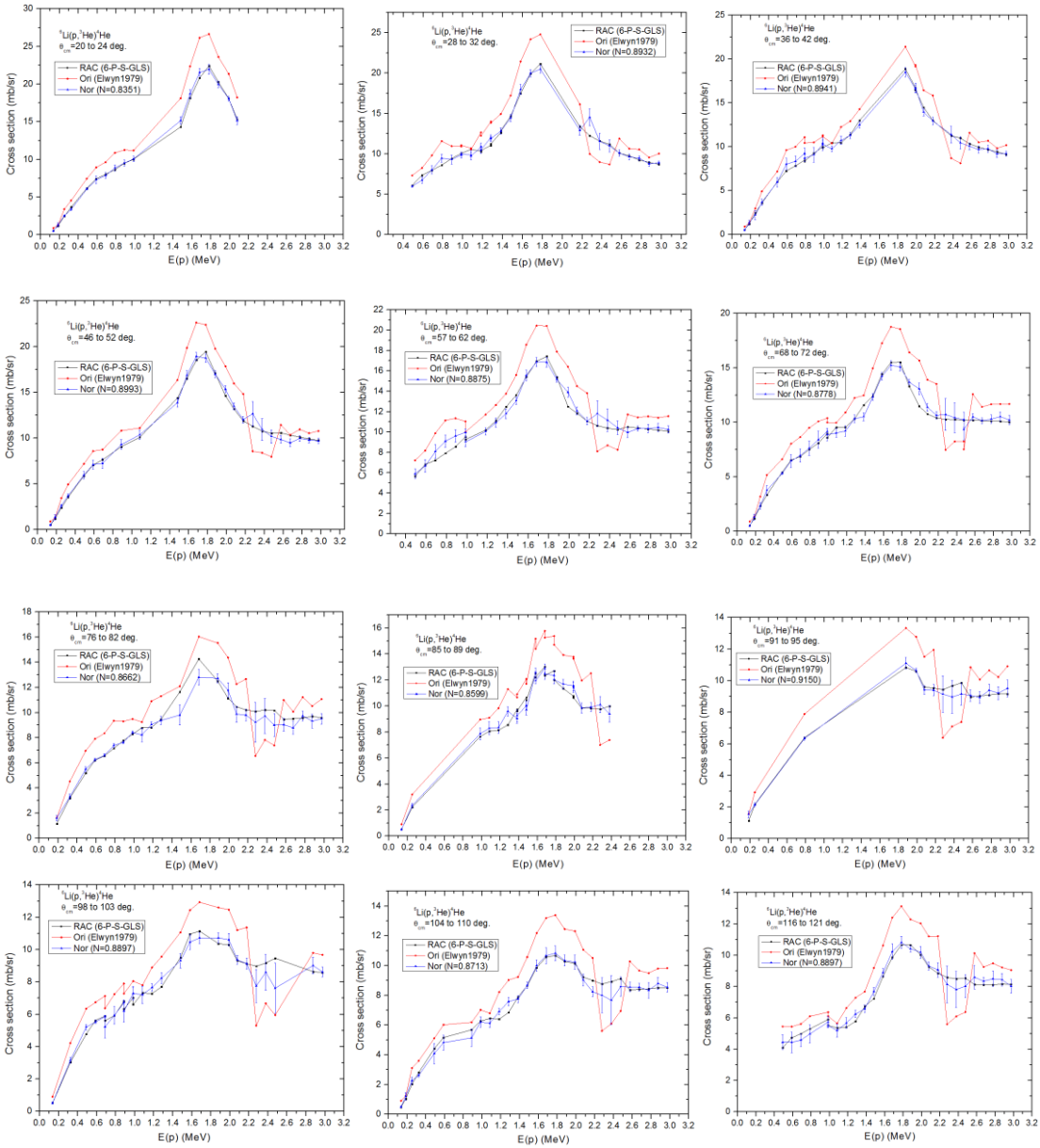

FIG 7.23(a). Evaluated DA of Elwyn [22] for ^{6}Li(p,^{3}He)^{4}He at 18 angles.

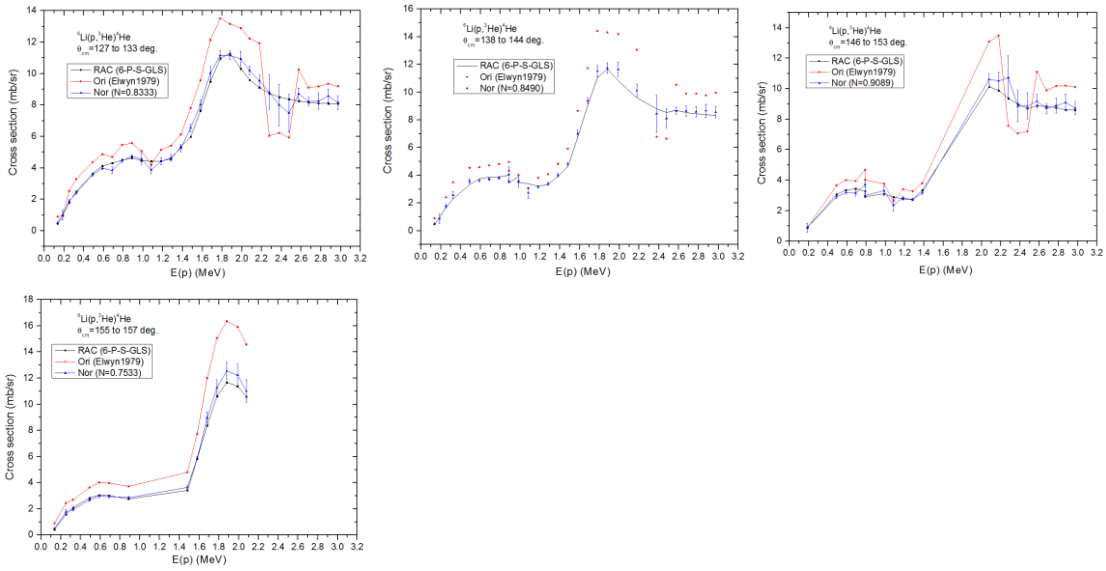

FIG 7.23(b). Evaluated DA of Elwyn [22] for $^{6}Li(p,^{3}He)^{4}He$ at 18 angles.

7.3.4. Data of Lin (1977)

This data set of Lin [23] includes 16 angles, with each angle having an angle range in the CM system, and each angle range corresponding to a detector set at a fixed LAB angle. The figures clearly show that the data at energies from 2.2 to 2.56 MeV vary smoothly with energy, and that no resonannce exists. For proton energies E_p from 1 MeV to 2.6 MeV, the data set of Lin [23] competes strongly with the data set of Elwyn [22]. Both the Lin and Elwyn data are absolute values, and for most of the data the corresponding nomorlization factors look reasonable, and lie within the range of systematic errors given in the original papers (9% to 10%).

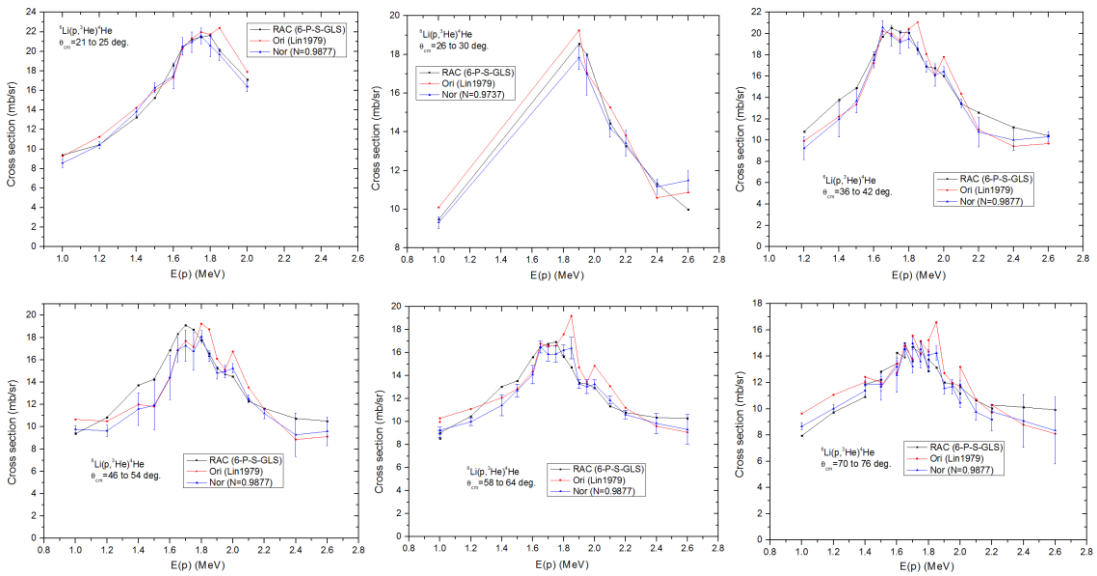

FIG 7.24(a). Evaluated DA of Lin [23] for $^{6}Li(p,^{3}He)^{4}He$ at 16 angles.

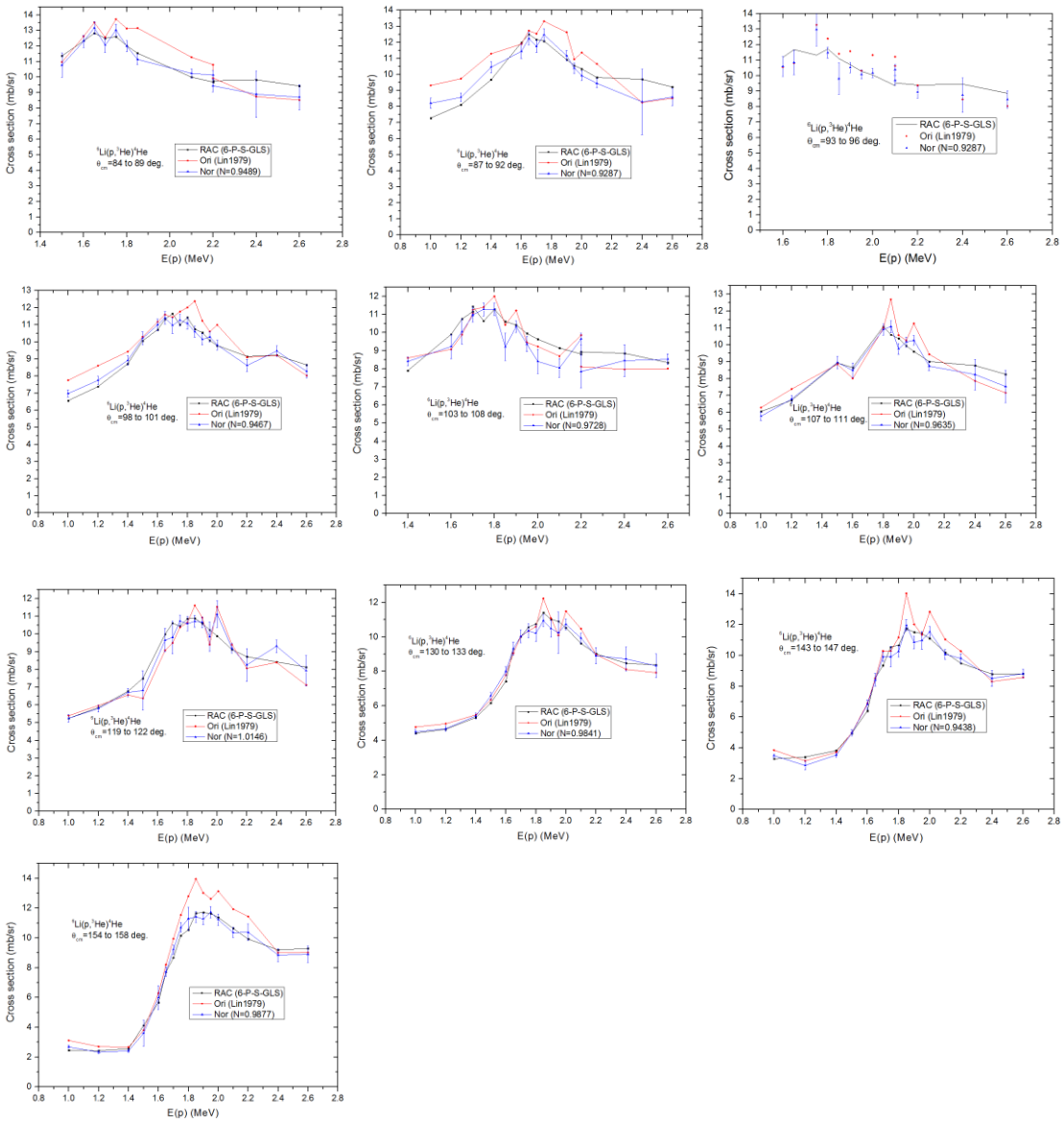

FIG 7.24(b). Evaluated DA of Lin [23] for ^{6}Li(p,^{3}He)^{4}He at 16 angles.

7.3.5. Data of Bas51

These relative data [36] were measured at the very large angle of 167.1 degrees. N = 1.2589 so the data have a very good shape.

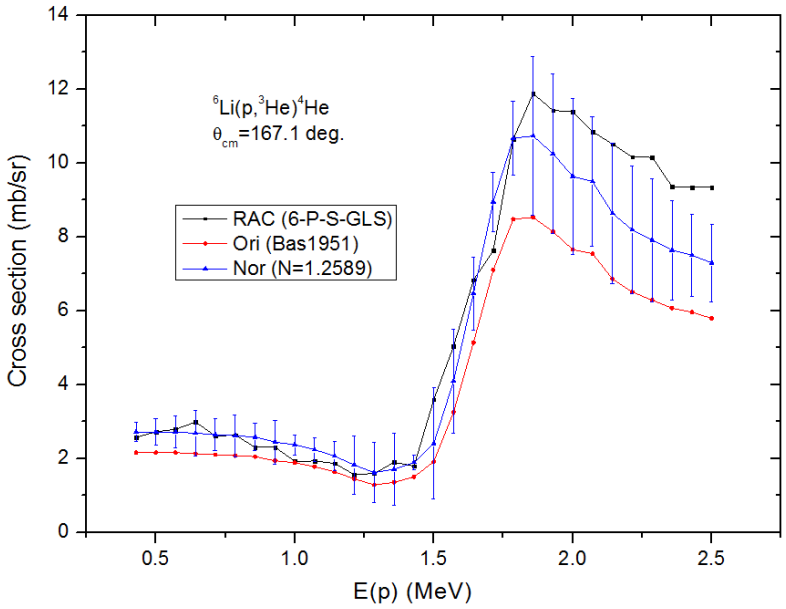

FIG 7.25. Evaluated DA of Bas51 [36] at mean 167.1 degrees.

7.3.6. DA of Gould (1974)

This data set [37] was measured at energies in the 'middle-energy region', i.e. at E_p = 4 to 10 MeV. In this middle-energy region, both these data and those of Schenk [37] contribute significantly to the fitting.

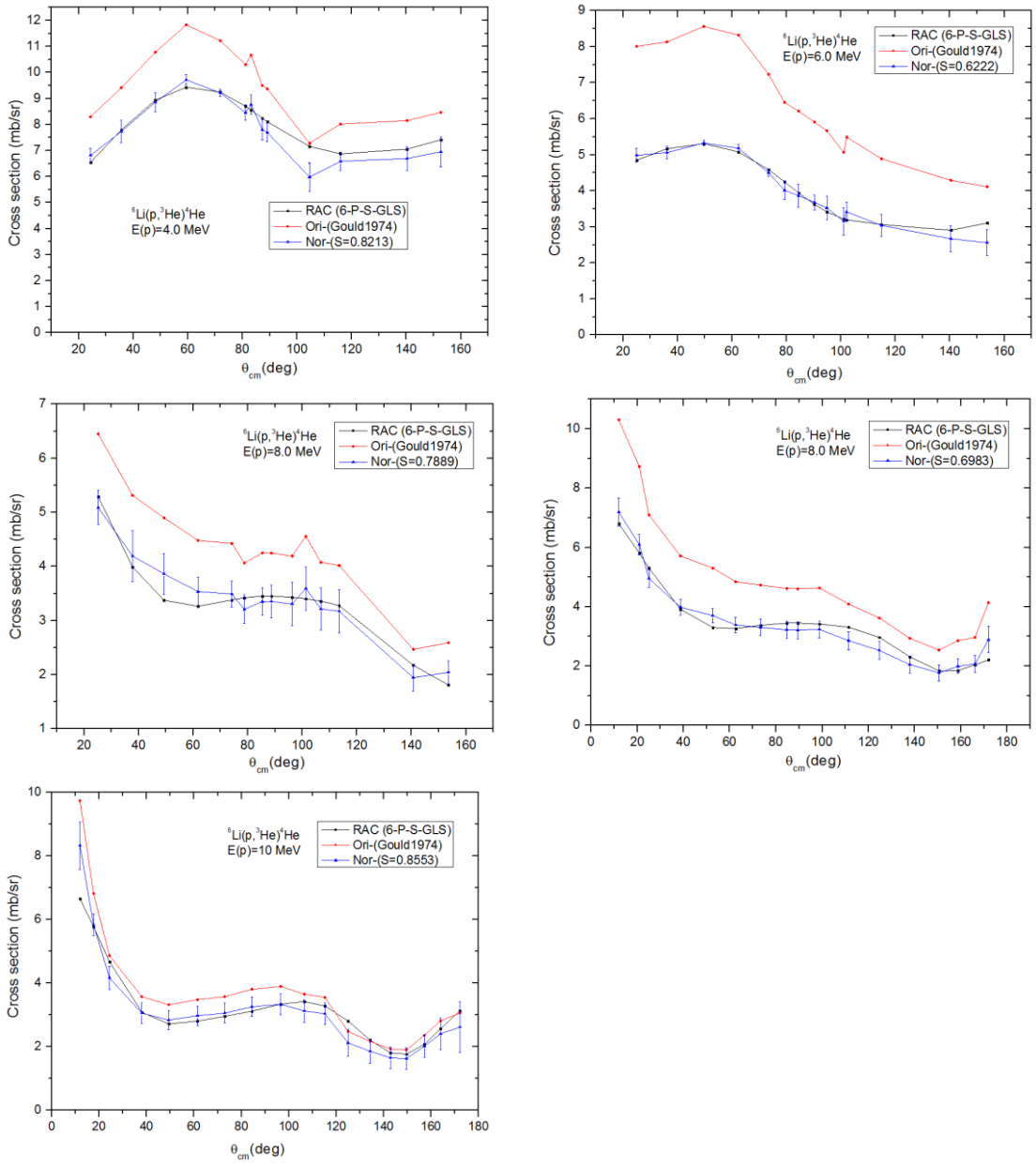

FIG 7.26. Evaluated DA of Gould [37] for $^6Li(p,^3He)^4He$.

7.3.7. DA of Schenk (1973)

This dataset [37] consists of anglular distributions measured in very wide energy region with proton energies E_p = 3.8 to 22.5 MeV. As a result, they play a key role in fitting the data in the higher energy region, which in fact is where the strong constraints on the distant level parameters are set, hence ensuring that the fitting of the data in the middle- and low-energy region is reasonable and reliable. The data at 15 MeV has a shape factor of 1.016 and are fitted very well. This is because there is no competition from other data sets at this energy. The fitting of the data at 22.5 MeV could still be improved to decrease the shape factor if one continued with further iterations.

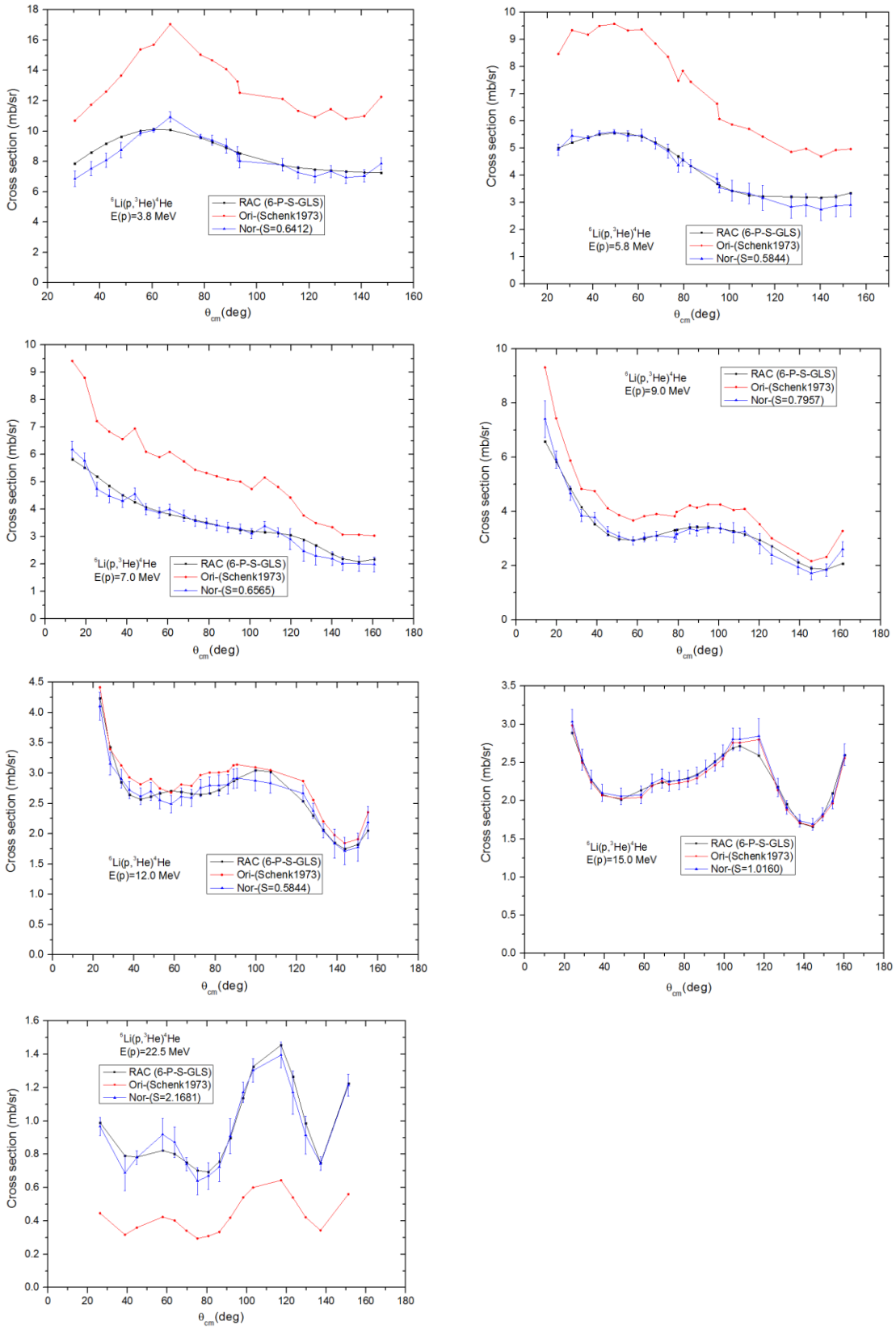

FIG 7.27. Evaluated DA of Schenk [37] for $^{6}Li(p,^{3}He)^{4}He$.

7.3.8. Analyzing Power data

The reproduction of the shapes of this data set of analyzing powers of ^{6}Li (p,^{3}He)^{4}He measured by Schenk [38] is reasonable.

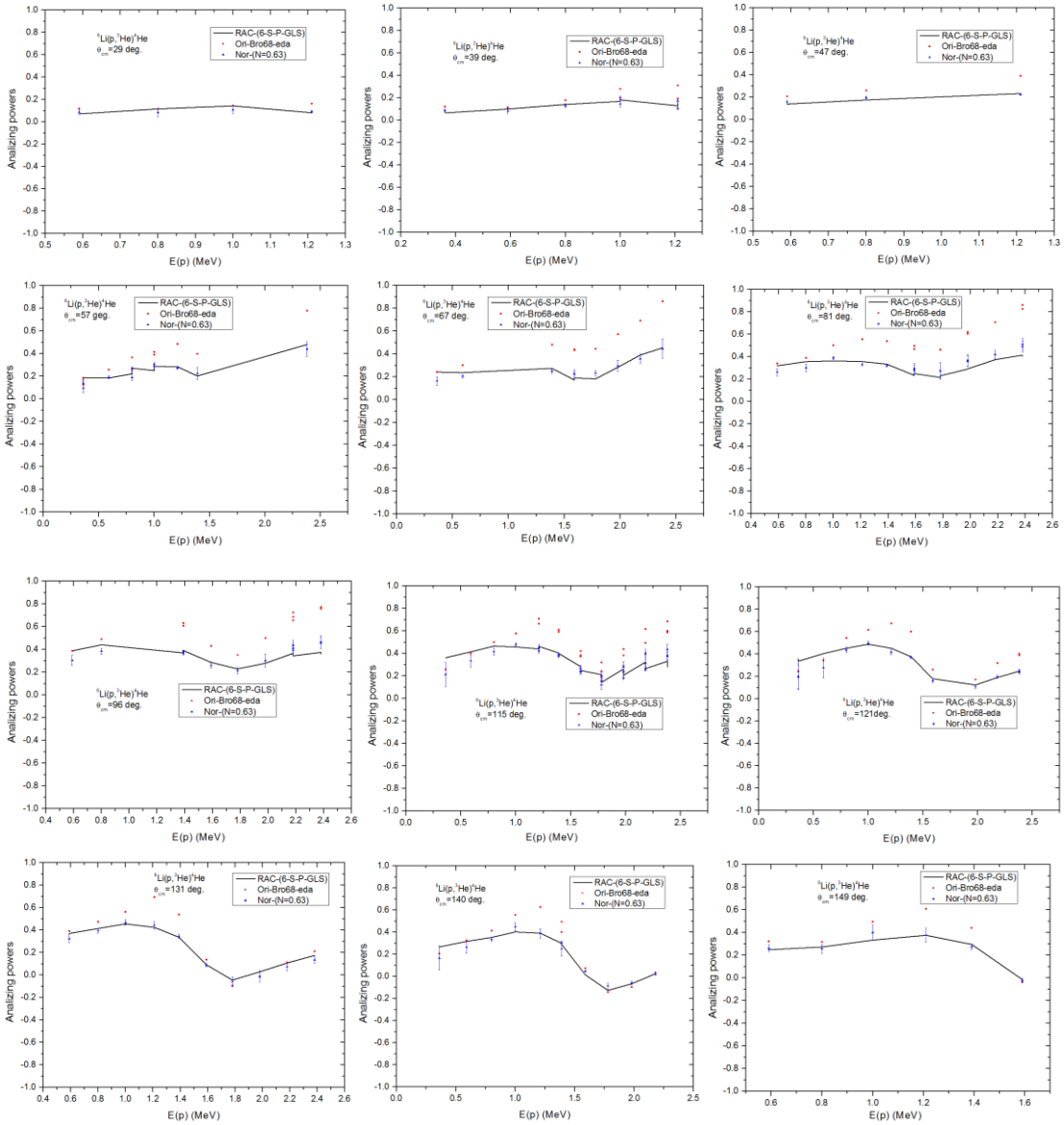

FIG 7.28. Evaluated analyzing powers of ^{6}Li(p,^{3}He)^{4}He [38].

7.4. Reaction channel $^{6}Li(p,p_1)^{6}Li^{*}$

7.4.1. Integrated cross sections

The integrated cross-sections of Harrison [27] play a key role in the fitting of the $^{6}Li(p,p_1)^{6}Li^{*}$ channel data by constraining the fit. The shape factor is fixed at N = 1.00.

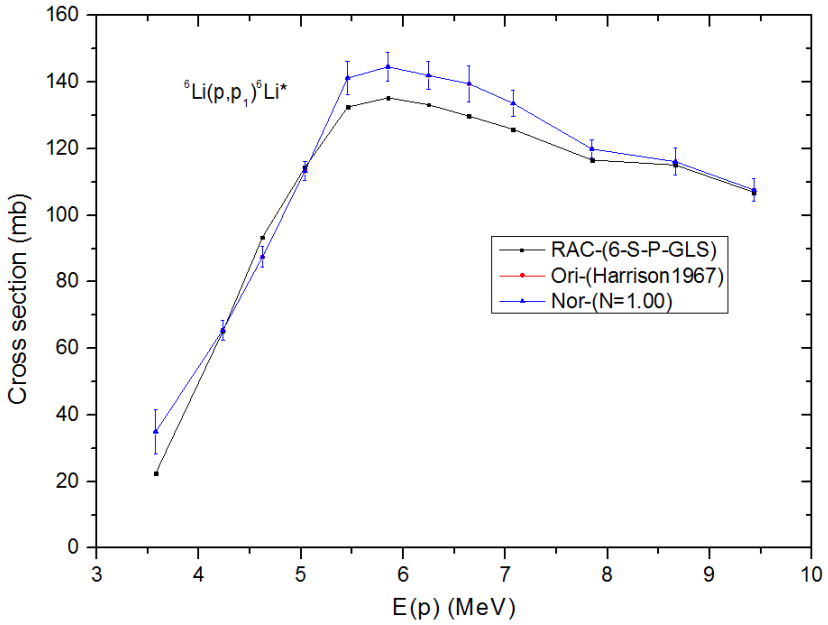

FIG 7.29. Evaluated cross sections of Harrison [27] for $^{6}Li(p,p_1)^{6}Li^{*}$.

7.4.2. DA of Laurat (1969)

The DA of Laurat [39] for $^{6}Li(p,p_1)^{6}Li^{*}$ is well reproduced. This data set is very important for fitting the ^{7}Be system in the middle-high energy region.

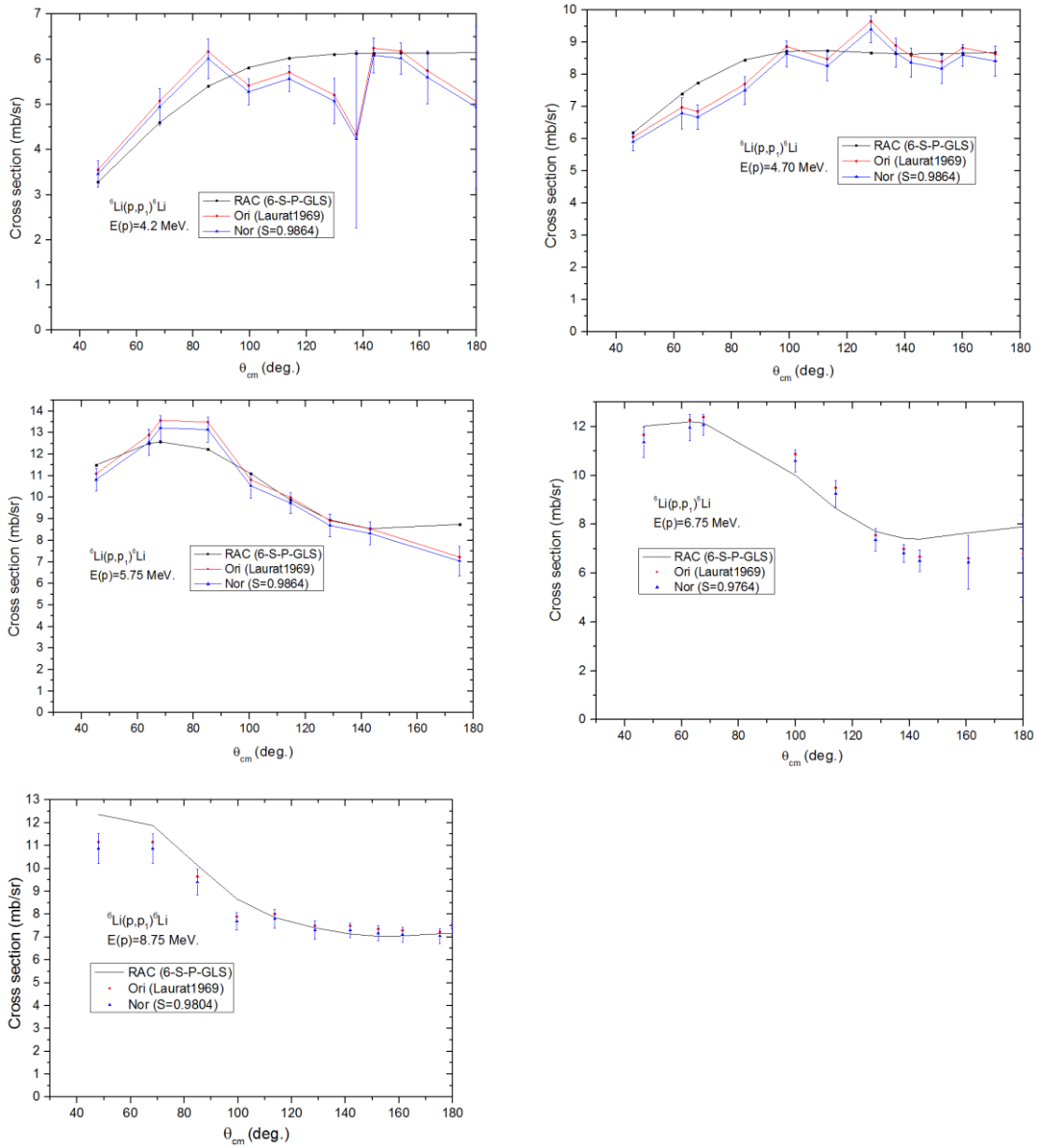

FIG 7.30. Evaluated DA of Laurat [39] for $^{6}Li(p,p_1)^{6}Li^{*}$ at low energies.

7.4.3. DA of Merchez (1968)

This DA data set of Merchez at 14 MeV [30] constrains the fitting of the $^{6}Li(p,p_1)^{6}Li^{*}$ data in the higher energy region, and has a shape factor fixed at N = 1.00.

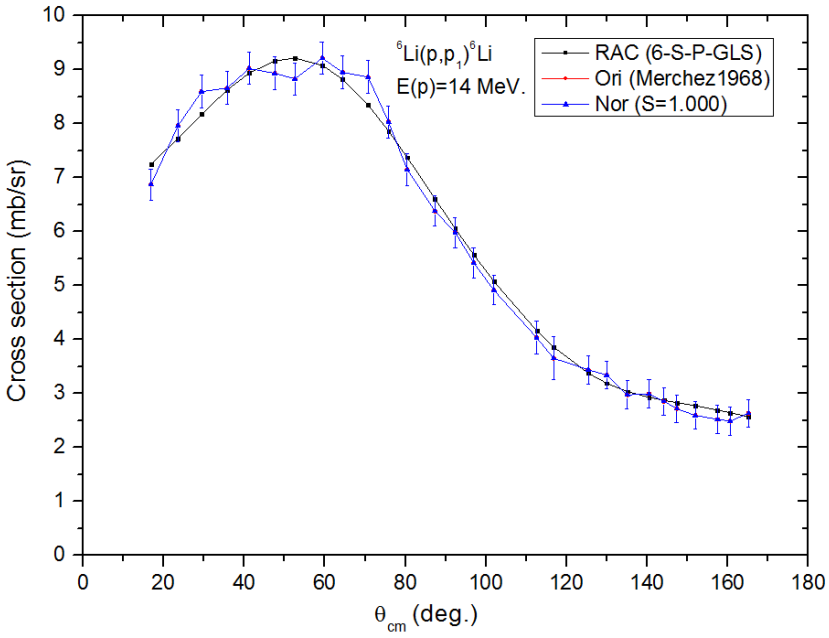

FIG 7.31. Evaluated DA of Merchez [30] for $^{6}Li(p,p_1)^{6}Li^{*}$ at 14 MeV.

7.4.4. DA of Harrison (1967)

This DA data set of Harrison [27] for $^{6}Li(p,p_1)^{6}Li^{*}$ constrains the global fit of $^{6}Li(p,p_1)^{6}Li^{*}$ data in the middle-high energy region, and has a shape factor fixed at N = 9864.

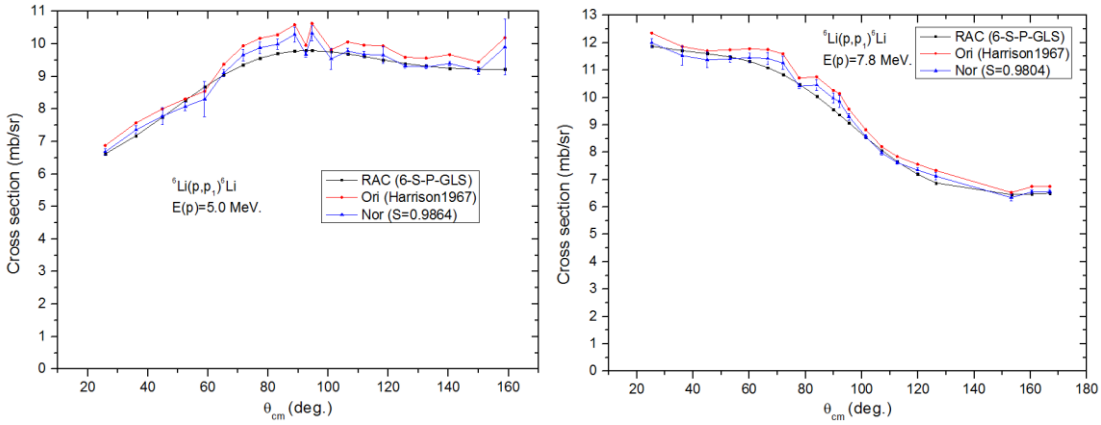

FIG 7.32. Evaluated DA of Harrison [27] for $^{6}Li(p,p_1)^{6}Li^{*}$.

7.4.5. Data of Laurat (1969)

This excitation function data of Laurat [38] contribute strongly to the fitting of the $^{6}Li(p,p_1)^{6}Li^{*}$ channel in the middle-high energy region.

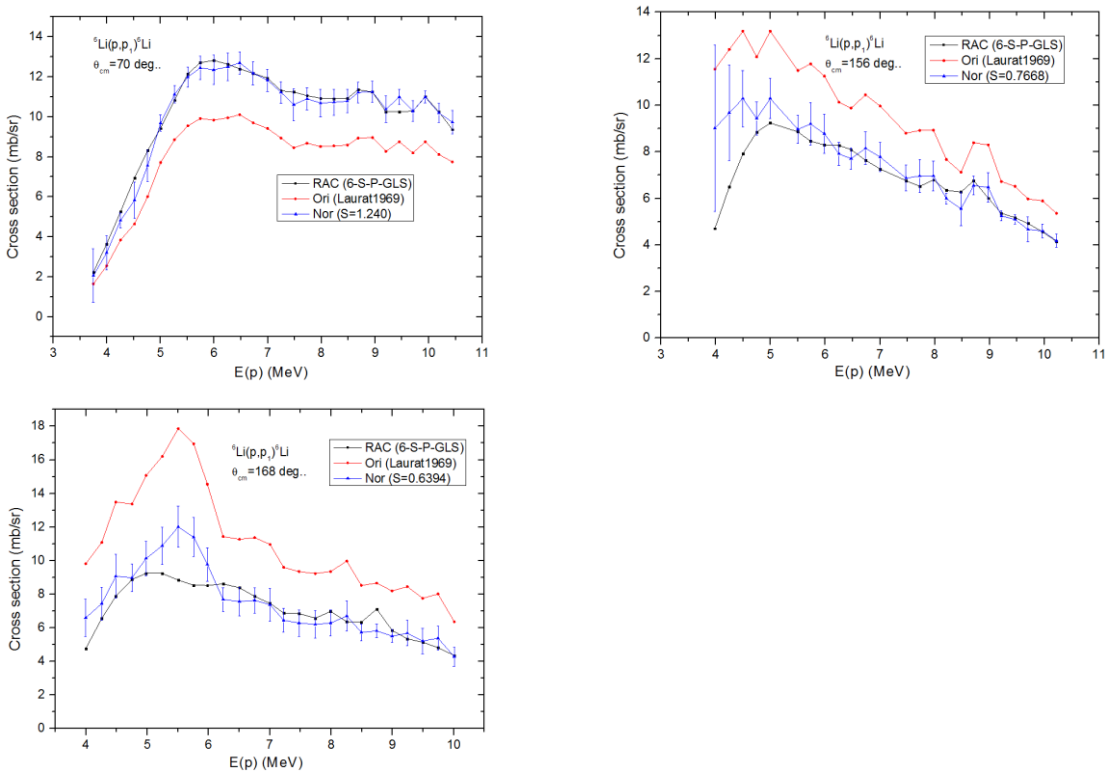

FIG 7.33. Evaluated DA of Laurat [38] for for $^{6}Li(p,p_1)^{6}Li^{*}$.

7.5. Reaction channel $^{6}Li(p,p_2)^{6}Li^{**}$

7.5.1. Integrated cross sections

The integrated cross sections of Harrison [27] for $^{6}Li(p,p_2)^{6}Li^{**}$ play a constraining role in the the fitting of the $^{6}Li(p,p_2)^{6}Li^{**}$ channel in the middle energy region, and the shape factor is fixed at N = 1.00.

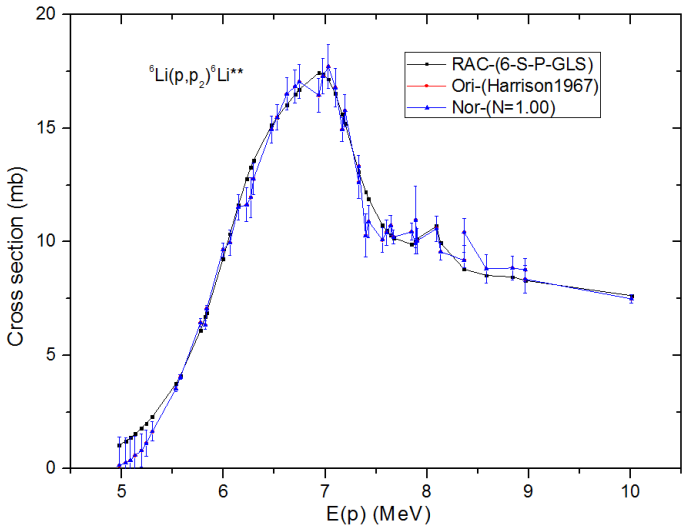

FIG 7.34. Evaluated integrated cross sections of Harrison [27] for $^{6}Li(p,p_2)^{6}Li^{**}$.

7.5.2. DA of Harrison (1967)

This DA data set of Harrison [27] is constrained by the integrated cross sections shown in Sect. 7.5.1 in the middle energy region. The shape factor at E_p = 5.8 MeV is much less than 1.00, but the shape factor at E_p = 7.8 MeV is higher than 1.00. The corresponding shapes look good.

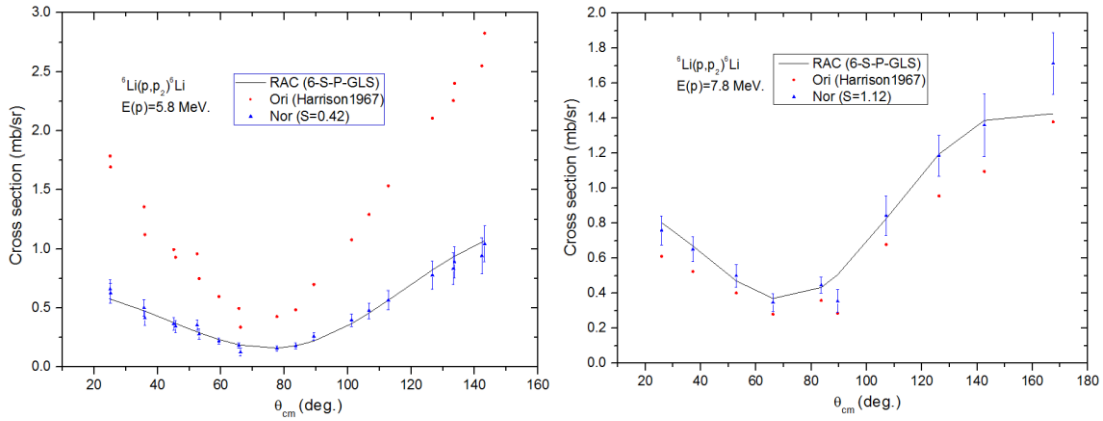

FIG 7.35. Evaluated DA of Harrison [27] for ^{6}Li(p,p$_2$)^{6}Li**.

7.5.3. DA of Merchez (1968)

This data set of Merchez [30] at 14 MeV constrains the fitting of the ^{6}Li(p,p$_2$)^{6}Li** channel in the higher energy region, and its shape factor is fixed at N = 1.00.

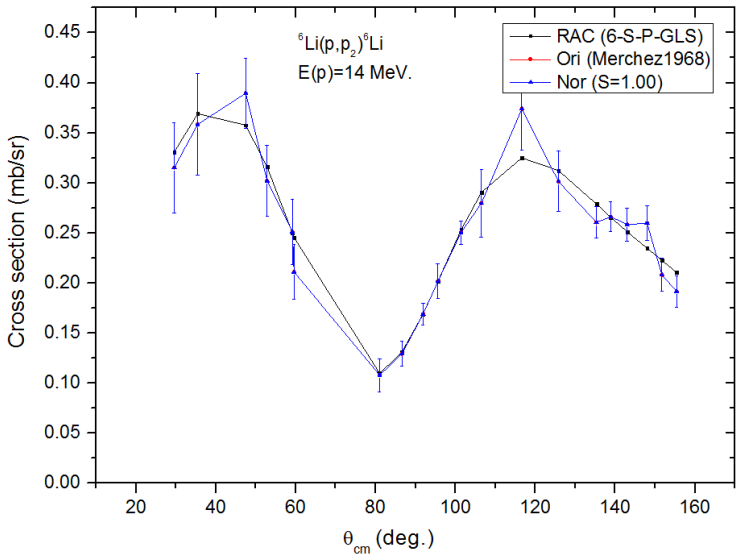

FIG 7.36. Evaluated DA of Merchez [30] for ^{6}Li(p,p$_2$)^{6}Li** at 14 MeV.

7.6. Reaction channel $^{6}Li(p,\gamma)^{7}Be$

7.6.1. Integrated cross sections

These integrated cross sections of Switkowski [39] for $^{6}Li(p,\gamma_0)^{7}Be$ and $^{6}Li(p,\gamma_1)^{7}Be^*$, respectively, are very hard to fit. Their shape factor is fixed at N = 1.00.

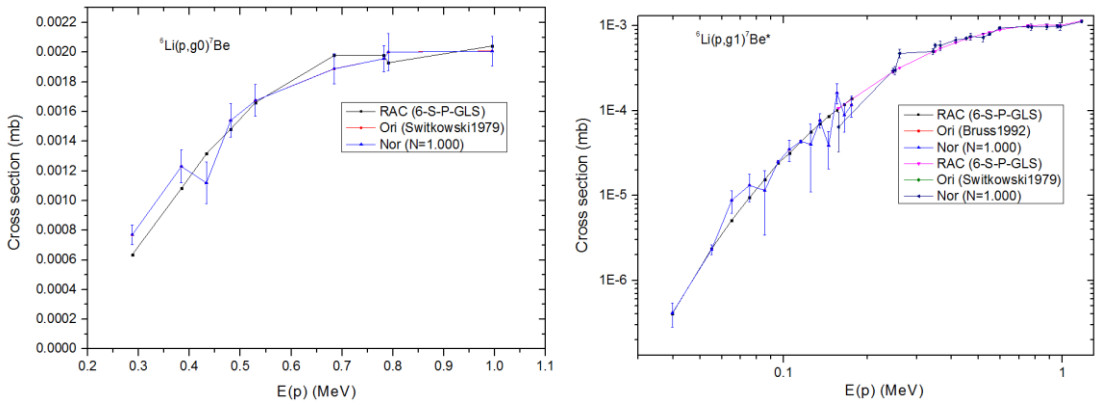

FIG 7.37. Evaluated integrated cross sections of Switkowski [39] for $^{6}Li(p,\gamma)^{7}Be$.

7.6.2. Data of Ostojic (1983)

These excitation functions of $^{6}Li(p,\gamma_0)^{7}Be$ and $^{6}Li(p,\gamma_1)^{7}Be$ measured at 90 degrees by Ostojic [40] are relative values. Their shape factor should be constrained by the integrated cross sections from previous Sect. 7.6.1.

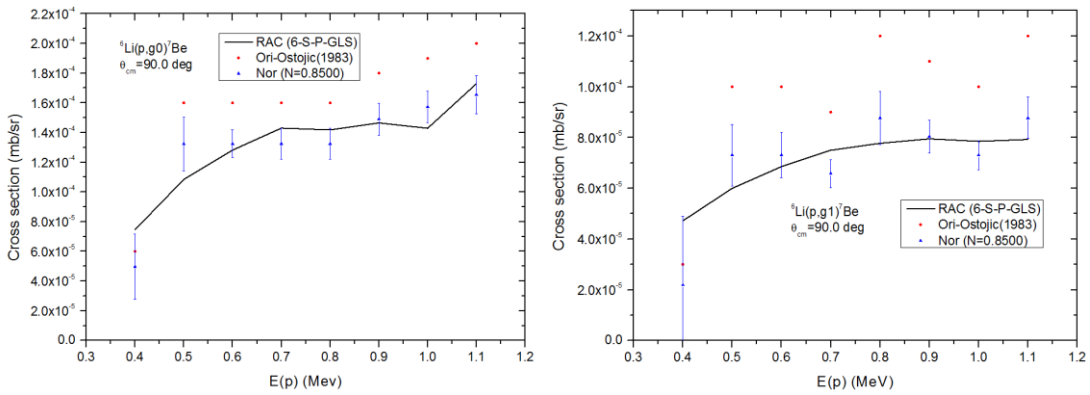

FIG 7.38. Evaluated excitation functions of Ostojic [40] for $^{6}Li(p,\gamma)^{7}Be$.

7.7. Reaction channel $^{4}He(^{3}He,^{3}He)^{4}He$

7.7.1. Data of Mohr (1993)

This set of data of Mohr [25] includes 14 angles and covers an energy range from $E_{^{3}He}$ = 1.2 to 3.12 MeV. It contributes significantly to the fitting procedure in the low energy region. The original data is relative to the Rutherford elastic scattering and the value of the first data point (1.2 MeV, 34.8 degree) agrees very well with the Rutherford cross section. This data point can actually be used to check the calculation accuracy of the R-matrix codes.

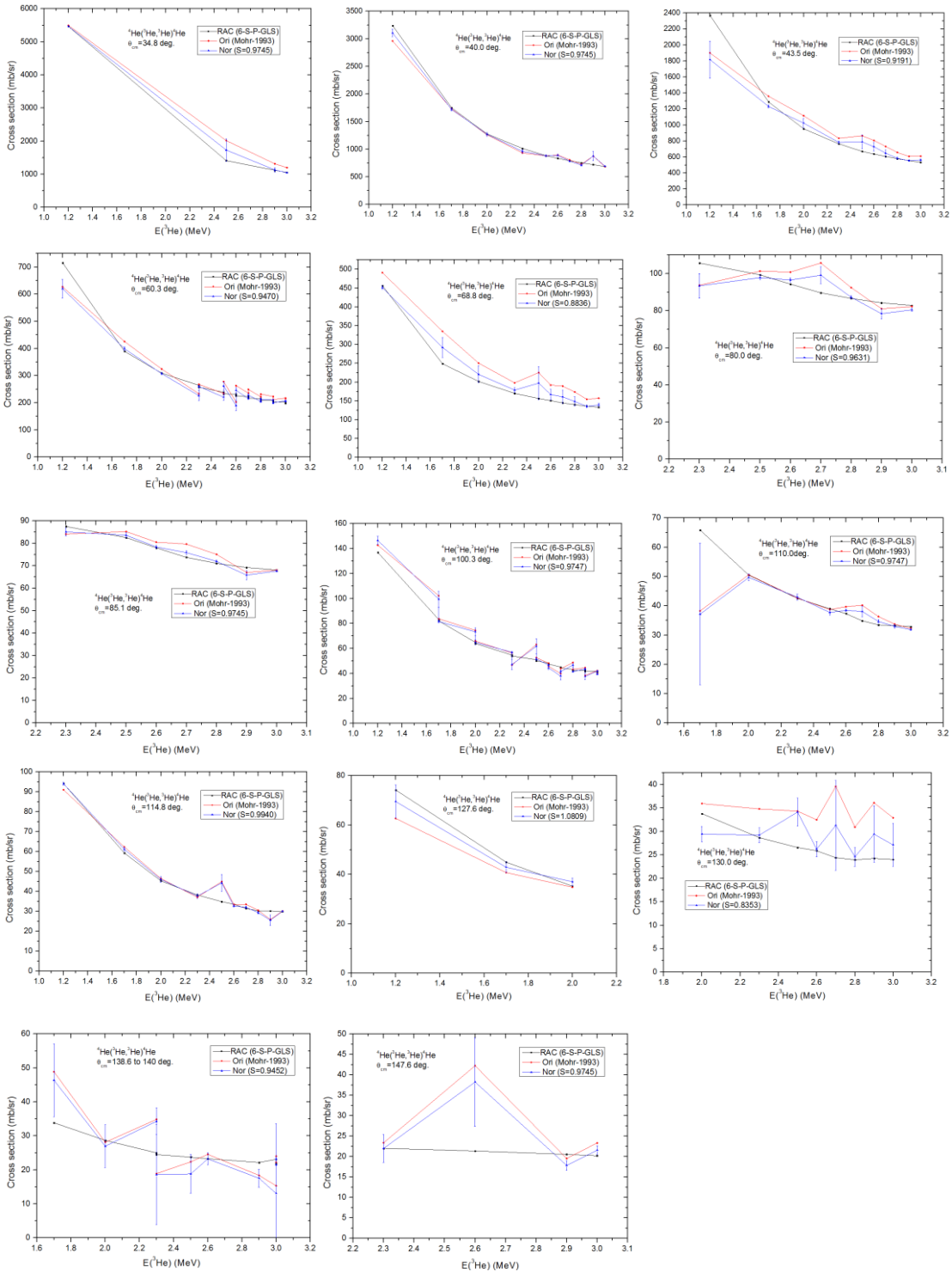

FIG 7.39. Evaluated excitation functions of Mohr [25] for $^{4}He(^{3}He,^{3}He)^{4}He$.

7.7.2. Data of Barnard (1964)

The data set of Barnard [21] includes 8 angles and energies from $E_{^3He}$ = 2.4 to 5.8 MeV at very small intervals (total of 840 data points). As a result, it dominates the fitting of the $^4He(^3He,^3He)^4He$ channel. From the energy of 4.4 to 5.8 MeV, there exist also data from Spiger [24] and Tombrello [26]. These 3 groups of data compete against each other in the fitting procedure.

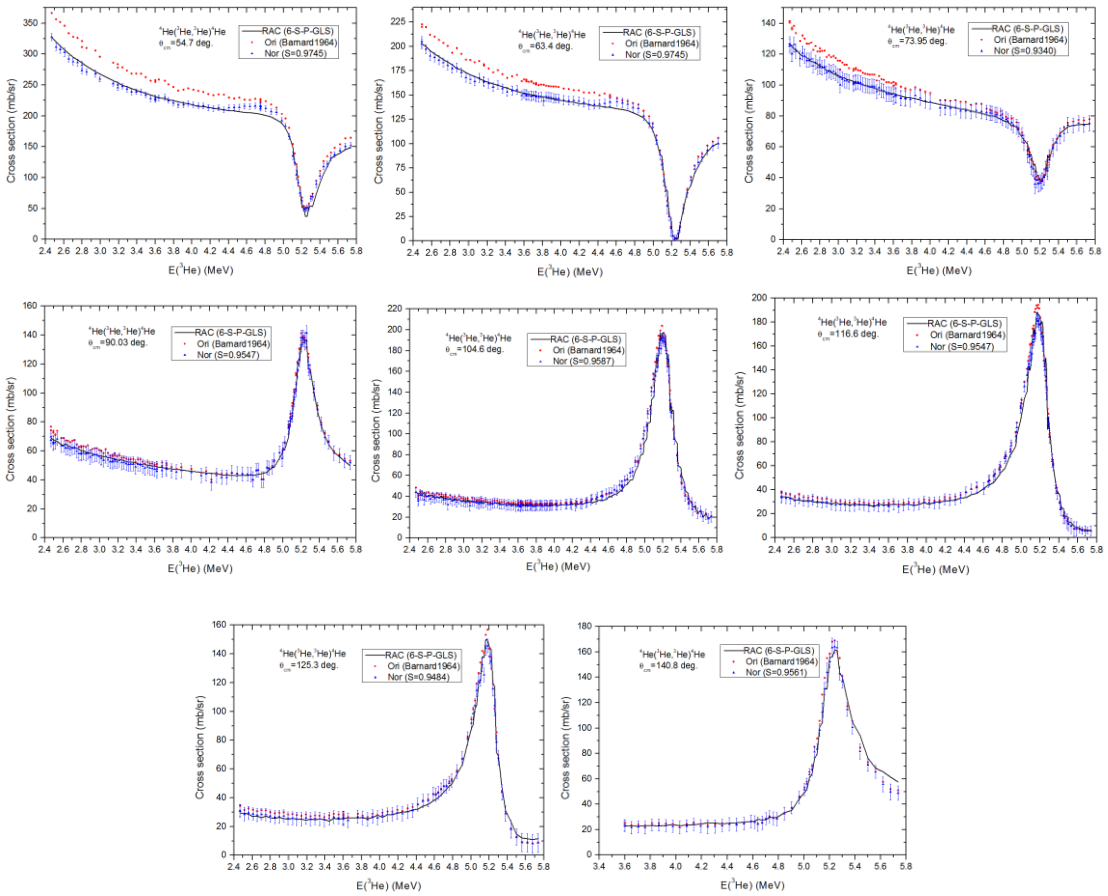

FIG 7.40. Evaluated excitation functions of Barnard [21] for $^4He(^3He,^3He)^4He$.

7.7.3. Data of Spiger (1967)

This set of data measured by Spiger [24] includes 19 angles and covers energies from $E_{^3He}$ = 4.2 to 10.8 MeV. The main feature is the very small systematic error (1.5%), however from the comparison with the data of Tombrello [26], it turns out the systematic error is positive and much larger in fact. In the energy range from 4.4 to 12.0 MeV, there exist also data from Tombrello [26] and Barnard [21]. These 3 groups of data are in a very strong competion in fitting procedure.

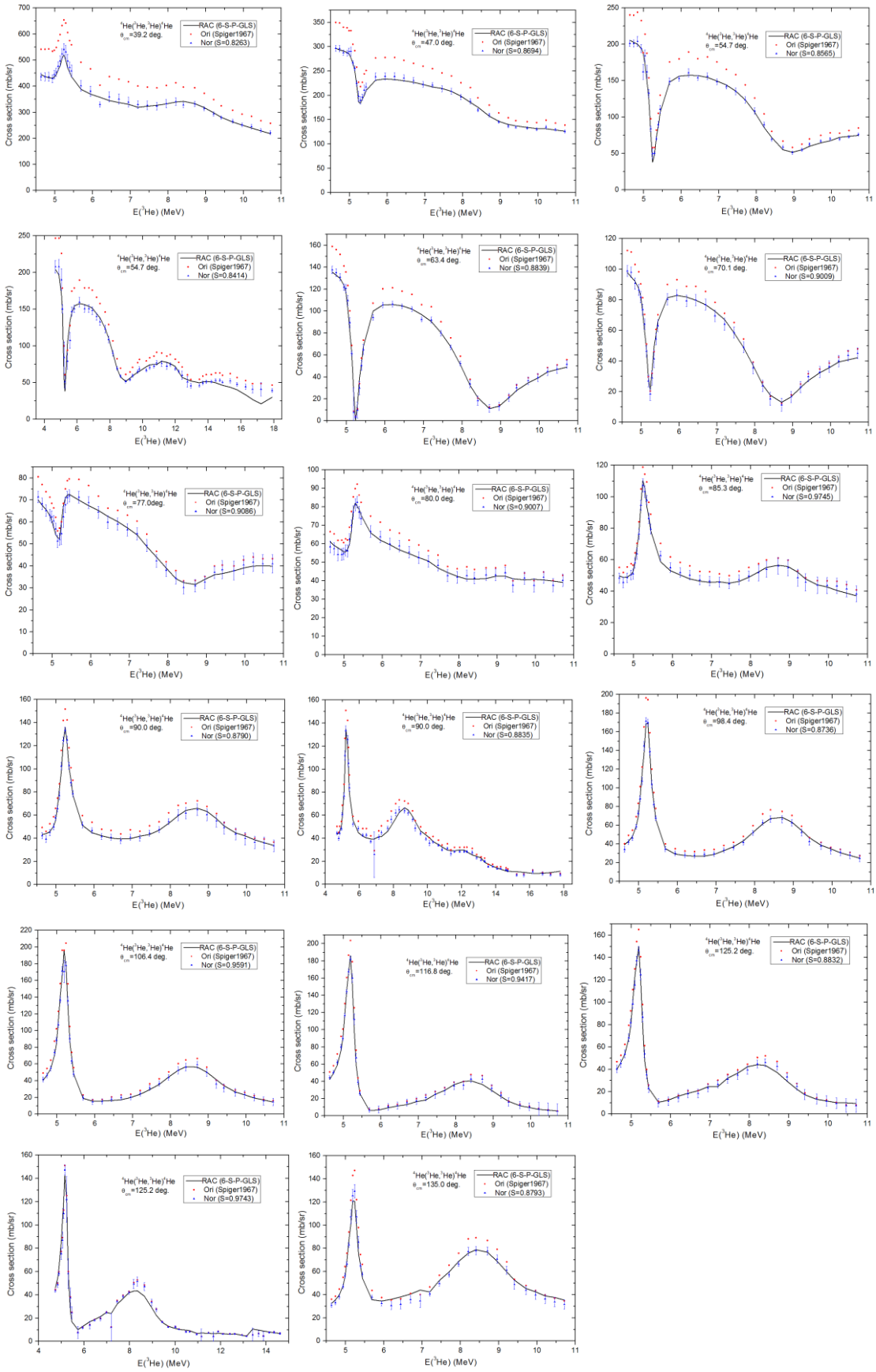

FIG 7.41. Evaluated excitation functions of Spiger [24] for $^{4}He(^{3}He,^{3}He)^{4}He$.

7.7.4. Data of Tombrello (1963)

This data set of Tombrello [26] includes 8 angles and covers energies from $E_{^3He}$ = 4.6 to 12.0 MeV. The main feature of these data is that they are in good agreement with the data of Barnard [21] in the low energy region, while from the comparison with the data of Spiger [24] they have a systematic error about 2% which is negative. In the energy range from 4.4 to 12.0 MeV, these data are in very strong competition with the data of Spiger [24] and Barnard [21].

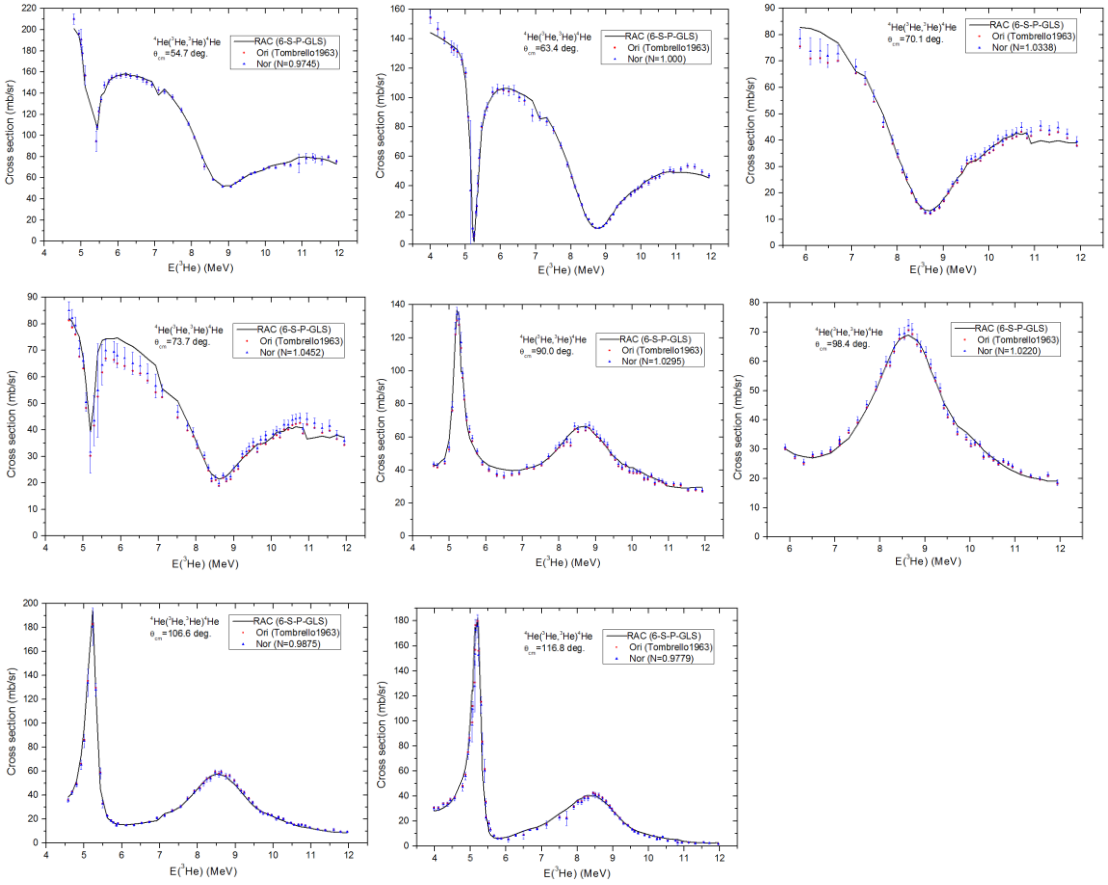

FIG 7.42. Evaluated excitation functions of Tombrello [26] for $^4He(^3He,^3He)^4He$.

7.7.5. DA of Tombrello (1963)

This set of data of Tombrello [26] includes angular didtribution with 18 angles at 4 energies. The fit at 9.69 MeV looks very good.

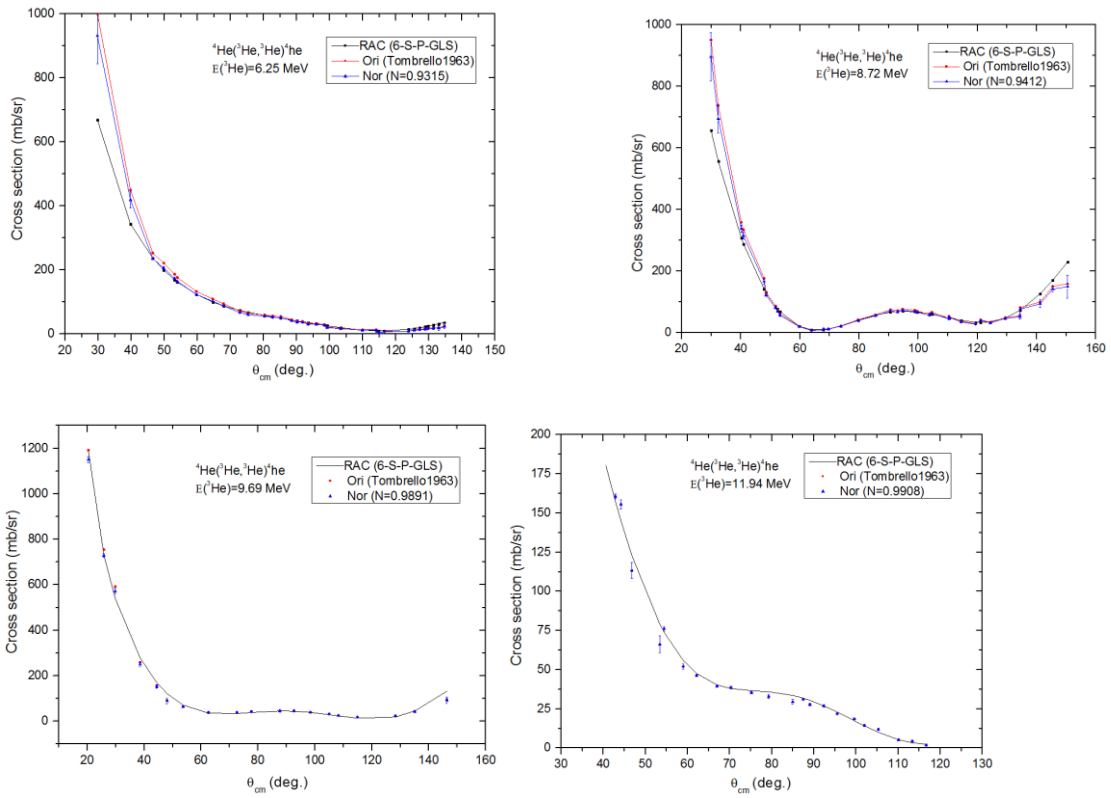

FIG 7.43. Evaluated DA of Tombrello [26] for $^4He(^3He,^3He)^4He$.

7.7.6. DA of Gorpinch (1992)

This data set of Gorpinch [41] has a different distribution compared to other data sets.

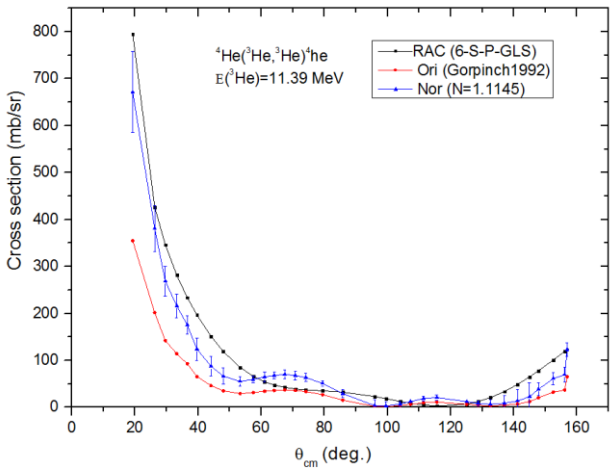

FIG 7.44. Evaluated DA of Gorpinch [41] for $^4He(^3He,^3He)^4He$.

7.7.7. DA of Jacobs (1970)

This data set of Jacobs [42] includes angular distributions with 38 angles at 7 very high energies, and therefore plays a key role in constraining the parameters of the distant levels.. All the fitted shapes look good.

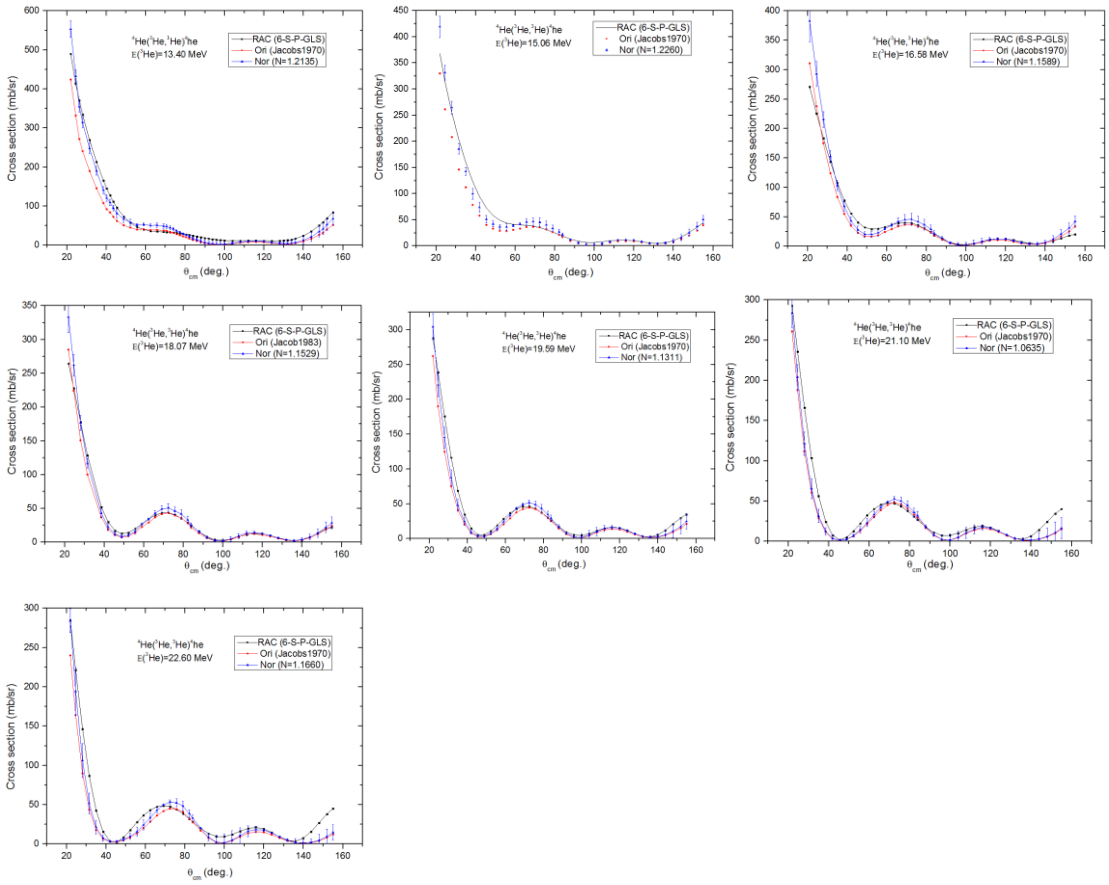

FIG 7.45. Evaluated DA of Jacobs [42] for $^{4}He(^{3}He,^{3}He)^{4}He$.

7.7.8. Analyzing powers of Harrison (1967)

This set of analyzing powers measured by Harrison [27] includes 3 angles and energies ranging from 6 to 11 MeV. The fits are fairly good.

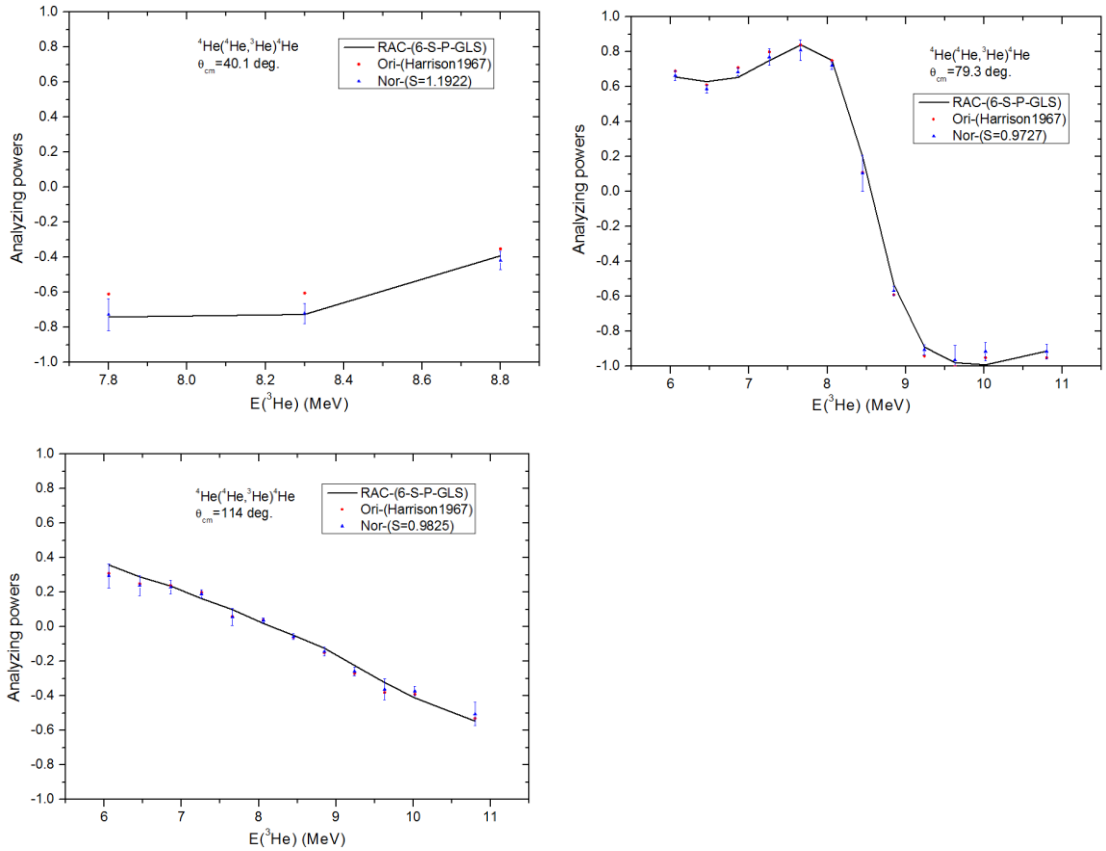

FIG 7.46. Evaluated analyzing powers of Harrison [27] for ^{4}He(^{3}He,^{3}He)^{4}He.

7.7.9. Analyzing powers of Boy (1972)

This set of analyzing powers of Boy [43] include 3 angles and energies ranging from 3.2 to 7 MeV. They are taken from the EDA evaluation file. The fit looks very good.

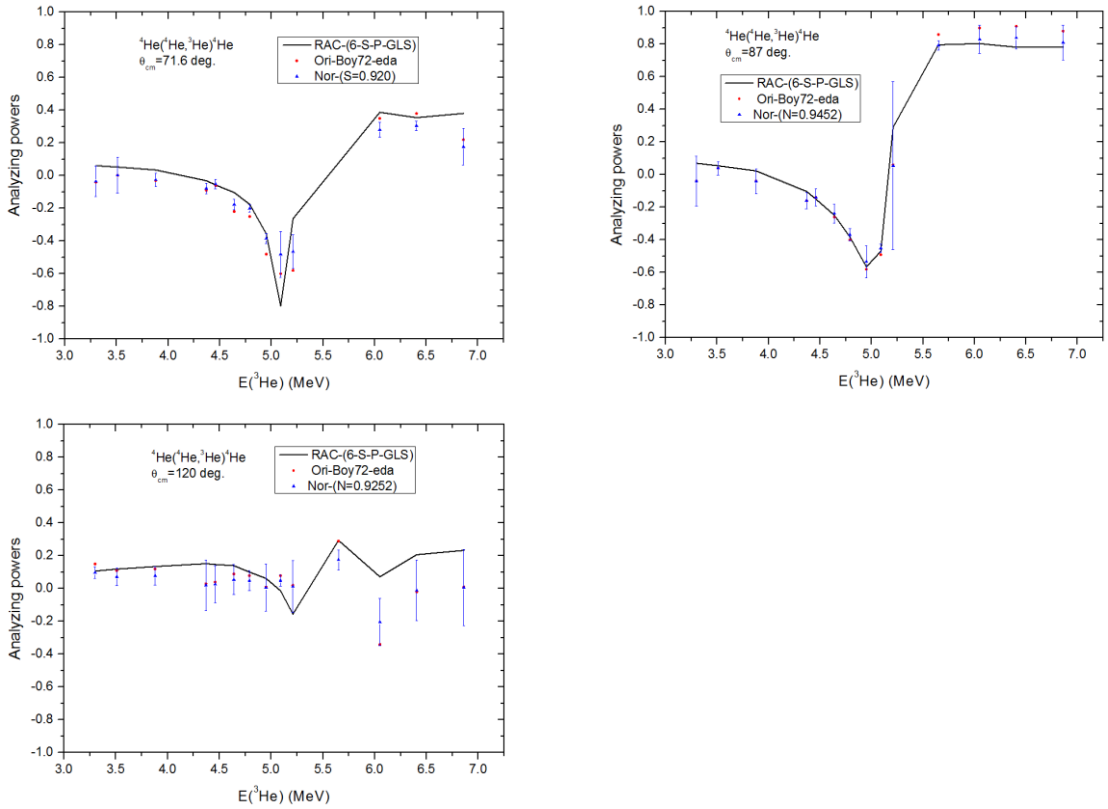

FIG 7.47. Evaluated analyzing powers of Boy [43] for $^{4}He(^{3}He,^{3}He)^{4}He$.

7.7.10. Comparison of data at 90 degree

This figure shows the excitation function of ^{4}He (^{3}He, ^{3}He) ^{4}He for 4 different data sets at 90 degree. These data sets have a large weighting factor in the fitting process.

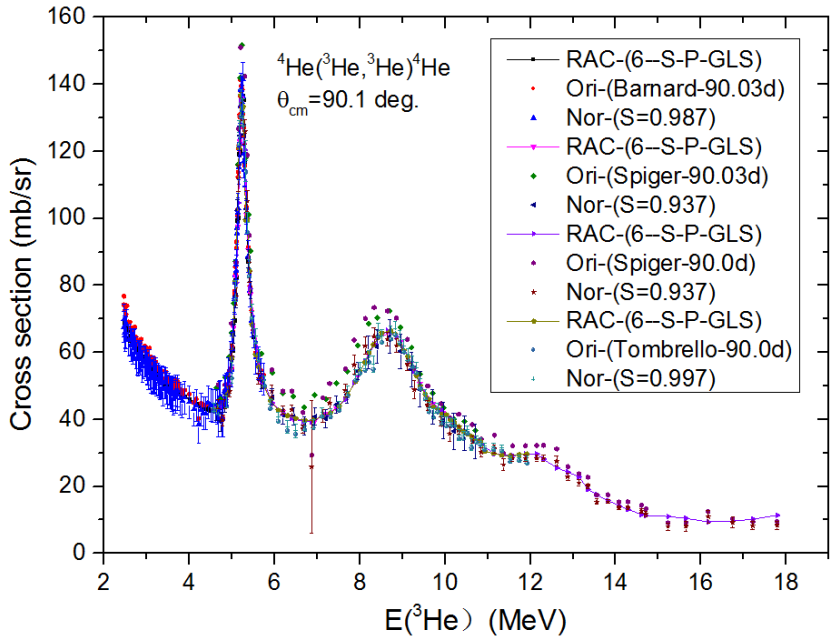

FIG 7.48. Evaluated excitation functions for $^{4}He(^{3}He,^{3}He)^{4}He$ based on data from Barnard [21], Spiger [24], and Tombrello [26].

7.8. Reaction channel $^{4}He(^{3}He,p)^{6}Li$

7.8.1. Data of Spiger (1967) – group *a*

This 'group *a*' data set of Spiger [24] includes 2 angles and energies ranging from 7.5 to 18 MeV. The fit looks good.

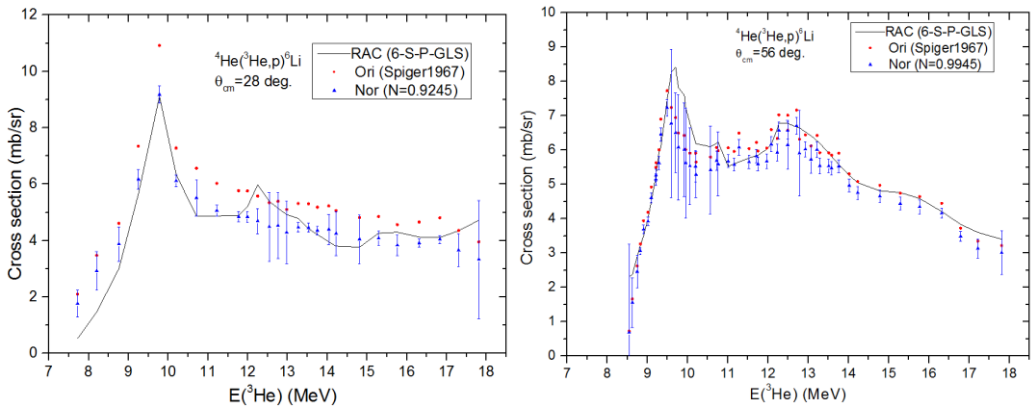

FIG 7.49. Evaluated excitation functions of Spiger [24] for $^{4}He(^{3}He,p)^{6}Li$ – group a.

7.8.2. Data of Spiger (1967) – group *b*

This 'group *b*' data set of Spiger [24] includes 13 angles and energies that range from 8.5 to 11 MeV. They too are taken from the EDA evaluation file. The statistical error is 6%.

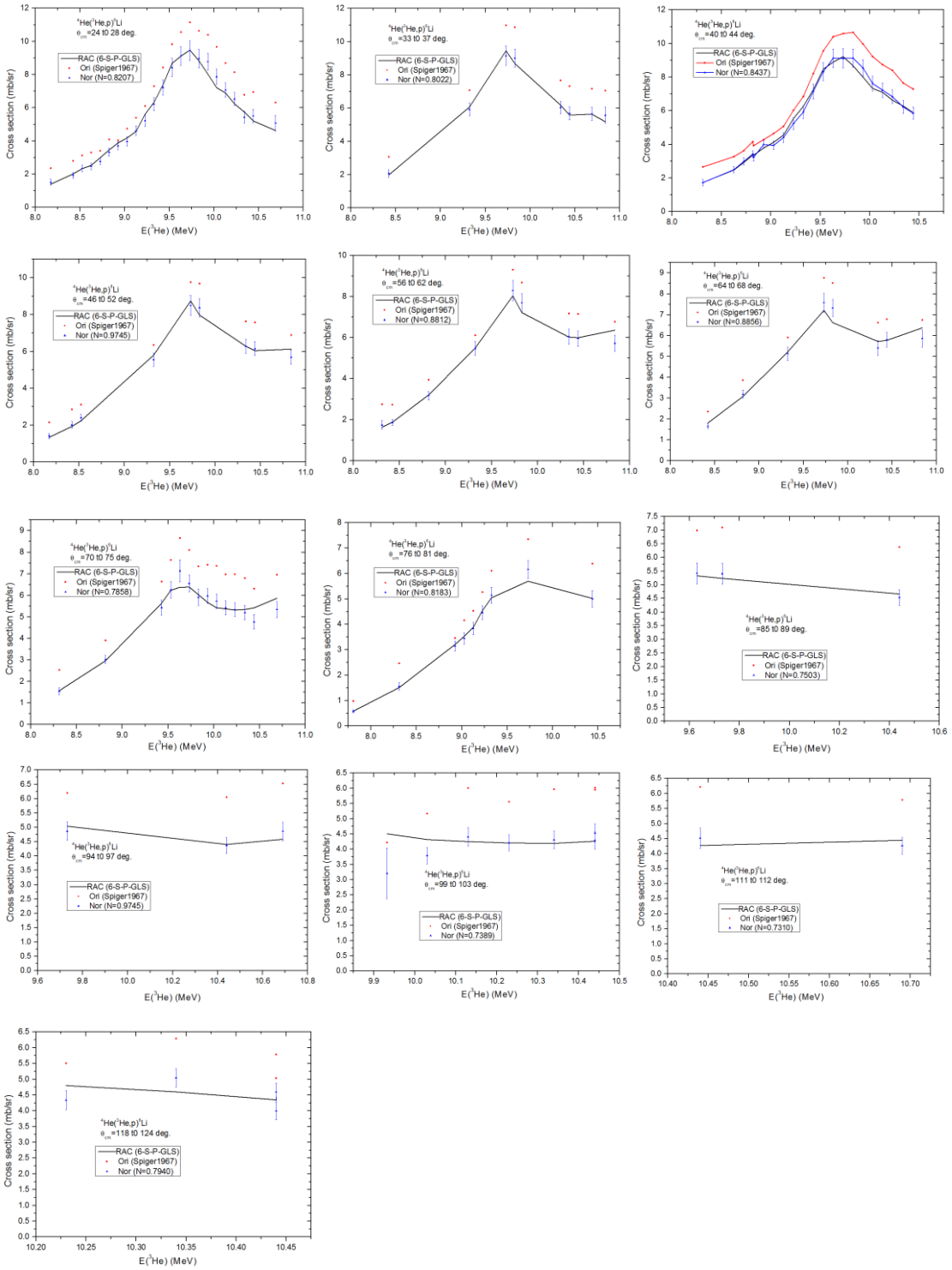

FIG 7.50. Evaluated excitation functions for the 'Spiger data [24] for $^{4}He(^{3}He,p)^{6}Li$ – group b.

7.9. Reaction channel $^{4}He(^{3}He,p1)^{6}Li^{*}$

7.9.1. Data of Spiger (1967)

This data set of Spiger [24] includes 2 angles and energies ranging from 11.5 to 18 MeV. The fit depends on other data sets.

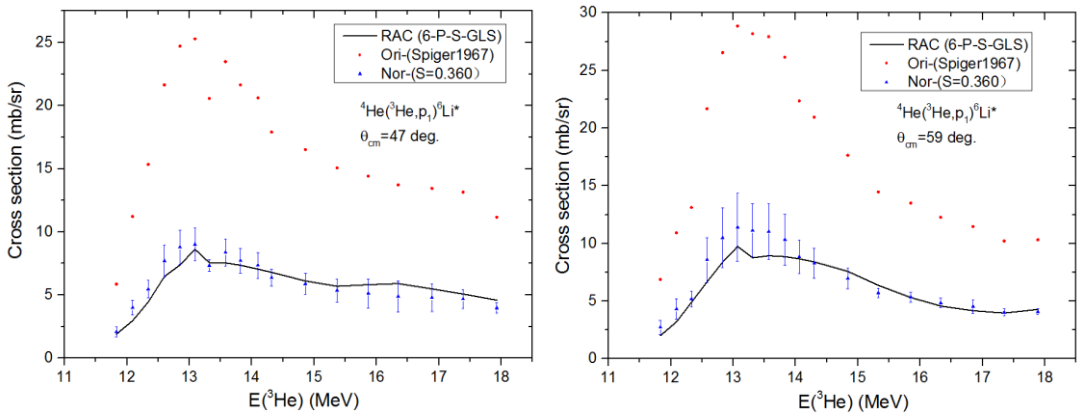

FIG 7.51. Evaluated excitation functions of Spiger [24] for $^{4}He(^{3}He,p_{1})^{6}Li^{*}$.

7.10. Reaction channel $^{4}He(^{3}He,\gamma)^{7}Be$

Integrated cross sections of $^{4}He(^{3}He,\gamma_0)^{7}Be^{4}$ and $He(^{3}He,\gamma_1)^{7}Be$ reaction from Osborne [44] and Singh [45]. The data are very hard to fit. The shape factor is fixed to N = 1.00.

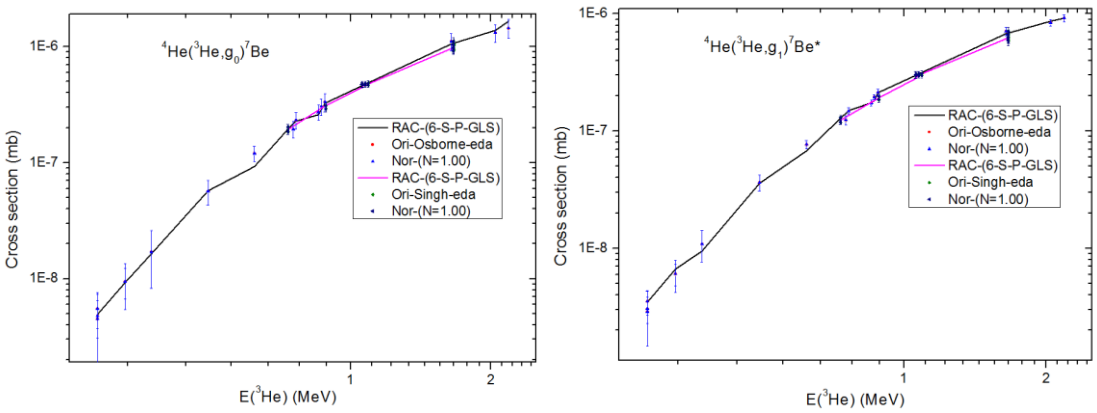

FIG 7.52. Evaluated excitation functions of Osborne [44] and Singh [45] for $^{4}He(^{3}He,\gamma)^{7}Be$.

7.11. Proposal for ENDF format

In Fig. 7.53 all the recommended DA resulting from the global fitting of ^{7}Be are plotted at different energies. The question is how one can store these evaluated data in the ENDF-6 format [47].

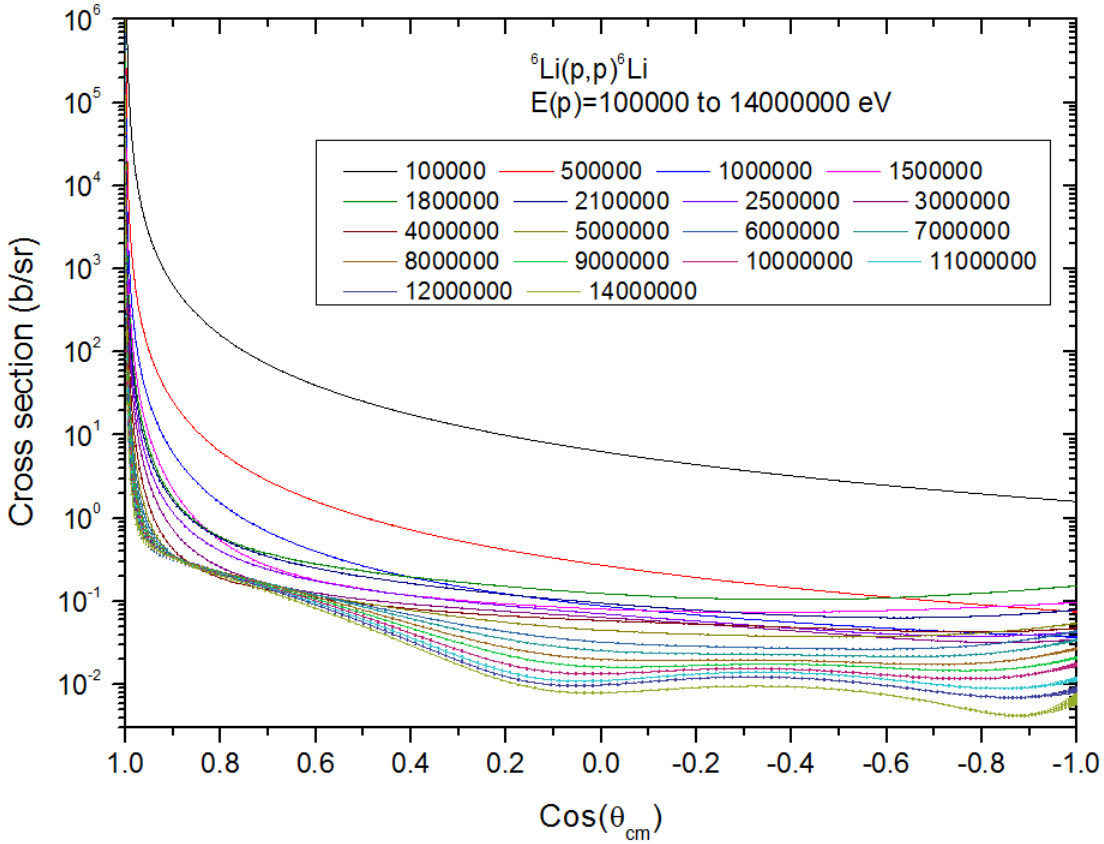

FIG 7.53. The final calculated DA for ^{6}Li(p,p)^{6}Li using the best R-matrix parameter set of RAC, which has been obtained from the global fitting of the ^{7}Be system.

In the currently adopted ENDF-6 format, the elastic scattering cross sections for incident charged-particles are defined by Eqs. (6.13-6.14) of the manual [47]. According to these equations, 'elastic scattering of charged particles includes components from Coulomb scattering, nuclear scattering, and the interference between them. The Coulomb scattering is represented by the Rutherford formula and electronic screening is ignored. Eqs. (6.13) describe the net elastic scattering differentinal cross sections, where the al are complex coefficients for expanding the trace of the nuclear scattering amplitude matrix and the bl are real coefficients for expanding the nuclear scattering cross section."

It is a very challenging task to get accurate al and bl, and there is no accurate way of producing their covariance matrix. Furthermore, it may happen that the non-Rutherford scattering effect is involved in the fitting process, in which case Eqs. (6.13) are not useful. For these reasons, it is recommended to use Tabulated Probability Distributions.

The proposal is to store charge-particle induced reactions as Tabulated Probability Distributions using the same form used for neutron-induced reactions, with the only difference being that an

4.2.2 Tabulated Probability Distributions (LTT=2, LI=0)

If the angular distributions are given as tabulated probability distributions, LTT=2, structure of a section is:

```
[MAT, 4, MT/  ZA, AWR,   0, LTT,  0,  0]HEAD   (LTT=2)
[MAT, 4, MT/ 0.0, AWR,  LI, LCT,  0,  0]CONT   (LI=0)
```

extra line 3 is added for DA (File=4, MT=2). An example is given below:

```
[MAT, 4, MT/ 0.0, 0.0,   0,   0, NR, NE/ E_int] TAB2
[MAT, 4, MT/   T,  E_1,  LT,   0, NR, NP/ μ_int/f(μ,E_1)]TAB1
[MAT, 4, MT/   T,  E_2,  LT,   0, NR, NP/ μ_int/f(μ,E_2)]TAB1
    ------------------------------------------
    ------------------------------------------
[MAT, 4, MT/   T, E_NE, LT,   0, NR, NP/ μ_int/f(μ,E_NE)]TAB1
[MAT, 4,  0/ 0.0, 0.0,   0,   0,  0,  0]SEND
```

Parameters T and LT are normally zero.

```
[MAT, 4, 2/  1.000000-1 1.000000+0 1.800000+2 1.000000+0    181 20]   3
```

The above excerpt is from Ref. [47] for a neutron as incident particle. For an incident charged particle, an additional line (line 3 highlighted) is added straight after line 2 marked with (LI=0) including the following items:

MAT 4 2 1.000000-1 1.000000+0 1.800000+2 1.000000+0 181 20 3

In the above line 3, '1.00000E-1' is the first angle, '1.00000E+0' is the second angle, '1.80000E+2' is the last angle, '1.00000E+0' is the uniform step, '181' is the total number of angles. '20' is the number of energy points. '3 is the line number in ascending order.

8. CONCLUSION

The R-matrix Analysis Code RAC with the CERNGEPLIS Evaluation Method has been used to perform a global fitting of the ^{7}Li and ^{11}B systems. The obtained results have been incorporated in the Neutron Cross-Section Standards of the IAEA [2,3]. Furthermore, the method has been implemented in the evaluation of the ^{20}O system to obtain the astrophysical S factor of ^{12}C (α,γ) ^{16}O with high precision (about 5%), and in the ^{7}Be system with perfect results for the IAEA coordinated project on "R-matrix Codes for Charged-particle Reactions in the Resolved Resonance Region" [1]. Recently the method has been used in the evaluation of the ^{10}Be system, with improved results for the n+^{9}Be cross sections. Our experience thus far proves that the code RAC combined with the CERNGEPLIS Evaluation Method is a reasonable, useful and powerful tool for nuclear data evaluation.

ACKNOWLEDGMENTS

The authors in Tsinghua University would like to thank Dr. Paraskevi Dimitriou for writing the Introduction and editing this document, and Dr. Vladimir Pronyaev and Dr. Roberto Capote for their valuable advice. They express their appreciation to D.L. Smith for his excellent book on "Probability, Statistics, and Data Uncertainties in Nuclear Science and Technology", and their gratitude to all the members of the project "R-matrix Codes for Charged-particle Induced

Reactions in the Resolved Resonance Region" for the fruitful discussions and help they have offered. This work is supported partially by a Special Service Agreement with the Nuclear Data section of IAEA; Science Challenge Project No. **TZ2018001**, China; the National Natural Science Foundation of China under Grants No. **11775029;** the Tsinghua University Initiative Scientific Research Program, China, No. **20111081104**.

REFERENCES

[1] H. Leeb, P. Dimitriou, I.J. Thompson, R-matrix Codes for Charged-Particle Reactions in the Resolved Resonance Region (1-5), INDC(NDS)-0703, INDC(NDS)-0726, INDC(NDS)-0737, INDC(NDS)-0767, INDC(NDS)-0787. http://www-nds.iaea.org/index-meeting-crp/CM-RMatrix-2019/

[2] A.D. Carlson, V.G. Pronyaev, D.L. Smith, N.M. Larson, Z.-P. Chen et al., Nucl. Data. Sheets **110** (2009) 215.

[3] A.D. Carlson, V.G. Pronyaev, R. Capote, G.M. Hale, Z.-P. Chen, et al., Nucl. Data Sheets **148** (2018) 142.

[4] A.M. Lane, R.G. Thomas, Rev. Mod. Phys. **30** (1958) 257.

[5] A.R. Barnett, D.H. Feng, J.W. Steed, L.J.B. Goldfarb, Comput. Phys. Commun. **8** (1977) 377.

[6] D.L. Smith, Probability, Statistics, and Data Uncertainties in Nuclear Science and Technology (Amer Nuclear Society, Chicago, 1991).

[7] F.C. Barker, T. Kajino, Ast. J. Phys. **44** (1991) 36.

[8] Z.P. Chen, R. Zhang, Y.Y. Sun, T.J. Liu, Science in China (Series G) **46** (2003) 225.

[9] EDA, Energy-Dependent Analysis code, Los Alamos National Laboratory.

[10] N.M. Larson, Technical Report ORNL/TM-9179/R8, Oak Ridge National Laboratory (2008).

[11] R.E. MacFarlane, et al., The NJOY Nuclear Data Processing System, Version 2012, LA-UR-12-27079, August 2013.

[12] X.D. Tang, K.E. Rehm, I. Ahmad, C.R. Brune, A. Champagne, et al., Phys. Rev. C **81** (2010) 045809.

[13] L. Buchmann, G. Ruprecht, and C. Ruiz, Phys. Rev. C **80** (2009) 045803.

[14] Z. Zhao, R.H. France, III, K.S. Lai, S.L. Rugari, M. Gai, et al., Phys. Rev. Lett. **70** (1993) 2066.

[15] I.J. Thompson, R.J. deBoer, P. Dimitriou, et al., Eur. J. Phys. A (2019) **55**: 92.

[16] A.C. Aitken, Statistical Mechanics, 8th Edition, Oliver and Boyd Press, London (1957).

[17] Zhen-Dong An, Zhen-Peng Chen, Yu-Gang Ma, et al., Phys. Rev. C **92** (2015) 045802.

[18] Z.D. An, Y.G. Ma, G.T. Fan, Y.J. Li, Z.P. Chen, and Y.Y. Sun, Astrophysical Journal Letters, **817**:L5 (pp. 6), January 2016.

[19] Z.P. Chen, Y.Y. Sun, Chinese Physics **13**/14 (2004).

[20] J A. McCray, Phys. Rev. **130** (1963) 2034.

[21] A.C.L. Barnard, C.M. Jones, and G.C. Phillips. Nucl. Phys. **50** (1964) 629.

[22] J. Elwyn, R.E. Holland, C.N. Davids, L. Meyer-Schützmeister, F.P. Mooring, and W. Ray, Phys. Rev. C. **20** (1992) 1984.

[23] Lin Chia-Shou, Hou Wan-Shou, Wen Min, and Chou Jen-Chang, Nucl. Phys. A **275** (1977) 93.

[24] R.J. Spiger and T.A. Tombrello, Phys. Rev. **163** (1967) 964.

[25] P. Mohr, H. Abele, R. Zwiebel, G. Staudt, H. Krauss, H. Oberhummer, A. Denker, J.W. Hammer, and G. Wolf, Phys. Rev. C. **48** (1993) 1420.

[26] T.A. Tombrello and P.D. Parker, Phys. Rev. **130** (1963) 1112.

[27] W.D. Harrison and A. Bruce Whitehead, Phys. Rev. **132** (1963) 2607.

[28] U. Fasoli, E.A. Silverstein, D. Toniolo, and G. Zago, Il Nuovo Cimento **34**/6 (1964) 1832.
[29] R.G. Seyler and H.R. Weller, Phys. Rev. C **20** (1979) 453.
[30] F. Merchez, R. Bouchez, R.A. Hoffswell, A.I. Yavin, Phys. Rev. **29** (1968) 969.
[31] M. Haller, M. Betz, W. Kretschmer, Nucl. Phys. A **496** (1989) 189.
[32] M. Skill, R. Baumann, G. Keil, Nucl. Phys. A **581** (1995) 93.
[33] Khanh (1961), taken from EDA file, see Ref. 46.
[34] I. Spinka,T. Tombrello, Nucl. Phys. A **164** (1971) 1.
[35] Bouchez, taken from EDA file, see Ref. 46.
[36] Bas (1951), taken from EDA file, see Ref. 46.
[37] D.R. Gould, R.O. Nelson, Nucl. Sci. Eng. **55** (1974) 267.
[38] L. Schenk,W. Buck, M. Morik, Int. Conf. on Nuclear Physics, Munich 1973, Vol.1, p.450 (1973).
[39] Bro (1968), taken from EDA file, see Ref. 46.
[40] R. Ostojic, L.Subotic, Nuovo Cimento A **76** (1983) 73.
[41] O.K. Gorpinich, V.I. Konfederatenko, V.V. Ostashko, et al., Bull. Russian Academy of Sciences – Physics 56 (1992) 439.
[42] C.G. Jacobs JR, R.E. Brown, Phys. Rev. C **1** (1970) 1615.
[43] Boy (1972), taken from EDA file, see Ref. 46.
[44] Sborne, taken from EDA file, see Ref. 46.
[45] Singh, taken from EDA file, see Ref. 46.
[46] EDA file for evaluation of ^{7}Be system, private communication (2017).
[47] ENDF-6 Formats Manual, edited by A. Trkov, M. Herman and D. A. Brown, February 2018. https://www-nds.iaea.org/public/endf/endf-manual.pdf

APPENDIX 1: Comparison of RAC and EDA for the ^{7}Li system

Figure A.1 (private communication of V. Pronyaev within IAEA Neutron Standards project, 2016) shows the correlation coefficients of ^{6}Li(n,n) and ^{6}Li(n,t) in the covariance matrix obtained with RAC and EDA. For neutrons on ^{6}Li, in the $E_n < 2$ MeV energy region only two outgoing reaction channels are open, ^{6}Li(n,n) and ^{6}Li(n,t), thus the neutron total cross section ^{6}Li(n,tot) ≡ ^{6}Li(n,n) +^{6}Li(n,t). The errors of the experimental neutron cross sections are very small thsu putting a strong constraint on the evaluated values of ^{6}Li(n,n) and ^{6}Li(n,t). As a result, the ^{6}Li(n,n) and ^{6}Li(n,t) cross sections have opposite tendency and the corresponding correlation coefficient is negative, not positive. All the correlation coefficients obtained with RAC are negative, which is perfectly reasonable from the physics point of view. In Fig. A.1 one sees the 'positive correlations observed for diagonal cross reaction correlations from EDA'.

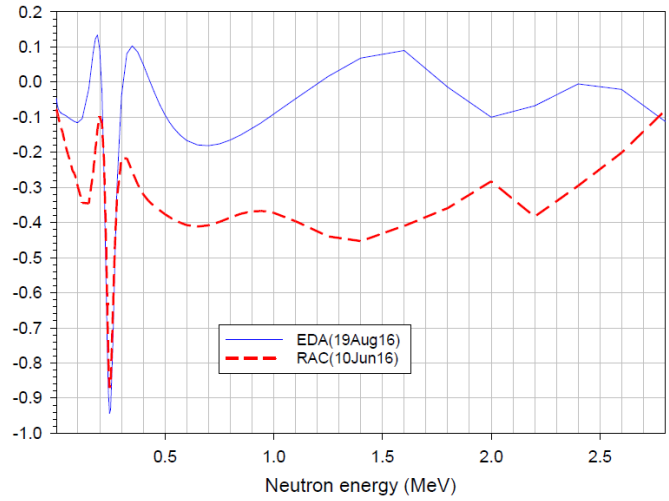

FIG A.1. Comparison of cross reaction correlations ^{6}Li(n,n)^{6}Li(n,t), the diagonal element of the square block with the maximum of cross correlations obtained with EDA and RAC. Positive correlations are observed for diagonal cross reaction correlations from EDA because of "confidence interval" approach.*

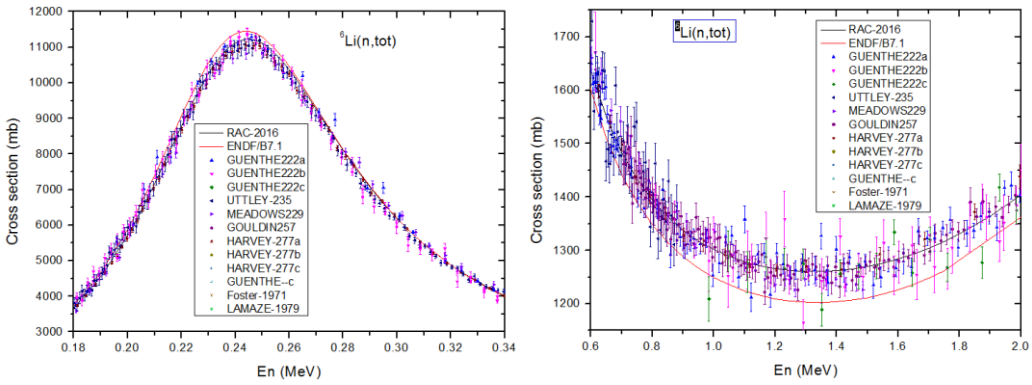

FIG A.2. The left panel shows that ENDF/B7.1 is systematically higher than experimental data for ^{6}Li (n,tot) at neutron energies E_n = 0.22 to 0.27 MeV. The right panel shows that ENDF/B7 is systematically lower than the experimental data for ^{6}Li (n,tot) at neutron energies E_n=0.6 to 2 MeV.

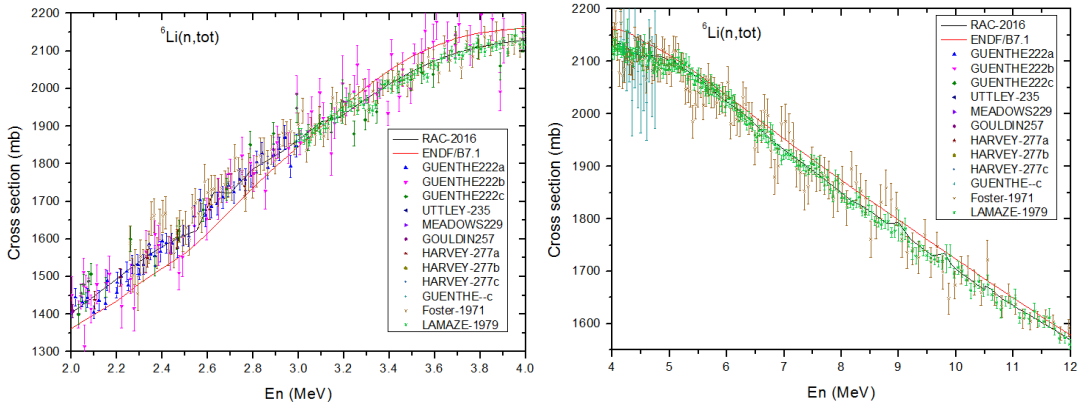

FIG A.3. The The left panel shows that ENDF/B7.1 systematically deviates from experimental data for ^{6}Li (n,tot) at energies E_n = 2 to 4 MeV，and the right panel shows it is systematically higher than experimental data for ^{6}Li (n,tot) at energies E_n=4 to 12 MeV.

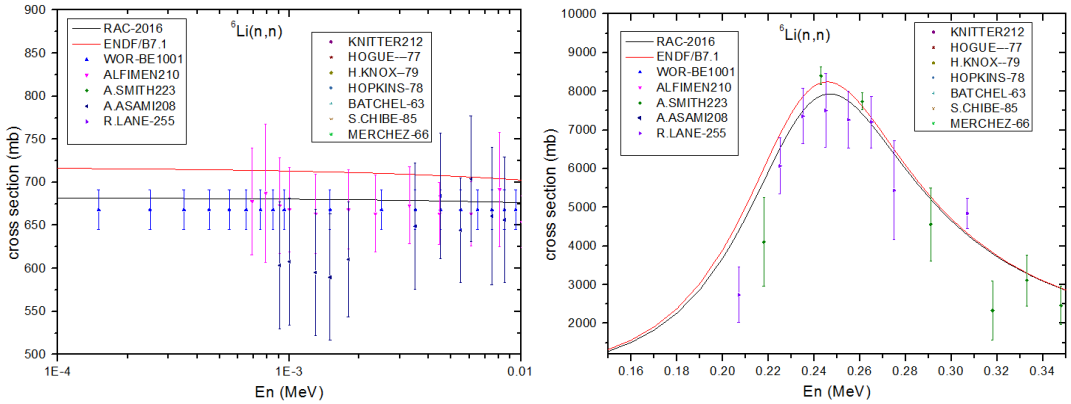

FIG A.4. The left panel shows that ENDF/B7.1 is systematically higher than experimental data for ^{6}Li (n,n) at neutron energies E_n = 0.0001 to 0.01 MeV, while the right panel shows that it is systematically higher than the experimental data of ^{6}Li (n,n) at energies E_n = 0.2 to 0.28 MeV.

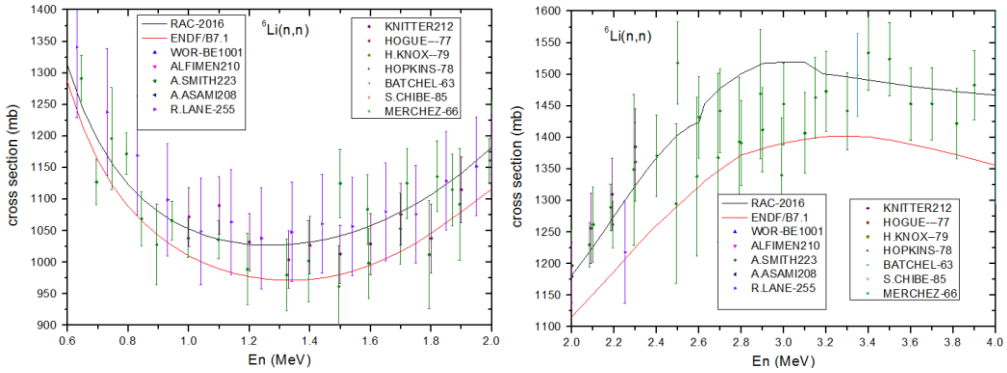

FIG A.5. The left panel shows that ENDF/B7.1 is systematically lower than the experimental data of ^{6}Li (n,n) for energies E_n = 0.6 to 2 MeV， and the right panel shows that it is systematically lower than the experimental data of ^{6}Li (n,n) for energies E_n = 2 to 4 MeV.

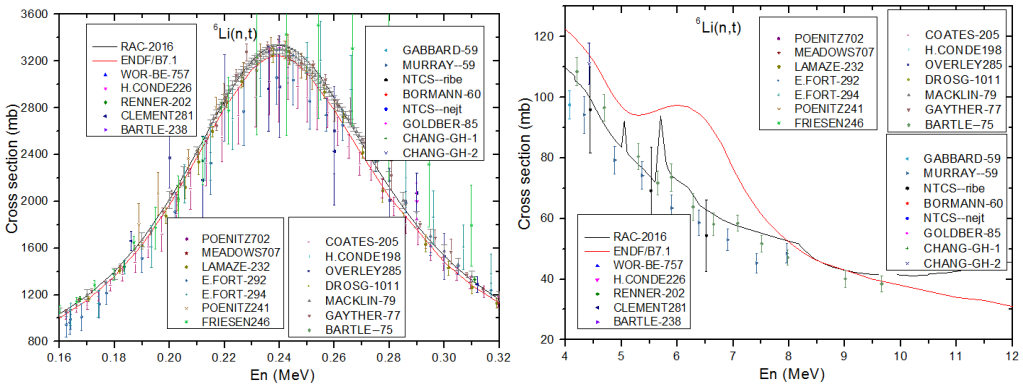

FIG A.6. The left panel shows that ENDF/B7.1 is systematically lower than the experimental data of ^{6}Li (n,t) for energies E_n = 0.22 to 0.27 MeV， and the right panel shows that it is systematically lower than experimental data of ^{6}Li (n,t) for energies E_n = 4 to 7 MeV.

Nuclear Data Section
International Atomic Energy Agency
Vienna International Centre, P.O. Box 100
A-1400 Vienna, Austria

E-mail: nds.contact-point@iaea.org
Fax: (43-1) 26007
Telephone: (43-1) 2600 21725
Web: http://nds.iaea.org